Mismatch responses in the awake rat: Evidence from epidural recordings of auditory cortical fields

Inaugural-Dissertation

zur

Erlangung des Doktorgrades

der Mathematisch-Naturwissenschaftlichen Fakultät

der Universität zu Köln

vorgelegt von

Fabienne Jung

aus Ludwigshafen

M & S Druckhaus GmbH, Köln

2013

Berichterstatter/in: PD Dr. Heike Endepols

Prof. Dr. Ansgar Büschges

Tag der mündlichen Prüfung: 27.06.13

1 Kurzzusammenfassung

Die Detektion von Veränderungen in einer sich rasch wandelnden Umwelt ist für Tiere und Menschen überlebenswichtig. Ein solcher automatischer Detektionsmechanismus existiert im auditorischen System des Menschen. Die sogenannte „Mismatch Negativity“ (MMN) ist eine spezielle Potentialkomponente akustisch evozierter Potentiale (AEPs) und reflektiert die Verletzung einer regulären Sequenz von vorhersagbaren akustischen Ereignissen. Die humane MMN ist besonders für klinische Anwendungen relevant, da gezeigt wurde, dass vielfältige Krankheitsbilder mit einer Reduktion der MMN-Amplitude assoziiert sind. Daher ist es von besonderem Interesse, Tiermodelle zu entwickeln, mit denen die der MMN zugrunde liegenden neurophysiologischen Mechanismen genauer untersucht werden können.

Bisher wurden solche Studien mit Nagetieren allerdings weitestgehend an narkotisierten Tieren durchgeführt, und die resultierenden Ergebnisse ließen keine eindeutigen Aussagen über MMN-analoge Phänomene und deren Mechanismen zu. Dies kann vermutlich hauptsächlich den gängigen Anästhetika zugesprochen werden, die die Generierung von AEPs im Allgemeinen beeinflussen.

In der vorliegenden Arbeit wurden AEPs in wachen „Black hooded“ Ratten abgeleitet, um zu untersuchen, ob ein analoges Phänomen zur humanen MMN existiert. Die elektrophysiologische Ableitung der Potentiale erfolgte bilateral mittels epidural positionierter Elektroden vom primären auditorischen Kortex (A1) und PAF („posterior auditory field“), einem sekundären auditorischen Feld. Als akustische Stimuli wurde schmalbandig gefiltertes weißes Rauschen verwendet, das hinsichtlich Frequenz und Dauer an das Hörvermögen der Ratten angepasst wurde.

In einem klassischen “Oddball”-Paradigma aus wiederkehrenden Standard-Stimuli und selten auftretenden abweichenden Tönen ("Deviants") wurden MMN-ähnliche Antworten sowohl von A1 als auch PAF abgeleitet. Diese entsprechen in wichtigen Charakteristika den beim Menschen gefundenen Potentialen. Beispielsweise konnte gezeigt werden, dass die Amplitude der MMN-ähnlichen Potentiale erhöht war, wenn die Wahrscheinlichkeit des Auftretens des Deviants erniedrigt wurde.

Um zwischen zwei konkurrierenden Mechanismen (Adaptation versus Verletzung einer Vorhersage) zu unterscheiden, die der Generierung der MMN zugrunde liegen könnten, wurden des Weiteren mehrere Kontrollexperimente durchgeführt. In einer Bedingung in der die Präsentationswahrscheinlichkeiten von Standard-Tönen und Deviants aneinander angenähert wurden, zeigte sich kein Unterschied zwischen den Potentialen. Dieses Ergebnis zeigt, dass auch Deviant-Potentiale aufgrund der hohen Anzahl präsentierter Töne von Adaptationsmechanismen betroffen waren. Andererseits kann hier auch mit der Generierung einer Vorhersage über die folgende akustische Sequenz argumentiert werden: Die hohe Anzahl von Deviant-Tönen könnte generell keine Vorhersage zugelassen haben, so dass für beide Stimuli Vorhersagefehler generiert wurden. In einer weiteren Kontrollbedingung zeigte sich darüber hinaus, dass keine Potentiale ausgelöst werden und daher auch keine MMN-ähnliche Komponente auftritt, wenn die Deviants in einer akustischen Sequenz komplett ausgelassen werden. Ein Potential, das nur durch das Ausbleiben eines erwarteten Stimulus auftritt konnte also nicht nachgewiesen werden. Darüber hinaus wurde eine spezielle Kontrollbedingung getestet, in der die Standardtöne durch Töne verschiedener Frequenzen, die zufällig auftraten, ersetzt wurden, so dass keine Vorhersage über zukünftige auditorische Ereignisse generiert werden konnte. Dies führte zu einer Reduktion der MMN-ähnlichen Aktivität, was dafür spricht, dass ein Teil der MMN die Verletzung einer Vorhersage oder die Detektion einer Abweichung widerspiegeln könnte. Trotz der verschiedenen Kontrollbedingungen erlaubte der experimentelle Aufbau es nicht, eindeutig zwischen Adaptationsmechanismen und einer Potentialgenerierung durch die Detektion einer Abweichung in der akustischen Umwelt oder der Verletzung einer Vorhersage zu unterscheiden.

Weiterhin wurden die zugrunde liegenden Mechanismen der MMN mit Hilfe einer Gruppe von mathematischen Modellen, den „dynamic causal models“, untersucht. Die Ergebnisse der Modellierung zeigen, dass Adaptation ein wichtiger Mechanismus bei der Generierung von MMN-ähnlichen Antworten bei wachen Ratten ist.

Der zweite untersuchte Mechanismus ist synaptische Plastizität. Bezüglich dieses Mechanismus wurde postuliert, dass synaptische Plastizität die Vorhersage über die akustische Sequenz generieren und diese sowie zugehörige Vorhersagefehler über

hierarchisch angeordnete Hirnareale signalisieren soll. Die Analyse mit Hilfe der Modelle ergab auch Anhaltspunkte für eine Beteiligung von synaptischer Plastizität an der Generierung der MMN-ähnlichen Antworten.

Darüber hinaus sollte untersucht werden, ob ein bestimmter Adaptationsmechanismus, „spike frequency adaptation“, der Generierung von MMN-ähnlichen Potentialen zugrunde liegt und ob die parametrische Manipulation dieses Prozesses mit Hilfe von DCM detektiert werden kann. Dazu sollte die Aktivität von muskarinischen Azetylcholin-Rezeptoren durch die Gabe eines Agonisten (Pilocarpin) und eines Antagonisten (Scopolamin) verändert werden. Nach Ableitung MMN-ähnlicher Antworten zeigte sich, dass die Potentiale auch nach Behandlung mit den Substanzen erhalten blieben. Eine Veränderung der „spike frequency adaptation“ konnte nicht nachgewiesen werden. Obwohl die Ergebnisse der Modellierung mit Tieren, die nur mit dem Lösungsmittel behandelt wurden, die zuvor beschriebenen Resultate replizierten, konnte DCM keinen weiteren Aufschluss über den Beitrag von „spike frequency adaptation“ zur Generierung der MMN geben. Dennoch wurde gezeigt, dass cholinerge Informationsweiterleitung bei der Generierung von AEPs eine Rolle spielt. Scopolamin verstärkte die AEP-Amplitude, während Pilocarpin zu einer Abschwächung der Potentiale führte.

Die vorliegende Studie demonstriert, dass MMN-ähnliche Antworten in wachen Ratten abgeleitet werden können. Dies bildet die Voraussetzung für zukünftige Experimente, mit denen die zugrunde liegenden physiologischen Mechanismen weiter untersucht werden können. Darüber hinaus ist es wichtig, Narkose-unabhängige experimentelle Ansätze zu wählen, um zu überprüfen, ob dem Menschen analoge MMN-Mechanismen in Tieren existieren. Diese Tiermodelle könnten zukünftig dazu beitragen, therapeutische Ziele auf zellulärer Ebene aufzudecken um Krankheitsbilder zu heilen oder zu verbessern, die mit reduzierten MMN-Amplituden assoziiert sind.

2 Abstract

The detection of sudden alterations in a rapidly changing environment is crucial for the survival of humans and animals. In the human auditory system the mismatch negativity (MMN), a special component of auditory evoked potentials (AEPs), reflects the violation of predictable stimulus regularities, established by the previous auditory sequence. Given the considerable potential of the human MMN for clinical applications, i.e. several diseases are associated with decreased MMN, the development of animal models that allow for detailed investigation of the underlying neurophysiological mechanisms is necessary. Rodent studies were so far almost exclusively conducted under anesthesia and have not provided decisive evidence whether an MMN analogue exists in rats. This may be due to several factors, most importantly, however, the effect of anesthesia.

In the present thesis, epidural recordings in awake black hooded rats were conducted to investigate whether an analogue to human MMN exists in rats. AEPs to bandpass-filtered noise stimuli that were optimized in frequency and duration were recorded bilaterally from two auditory cortical areas. Using a classical oddball paradigm with frequency deviants, mismatch responses were detected in primary (A1) and secondary auditory cortex, namely the posterior auditory field (PAF). Those responses share key properties with the human MMN, *i.e.* large amplitude biphasic differences that increased in amplitude with decreasing deviant probability.

For distinguishing between adaptation and other mechanisms that may explain MMN-like phenomena like deviance detection or prediction error signaling, several control conditions were conducted. Converging probability of deviant and standard stimuli for example led to a disappearance of the overall difference between both potentials. This may be due to adaptation affecting also deviant potentials due to the high number of stimuli presented. On the other hand, arguing with prediction error signaling, the presented sequence may not have allowed the brain to establish a prediction about the upcoming sequence in general thus generating prediction errors for both stimuli. The complete omission of deviant sounds in an otherwise homogenous sequence did not lead to evoked activity. Furthermore, in a control condition that removed the predictive

context while controlling for the presentation rate of deviants MMN-like activity diminished. This finding may suggest that mismatch responses are even partly generated by deviance detection or prediction error signaling. However, the chosen experimental design does not allow for disambiguating precisely the overall contribution of adaptation and other mechanisms that may explain MMN generation to the observed responses.

In addition, a modeling approach was conducted using dynamic causal modeling (DCM) in order to differentiate between the above mentioned mechanisms. The results suggest that adaptation is a key factor for the generation of mismatch responses in awake rats. DCM also revealed evidence for a second mechanism, namely synaptic plasticity. Synaptic plasticity was suggested as underlying mechanism responsible for establishing a prediction about upcoming stimuli by learning the standards and signaling this and related prediction errors across hierarchically organized brain areas.

In order to investigate whether spike frequency adaptation underlies MMN generation, a pharmacological alteration of this mechanism via the manipulation of muscarinic acetylcholine receptors was intended, accompanied by the detection of the resulting changes with DCM. Therefore, an agonist (pilocarpine) and antagonist (scopolamine) of the muscarinic receptor were applied. Mismatch responses were preserved after the injection of muscarinic drugs while a change of spike frequency adaptation was not observed. Although results from vehicle treated animals resemble previous modeling results, DCM could not further contribute to the assessment of the impact of spike frequency adaptation to the generation of MMN-like potentials. However, it has been shown that cholinergic signaling is involved in the generation of AEPs elicited with an oddball paradigm in awake rats. Scopolamine was shown to enhance the overall potential waveform whereas pilocarpine led to a reduction of AEPs.

This study demonstrates that robust MMN-like responses can be obtained in awake and unrestrained rats and therefore provides a basis for future experimental investigations of the mechanisms that underlie MMN generation. Establishing anesthesia-independent settings for probing rodent analogues to human MMN are important for facilitating the detection of therapeutic targets at the cellular level. Knowledge of these targets may

guide the development of drugs for treating disorders that have been shown to be accompanied by reduced MMN responses.

Index of contents

3 Introduction

The main focus of this thesis is the Mismatch Negativity (MMN), a special component of event-related brain responses, elicited by any irregular auditory event occurring in an otherwise homogenous sequence of acoustic stimuli (Näätänen *et al.*, 1978). The MMN can be evoked reasonably easy without a subject paying attention or reacting to the acoustic stimulation. This allows for its detection even in freely moving animals without combining the electrophysiological recording with a behavioral task. Although the MMN is considered a very basic mechanism, it is related to higher order auditory processing or even to the first step of a pre-attentive processing chain gating an acoustic stimulus to consciousness.

Beyond its attractiveness for a basic understanding of sensory processing, the MMN has gained a lot of interest since it is impaired in numerous diseases like schizophrenia (Shelley *et al.*, 1999; Näätänen, 2003; Umbricht & Krljes, 2005), dyslexia (Baldeweg *et al.*, 1999), Parkinson (Pekkonen *et al.*, 1995b) and Alzheimer's disease (Pekkonen *et al.*, 1994). For this reason, the MMN has great translational potential for clinical neuroscience. Deeper understanding of its generation could reveal therapeutic targets at the cellular level for ameliorating or treating the disorders that are accompanied by reduced MMN responses. In addition to human experiments, this requires invasive recordings in corresponding animal models and pharmacological perturbations. However, for making appropriate use of animal data, it has to be established first under which conditions mismatch responses can be obtained that are comparable to human MMN.

For this purpose, we set up a telemetric system for recording auditory evoked potentials (AEPs) in the awake and unrestrained rat. Recording in the awake state is crucial for unambiguous interpretation of AEPs because it has been shown that response properties of auditory neurons change under anesthesia (Zurita *et al.*, 1994; Cheung *et al.*, 2001; Gaese & Ostwald, 2001) along with morphology, latency and amplitude of mismatch responses (Nakamura *et al.*, 2011).

Beyond the aim of investigating mismatch responses rats in general, these potentials were used with the objective to validate a new class of mathematical models, namely Dynamic

causal models (DCM). This part of the project was elaborated in cooperation with the group of Prof. Klaas Enno Stephan (Translational Neuromodeling Unit (TNU), Institute for Biomedical Engineering, University of Zurich & ETH Zurich). The experimental approach was based on a parametric modulation of muscarinic signaling in the auditory cortex by the use of two drugs that have opposite effects on the muscarinic acetylcholine receptor. In particular, we ask whether manipulations of the muscarinic receptor can be detected with DCM and, if successful, these models should be used for distinguishing between two opposing theories explaining MMN generation.

3.1 The mammalian auditory system

Sound perception per se requires a highly complex system that is similarly structured in all mammals. The sound travels through the air as a mechanical wave and is effectively captured by the pinna (or auricle). This structure acts like a funnel and focuses the sound wave into the external auditory meatus, which ends at the tympanum (*membrana tympani*), a thin diaphragm that separates the external ear from the middle ear. The middle ear, an air-filled cavity, contains three tiny bones, the auditory ossicles named malleus, incus and stapes. A sound wave reaching the tympanum leads to vibrations of the membrane, which sets the auditory ossicles in motion. Through this chain of moving ossicles, the sound pressure is transmitted from air to the subsequent fluid-filled compartment, the inner ear. The inner ear is sealed by the “oval window” (*fenestra ovalis*), a diaphragm, which is directly connected to the footplate of the stapes. When the stapes deflects the membrane of the oval window, pressure changes of the fluid in the inner ear are produced. Part of the inner ear is the cochlea, which is the central organ for transducing mechanical into electrical energy. The cochlea consists of three compartments, which are fluid-filled tubes, arranged on top of each other and coiled around a bony core. The scala vestibuli and the scala tympani are filled with perilymph and communicate through the helicotrema, an interruption of the cochlear duct at the cochlear apex. Between those structures the scala media is located. This tube is separated from the other ducts by the basilar membrane and the Reissner’s membrane, respectively. The scala media is filled with endolymph that provides a specialized ionic environment for

the mechano-transducing membranes of the sensory hair cells (Ashmore, 2008). The transmitted sound wave leads to fluctuating pressure differences between the scala vestibuli and the scala tympani resulting in an up and down movement of the basilar membrane. Along the full length of the basilar membrane, the organ of Corti is located, an innervated sensory epithelium (Figure 1 a), which is the actual "site of mechano-electrical transduction" (Hudspeth, 2000). The human organ of Corti contains about 14,500 hair cells (Ashmore, 2008) which are coupled to the overlying tectorial membrane. Differential movement of the basilar and tectorial membrane leads to lateral shearing movements of the hair cell stereocilia, which opens mechano-transducer channels followed by a K^+ inward current (Vollrath et al., 2007). In the mammalian auditory system two classes of hair cells have to be distinguished: the inner and the outer hair cells. The inner hair cell receptor potential triggers the release of the neurotransmitter glutamate (Glowatzki & Fuchs, 2002). Inner hair cells are innervated by dendrites of the cochlear spiral ganglion where the first action potentials occur. The outer hair cells, on the contrary, have less pronounced afferent innervation but exhibit a large amount of efferent innervation (Ashmore, 2008). They are non-sensory supporting cells that are thought to mediate the fine-tuning of frequency selectivity by mechanical feedback amplification (Dallos & Corey, 1991).

A special building principle of the auditory system that is expressed for the first time in the cochlea but continues through various auditory structures to the cortex is tonotopy. Auditory nerve fibers are most sensitive to one frequency called the "best frequency" of a neuron whereas sound frequencies that are close to each other are processed by neighboring neuronal fibers. In the cochlea, the tonotopic principle is expressed in terms of low frequency sounds excite hair cells at the apex of the cochlea whereas high frequency sounds excite cells at the base of the cochlea (Figure 1 b). Information about the frequency of the sound can be gained through its position in the tonotopic map ("place code") or the rate of action potentials ("frequency code"), respectively (Hudspeth, 2000).

3.1.1 Central auditory processing

After mechano-electrical transduction the signals are processed over several stations starting at the eighth cranial nerve that is formed by the axons of cochlear spiral ganglion neurons. At this stage, the first action potentials are generated and from that point on the initial mechanical energy is exclusively transmitted electrically to the cortex. The first central processing step takes place at the cochlear nucleus (CN) complex (Figure 1 c) that is located laterally and superficially in the pons (Malmierca & Hackett, 2010). This nucleus consists of three major components, the dorsal cochlear nucleus (DCN) and the anteroventral (AVCN) and posteroventral cochlear nuclei (PVCN) (Rose *et al.*, 1959). Each of the three subnuclei is tonotopically organized. The auditory nerve enters the brainstem and subsequently branches into three pathways whereas each fiber bundle targets one of the three subnuclei. Some of the various cell types located in the CN are known to optimize the timing information that has been obtained in the cochlea.

From the three subnuclei of the CN three parallel pathways ascend: The dorsal acoustic stria arises from the dorsal cochlear nucleus whereas the intermediate acoustic stria has its source in the posterior part of the PVCN (Strominger, 1973). Both pathways target the inferior colliculus (IC) via the contralateral nucleus of the lateral lemniscus. The third and most prominent fiber bundle, the ventral acoustic stria or trapezoid body arises from the AVCN and the anterior portion of the PVCN. It targets the superior olivary complex (SOC) in the brainstem bilaterally. At the SOC, which consists of the lateral (LSO) and medial superior olive (MSO) as well as the nucleus of the trapezoid body, the first binaural information processing occurs. Interaural time differences for localizing sound in the horizontal axis are processed in the MSO. This structure is interpreted as a coincidence detector for binaural excitatory input because neurons are excited by inputs from both ears reaching the neuron synchronously (Colburn *et al.*, 1990). The LSO receives excitatory input from the ipsilateral AVCN. The fibers from the contralateral AVCN, however, pass another relay station in the ipsilateral medial nucleus of the trapezoid body (MNTB) (for review see Tollin, 2003) and target the LSO with inhibitory projections. The LSO is also involved in localizing a sound source in the horizontal axis but employs bilateral intensity cues instead of interaural time differences. Moreover, from the LSO descending efferent

fibers arise, which innervate the inner hair cells of the cochlea, whereas the MSO sends innervating fibers to the outer hair cells (Warr & Guinan, 1979).

The fibers ascending from the SOC form the tract of the lateral lemniscus that carries information to the IC. In addition, cell assemblies or nuclei, namely the nuclei of the lateral lemniscus, are embedded in the fibers of the lateral lemniscus. The dorsal nucleus of the lateral lemniscus receives bilateral input from the AVCN whereas the ventral nucleus of the lateral lemniscus is targeted by fibers ascending from the dorsal and ventral division of the contralateral CN (Moore, 1991). The neurons of the ventral nucleus of the lateral lemniscus encode temporal events with a very high resolution (Covey & Casseday, 1991) whereas the dorsal nucleus of the lateral lemniscus plays an important role in binaural processing, *i.e.* sound localization (Malmierca & Hackett, 2010).

The subsequent relay station, the IC, receives input from the dorsal and intermediate acoustic stria as well as direct, monosynaptic projections from the SOC and projections from different nuclei of the lateral lemniscus. The majority of auditory pathways that diverge from lower auditory centers converge on the IC but there are also a few ascending projections that circumvent this structure and project directly to the medial geniculate body (MGB) or areas of the forebrain. The IC comprises a central nucleus surrounded by shell regions. From the core region of the IC the so called “lemniscal pathway” or “core projection” arises, which crosses the ventral nucleus of the MGB and targets the core region of the primary auditory cortex (A1). In this pathway the tonotopic organization is exactly preserved. In addition, there is a parallel pathway arising from the shell or cortex regions of the IC. This “non-lemniscal pathway” or “belt projection” exhibits no clear tonotopic organization and targets the belt regions of the auditory cortex via the dorsal division of the MGB (for review see Hu, 2003).

The MGB of the thalamus is the last subcortical auditory structure to be passed before auditory information reaches the cortex. It is divided into three parts, the ventral, dorsal and medial division (Morest, 1964). The majority of neurons in the ventral nucleus of the MGB (MGv) show low threshold and short latency responses to tones and complex sounds. They are tuned to one best frequency and are also sensitive to interaural time and intensity differences (Malmierca & Hackett, 2010). This structure is part of the lemniscal

auditory pathway and targets – as described above – the A1 (Romanski & LeDoux, 1993). The dorsal part of the medial geniculate body (MGd) is a key structure of the non-lemniscal pathway and exhibits fewer cells than the ventral division. It has no laminar structure, no tonotopic organization, shows rapid habituation to repeated stimuli and the frequency tuning of the neurons is broader in general (Bordi & LeDoux, 1994). Extensive axonal tracing studies conducted in rats show that non-lemniscal structures of the auditory thalamus (MGd and posterior intralaminar nucleus) send efferent fiber bundles to several limbic structures like the amygdala, insular cortex and striatum (Deschenes *et al.*, 1998). The medial nucleus of the medial geniculate body (MGm) targets core as well as belt regions of the auditory cortex and receives input from auditory and non-auditory structures (Malmierca & Hackett, 2010). Auditory inputs are arising from the IC (excitatory and inhibitory), the thalamic reticular nucleus (reciprocal inhibitory inputs) and the auditory cortex (strong reciprocal inputs). Non-auditory inputs terminating on the medial nucleus are not as well defined but are thought to comprise afferents from deep layers of the superior colliculus and polysensory regions like the midbrain tegmentum (Winer & Morest, 1983).

The last structure in the auditory pathway that is essential for the perception of sounds is the auditory cortex. It exhibits the same organization principle in all mammalian species: a central core region with a precise tonotopic alignment is surrounded by several “belt” areas. The number of regions comprising the core differs across species, whereas it consists of A1 and up to two other tonotopically organized areas (Malmierca & Hackett, 2010). The core auditory cortex exhibits a six-layered structure with at least eight classes of pyramidal and non-pyramidal neurons. Layer I comprises the fewest cells with 90 % being small GABAergic neurons. Layer II contains pyramidal and non-pyramidal neurons whereas pyramidal cells are mostly glutamatergic and concentrate in layer III and V. The latter are the main targets of fibers connecting both hemispheres (Malmierca & Hackett, 2010). Areas dedicated to the processing of the same or neighboring frequencies are most strongly linked by callosal fibers (Wallace & Harper, 1997). Layer III and IV are targeted by ascending projections from the MGv (Winer, 1985). Descending projections targeting the

MGm and IC originate from the most superficial layer V and VI (Malmierca & Hackett, 2010).

The belt region of the auditory cortex receives a more diffuse input and exhibits less or no tonotopic organization. In every mammalian species, the number of belt areas exceeds the number of core areas. Those areas have widespread connections to areas outside the auditory cortex, for example the prefrontal cortex (Romanski *et al.*, 1999) and are thought to be involved in higher order processing (Howard *et al.*, 2000).

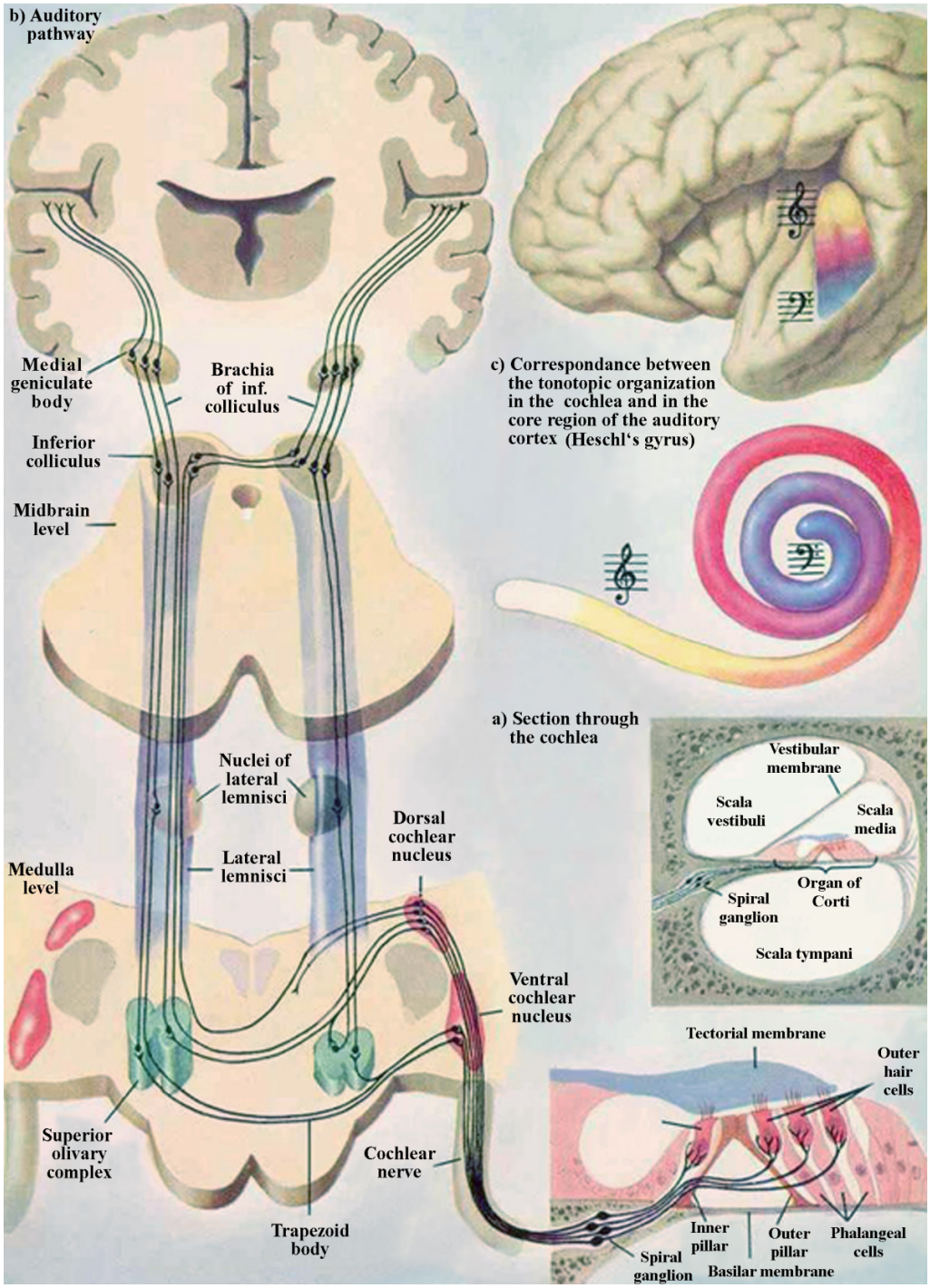

Figure 1: The human auditory pathway. a) Section through the cochlea showing the organ of Corti and the three fluid-filled compartments. b) Electrical signals generated by hair cells in the cochlea are transferred in the form of action potentials to the dorsal and ventral cochlear nuclei, which project to the lateral lemniscus. After further relays, the neuronal fiber bundles target the medial geniculate bodies of the thalamus, which send projections to the primary auditory cortex. c) Color-coded correspondence between the frequency representation in the cochlea and the auditory cortex. Modified after Mulroney & Myers (2009).

Comparison between the rat and human auditory system

Although the central auditory processing is similar in all mammals, small differences can be found in several stages of the auditory pathway. The most obvious discrepancy between the rat and human auditory pathway is the large difference in size and the lissencephalic nature of the rat brain compared to the gyrencephalic human auditory cortex. Central auditory conduction time, *i.e.* the time for an afferent volley to travel through the auditory pathway, is lower in rats (6.6 ms) compared to humans (12 ms) (Shaw, 1990; 1995), reflecting the shorter fiber lengths in rats. In contrast to humans, rats are able to perceive very high frequency sounds. Rats can detect carrier frequencies between 0.39 and 72 kHz whereas human hearing ranges from 0.03 to 19 kHz at 60 dB SPL (West (1985). First of all, this difference is due to variations in the length of the basilar membrane and the number of spiral turns of the cochlea. While the overall audible range of octaves is positively correlated with the number of turns of the cochlea (2 ¾ in humans vs. 2 ¼ in the laboratory rat) the upper and lower limits of hearing are related to the length of the basilar membrane (33.5-35 mm in humans vs. 9.7 mm in rats; West (1985)).

Besides differences present in the cochlea, several other discrepancies can be observed. In contrast to the VCN, the DCN exhibits variations among species with respect to the lamination of the structure: it is only laminated in rodents and carnivores (for review see Malmierca, 2003). Anatomical differences relating to the SOC are thought to reflect differences in the hearing range of humans and rats. The three main nuclei (LSO, MSO and MNTB) can always be identified, but the MSO has been shown to be small in the rat while it is well developed in cats and humans. Since the MSO responds mainly to low frequency sounds and solely to a narrow range of high frequencies, this finding is in line with the ability of the human auditory system to process low frequencies, whereas the auditory system of rats is specialized in high frequency processing. On the other hand, the LSO and MNTB are well developed in rats and cats, while they are diminutive in humans (for review see Malmierca, 2003). Furthermore, rodents exhibit a fourth nucleus additionally to the three main SOC nuclei named the superior paraolivary nucleus (Osen *et al.*, 1984). With respect to the nuclei of the lateral lemniscus, there have been distinctions proposed by

several authors based upon cytoarchitectonic studies of different species (as summarized by Malmierca *et al.*, 1998). However, the subdivision into DNLL and VNLL is in line with the presence of two functionally separated systems (Malmierca & Hackett, 2010). In the IC the distinction into the three main nuclei (central nucleus, dorsal shell, lateral shell) persists but the absolute dimension differs. For example, the low frequency representation of the central nucleus is contracted in rats compared to cats whereas the lateral shell region is expanded in rats (Loftus *et al.*, 2008). In the last subcortical station of the auditory pathway, the MGB, a large concordance in between species exists. However, there seem to be large interspecies differences regarding the total number of GABAergic neurons in the MGv with ranges varying from < 1 % in bats and rats compared to 25 % or more in cats and monkeys (Winer & Larue, 1996).

The largest interspecies differences can be seen in the auditory cortex. Mice and rats exhibit 5 to 6 auditory areas whereas the primate auditory cortex is thought to comprise 10 to 12 different areas (Malmierca & Hackett, 2010). Differences include not only the number of auditory areas but also their alignment, cell density and connections. The human auditory cortex is located in the superior portion of the temporal lobe including parts of the supratemporal plane and supratemporal gyrus. Core areas of the auditory cortex are situated on Heschl's gyrus also known as the transverse temporal gyrus buried within the lateral sulcus of the temporal lobe. Brodmann's area 41 designates the primary auditory cortex whereas area 42 refers to the secondary auditory cortex (Brodmann, 1909) (Figure 2). The auditory cortex of the rat is located in the temporal cortex on the lateral surface of the brain and is therefore reasonably easy to access experimentally. The temporal cortex of the rat comprises three areas TE1, TE2 and TE3 from which only TE1 is tonotopically organized. It contains the core region of the auditory cortex that is subdivided into an anterior auditory field (AAF), A1 and a posterior auditory field (PAF) (Polley *et al.*, 2007; Pandya *et al.*, 2008). A1 exhibits a precise tonotopic pattern with high frequencies represented in the anterior part and low frequencies in the posterior part. From A1 to both AAF and PAF, a reversal of the tonotopic frequency organization exists at the border of each area (Doron *et al.*, 2002). In addition to the direction of the frequency representation, auditory areas differ with regard to single neuron properties. Intracortical

recordings have shown that the cells located in AAF or PAF exhibit longer latencies than neurons in A1 (Simpson & Knight, 1993a; Doron *et al.*, 2002), suggesting these areas to be involved in higher order processing (Simpson & Knight, 1993a). The entire area TE1 receives input from the MGv of the thalamus (Scheel, 1988; Romanski & LeDoux, 1993). TE2 and TE3 consist of the belt regions of the rat's auditory cortex. Those areas are targeted by afferent fibers from non-tonotopic parts of the MGB and also polymodal input from other thalamic and cortical non-auditory modalities (Shi & Cassell, 1997).

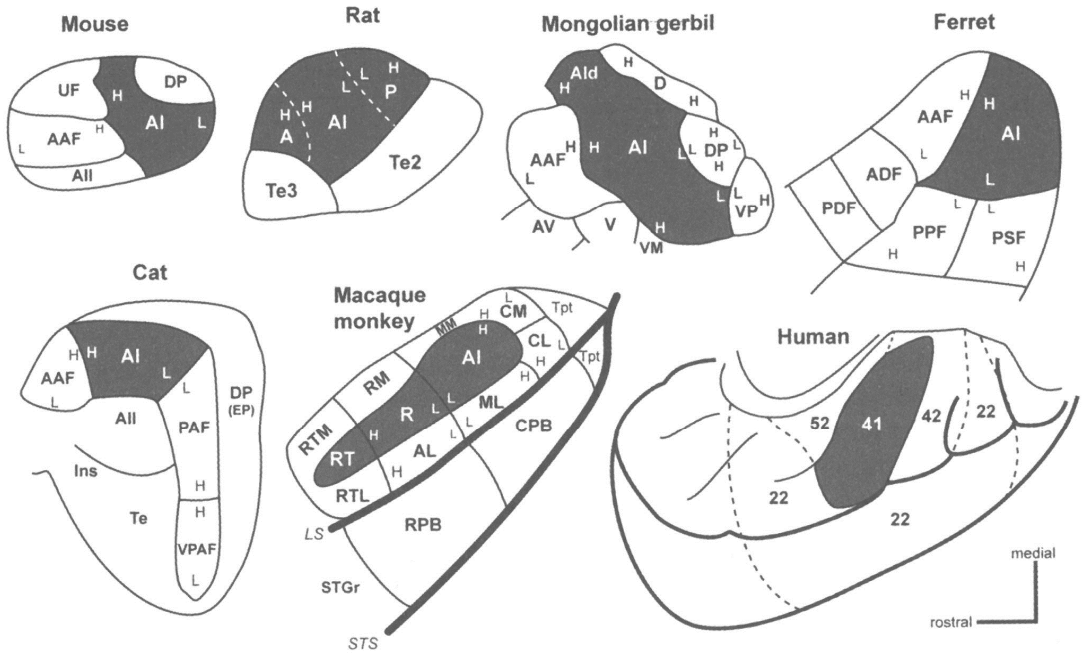

Figure 2: Comparison of auditory areas in several mammalian species. Core areas are displayed in black whereas belt areas are uncolored. Tonotopic gradients are denoted with H for the high frequency representation and L for the low frequency representation. A = anterior area (referred to as AAF in the main text throughout this thesis); A1 = primary auditory area; AAF = anterior auditory field; AV = anterior ventral area, CL = caudolateral area; CM = caudomedial area; D = dorsal area; DC = dorsocaudal area; DCB = dorsocaudal belt area; DP = dorsal posterior area; DRB = dorsorostral belt area; PAF = posterior auditory field; VPAF = ventral posterior auditory field; Ins = insula; MM = middle medial area; P = posterior area (referred to as PAF in the main text throughout this thesis); PDF = posterior dorsal field; R = rostral area; RM = rostromedial area; RT = rostrotemporal area; RTL = rostrotemporal lateral area; RTM = rostrotemporal medial area; Te = temporal area; V = ventral area; VCB = ventrocaudal belt area; VM = ventral medial area; VRB = ventrorostral belt area. Numbers denote Brodmann's areas. From Malmierca & Hackett (2010).

Despite the above-mentioned differences, it can be concluded that the gross anatomy and physiology of hearing in humans and rats is comparable. Therefore, rats can be used as model organisms for studying auditory processing in order to gain information that can be translated to human subjects in the future.

3.2 Electroencephalography

In the present study, electrical activity was recorded by the use of electrodes placed above the rat's auditory cortex. The recording of electrical brain activity from the scalp surface is referred to as electroencephalography (EEG). The first recording was made in 1924 by the German neurologist Hans Berger (Berger, 1929). Later on, this method became one of the widely used techniques for studying brain activity. Although this technique was developed nearly 90 years ago, the relationship between activity of single neurons in the brain and the surface recorded voltage shifts is not completely understood until today. It is well-established that the recorded activity is related mostly to cortical but- to a lesser degree- also to subcortical auditory processing. However, solely cortical structures contributing to the surface recorded electrical fields are well investigated whereas subcortical structures that influence the rhythm of the EEG remain poorly understood (Zschocke, 2012).

For the interpretation of EEG-recordings it is necessary to examine the cellular processes leading to electrical brain activity more closely. Therefore, these processes are elucidated in the following.

3.2.1 Cellular processes

The voltage measured at the head surface is generated by any active cellular processes in brain tissue. Every transmembrane current contributes to the generation of extracellular electrical fields and consequently to the surface recorded voltage. The relative contribution to the overall voltage, however, depends on whether the membrane is a spine, dendrite, soma, axon or axon terminal (Buzsaki *et al.*, 2012). Action potentials (APs), for example, produce transmembrane currents of large amplitudes at the soma of a

neuron. However, until recently, APs were thought to contribute only very little to the EEG because they cause charge displacements lasting only for 1-2 ms (Zschocke, 2012). Nonetheless, synchronized action potentials from many neurons can contribute to the electrical extracellular field (Buzsaki *et al.*, 2012) because ionic processes are able to superimpose and summate at a given time and location. Indeed, the most important source of the EEG under physiological conditions is the synapse. Action potentials arriving at the synapse cause a release of neurotransmitter from the presynaptic terminal. At the postsynaptic membrane, binding of the transmitter to its receptor leads to either a long lasting depolarization, the excitatory postsynaptic potential (EPSP), or to a hyperpolarization, the inhibitory postsynaptic potential (IPSP) depending on the type of neurotransmitter that is released. Postsynaptic potentials exhibit a slower time constant than APs (10-100 ms) and consequently superimpose more effectively (Zschocke, 2012). Crucial for the relative contribution of a single postsynaptic potential to the entire recordable field is the orientation of neurons from which potential fields emanate. Pyramidal cells that are located perpendicular to the cortical surface constitute the main source of the EEG because they form open dipoles (Eccles, 1951). Hence, it is important to note that in the cortex, only one third of cells exhibit this configuration (Zschocke, 2012).

Electric dipoles arise through excitatory or inhibitory inputs to pyramidal neurons. EPSPs are generated mostly at the apical dendrites and are mediated through AMPA (α-amino-3-hydroxy-5-methyl-4-isoxazolepropionic-acid) or NMDA (n-methyl-d-aspartic-acid) receptors. Their activation leads to synaptic Na^+ or Ca^{2+} influx. On the outside of the membrane, a current "sink" emerges that has to be compensated. As a consequence, current flows from the non-excited part of the soma and the basal dendrites that constitute the current "source" to the apical dendrites.

IPSPs are mediated through GABA (γ-aminobutyric acid) receptors (subtype A), which are located mainly at the soma of pyramidal neurons and are conveyed by Cl^--ions. Those potentials were thought to contribute only little to the extracellular field because the Cl^- equilibrium potential is very close to the resting membrane potential thus resulting only in a marginal charge displacement. In spiking neurons, however, the membrane is depolarized and shifted away from the Cl^--equilibrium potential. In this situation,

inhibitory currents can provide substantial contributions to the extracellular electrical field (Buzsaki *et al.*, 2012). Depending on the distance between current source and sink an open dipole field emerges. Pyramidal neurons that are synchronously activated, give rise to large dendritic summation potentials that cause charge displacements at the cortical surface (Figure 3).

Apart from APs and postsynaptic potentials, gap junctions, also named "electrical synapses", are able to influence the EEG indirectly. They can modify the EEG due to direct electrical coupling between neurons. Moreover, glial cells, which exceed the number of neurons 5 times, are important (Zschocke, 2012). Astrocytes support neurons mechanically but sustain also the extracellular K^+ concentration. On the one hand this protects the neurons from a functional failure due to high K^+ concentration, on the other it leads to a depolarization of the glial cell due to higher intracellular levels of K^+. Since glial cells themselves are connected via gap junctions, this can result in locally restricted glial cell depolarization.

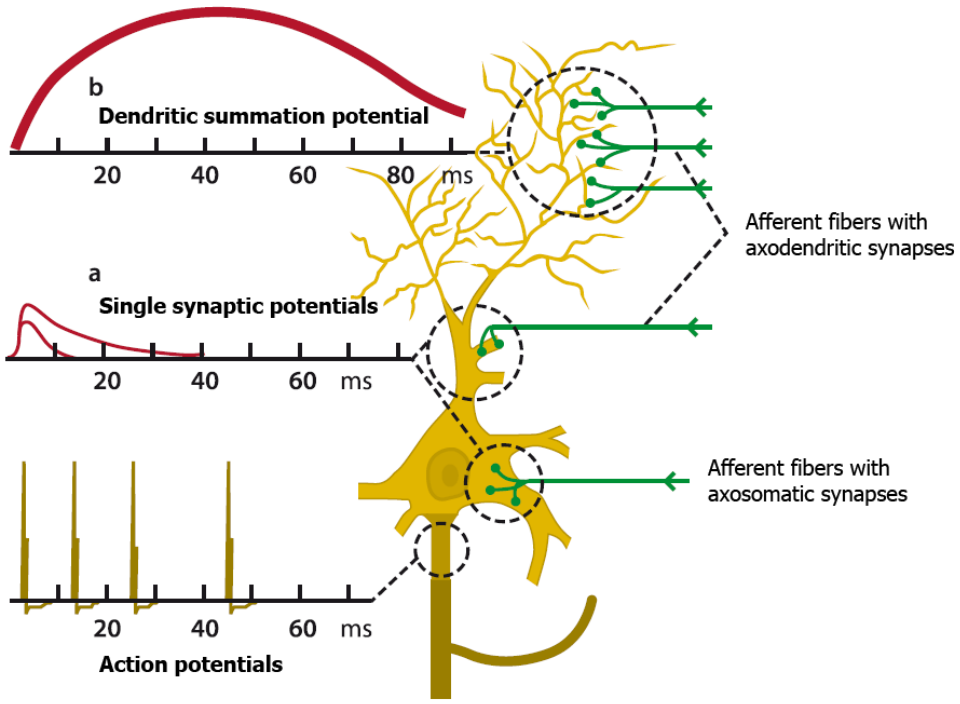

Figure 3: Schematic drawing of a cortical pyramidal cell with an illustration of its synaptic contacts. Synapses from afferent fibers reach either the soma or the dendritic tree. On the left side the relative contributions of summation of single synaptic potentials are depicted (a). The dendritic potential is the sum of the postsynaptic potentials at the strongly branched dendrites of the neuron (b). Modified after Zschocke (2012).

3.2.2 Rhythmic activity of the EEG

A characteristic feature of neuronal networks that contributes substantially to the detectable electrical field and is present in several brain regions like the hippocampus, thalamus and neocortex, is oscillatory activity (Buzsaki & Draguhn, 2004). In animal experiments, isolated or deafferented cortical areas show brief bursts of activity but oscillating activity patterns are absent (Creutzfeldt & Struck, 1962). This finding clearly demonstrates that oscillatory activity is not spontaneously generated but driven by subcortical structures like the thalamus. The thalamus is the most important subcortical structure influencing the EEG and is itself modulated by inputs from the *Formatio reticularis*, a diffuse network of nuclei in the brainstem. Two functionally distinct systems arise from the *Formatio reticularis*: the first originates from the midbrain reticular

formation, whilst the second has its source at the medullar reticular formation. The former controls wakefulness and modifies the overall activation level of the brain by the projection of afferent cholinergic neurons via muscarinic and nicotinic acetylcholine receptors (Curro Dossi *et al.*, 1991). This fiber system is also named the ascending activating reticular system. The latter tract with its respective source at the medullar reticular formation is responsible for inducing and maintaining sleep (Moruzzi & Magoun, 1949).

Overall, network oscillations exhibit six different main frequencies (delta, theta, alpha, gamma, beta, mu) with characteristic spatial distributions that are associated also with different mental states (*e.g.* sleep stages, waking). Gamma activity, for example, was shown to be enhanced by sensory input (Adrian, 1942). In addition, it seems as if synchronous brain activity has also a functional role in "binding" the regionally distributed output of several sensory processing streams together to form one perceptual object (for review see Singer & Gray, 1995).

3.2.3 Auditory evoked potentials in humans

Besides background EEG, specific voltage changes elicited by sensory, perceptual or cognitive stimuli can be recorded. These characteristic potentials are named event-related potentials (ERPs). Due to their lower amplitude compared to the background EEG, ERPs can only be obtained by averaging the electrical activity that is time-locked to a series of stimuli. Any component or background activity that is not temporally related to the stimulation averages to zero. Today, event-related potentials are used for diagnosing neurologic or psychiatric diseases like schizophrenia (McCarley *et al.*, 1991), dementia (Brown *et al.*, 1982), depression (Sumich *et al.*, 2006) and Alzheimer's disease (Chapman *et al.*, 2007), because they can be applied non-invasively, exhibit a high temporal resolution and directly reflect brain activity. In this thesis the emphasis is on a subgroup of event-related responses namely the auditory evoked potentials (AEPs).

Human AEPs are subdivided into fast, middle and long latency potentials and reflect the various steps of information processing throughout the auditory system. The recordable waveforms exhibit positive and negative deflections that are named "peaks", "waves" or

"components". Early potentials are referred to as brainstem or fast auditory evoked potentials (FAEPs) and emerge until 10 ms after stimulus presentation. In this class of potentials, each peak is thought to reflect sequential activation of relay nuclei from the cochlea to the CN, SOC, and the IC of the midbrain (Stone *et al.*, 2009). In general, FAEPs consist of seven components (Picton *et al.*, 1974; Grundy *et al.*, 1982) which are named with Roman numerals to indicate their order of occurrence. FAEPs are little susceptible to sleep (Campbell & Bartoli, 1986) or anesthesia (Grundy *et al.*, 1982) and are therefore widely used in sleeping newborns or sedated children to assess hearing thresholds and the integrity of the auditory pathway. Middle and long latency evoked potential peaks are labeled with "P" or "N" indicating their polarity at the head surface (vertex) (Davis *et al.*, 1966). Middle latency auditory evoked potentials (MAEPs) exhibit largest amplitudes when recorded at the vertex and arise about 10 to 50 ms after stimulus onset. MAEPs are generated in the ascending auditory pathway and partially even in the auditory cortex (McEvoy *et al.*, 1994; Pekkonen *et al.*, 1995a). In contrast to FAEPs, particularly the late middle latency components are modulated by sleep and sedation, *e.g.* can be dose-dependently depressed by volatile anesthetics (Schwender *et al.*, 1996).

This thesis focuses on long latency or slow auditory evoked potentials (SAEPs) that arise approximately 50 to 300 ms after the onset of an acoustic stimulus (Figure 5) and are generated in or near the auditory cortex (Picton *et al.*, 1999). An auditory stimulus enhances the specific information flow from the thalamus to the cortex. In other words, the activity of afferent fibers arising from the MGv is increased. Those fibers target mostly pyramidal neurons in cortical layers III and IV of the core auditory cortex. In addition, inhibitory interneurons contact the soma of pyramidal cells and some neurons decrease the activity of neighboring cells via intracortical connections each time they are excited (lateral inhibition). After acoustic stimulation, all these processes contribute directly to the surface recorded SAEPs. However, sensory stimuli activate also non-specific thalamo-cortical afferent fibers that lead to summation of EPSPs in superficial cortical layers. EPSPs arriving at the apical dendrites of neurons close to the cortical surface result in a pronounced negativity ("N-peak") at the cortical surface. This applies also for IPSPs generated at the soma of a pyramidal neuron far from the cortical surface (Figure 4).

Therefore, it is not possible to directly relate inhibitory or excitatory activity to positive or negative peaks in AEPs. Furthermore, it has to be born in mind that peak polarity is also dependent on the position of the reference electrode.

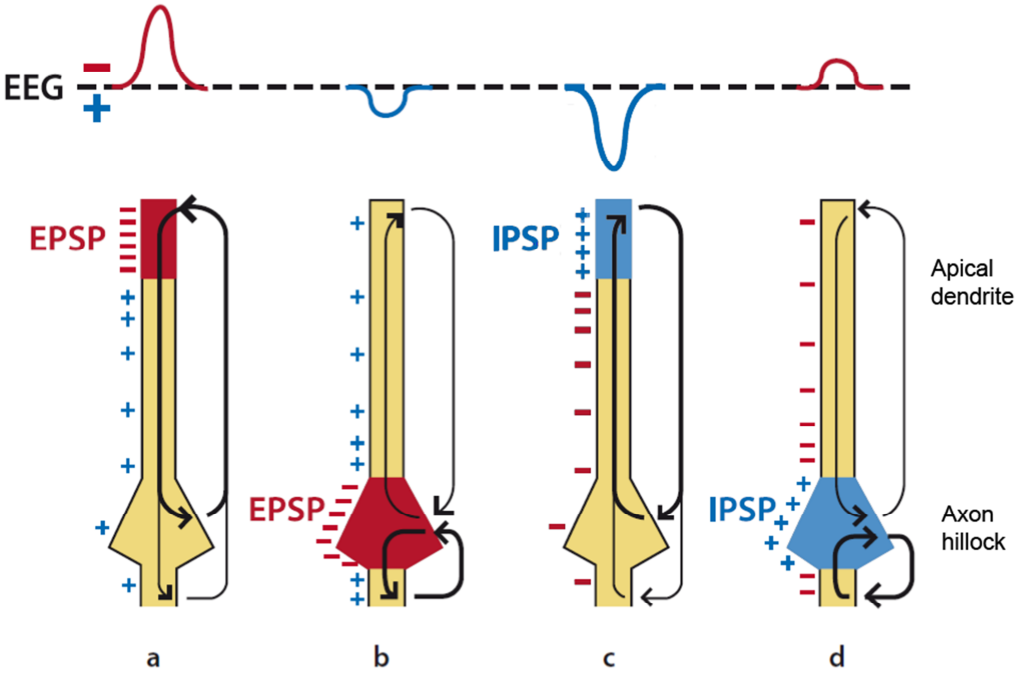

Figure 4: Schematic drawing of extracellular fields and the resulting EEG voltage generated by cortical pyramidal neurons. a) EPSP at the apical dendrite results in a negative voltage shift in the EEG; b) EPSP at the soma results in a positive voltage shift in the EEG; c) IPSP at the apical dendrite of a neuron result in a positive voltage deflection; d) IPSP at the soma of a cell results in a positive voltage shift in the EEG. Modified after Zschocke (2012).

SAEPs that are recorded at the human vertex (Figure 5) consist of three characteristic peaks: P1 (around 50 ms), N1 (around 100 ms) and P2 (around 180 ms) (Picton *et al.*, 1999). Intracortical recordings have shown that a major source of the P1 peak is located in the lateral portion of Heschl's gyrus, 7-15 mm from the insular plane (Liegeois-Chauvel *et al.*, 1994). This peak is followed by the N1 peak that consists of several components that overlap temporally (McCallum & Curry, 1980). Early EEG and magnetencephalography (MEG) studies argue for a source of the N1 in or slightly posterior to A1 (Hari *et al.*, 1980), while more recent studies using intracortical recordings (Liegeois-Chauvel *et al.*, 1994) or MEG (Lütkenhoner & Steinsträter, 1998) detected activity in the supratemporal plane,

more precisely the planum temporale (secondary auditory cortex). The latter is at the extreme posterior pole of the supratemporal gyrus and overlaps with parts of Wernickes area. In addition, frontal and parietal generators were suggested (Giard *et al.*, 1994). The N1-peak is thought to reflect conscious detection of acoustic stimuli in the environment (Hyde, 1997) and there might be also one source responsible for the switch of attention towards the sound (Alcaini *et al.*, 1994). However, the source of the N1 peak seems to vary with the frequency of a presented stimulus (Verkindt *et al.*, 1995) and the amplitude is strongly dependent upon the loudness of a stimulus as well as the interstimulus interval of the presented sounds (Davis *et al.*, 1966). The subsequent wave, P2 emerges mainly together with the N1 peak but is generated by a different process because both peaks can be dissociated experimentally, developmentally (Ponton *et al.*, 2000), topographically (Vaughan *et al.*, 1980) and also within lesion studies (Knight *et al.*, 1988). It is not generated in the temporal cortex but may reflect activation of the mesencephalic reticular activating system.

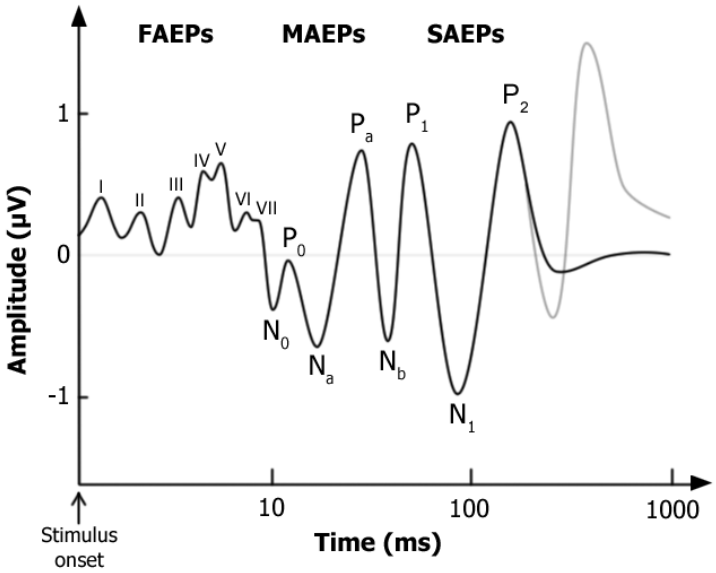

Figure 5: Human auditory evoked potentials. The black curve displays fast auditory evoked potentials (FAEPs), middle latency evoked potentials (MAEPs) and slow evoked potentials (SAEPs). The grey curve shows components that are elicited only with special stimulation protocols. The time scale is displayed logarithmically. Modified after Picton *et al.* (1974).

3.2.4 Auditory evoked potentials in rats

In rats, potentials are mostly recorded from the vertex and potential classes are divided analog to human AEPs into three different classes (FAEP, MAEP, SAEP). Compared to humans, however, AEPs in rats emerge with shorter latencies due to the smaller size of the auditory pathway and consequently shorter conduction times. BAEPs, for example, exhibit latencies from 1.5 to 4 ms (Edwards *et al.*, 1983) and consist of solely four principle components (Shaw, 1988). As in humans, the BAEP is the most invariant and stable waveform. The first peak is generated in the auditory nerve. In humans it is thought that one peak is generated by the peripheral and one peak by the central partition of the nerve (Moller *et al.*, 1981) leading to two BAEP components generated at the auditory nerve in humans versus one in rats. The longer distance of the human pathway may be the reason for a larger overall number of BAEP components. Latencies of the subsequent waves II, III and IV in rats seem to relate to activity recorded from depth electrodes inserted in or near the CN, the SOC and IC, respectively (Shaw, 1988).

Vertex recorded MAEPs (latency: 17-38 ms; Knight *et al.* (1985)) and SAEPs (latency: 50-130 ms; Knight *et al.* (1985)) in rats are generated by nonspecific auditory input from the extralemniscal pathway. These potentials are known to be very susceptible to levels of arousal (Knight *et al.*, 1985) and muscarine receptor modulation (Campbell *et al.*, 1995). In rats, activity of the primary auditory cortex seems not to contribute to the responses detectable at the vertex (Knight *et al.*, 1985). Potentials generated inside the primary auditory cortex can be recorded only at a very small area on the lateral surface of the cortex (Barth & Di, 1990; Simpson & Knight, 1993a). In order to distinguish AEPs detected as near-field potentials from the auditory cortex from vertex-recorded AEPs, they are named cortical auditory evoked potentials (CAEPs).

CAEPs recorded with an electrode array in several layers of the temporal cortex of anesthetized rats consist of a fast positive-negative deflection followed by a slower positive-negative wave (Barth & Di, 1990) (Figure 6). P1 emerges approximately 15-20 ms after stimulus onset and - if the response complex is taken to be excitatory- (see 3.2.3 and Figure 4) reflects the depolarization of supragranular pyramidal neurons in layer I, II and III

due to afferent input from the MGv. The subsequent N1 peak has a latency of 25-30 ms and can be recorded in an area twice the size of the P1 area. It is likely to mirror depolarization of apical dendrites in infragranular layers and/ or hyperpolarization at the soma. Electrical activity might also be mediated by axon collaterals from neurons located in supragranular layers. Overall, N1 and P1 are more confined to one area than the later potential components. Thus, it has been proposed that P1 and N1 are generated by stimulus-specific thalamo-cortical inputs while later components are generated by non-specific thalamo-cortical inputs and cortico-cortical connections (Hall & Borbely, 1970; Shaw, 1988).

P2 has a latency of 50-60 ms and emerges from two distinct processes: repolarization of the neurons that were excited during P1 and N1 generation and depolarization resulting from the thalamo-cortical input arising from the MGm, whereas activities from supra- and infragranular neurons overlap. The following component N2 exhibits latencies between 100 and 175 ms and is generated by active inhibition in supra-and infragranular layers together with a depolarization from afferent fibers of the MGm.

The results summarized above derive mostly from one study in which potentials were recorded from ketamine-xylazine anesthetized rats (Barth & Di, 1990). This drug appeared to have little effect on the AEP waveform.

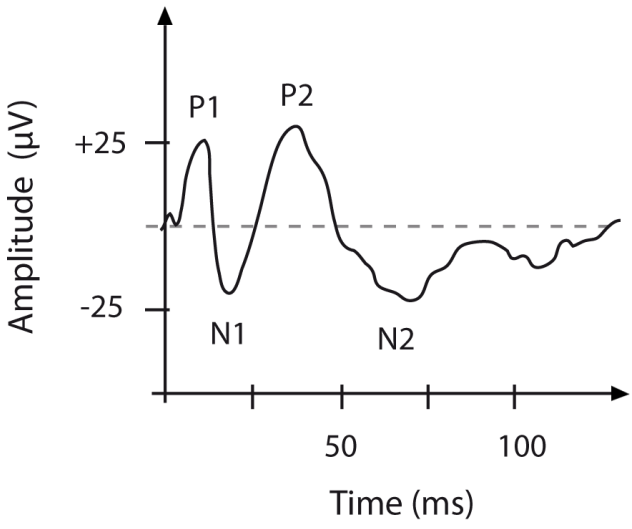

Figure 6: Click evoked CAEPs in the rat. CAEPs were recorded epidurally from the contralateral auditory cortex during waking (modified after Hall & Borbely (1970)). The potentials consist of a fast positive-negative deflection (P1/N1-complex) that is followed by a slower positive-negative deflection (P2/N2-complex).

3.3 Mismatch negativity

The mismatch negativity (MMN), which is the main focus of this thesis, is a special component of SAEP. It is a neural correlate, reflecting an automatic detection mechanism of novel or deviating auditory information. The detection of differing sensory information amongst frequent, familiar input and environmental background noise is crucial for the survival of humans and animals. Attention can be focused only on a few parameters at the same time, but gradually scanning the environment would be highly inefficient. As a consequence, there needs to be a way to gate important and behaviorally relevant sensory information to consciousness in a rapid "bottom-up" manner whereas irrelevant information has to be filtered out (Jääskelainen *et al.*, 2004).

3.3.1 MMN in humans

The MMN is characterized by a more negative response to sudden changes in a previously homogenous auditory sequence. It peaks at about 100 to 200 ms after stimulus onset (Näätänen, 1990) depending on the type of violation (frequency[1], intensity, duration, inter-stimulus interval) that is encountered and on the magnitude of deviance (Tiitinen *et al.*, 1994). The MMN is often followed by a special potential component, the P3a that is considered to be related to the involuntary switch of attention towards the deviant sound (Escera *et al.*, 1998; Schröger & Wolff, 1998).

Experimentally, the MMN is elicited during a so called "oddball paradigm", a sequence of frequent "standard" stimuli et al., 2006) in which low probability "deviant" sounds are interspersed. The traditional experimental design that is used to evoke MMN with a frequency mismatch is a "flip-flop" design in which the frequencies of standard and deviant stimuli are swapped in two consecutive sessions. In order to control for effects of carrier frequency, MMN is defined as the difference between the averages (across sessions) of the standard-evoked and the deviant-evoked potentials (Figure 7). The MMN

[1] Throughout this thesis, the term "frequency" is referring to the acoustic carrier frequency or tone pitch of an acoustic stimulus. The frequency of stimulus presentation will be termed "rate" hereafter, whereas the frequency of a certain stimulus within a sound sequence will be designated by "probability"

is procedurally defined as the difference between deviant- and standard-AEPs whereby standard and deviant stimuli can differ in a number of dimensions like, for example, frequency (Sams *et al.*, 1985b), intensity (Näätänen *et al.*, 1978; Näätänen *et al.*, 1989a) or duration (Näätänen *et al.*, 1989b). In addition, it has been shown that a lower probability of deviant occurrence leads to an increased in MMN amplitude (Näätänen, 1992 ; Imada *et al.*, 1993; Javitt *et al.*, 1998; Shelley *et al.*, 1999; Sato *et al.*, 2000; Sabri & Campbell, 2001; Sonnadara *et al.*, 2006).

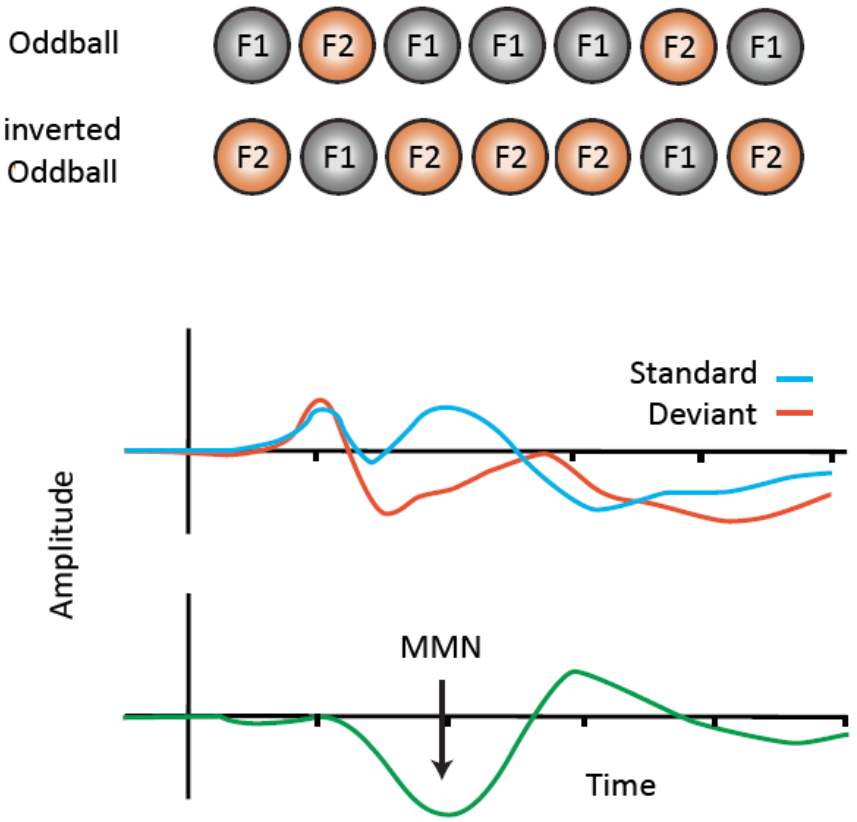

Figure 7: "Flip-flop" design of an oddball paradigm. A low and a high frequency stimulus are presented in two consecutive trials whereby each frequency is presented once as standard and once as deviant stimulus. Below, the electrical response to the acoustic stimulation recorded with EEG is shown. The blue waveform represents the averaged evoked potential to both frequencies used as standard stimulus and the red waveform the averaged evoked potential to both stimuli used as deviant. The averaged deviant potential is subtracted from the averaged standard potential to obtain the MMN (green curve). Adapted from Moore (2003).

The human MMN is not only elicited by deviations from regular stimulus trains, but by any violation of established expectancies or predictions, including abstract rules. A MMN has been elicited with a sound sequence that followed the rule “the higher the frequency the louder the acoustic stimulus”, when this rule was violated by sounds of either high-frequency tones and low intensity or low-frequency tones and high intensity (Paavilainen *et al.*, 2001). In addition, also an ascending tone pair in a sequence of descending tone pairs did evoke an MMN (Saarinen *et al.*, 1992; Carral *et al.*, 2005) and also to linguistic differences (Obleser *et al.*, 2006).

3.3.2 Loci of human MMN generation

It has been demonstrated with dipole analyses of the magnetic counterpart of MMN (recorded with magnetencephalography) (Sams *et al.*, 1985a; Sams & Hari, 1991) and also with dipole analyses of electrical recordings (Sams *et al.*, 1985b; Giard *et al.*, 1990; Scherg & Berg, 1991) that the neuronal source of the MMN is located within the supra-temporal plane in or near A1. Direct evidence for a neuronal source inside the auditory cortex was obtained by intracranial recordings during brain surgery (Halgren *et al.*, 1995; Kropotov *et al.*, 1995). The maximal EEG amplitude of the MMN (about 5 μV), however, is detected in fronto-central scalp electrodes (Sams *et al.*, 1985b; Alho *et al.*, 1986; Näätänen & Picton, 1987) because the electrical components generated on the superior planes of both temporal lobes summate at fronto-central areas (Vaughan & Ritter, 1970). In addition, there is experimental evidence that a prefrontal generator is also involved. Temporal MMN components have been shown to diminish together with frontal components in patients with prefrontal lesions (Alho *et al.*, 1994; Alain *et al.*, 1998).

Notably, several studies (Paavilainen *et al.*, 1991; Molholm *et al.*, 2005) found slightly different MMN sources depending on the type of violation that is encountered (frequency, intensity, duration). Hence, all these sources were consistent with generators in the auditory cortex. These findings indicate that the MMN not only signals that a change was detected but also the nature of the change.

3.3.3 Theories explaining MMN generation

With respect to MMN generation a variety of mechanisms have been proposed and theories have been constantly updated after new experimental evidence was gained. Early work of Näätänen and his colleagues (Näätänen *et al.*, 1989a) suggests that the MMN is an error signal that is generated when an incoming auditory stimulus does not match the "memory trace", that has been formed during previous acoustic stimulation. The time period in which the memory trace is active is called "echoic memory", a special form of auditory memory, which has been shown to last approximately 10 s (Böttcher-Gandor & Ullsperger, 1992; Sams *et al.*, 1993b) after stimulus presentation. As cellular basis, a release from tonic inhibition was suggested, whereas the selective release involves only neurons that are specialized to physical attributes of stimuli that are currently not presented (Javitt *et al.*, 1996). The presentation of deviant stimuli results in a larger response because it is generated by a neuronal population that was previously released from inhibition (Javitt *et al.*, 1996). A critical point in this theory, however, is that this mechanism can only explain the very basic forms of MMN, while complex responses like for example MMN to the violation to linguistic differences have to be processed differently.

In agreement with this theory, later on, the "model adjustment hypothesis" has been postulated. It states that the MMN is generated by a fronto-temporal network whenever a break of regularity in an auditory sequence occurs. The MMN is thought to reflect online adjustment of a perceptual model that is reformed when an auditory input violates its predictions (Winkler *et al.*, 1996; Näätänen & Winkler, 1999; Sussman & Winkler, 2001). Furthermore, it has been claimed that the MMN is generated by two different processes that have also different neuronal sources. The temporal source of the MMN is thought to reflect a process that is related to sensory memory. The frontal generator, on the contrary, could represent a cognitive component or comparator based mechanism (Giard *et al.*, 1990) that causes an involuntary attention switch (Näätänen & Michie, 1979; Escera *et al.*, 1998). Therefore, the MMN might be one part of a pre-attentive processing chain that allows the switch of the attentional focus to sudden changes in the auditory environment (Näätänen, 1990).

However, an opposing theory referred to as the "adaptation hypothesis" (Jääskelainen *et al.*, 2004) states that the MMN can be explained by stimulus-specific adaptation (SSA) of neurons in A1 only. Authors hypothesize that the MMN is not distinct from the N1-peak but results from a delayed and diminished N1 to repeated standard presentation, and a larger peak with shorter latency evoked by the deviant. The deviant-evoked potential is thought to be generated by neuronal elements, which are not adapted. Therefore, the characteristic MMN waveform results from the calculation of the difference of an adapted and a non-adapted component of the N1 response. Whether the MMN and the N1 derive from different neuronal sources is a matter of debate. Several MEG studies have shown that the source of the MMN is located 7-10 mm anterior to that of the N1 (Hari *et al.*, 1992; Tiitinen *et al.*, 1993; Korzyukov *et al.*, 1999) and intracranial recordings found differences in peak topographies with the MMN originating slightly more anterior (Halgren *et al.*, 1995). On the contrary, Jääskelainen *et al.* (2004) argue that there are two distinct auditory cortex sources that contribute to the N1 response: an early posterior N1 at 85 ms and an additional neuronal population that is activated later (at about 150 ms) which is located more anterior and closely matches the source of the MMN (Sams *et al.*, 1993a). Authors interpret the posterior N1 as reflecting a pre-attentive gating mechanism that determines to what extent an acoustic stimulus enters consciousness, whereas the process that underlies the anterior N1 might be an analysis of the physical stimulus features. Earlier studies supporting the opposing "memory trace hypothesis" have shown that repetition of standards constitutes a prerequisite for MMN elicitation. However, Jääskelainen *et al.* (2004) elicited a robust MMN with deviant sounds that were preceded by only one "standard" tone.

There are several experimental findings that argue against the "adaptation hypothesis" (for review see Näätänen *et al.*, 2005). Tervaniemi *et al.* (1994) observed for example that a tone repetition in a sequence of steadily descending tones elicits an MMN even though there is no tone repetition of "standards" that could cause adaptation. Deviants of reduced sound intensity can cause an MMN as well Näätänen *et al.* (1989a) and this cannot be explained by SSA alone. The MMN can also be evoked without elicitation of any

N1 component as it was shown in a study of Yabe *et al.* (1997) who omitted stimuli in an otherwise homogenous sequence.

In any case, from the experimental evidence and attempts to model the observed responses, it seems likely that both proposed mechanisms play a role in MMN generation (Garrido *et al.*, 2008; Garrido *et al.*, 2009b). Recently, the two competing theories have been combined in a unified explanation of MMN. This is a predictive coding framework in which the MMN reflects the prediction error dependent updating of a hierarchical model that infers on the causes of sensory stimuli and predicts future events (Friston, 2005; Baldeweg *et al.*, 2006). In this theory of MMN generation, model adjustment corresponds to prediction error dependent synaptic plasticity of inter-regional connections and adaptation serves to balance the postsynaptic sensitivity to top-down predictions and bottom-up stimulus information, respectively (Garrido *et al.*, 2008; Garrido *et al.*, 2009b).

3.3.4 Control conditions

If frequent standards are compared to rare deviants only, as it is done in “flip-flop” designs, differences between the potentials caused by deviance detection cannot be distinguished from differences caused by unequal presentation rates of standard and deviant stimuli. Several control conditions have been proposed to overcome this problem. An early control is the “deviant alone” condition (Sams *et al.*, 1985a) in which standards are replaced by silence and deviants are presented with the same randomly changing interstimulus interval as in the oddball experiment. In the “deviant alone” condition there is no regularity to break by the deviant but the presentation rate of deviants from the oddball paradigm is preserved. However, this control neglects the fact that neuronal responses are strongly dependent on the overall presentation rate of stimuli, meaning that the "deviant alone" condition mixes the effect of stimulation duty cycle with the effect of the rarity of the deviant.

The “deviant within many standards” that was initially designed by Jacobsen & Schröger (2001) controls for effects of the presentation rate of deviants and has been convincingly applied in human experiments. Here, the overall presentation rate of deviants is the same as in the oddball condition but standards are replaced by a number of acoustic stimuli

with different frequencies. Each stimulus is presented randomly with the same probability, so that no regularity is present. The term “deviant within many standards” might be unclear because each stimulus is presented with the same probability and in random order so that no stimulus functions as deviant or standard. Therefore, the term “equiprobable control condition” (Astikainen *et al.*, 2011) will be used throughout this thesis.

In order to identify neuronal mechanisms of MMN generation, not only human but also animal studies are necessary. Animal studies allow for a number of invasive interventions like, for example, pharmacological perturbations and intracranial or intracortical recording, providing valuable physiological information that can be translated to human studies. In the following, animal studies that have been published so far are reviewed.

3.3.5 MMN in animals

As described above, the human MMN is a scalp-recorded phenomenon that summates over several cortical areas. Therefore, intracortically recorded phenomena like multi-unit activity or single-neuron responses can never be referred to as MMN even though both phenomena might share key properties (Nelken & Ulanovsky, 2007). Epidural potentials, which are recorded with electrodes placed directly onto the *dura mater*, detect more spatially confined sources than scalp-electrodes (Destexhe *et al.*, 1999). The cortical volume, in which electrical activity can be detected with epidural electrodes, is about 3 mm (Freeman *et al.*, 2003). However, it is conceivable that true MMN-like phenomena can be detected at this spatial scale (Nelken & Ulanovsky, 2007).

In several non-human species, differential waveforms (“deviant minus standard” averaged potential) have been reported using epidural recordings. These waveforms share key features with the human MMN but may be of different polarity and/or latency. In order to distinguish those from their human counterpart they are referred to as “MMN-like” or “mismatch responses”. MMN-like activity in cats has been reported in several studies (Csépe *et al.*, 1987; Csépe, 1995; Pincze *et al.*, 2001; Pincze *et al.*, 2002). Csépe *et al.* (1987) and Csépe (1995) argue that they have found an analogue of human MMN in primary, secondary and association cortices of the cat with shorter latency than human

MMN, that was detectable during wakefulness and slow wave sleep. The difference waveform reached its maximum amplitude at about 50 ms after stimulus onset above the auditory cortex. However, a clear limitation of this study is that no “flip flop”-design was applied (*cf.* 3.3.1) and there may be frequency specific effects mimicking mismatch responses. Pincze *et al.* (2001) detected MMN-like potentials in awake cats with chronically implanted epidural electrodes. The potentials originated from the rostroventral part of secondary auditory area and were well separated from the generation loci of the obligatory peaks N1 and P2. In a later study, it was also demonstrated that cat MMN-like potentials were sensitive to interstimulus interval and deviant probability, a finding that mirrors results from human MMN studies (Pincze *et al.*, 2002).

In the macaque monkey, MMN-like activity to soft and loud click sounds was recorded epidurally from the cortex (Javitt *et al.*, 1992). In this study, differences between standard and deviant potential were maximal at the frontal recording site. This is in line with human MMN studies whereas the latency of MMN-like activity was somewhat shorter in macaque monkeys (maximal amplitude at about 80 ms). The authors state that the latency of the monkeys’ mismatch response is intermediate between that of cat (30-70 ms, Csépe *et al.* (1987)) and human MMN (100-200 ms, Näätänen (1990)) under analogous circumstances. This finding conforms also with the size and complexity of the monkey brain relative to that of cat and human. In a recent study (Fishman & Steinschneider, 2012) using awake macaque monkeys, however, deviant potentials were enlarged compared to standard potentials with respect to “obligatory” potential components. The emergence of new or additional features in deviant elicited potentials that has been shown in human subjects could not be demonstrated. In addition, oddball deviant responses were comparable to deviants presented in the equiprobable control condition. From the experimental findings with electrodes recording from A1, the authors interpret the differential responses between standard and deviant potential as derived from adaptation rather than deviance detection.

However, MMN-like potentials were reported in ketamine-xylazine guinea pigs (Kraus *et al.*, 1994b) but were only detectable in non-primary auditory areas (non-primary thalamus, *i.e.* caudomedial MGB and surface recorded at the midline of the cortex).

Umbricht *et al.* (2005) detected "deviance-related" activity to frequency and duration mismatch in mice but the authors interpret only results from duration mismatch experiments as "MMN-like". In the frequency mismatch condition, they detected only enhancement of obligatory peaks in deviant potentials but also "qualitative" changes in the duration mismatch.

Today, there are several studies attempting to detect MMN-like potentials in rats. The results are inconsistent regarding the polarity or time course of the detected potentials. This discrepancy across studies may be due to several factors, including differences in recording sites, stimulus properties, experimental design, especially the use of different control conditions and anesthesia. MMN-like potentials were observed under pentobarbital-sodium (Tikhonravov *et al.*, 2008; Tikhonravov *et al.*, 2010) and urethane anesthesia (Ruusuvirta *et al.*, 1998; Astikainen *et al.*, 2006). Tikhonravov et al. (2008; 2010) defined MMN-like responses by comparing deviant potentials elicited in the oddball condition to deviants elicited in the "deviant alone" control. However, Lazar & Metherate (2003) did not find MMN-like responses under similar conditions. Roger *et al.* (2009) reported mismatch responses in awake and freely moving rats for the first time in a duration mismatch paradigm. True mismatch responses have been demonstrated using the "equiprobable" control condition (*cf.* 3.3.4) in awake (Nakamura *et al.*, 2011) and anesthetized rats (Nakamura *et al.*, 2011; Astikainen *et al.*, 2011).

To date there is only one animal study reporting MMN-like potentials to violations of abstract rules. Ruusuvirta *et al.* (2007) detected mismatch responses in urethane-anesthetized rats whenever the deviant and standard stimuli were physically the same but deviants differed from standards with respect to the melodic ordering (ascending or descending) of a tone pair.

Although some animal studies used speech sounds as acoustic stimuli (rat: Eriksson & Villa (2005), Ahmed *et al.* (2011); guinea pig: Kraus *et al.* (1994a)), these studies are not

discussed in detail at this point, because results are very difficult to interpret and not comparable to other animals studies discussed in this thesis. In addition, there are studies showing MMN-like potentials recorded from the hippocampus of rabbits (Ruusuvirta *et al.*, 2010). Since those studies are also not comparable to our experiments, they will not be presented.

In this section, epidurally recorded MMN-phenomena in animals have been reviewed. Although intracortically recorded activity to oddball stimulation has to be distinguished from the surface recorded MMN (see above), multiunit and single-neuron responses have substantially contributed to the understanding of MMN generation. Therefore, these studies are listed and discussed in detail below.

3.3.6 Intracortical responses to oddball stimulation in animals

The first animal studies demonstrating intracortical responses to oddball stimulation were performed by Javitt and his colleagues (1992; 1994). Recordings with multichannel electrodes inserted into A1 of the awake macaque monkey showed a distinct contribution of this area to scalp-recorded MMN-like activity and a larger response to soft as well as loud deviants (Javitt *et al.*, 1994). The initial thalamo-cortical activation was similar for standard and deviant stimuli, but MMN-like activity was associated with increased activation of pyramidal cells within supragranular laminae. Surprisingly, intracortical correlates of MMN were found as early as 15 ms after stimulus onset while surface recorded mismatch responses commence not earlier than 60 ms (Javitt *et al.*, 1992).

In A1 of halothane-anesthetized cats, Ulanovsky *et al.* (2003) recorded single-neuron responses to an acoustic oddball stimulation and found a reduced response to the same or a similar stimulus when it was repeatedly presented. The initial response amplitude was restored by the presentation of a deviant sound. These results potentially reflect a single neuron correlate of MMN namely stimulus specific adaptation (SSA). A strength of this study is the application of the equiprobable control condition (*cf.* 3.3.4). Neuronal responses to the deviants in the oddball condition were significantly larger than to deviants presented in a random background of stimuli (equiprobable control condition). The findings argue against activity-dependent adaptation in terms of “fatigue” of the

neurons because this process can never be stimulus-specific. However, the authors suggest a contribution of mechanisms operating at the inputs to the neuron like synaptic depression or stimulus-specific inhibition. In a later review Nelken & Ulanovsky (2007) state that the discovered mechanism is a “single-neuron habituation” rather than SSA because the decline in neuronal response is not use-dependent (refractoriness, changes in ion concentrations leading to less excitability).

Later on, the existence of this mechanism has also been verified in the A1 of awake rats (von der Behrens *et al.*, 2009; Farley *et al.*, 2010). Whether SSA alone can account for the surface recorded MMN is a matter of debate. It has been argued that SSA is a non-trivial mechanism and can explain the findings in human experiments (Ulanovsky *et al.*, 2004). Moreover, experimental evidence revealed several similarities between MMN and SSA. The magnitude of MMN as well as SSA increases with decreasing deviant probability and with increasing difference between standard and deviant. Additionally, the latency of both phenomena decreases with increasing difference. On the contrary, it has been shown experimentally that the MMN diminishes after pharmacological treatment with NMDA-receptor antagonists (*cf.* 3.3.8) whereas SSA is left intact in a rat model (Farley *et al.*, 2010). Modeling attempts also show a mechanism contributing to MMN-like potentials that is distinct from SSA (Taaseh *et al.*, 2011).

After all, animal studies found evidence for intracortical correlates of the surface recorded MMN. However, the relative contribution of the cellular mechanisms that have been discussed (synaptic depression, inhibition, refractoriness) has not been clarified conclusively. Further information was gained from pharmacological perturbations suppressing or disrupting MMN-like phenomena.

3.3.7 The neuropharmacology of MMN and MMN-like potentials

The MMN is significantly attenuated by NMDA receptor antagonists in humans (Umbricht *et al.*, 2000; Kreitschmann-Andermahr *et al.*, 2001) and macaque monkeys (Javitt *et al.*, 1996) suggesting an important role of these receptors for MMN generation. This finding is in line with the above-mentioned rat study that found no alteration of SSA after application of an NMDA-receptor antagonist (Farley *et al.*, 2010).

Nevertheless, studies modulating the activity of dopamine receptors are not as consistent. Parkinson's patients that exhibit an overall reduced dopamine level show lower MMN amplitudes (Pekkonen *et al.*, 1995b) as well as healthy subjects treated with haloperidol, a D2-receptor antagonist (Kähkönen *et al.*, 2001). While one study failed to replicate these results, but observed a shorter MMN latency after haloperidol treatment (Pekkonen *et al.*, 2002), another study did not find any effect of dopamine agonists (D1- and D2-receptor) on the MMN (Leung *et al.*, 2007).

Modulations of serotonin levels in the brain or direct manipulations of serotonin receptors resulted also in ambiguous findings. One study demonstrated a reduction in MMN amplitude and latency after acute depletion of the serotonin precursor tryptophan (Kähkönen *et al.*, 2005). In another study, tryptophan depletion did not modulate the MMN (Leung *et al.*, 2010), Likewise, the $5HT_2A$-receptor agonist psilocybin did not alter the MMN but was shown to induce cognitive deficits (Umbricht *et al.*, 2003).

There are also two studies investigating the effect of $GABA_A$-receptor manipulation with benzodiazepines on MMN. Both studies consistently show a reduction of MMN after benzodiazepine treatment (Nakagome *et al.*, 1998; Rosburg *et al.*, 2004).

The modulation of nicotinic acetylcholine receptors certainly alters the MMN. Treatment with nicotine or nicotinic agonists, for example, enhanced MMN amplitudes (Engeland *et al.*, 2002; Baldeweg *et al.*, 2006; Dunbar *et al.*, 2007) and shortened its latency (Inami *et al.*, 2005; Dunbar *et al.*, 2007). The effect of muscarinic acetylcholine receptor modulation on the MMN, however, is not well investigated and yet no conclusive results exist. In one study (Pekkonen, 2001), the amplitude of the magnetic MMN to frequency changes was attenuated by the application of the muscarinic antagonist scopolamine whereas the MMN to duration mismatch was not affected. A later study, however, did not report an effect of scopolamine on the electric and magnetic MMN (Pekkonen *et al.*, 2005).

3.3.8 Pharmacological treatment

One theory of MMN generation referred to as the "adaptation hypothesis" states that the difference wave can be explained by local adaptation of neurons in A1 to the repeated

presentation of the standard stimulus. Pharmacologically, spike frequency adaptation, *i.e.* the decrease in response rate after repeated activation, is influenced particularly through muscarinic acetylcholine receptors. It is regulated by slow afterhyperpolarizing potassium currents that are calcium and voltage independent (Benda & Herz, 2003). These currents cause a prolonged hyperpolarization of the neuron and thereby reduce the rate with which action potentials can be generated (Faber & Sah, 2003). Activation of muscarinic receptors reduce the afterhyperpolarizing potassium currents through a cGMP-dependent second messenger mechanism eliciting a shift towards higher EEG frequencies (Liljenstrom & Hasselmo, 1995). Muscarinic-dependent oscillations in vivo have been described in the gamma range in auditory cortex (Metherate *et al.*, 1992) and visual cortex (Rodriguez *et al.*, 2004), as well as in the theta range in the hippocampus (Rowntree & Bland, 1986; Golebiewski *et al.*, 2002). Selective antagonists of muscarinic receptors increase adaptation, while conversely, agonists reduce adaptation, resulting in opposite effects (for review see Hasselmo, 1995).

For our study we chose the two naturally occurring alkaloids scopolamine and pilocarpine to manipulate the state of the muscarinic receptor. Pilocarpine is a non-specific agonist of the muscarinic receptor and can be obtained from the leaflets of South American shrubs of the genus *Pilocarpus*. It was first isolated in 1875; thereafter the actions of pilocarpine on the sweat and salivary glands were described. It has a predominant effect on the muscarinic acetylcholine receptor and no or very little nicotinic activity (Brown & Taylor, 2005). Scopolamine on the contrary is a non-specific antagonist of the muscarinic receptor and stems, like atropine, from belladonna (Solanaceae) plants. It is found mainly in *Hyoscyamus niger* and was previously smoked in India to treat asthma. There, British colonists observed this form of therapy and introduced belladonna alkaloids to western medicine early in the 1800 (Brown & Taylor, 2005). In general, antagonists prevent the effects of ACh by blocking its binding to the muscarinic receptor on smooth muscles, cardiac muscles and gland cells, but also in peripheral ganglia and the CNS.

In the present thesis the effects of muscarinic receptor modulation on mismatch responses in awake rats were investigated. Moreover, it was attempted to detect the

induced alterations using dynamic causal modeling. As mentioned above, this part of the project was done in cooperation with the group of Prof. Klaas Enno Stephan.

3.4 Dynamic causal modeling

Dynamic causal modeling (DCM) was originally developed for analyzing the effective connectivity of brain areas with fMRI data (Friston *et al.*, 2003) but later on adapted also for the analysis of ERPs measured with EEG (David *et al.*, 2006). The aim of DCM is to infer the effective or causal connectivity of coupled dynamical systems, *i.e.* it is used to investigate how the activity of one neuronal population influences the activity of a second population under specific experimental perturbations. In practice, this is done by comparing different models of competing theories explaining the generation of neural activity within a network of interconnected sources. In this study, specifically DCMs for ERPs were used. Those models are predicated on the assumption that ERPs are generated by temporal dynamics of a network of several sources and that these temporal dynamics can be described by differential equations. In addition, each source is assumed to project to the sensors (electrodes) following physical laws.

A single source model is based on a simplified neurophysiological model of a cortical column. It rests upon the neural mass model that was first developed by Jansen & Rit (1995). This model generates the average postsynaptic membrane potentials from the firing rates of three neuronal subpopulations (pyramidal cells, spiny stellate cells and inhibitory interneurons) which are arranged in a layered structure and interconnected with intrinsic connections. With several of the described cortical elements, a neurobiological plausible model of hierarchically interconnected neuronal sources can be build. The connectivity rules which are applied for these (extrinisic) cortico-cortical connections are based on a partitioning of the cortex in infragranular, supragranular and granular layer 4, which was established in experimental studies of the visual cortex in monkeys (Felleman & Van Essen, 1991). It has to be noted, however, that applying these models to networks in the auditory cortex is a simplification, because connectivity differences between visual and auditory cortices exist (Smith & Populin, 2001). Based on the study of Felleman & Van Essen (1991) three types of direct connections are classified

as either a) forward connections that originate in agranular layers and terminate in layer 4, b) backward connections that connect agranular layers or c) lateral connections that originate in agranular layers and target all layers (David *et al.*, 2005). These connections are always excitatory and encompass the axonal processes of pyramidal cells (David *et al.*, 2006).

An important factor making DCM unique compared to other ERP reconstruction techniques, are prior constraints that are applied to the parameters of the model. Priors are used to specify how regions are interconnected, which regions are targeted by subcortical structures and which cortico-cortical connections change with the experimental perturbations (David *et al.*, 2006). The priors thereby specify how a specific stimulus is allowed to change the synaptic coupling strength among sources (synaptic plasticity) and the postsynaptic gain (local adaptation). These values build a prior distribution of the parameters and are subsequently combined with recorded data via a likelihood distribution that results in a posterior distribution according to Bayes' rule. (David *et al.*, 2006). As a consequence, the variance of each parameter reflects the uncertainty about the parameter itself after observing the data. The uncertainty about a particular model, however, is addressed with Bayesian model comparison based on an approximation to the model evidence (Penny *et al.*, 2004). The model evidence can be seen as a trade-off between the complexity of a model and the goodness of its fit to the data.

It has been demonstrated previously that DCM is suitable for inferring on synaptic mechanisms underlying the generation of EEG data recorded from A1 and PAF in isoflurane-anesthetized rats (Moran *et al.*, 2011) or awake mice with recordings from the hippocampus and amygdala (Moran *et al.*, 2009) by fitting DCM to macroscopic electrophysiological data.

3.4.1 Dynamic causal modeling of mismatch responses

In the present thesis, DCM was used to investigate mechanisms underlying MMN generation. As summarized above (*cf.* 3.3.1), the theories explaining MMN generation can be mainly divided into two parties: the most widespread theory states that the MMN is

generated by a temporo-frontal network whenever an auditory stimulus does not match a memory trace which was established during previous acoustic input (for review see Näätänen *et al.*, 2005). An update of this theory was formulated as the "model adjustment hypothesis" (Winkler *et al.*, 1996). However, there are also studies explaining the MMN by a much simpler mechanism, namely adaptation (Jääskelainen *et al.*, 2004). A contemporary theory, that is referred to as the "predictive coding framework" (Friston, 2005) combines these mechanisms. MMN is thought to reflect a prediction error dependent updating of a hierarchical model that infers the causes of sensory stimuli and predicts future inputs (Friston, 2005; Baldeweg *et al.*, 2006). In this theory of MMN generation, model adjustment conforms to prediction error dependent synaptic plasticity of fibers connecting hierarchically organized regions and, in addition, adaptation regulates the postsynaptic sensitivity to top-down predictions and bottom-up stimulus information. This means that adaptational mechanisms may act locally in the auditory cortex and modulate how ascending fibers transmit prediction error to higher cortical levels and how descending connections provide information to lower levels. Within this theory, the MMN represents a failure to predict bottom-up inputs and suppress prediction error (Garrido *et al.*, 2008; Garrido *et al.*, 2009a).

During this thesis, I investigated the relative contribution of the above named mechanisms to mismatch response generation using DCM. This was done on the basis of a network that consisted of four neuronal sources (each targeted with an epidural electrode): A1 on the left and on the right hemisphere and PAF on the left and on the right hemisphere. In this network architecture, A1 receives the primary auditory input whereas PAF is supposed to lie downstream of A1 and is thought to be involved in higher auditory processing (Simpson & Knight, 1993b). The question we wanted to answer using this design was, how perturbations of the network (the presentation of the deviant sound) change the connection strength between A1 and PAF as well as adaptation in A1.

Furthermore, with the parametric modulation of muscarinic acetylcholine receptors we aimed to investigate the effect of changes in the properties of spike frequency adaptation on mismatch responses in general. In addition, we ask whether we can successfully detect these manipulations with DCM.

4 Materials and Methods

4.1 Subjects

All experiments were performed on male rats (*Rattus norvegicus*). In preliminary studies, Lister hooded rats (Harlan® Rossdorf, Germany), an outbred line originally bred at the Lister Institute, were used. Due to great problems with the detection of auditory evoked potentials (AEPs) at the beginning, a setup for determining the hearing ability of rats was developed and the hearing threshold of Lister hooded rats was compared to Black hooded rats. The results guided our choice to use Black hooded rats (Janvier®, Le Genest St Isle, France) for all further experiments. Those rats originally stem from the same strain of the Lister institute but were bred further on as an inbred line.

Animals were housed in a temperature (22 ± 1°C) and humidity (55 ± 5 %) controlled room. Prior to electrodes implantation, animals were housed pairwise in type 4 makrolon cages that were enriched with nestboxes and horizontal tubes for climbing and filled with the bedding material Lignocel® (hygiene animal bedding). After the operation, animal were kept in pairs in cages equipped with elevated lids. Nestboxes as well as tubes were removed to reduce the risk of tearing apart the implanted telemetry sockets.

Rats were housed with an inverse 12 hours day-night cycle with lights on at 8:30 pm to 8:30 am. Rats are nocturnal animals that sleep about 80 % during the light phase but only 30 % during the dark phase (Antle & Mistlberger, 2005). By inverting their day-night cycle we were able to conduct all experiments in their active phase. During the dark phase, persons entering the animal room switched on red light (> 660 nm, 2 Lux). Rats exhibit three photoreceptors: rods show an absorption maximum λ_{max} at 486 nm, cones two maxima at λ_{max} 358 nm and λ_{max} 510 nm. Above 600 nm, even the blue-green sensitive cones (λ_{max} = 510 nm) exhibit very little sensitivity (Yokoyama, 2000). As a consequence it can be assumed that red light does not disturb the circadian rhythm of the animals and can therefore be used for illumination during the dark phase.

Animals were kept on a diet to avoid a fast increase of weight during the experimental period. Each animal received 18 g of normal rodent chow (R/H-M, Sniff®, Spezialdiäten

GmbH, Soest, Germany) per day, which corresponds to about 80 % of the free-feeding food amount. For three days after electrodes implantation, the animals were fed additionally with baby mush. After the surgery, rats were weighed daily to ensure that they were eating normally.

In order to evaluate the hearing ability of the rats in preliminary studies, overall 12 rats, *i.e.* six Black hooded and six Lister hooded rats were compared. Afterwards, all experiments were conducted with Black hooded rats. In preliminary experiments, for evaluating the optimal stimuli four Black hooded rats were utilized. The main experiments that comprised electrophysiological recording during oddball stimulation were conducted with a group of 16 rats. For the pharmacological study, a subgroup of nine rats was used.

All experimental procedures were approved by the local governmental and veterinary authorities of Cologne (file number 9.93.2.10.35.07.056).

4.2 Anesthesia

The implantation of electrodes, attachment of the telemetry transmitter, injection of drugs as well as the recording of BAEPs were conducted under anesthesia. For inducing anesthesia, rats were placed in an anesthesia box, perfused with isoflurane (5 %) mixed with 30 % O_2 and 70 % nitrous oxide (N_2O). For attaching the telemetry transmitter to the implanted socket and the injection of muscarinic drugs, the animals had to be only lightly anesthetized. In order to achieve a deeper state of anesthesia for surgery and BAEP-recording, the animals received anesthetic gases until no eye lid closure reflex was present.

For electrode implantation, the rats were fixed in a stereotactic frame (*cf.* 4.3.2). For the recording of BAEPs animals were placed on a special holder (*cf.* 4.6). During the operation and brainstem audiometry, animals inhaled the anesthetic gases (isoflurane reduced to 2-3 % in case of surgery and 1.5-2 % during BAEP-recording) through a mask. The animals' body temperature was maintained stable at 37 ± 0.5 °C by a heating pad during brainstem audiometry or a temperature control unit (medres®, medical research GmbH, Köln, Germany) during surgery, which were both regulated with a rectal probe. To avoid drying

out of the eyes during long anesthesia, Bepanthen (5 % Dexpanthenol, Bayer Vital GmbH, Leverkusen, Germany) was dispersed on the eyes of the animals.

4.3 Implantation of electrodes

4.3.1 Fabrication of electrodes

For epidural recordings, self-fabricated silverball electrodes were used. A 0.2 mm thick silver wire was heated with a Bunsen burner until the tip of the wire formed a ball with an approximate diameter of 1 mm. The silverballs were chlorinated by electrolysis to reduce the input resistance. Afterwards, the silver wire was cut about 2 mm from the silverball and soldered to an insulated copper wire, which was itself soldered to conducting pins of the telemetry socket.

4.3.2 Surgical procedure

For chronic implantation of electrodes which was conducted under anesthesia (*cf.* 4.2) animals were fixed in a stereotactic frame with earbars and toothbar. The placement of the earbars had to be done very cautiously to avoid injury of the eardrum. Prior to surgery, rats were given an intraperitoneal (i.p.) injection of 5 mg/kg Carprophen (Rimadyl®, Pfizer, Berlin, Germany) as analgetic. For placing the electrodes the temporalis muscle was partly removed and the cranial bone was grinded with a dental drill (Prolab Basic, Bien Air® Medical technologies, Switzerland). An additional smaller window for the placement of the reference electrode was opened 5 mm anterior to bregma at the midline. In order to achieve a strong bonding between the scull and the telemetry socket, an additional fixation was needed. Therefore, three burr holes were drilled: one near the exposed area on the left side, one near the exposed area on the right side and one close to the reference electrode next to the midline. Into these burr holes, three fixation screws (cylinder head, 1.0 x 3 mm, Knupfer Modell-und Feinwerktechnik, Schorndorf, Germany) were tightened.

Guided by stereotaxic coordinates two electrodes were positioned above the right and two above the left hemisphere. They covered the primary auditory area, A1 (coordinates

relative to bregma: 4 mm posterior, 8 mm lateral, 4 mm ventral) and the posterior area, PAF (6 mm posterior, 8 mm lateral, 4 mm ventral), thereby targeting a primary and a non-primary auditory area, respectively (Doron et al. (2002), 2002; Figure 8). A reference electrode was placed 5 mm anterior to bregma at midline over the frontal sinus.

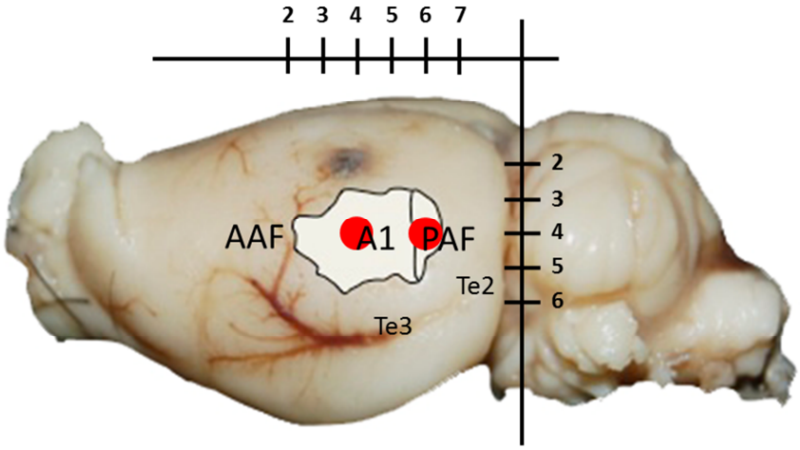

Figure 8: Positioning of silverball electrodes above the left auditory cortex. The white area labels the auditory cortex (taken from Doron *et al.* (2002)) and superimposed onto the picture of a dissected rat brain. The core auditory areas (the anterior auditory field (AAF), primary auditory cortex (A1) and posterior auditory field (PAF)) are labeled. The red dots represent the location of the electrodes. The hematoma above A1 resulted from the fixation screw.

The telemetry socket, to which electrodes were soldered, was fixed onto the skull with dental cement (Technovit 3040, Heraeus Kulzer GmbH, Wehrheim, Germany). After surgery rats were given an additional analgetic (0.3 mg/kg Buprenorphine (Temgesic®, Nycomed GmbH, Singen, Germany), i.p.). Animals were allowed to recover at least ten days after surgery and received analgetics for three days after surgery (Carprophen twice a day and Buprenorphine once).

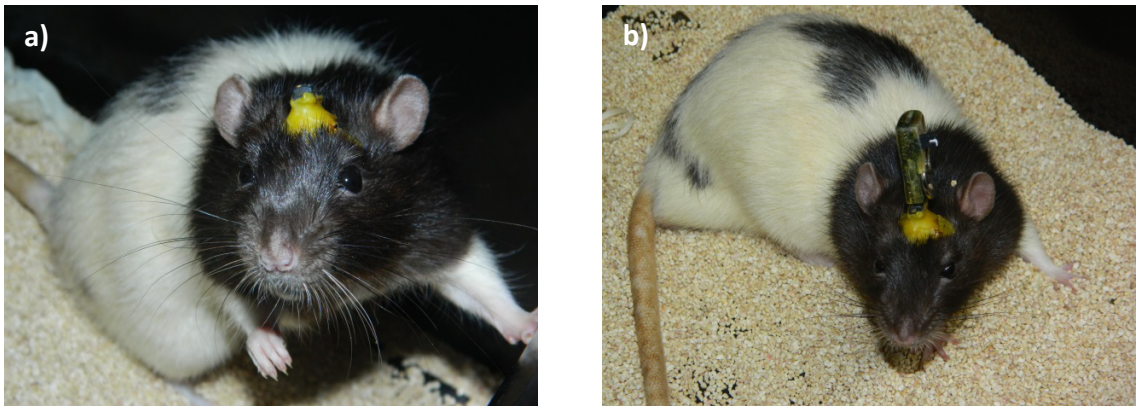

Figure 9: Black hooded rat after electrodes implantation. a) Rat with implanted telemetry socket fixed to the scull with dental cement (yellow material). b) Telemetry transmitter attached to the implanted socket.

4.4 Experimental setup

4.4.1 Sound-attenuated chamber

All electrophysiological experiments were performed in a sound-attenuated chamber which was surrounded by a Faraday cage (Figure 10). The recording chamber was isolated with a special sound proof foam material and illuminated with red light (> 660 nm) by a LED panel, which was needed to observe the rats with a camera (S7500 webcam, Logitech®, Morges Switzerland). Two speakers were mounted at a height of 10 cm and with a distance of 25 cm to the left and right from the middle of the cage. In order to keep the spacing between the rats and the speakers reasonably constant the animals were placed in a wire cage (21 x 35 x 22 cm) located between two loudspeakers.

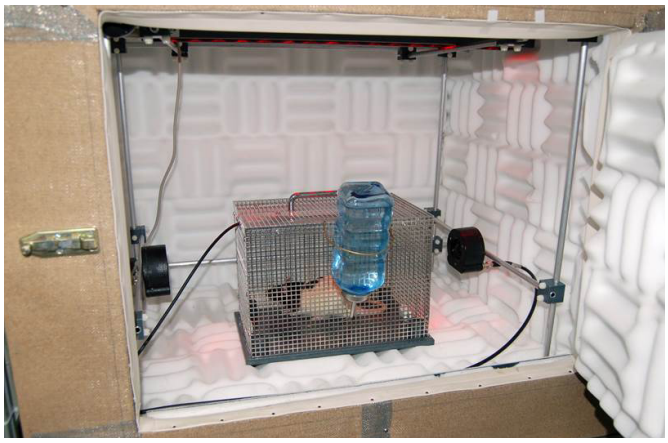

Figure 10: Sound-attenuated chamber. During acoustic stimulation, the rat was placed into a cage to keep the distance between the speakers and the animal reasonably constant. The chamber was isolated with a soundproof foam material and illuminated with red LED light.

The experimental setup consisted of three main hardware components: the telemetry system that allowed wireless transmission of the EEG-signal, a system for acoustic stimulation and a data acquisition system (Figure 11).

4.4.2 Telemetry system

The telemetry system was purchased from TSE Systems (TSE Systems GmbH, Bad Homburg, Germany) and permits the wireless transmission of electrophysiological data via radio waves. This experimental setup allows us to record the EEG in the awake rat without any anesthesia effects. A great advantage compared to the transmission via cables with swivel connectors is that the animals can move completely unrestrained. Hence, the wireless approach is less stressful for the animal (Kramer *et al.*, 2001).

The telemetry system consisted of a transmitter, an implantable socket, a receiver system with antenna and a control unit. The transmitter was equipped with an internal antenna and electrically supplied by a coin cell. Prior to the experiments, the transmitter was attached to the implantable plastic socket which itself was connected to the electrodes. The EEG signal was pre-amplified in the transmitter (1000 x), processed by the internal multiplexer and coded using a pulse spacing modulation. The modified signals were sent via the transmitter antenna as radio waves (433.7 MHz) to a receiver-antenna that was connected to a high frequency (HF)-receiver. The receiver stabilized and amplified the signals (10 x) and passed them on through a serial port to a control unit which includes an interface for decoding and modifying the analogue signals. From the control unit, coaxial cables ran to the A/D-converter of the data acquisition system. Each cable transmitted the signal of one single electrode and was connected to the A/D-converter via BNC connectors. The data was bandpass filtered (0.6-60 Hz) by the system.

4.4.3 Acoustic stimulation system

Acoustic stimuli were generated and presented with Tucker Davis Technologies® (TDT, Alachua, USA) System 3 and delivered via free-field magnetic speakers (FF1, TDT). The RX6 Piranha Multifunction Processor of the TDT system was connected to a PC via fiber cables

that were running from a PCI card to the gigabit-interface (PO5 und FO5, TDT). This setup allows exact timing of stimuli. Synchronously to stimulus presentation, a trigger pulse was sent to the data acquisition system to indicate the occurrence of a stimulus.

4.4.4 Data acquisition system

The data acquisition system consisted of a windows computer running the software DasyLab (National Instruments®, Austin, Texas) which was additionally equipped with special PCI-interfaces that were connected to an A/D-converter.

From the control unit of the telemetry system four coaxial cables, each transmitting the signal of one recording electrode, were connected via BNC connectors to the input of the A/D-converter. The telemetrically recorded EEG was sampled with a frequency of 2 kHz. For recording brainstem potentials (*cf.* 4.6), the sampling rate was set to 20 kHz in order to detect the very fast potential peaks.

The TTL-trigger-signals that were emitted by the acoustic stimulation system synchronously to stimulus presentation were transmitted via coaxial cables and connected with BNC connectors to the inputs of the A/D-converter. The number of trigger signals depended on the stimulation paradigm that was conducted. For oddball experiments, for example, two trigger signals were needed: one trigger indicated the presentation of a standard sound and one the presentation of a deviant sound.

A general advantage of the program DasyLab is that the data stream can be visualized at the graphical user interface. For each paradigm, a worksheet had to be generated that matched the requirements of an experiment. The trigger signals indicating the different acoustic stimuli were used for online averaging of AEPs. In addition, the raw data stream was stored.

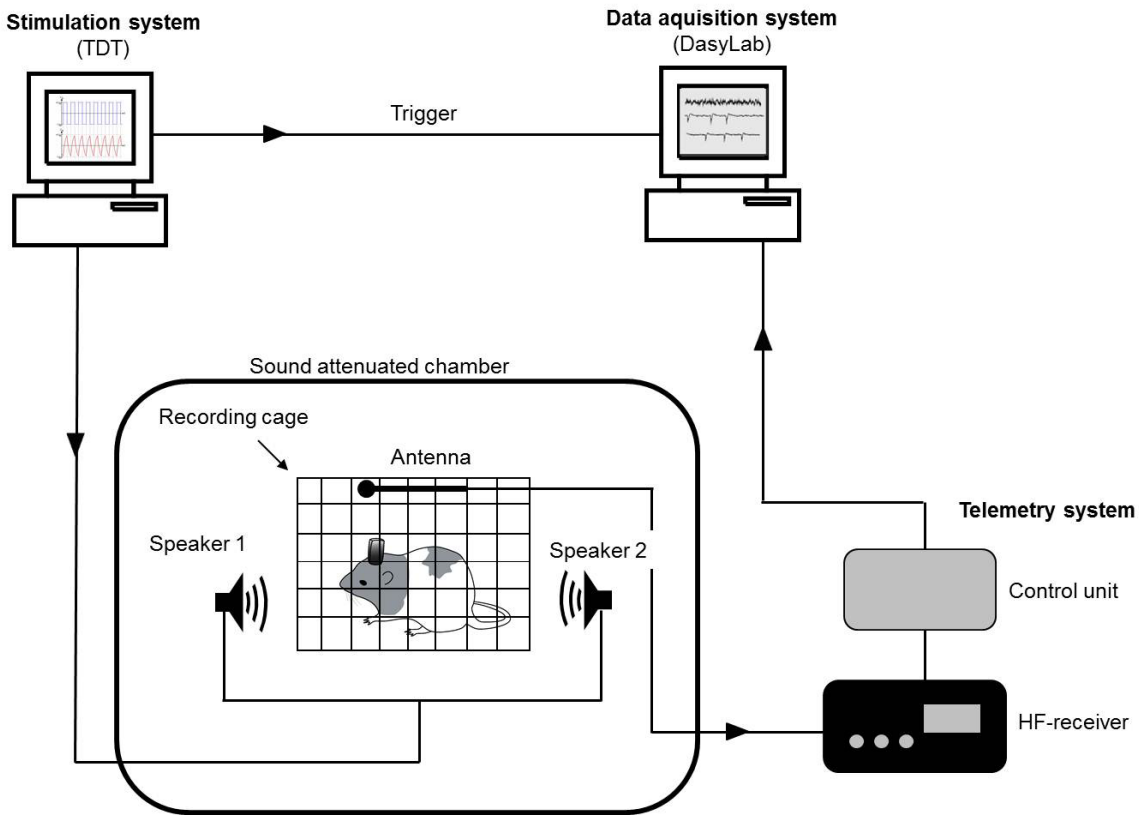

Figure 11: Experimental setup. The rats were sitting in a cage during the recordings. On each side of the cage one speaker was positioned. The EEG-signal that was emitted by the telemetry transmitter was captured by the antenna (mounted at the top of the cage) and transferred to a HF-receiver from which it was sent to a control unit and passed on to the A/D-converter of the data acquisition system (DasyLab). The stimulation system (TDT) controls the two speakers and sends trigger pulses to the data acquisition system synchronously with the acoustic stimuli.

4.5 Acoustic stimuli

4.5.1 Generation

All sounds were generated with the program SigGen (TDT). As mentioned above, in the preliminary study, individual hearing thresholds have been determined (*cf. 4.1*). For this purpose, click stimuli have been used. Those stimuli are most effective for activating a large number of neurons simultaneously because they combine a rapid on- and offset, a very short overall duration (50 µs in this study) and a broad range of frequencies (1 to 20 kHz). For establishing an audiogram of Black hooded rats, short sine tone-bursts

(2 ms duration with a rise- and fall-time of 1 ms) of five different frequencies (4, 8, 16, 32 and 43 kHz) were used.

The resulting audiogram lead us to choose stimuli of 7-9 kHz and 16-18 kHz in the main oddball experiments. We used bandpass-filtered noises rather than sine tones since neurons in the auditory cortex adapt rapidly to pure tone stimuli and we wanted to ensure the largest response amplitude over time. In preliminary experiments, the duration of the stimuli varied from 40 ms to 100 ms in 10 ms steps. Those experiments guided our choice to use stimuli of 100 ms duration with a rise- and fall-time of 10 ms. For the control conditions, 10 different band pass filtered noise stimuli (7-9, 8-10, 9-11, 10-12, 11-13, 12-14, 13-15, 14-16, 15-17, 16-18 kHz) were generated.

4.5.2 Calibration

The system was calibrated using the program SigCal (TDT) to flatten the non-linear frequency-response of the speakers. The calibration program plays a series of tones that are recorded with a microphone (model 7016, ACO Pacific, Belmont, California, USA). Subsequently, the output and the actual sound pressure level are compared. For each stimulus, a correction factor was automatically calculated and saved in a normalization file. Afterwards, the acoustic stimuli are generated and the normalization file is applied to each stimulus while playing. The actual sound pressure level was afterwards adjusted using a sound pressure level (SPL)-meter (NL 32, RION Co. Ltd, Tokyo Japan). The frequency weighting for the measurement was set to linear. Other frequency weightings implemented in the SPL-meter, for example A-weighting, could not be used because those account for sound pressure levels perceived by the human ear. As there is no comparable weighting available for rats, linear weighting had to be employed.

All stimuli that were used in brainstem audiometry were calibrated as described above but with the use of an artificial ear canal. The artificial ear canal was a self-made cast of an external auditory meatus of a Black hooded rat. The rat was therefore sacrificed and the outer ear was filled with dental cement (Technovit 3040, Heraeus Kulzer GmbH, Wehrheim, Germany). After dissecting the cast out of the rat's ear, it was used as a negative to produce the artificial ear canal with a silicon modeling material (Selva Technik

GmbH & Co.KG, Trossingen, Germany). The ear canal was used afterwards as a coupler between the microphone of the SPL-meter and the plastic tube of the closed-field speaker. This holds the membrane of the microphone at the place where the eardrum of the rat would be located. This method allowed for an exact calibration of the sound pressure level. For measuring very brief sounds with the SPL-meter the option "L_{pk}" that employs no time constant but resembles the actual peak of the sound pressure was used. All dB-values for the short stimuli are therefore given in "dB peak sound pressure level" (dB pSPL). Tone bursts implemented for establishing an audiogram of Black hooded rats were calibrated as "peak equivalent sound pressure level" (dB peSPL) due to the longer stimulus duration (Burkard, 2006). For the use in brainstem audiometry, stimuli with various sound pressure levels (from 100 dB pSPL or peSPL decreasing in 10 dB steps) had to be generated.

The bandpass-filtered noise stimuli for the main experiments which were intended to be used during stimulation with the two free-field speakers on each side of the recording cage were set to 75 dB ± 3 dB measured with the microphone of the SPL-meter located in the middle of the recording cage. Sound pressure levels were determined with fast time weighting.

4.5.3 Presentation

The acoustic stimuli were presented with the program SigPlay (TDT). During brainstem audiometry overall 1000 stimuli were delivered at a rate of 4 Hz.

For all main experiments a slower rate of 2 Hz was used. This was done in order to preserve comparability to other MMN-studies with rats (*e.g.* Tikhonravov *et al.* (2008), Tikhonravov *et al.* (2010); Nakamura *et al.* (2011); Lazar & Metherate (2003)). Adapted to the aim of the individual paradigm, either a pseudorandomized protocol or a homogenous sound sequence was used. In the oddball paradigms in which standard and deviant stimuli were randomly presented, the overall number of stimuli was kept constant (on average 1000 stimuli) but the probability of the deviant stimulus (0.4, 0.2, 0.1) varied. A new randomization was used for each session. For the stimulation with a homogenous sequence of sounds, 100 stimuli were applied.

For the control sequences, a special protocol playing either ten or five sounds randomly was required. This was achieved with a so called “circuit file” that was designed by TDT especially for our control experiments. This file was loaded directly onto the processor without the use of the program SigPlay, where it triggered the randomized play back of stimuli. As a prerequisite of the control condition succeeding frequencies were never identical.

4.6 Brainstem audiometry

As mentioned before, in the preliminary study the hearing ability of Lister and Black hooded rats were compared to select the most suitable strain for the study. The experimental setup was developed together with Felix Neumaier, a Bachelor student who did an internship in our group and conducted the experiments under my supervision.

Testing the rats’ hearing capacity can be done reasonably easy by recording brainstem evoked potentials (BAEPs) in the anesthetized state (Figure 12). BAEPs in rats consist of four peaks which are generated at various stations of the auditory pathway starting at the auditory nerve and comprising also the cochlear nucleus (CN), the superior olivary complex (SOC) and the inferior colliculus (IC), respectively (Shaw, 1988).

BAEPs were recorded as difference recording between mastoid and vertex. Therefore, two platinum needle electrodes were inserted subcutaneously: the recording electrode was placed at the left or right mastoid depending on the ear that was stimulated; the reference electrode was inserted at the vertex. A third electrode that represented the ground wire was inserted subcutaneously at the back of the rat near the base of the tail.

The acoustic stimuli were presented with the acoustic workstation, but in this setup the stimuli were directly into the rats’ outer ear with closed-field speakers (CF1, (TDT), Alachua, USA) that were equipped with plastic tubes for insertion into the ear channel.

BAEPs were recorded with a sample-rate of 20 kHz. Before A/D-conversion, signals were amplified (x 1000) and passed through an analogue low-pass-filter with a cut-off-frequency of 3 kHz. Signals were delivered to the acquisition system (Dasy Lab, *cf.* 4.4.4), again amplified by 1000 and low-pass-filtered digitally with a cut-off at 100 Hz.

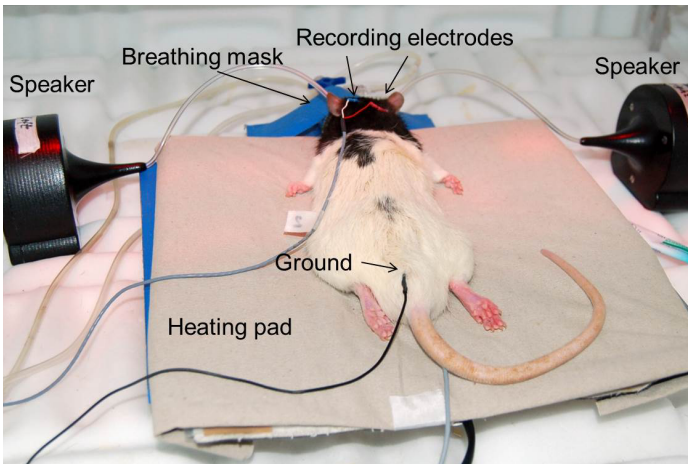

Figure 12: Experimental setup for recording of brainstem potentials. Recording was conducted under inhalation anesthesia. The special closed-field speakers were equipped with plastic tube for insertion into the ear channel to deliver the acoustic stimuli directly the eardrum of the rats.

4.6.1 Estimation of hearing thresholds with click stimuli

For a gross estimation of hearing thresholds, click stimuli were used. During stimulation, the contralateral ear was masked with white-noise of an amplitude 30 dB below stimulus-level to avoid stimulation through bone-conduction. The loudness of the clicks was reduced from initially 100 dB pSPL in steps of 10 dB pSPL. Because BAEPs could be averaged online in DasyLab and were directly visualized on the screen, the loudness of the click-stimuli could be reduced stepwise until no evoked activity was present in the average.

The individual hearing threshold of each animal was determined as an average between the last sound pressure level that evoked BAEPs and the next lower sound pressure that was used. For example, if there were potentials visible in the recording tracks for the stimulation with 40 dB pSPL, but no potentials for 30 dB pSPL the individual hearing threshold for an animal is given as 35 dB pSPL. For assuring the stability of the recordings, each animal was measured twice on two different days and hearing thresholds were averaged.

4.6.2 Tone-burst evoked audiograms

After it was decided to use Black hooded rats for all further experiments, a precise audiogram for this strain was established in order to assure that the acoustic stimuli that should be used for mismatch experiments fit the rats hearing ability. Therefore, tone-bursts of five different frequencies were presented and, again, the loudness of the stimuli was reduced in 10 dB peSPL steps until no brainstem activity was evoked. The analysis was conducted as described above (*cf.* 4.6.1).

4.7 Paradigms

4.7.1 "Flip-flop" oddball paradigm

As oddball paradigm, a classical "flip-flop" experiment was employed that comprised two blocks: In the first block the low frequency stimulus (7-9 kHz) was used as standard and the high frequency stimulus as deviant sound (16-18 kHz). In the subsequent block, stimuli were swapped so that the high frequency stimulus served as standard and the low frequency stimulus as deviant. The high and the low frequency standard as well as the high and the low frequency deviant were averaged afterwards. This was done in order to eliminate frequency specific effects arising in the recorded waveforms that could mimic mismatch responses.

In human subjects, it has been shown that the probability of deviant sounds affects the amplitude of the mismatch negativity (MMN), *i.e.* a lower deviant probability leads to an increased MMN (Näätänen, 1992 ; Imada *et al.*, 1993; Javitt *et al.*, 1998; Shelley *et al.*, 1999; Sato *et al.*, 2000; Sabri & Campbell, 2001; Sonnadara *et al.*, 2006). Therefore, in the main oddball paradigms with 16 rats, the following two probabilities were applied: 0.1 (100 deviants vs. 900 standards) and 0.2 (200 deviants vs. 800 standards).

Due to the randomization implemented in the sound presentation program, the number of standard stimuli varied around the mean (*e.g.* main oddball experiments: 0.1 probability condition: 908 standards (SD = 32); 0.2 deviant probability: 805 standards (SD = 11)).

In a subgroup of rats (n = 6) the deviant probability was further increased to 0.4 (600 standards vs. 400 deviants) and a deviant omission paradigm was presented, in which a homogenous sequence of standards was presented that was interspersed with gaps of 0.1 probability.

For the pharmacological study (n = 10) an oddball paradigm of deviant probability 0.1 was used to compare the effect of the different treatments.

4.7.2 Control conditions

Overall, two control conditions were used in a subgroup of rats (n = 6). In MMN research, control conditions are indispensable because differences between standard and deviant potentials can be either due to the rarity of the deviant (*i.e.*, less adaptation or refractoriness) or to the violation of predictions based on the previous acoustic sequence.

A control condition that was used in early MMN research is the “deviant alone” condition (Sams *et al.*, 1985a). In this condition, standards are replaced by silence and deviants are presented with the same randomly changing interstimulus intervals as in the oddball experiment. As there is no auditory stimulation present before the deviant, no prediction about the upcoming auditory sequence can be established and no MMN should be evoked. However, this control mixes the effect of stimulation duty cycle with the effect of the rarity of the deviant (*cf.* 3.3.4).

A more recent control that was suggested by Jacobsen and Schröger (2001) is the “deviant in many standards”-control condition. The overall presentation rate of deviants is again preserved but standards are replaced by stimuli with different carrier frequencies. Because the denotation “deviant in many standards” might be misleading the term “equiprobable” control condition introduced by Astikainen *et al.* (2011) will be used throughout this thesis. Overall, two control conditions were designed, one condition matching each deviant probability (0.2 and 0.1) that was used in the main oddball experiments. In other words, for the control condition with deviant probability 0.1, 10 different band-pass filtered noise stimuli (7-9, 8-10, 9-11, 10-12, 11-13, 12-14, 13-15, 14-16, 15-17, 16-18 kHz) were used, each presented 100 times in random order (equiprobable control 0.1). The second control with deviant probability 0.2 comprised 5

stimuli (7-9, 10-12, 13-15, 16-18, 19-21 kHz) each presented 200 times in random order (equiprobable control 0.2).

4.8 Pharmacological treatment

The drugs scopolamine hydrobromide and pilocarpine hydrochloride (Sigma Aldrich®, Hamburg, Germany) were used in the pharmacological study to modify the state of the muscarinic acetylcholine receptor and to evaluate the effects on mismatch responses.

Scopolamine hydrobromide is a non-selective antagonist of the muscarinic receptor that blocks cholinergic signaling. In addition, it enhances afterhyperpolarising potassium currents through a cGMP-dependent second messenger mechanism (Krause & Pedarzani, 2000) thus increasing spike frequency adaptation.

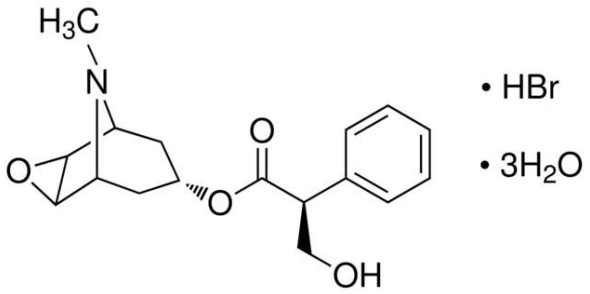

Figure 13: Chemical structure of scopolamine hydrobromide trihydrate. The illustration is taken from http://www.sigmaaldrich.com/catalog/product/sigma.

Pilocarpine hydrochloride is a non-selective muscarinic acetylcholine receptor agonist that activates muscarinic acetylcholine receptors and therefore results in opposing effects of those of scopolamine. At very high doses (about 30 mg/kg and higher), pilocarpine is used to induce epilepsy in an animal model.

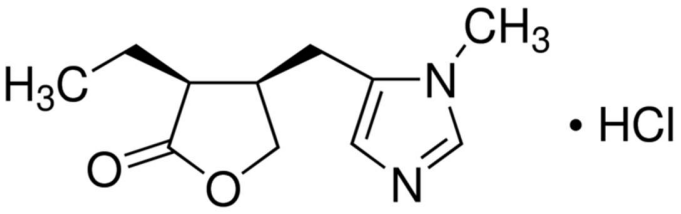

Figure 14: Chemical structure of pilocarpine hydrochloride. The illustration is taken from http://www.sigmaaldrich.com/catalog/product/sigma.

The drugs were solved in NaCl and injected i.p. in doses of 1 and 2 mg/kg (scopolamine) and 3 and 6 mg/kg (pilocarpine). Doses were adjusted after personal communication with PhD Rosalyn J. Moran who did the analysis of the preliminary data. In order to control for effects of the i.p. injection or the solvent itself, all animals received a vehicle (only NaCl) injection as well.

Prior to the experiment, the animals were weighed to determine the correct injection dose. For injection, the rats were anesthetized briefly (*cf.* 4.2.). 20 minutes after the injection, the acoustic stimulation was started.

For both substances there is only little data available describing its pharmacokinetics and no information especially for rats. In humans, scopolamine is known to exhibit a plasma half-live of 3 hrs (Brown, 1992). After i.v. injection of 15 mg/ml pilocarpine nitrate in dogs, the substance exhibits a plasma half-live of approximately 1.3 hr (Weaver *et al.*, 1992). Oral doses of 5 mg pilocarpine hydrochloride exhibited 0.76 hr plasma half-live in human subjects and salivary secretion that started at 20 min and lasted 3 to 5 hr (MGIPharma, 2001).

To assure that the applied drug does not interact with the subsequent treatment, there has to be a break between injections which is about five times the substances half-life Therefore, the animals underwent drug injections every third day. The order of injections and time of day was counterbalanced across the animals.

4.9 Data analysis

The recorded EEG signals were preprocessed offline using MATLAB®(Version 2011b, Mathworks, Natick, Massachusetts). The data were stored in ASCII format containing a

time column, four columns of voltage values (one for each recording electrode) and, depending on the paradigm that was conducted, additional columns comprising the trigger pulses. For the oddball experiments, for example, two different trigger signals were needed: one indicated the presentation of standard sounds and one indicating deviants. The data were down sampled for the whole analysis (except for dynamic causal modeling, *cf.* 4.10.3) from 2 kHz to 1 kHz.

The electrodes that recorded no evoked activity were eliminated from the analysis. AEPs were calculated for homogenous sequences of stimuli as an average over all stimuli presented. For oddball experiments, standard (mean of the high and the low frequency standard) and deviant potentials (mean of the high and low frequency deviant) were averaged separately. The potentials were baseline corrected by subtracting the average value of the 100 ms prestimulus baseline. Subsequently, differences waveforms, *i.e.* MMN-like activity was calculated as "deviant minus standard" evoked potential. For the analysis of the equiprobable control condition, responses to the stimuli 7-9 kHz and 16-18 kHz were averaged and served as control deviant.

4.9.1 Latency and amplitude of the most prominent peaks

In order to compare the amplitudes and latencies of the most prominent peaks between deviant and standard potentials, the respective values were detected in the averaged potential waveforms separately for the two stimulus types (standard, deviant). For the first negative peak (N1), the minimum value was detected in a time window of 10 to 40 ms after the beginning of the stimulus. The latency and amplitude of the corresponding peak were determined using the MATLAB command "min". For the subsequent positive peak (P2) the maximum value between 40 to 140 ms after stimulus onset was detected and the latency of occurrence and amplitude established using the MATLAB command "max".

4.9.2 Integrals

In order to compare the whole potential waveform and amplitude in two distinct conditions, integrals of the AEPs were calculated. Therefore, the voltage values were transformed in absolute values by squaring and extracting the square root. Afterwards,

the absolute values were added for 0 to 250 ms after stimulus onset to obtain an integral over the first 250 ms. In the time range of 250 to 500 ms no evoked activity was observed, therefore, no analysis was performed for this latency range.

4.9.3 Statistical analysis

For the statistical analysis the significance level α was set to 0.05. For p-values smaller than 0.05 the null hypothesis was rejected and the detected differences were designated as significant. As some data sets were not normally distributed, most likely due to the relatively small sample, only non-parametric statistical tests were used.

For statistical analysis of waveforms in which a large number of point by point comparisons were needed MATLAB was used. Those comparisons were done from 1 to 250 ms after stimulus onset using a Wilcoxon Signed Rank Test for corresponding sample points (time bin 1 ms). Due to the problem of multiple comparison the resulting p-values were FDR-corrected with a MATLAB script developed by Groppe *et al.* (2011) adapted to the present data.

Latency values, peak amplitudes and integrals were compared statistically using the software Sigma Plot® (Systat Software Inc, Version 11.0). Again, all tests were performed non-parametrically. Therefore, all analyses of variance were calculated on rank-transformed data.

In order to evaluate the effect of treatment on the latencies and integrals of the evoked potentials a two-way repeated measures ANOVA on ranks was calculated separately for the four electrodes. Resulting p-values were corrected for multiple comparisons using the Bonferroni procedure.

For better visualization, data were down-sampled to 0.5 kHz before plotting and the standard error of the mean (SEM) was used in figures displaying waveforms. For illustrating latencies and amplitudes in bar graphs, the standard deviation (SD) was employed.

4.10 Dynamic causal modeling

The modeling part of this thesis was done in cooperation with Andreea Oliviana Diaconescu Post-doctoral fellow in the group of Prof. Dr. Dr. Klaas Enno Stephan(Translational Neuromodeling Unit (TNU), Institute for Biomedical Engineering, University of Zurich & ETH Zurich). Biologically plausible forward models can be used for investigating how event-related potentials (ERPs) are generated. One possible approach is dynamic causal modeling (DCM), which was originally developed for connectivity analysis of fMRI data (Friston et al. 2003) and afterwards implemented for several other data modalities and features, like ERPs measured with EEG (*cf.* 3.4). DCM uses a biologically informed causal model to make inferences about the underlying neural mechanisms that generate ERPs. The parameters that are estimated during model inversion have a specific neuronal interpretation and thereby encode the coupling among brain regions and how the coupling depends upon experimental manipulations (David *et al.*, 2005; David *et al.*, 2006).

The implementation of DCM for ERPs was performed using Statistical Parametric Mapping (SPM8 version 5236; http://www.fil.ion.ucl.ac.uk/spm/software/spm8/). The differential equations that govern the neural mass model and the details of the model inversion are not explained in detail in the context of this thesis. At any point, references to the original publications, where the mathematical equations can be found, are provided.

The DCM framework has two main components: biophysical modeling and statistical data analysis (probabilistic inference). As with any modeling attempt, both components rest on the plausibility of the modeling assumptions and the simplifications that modeling inevitably entails (see for example Moran *et al.*, 2009; Stephan *et al.*, 2010; Litvak *et al.*, 2013).

4.10.1 Neuronal mass model

DCM uses a neural mass model of a single cortical source which was originally developed by Jansen and Rit (Jansen & Rit, 1995) to simulate electrophysiological responses. The model contains interacting inhibitory and excitatory subpopulations of neurons.

Specifically, each source is described in terms of the average post-membrane potentials and firing rates of three neuronal subpopulations of pyramidal cells, spiny stellate cells and inhibitory interneurons. The neuronal mass model itself is able to generate a cortical α-rhythm with a certain input, such as white noise and can be depicted as an electrical circuit diagram (Figure 15) This illustrates how the neuronal populations were allowed to interact and how the six differential equations (see Jansen & Rit, 1995) the neuronal dynamics, were obtained.

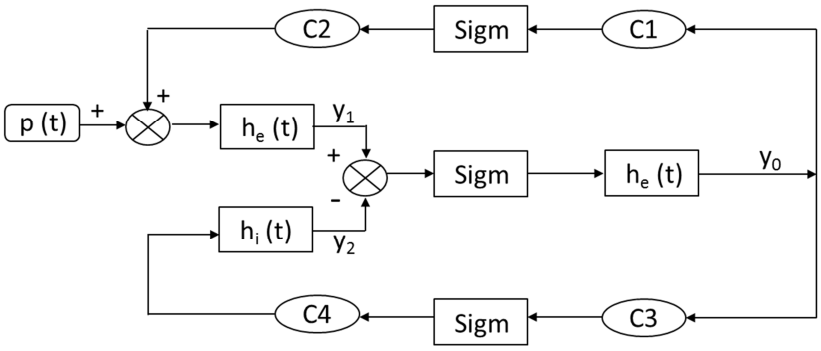

Figure 15: Simplified model of cortical α-rhythm generation taken from Jansen & Rit (1995). Each neuronal block is modeled with a "postsynaptic potential" block (h_e, h_i) converting spiking input into average postsynaptic potentials and, furthermore with a sigmoid function (Sigm) that transfers postsynaptic potentials into an average spike rate of action potentials. C1 to C4 represent time constants. y_0, y_1 and y_2 represent the outputs of the three postsynaptic potential blocks.

P(t) represents the input to the system that is allowed to target excitatory spiny stellate cells. Each neuronal population is modeled with two blocks: the first block is referred to as the "postsynaptic potential block" that transforms the average pulse density of actions potentials that arrive at a population (either as an input from outside the circuit or from another neuronal population in the circuit) into an average postsynaptic membrane potential. The membrane potential can be inhibitory (h_i) or excitatory (h_e) depending on the population. Activity of inhibitory interneurons is modeled with h_i whereas pyramidal cells and stellate cells are modeled with h_e. In the equation describing the postsynaptic kernel, there is an additional constant accounting for the maximum permitted membrane

potential, and one further constant that accounts for the passive membrane properties and other time delays in the dendritic network.

The second block is used to transform the average postsynaptic membrane potential into an average pulse density of action potentials, which is used as an input into another neuronal population. This transformation is done using a sigmoid function (designated by "Sigm" in the circuit).

The remaining four constants C1 through C4 represent connectivity constants that account for the number of synaptic contacts established between the neuronal populations. The outputs of the three postsynaptic potential blocks are y_0, y_1 and y_2. The six differential equations underlying the neuronal mass model were consequently obtained by following the circuit along the given hierarchy and combining the postsynaptic potential block and the sigmoid block accordingly for each population. The output of excitatory spiny stellate cells and the inhibitory interneurons, for example, was subtracted from each other, before the transformation into action potentials, which then reaches the pyramidal cells. Consequently, the activity of the population of pyramidal neurons always depended on the feedforward information from stellate cells and inhibitory interneurons.

4.10.2 DCM for event-related responses

In DCM for ERPs (David *et al.*, 2006), several of the single source models are connected to obtain a neuronal network. The active cortical sources are interconnected according to the connectivity rules described in Felleman & Van Essen (1991) and conform to a hierarchical model of intrinsic and extrinsic connections within and between multiple sources as described in David *et al.* (2005) and Kiebel *et al.* (2007)

Applying this to the auditory cortex, like it was performed in our study, is a simplification of this model, due to differences between visual and auditory cortices (*cf.* 3.4). Based on the study of Felleman & Van Essen (1991) three types of extrinsic connections were introduced into the model a) forward connections that originate in agranular layers and terminate in layer IV, b) backward connections that connect agranular layers and c) lateral connections that originate in agranular layers and target all layers (David *et al.*, 2005).

These connections are always excitatory and are modeled like pyramidal cells (David *et al.*, 2006). The neuronal state equations (David *et al.*, 2006) contain these connectivity rules, whereas the strength of the intrinsic connections and the total number of synapses are again expressed by the constants.

In the present application of DCM, the coordinates of the electrodes, which were used to record ERPs, defined the source locations, *i.e.* the coupled brain regions.

An important factor making DCM unique compared to other biophysical modeling techniques, is that it uses prior constraints on the parameters of the model. Priors are used to specify how neuronal populations are interconnected, and which cortico-cortical connections change with the experimental perturbations (David *et al.*, 2006). The priors thereby specify how a specific stimulus is allowed to change the synaptic coupling strength among sources (synaptic plasticity) and the post-synaptic gain parameters (local adaptation, *cf.* 4.10.1).

4.10.3 Data preprocessing

For modeling mismatch responses, the AEP data recorded under the “flip-flop” oddball paradigm (*cf.* 4.7.1) was used. In the untreated condition, deviant probability 0.1 and 0.2 were compared. Because a network of four sources was investigated, only animals with four intact electrodes (n = 12) were included into the analysis. Furthermore, DCM was performed for mismatch responses after treatment with muscarinic drugs. Here, five drug conditions were compared for the oddball paradigm with deviant probability 0.1 (n = 9). The averaged standard and deviant potentials of each animal were used as an input to SPM8. Electrophysiological data were down-sampled to 300 Hz, and bandpass filtered between 0.5 and 30 Hz. DCM was performed on the preprocessed channel data for 0 to 250 ms after stimulus presentation. SEP models were selected (Kiebel *et al.*, 2006) because those were show in preliminary analyses to fit the underlying data best and account for faster time constants than ERP models (personal communication Prof. Klaas Enno Stephan).

4.10.4 Model specification for evaluating mismatch responses

DCM is a hypothesis driven method that does not explore all possible models, but tests a specified model space based on prior knowledge about the system of interest. In our study, DCM was performed on the basis of a four sources network (each targeted with an epidural electrode): A1 on the left and on the right hemisphere and PAF on the left and on the right hemisphere. In this network architecture, A1 receives the primary auditory input whereas PAF is supposed to lie downstream of A1 and is thought to be involved in higher auditory processing (Simpson & Knight, 1993b). For evaluating the mechanisms underlying MMN generation, overall eight different models were compared. These models were created by systematic combinations of the two key mechanisms proposed by predictive coding theories explaining MMN generation (Garrido *et al.*, 2008; Garrido *et al.*, 2009b) allowing for different changes of the network caused by the deviant (Figure 16). The first mechanism was short-term plasticity of glutamatergic long-range connections. This is typically modeled by allowing for a modulation of the synaptic coupling strength of inter-regional forward and backward connections when the deviant tone is presented (Garrido *et al.*, 2008; Schmidt *et al.*, 2012). The corresponding DCM parameters express the coupling change relative to the standard tone. We allowed for different expression of this type of plasticity, creating four models: Model 1 included no modulation of connections by the deviant, model 2 and 3 comprised modulation of either forward or backward connections among A1 and PAF, respectively, model 4 comprised modulations of both forward and backward connections among the two regions.

The second mechanism concerned neuronal adaptation: In models 5 through 8 we repeated the same variations in synaptic plasticity as for the first four models, but additionally we allowed for variations in adaptation, expressed in terms of deviant-induced modulation of the post-synaptic gain modulation (expressed via h_e) in the left and right A1.

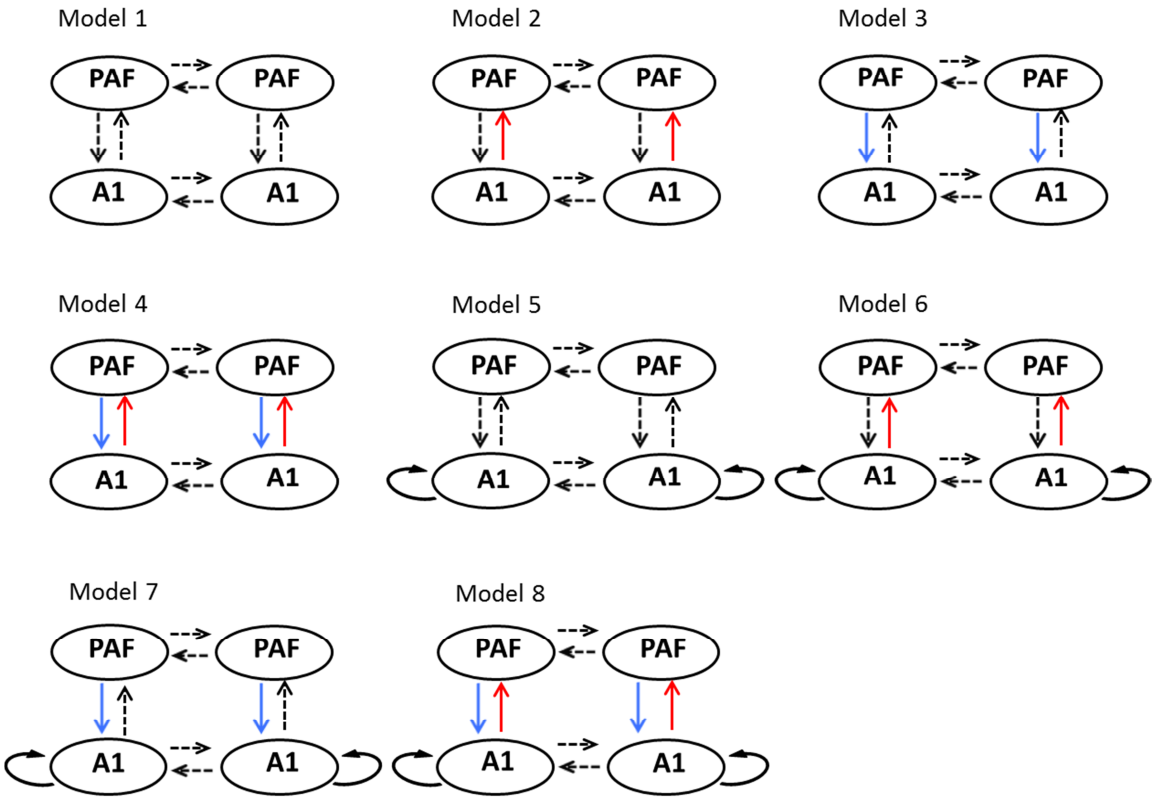

Figure 16: Neuronal network model of the rats' auditory cortex. The network that was investigated consisted of four sources: A1 on the left and right hemisphere and PAF on the left and right hemisphere. Model 1 comprised no modulation of the network by the deviant stimulus. Therefore, the existing connections are displayed as dotted arrows. From model 2 to model 8 the deviant stimuli were allowed to alter either forward (red arrows) or backward (blue arrows) connections. In addition, adaptation in A1 was allowed to vary (bent arrows, model 5 to 8). The input to the network was always set to A1 in both hemispheres (due to clarity the input is not shown in this illustration).

4.10.5 Bayesian model selection (BMS)

The selection of the model that best explains the underlying data was evaluated after model inversion by comparing their log-evidence. The log-evidence corresponds to the probability of the data given a specific model that represents a principle measure that is derived from probability theory, *i.e.* a trade-off between model fit and model complexity. Since the log-model evidence cannot be computed analytically except for linear Gaussian models, approximations are usually required. The approximation used here is the (negative) free energy that provides a bound-approximation on the log-evidence and can be obtained using Variational Bayes (Friston et al. 2007).

The evidence consists of two components: the accuracy term, which quantifies the data fit, and a complexity term which penalizes models with many degrees of freedom (*e.g.*, many and/or uninformed parameters). The best model is the one with the largest log-model evidence, ln$p(y|m)$.

BMS can be done either in a fixed effects approach that assumes that the data from each subject can be explained using the same model or with a random effects approach that proposes different models for each subject. Random effects BMS is robust to potential outliers in the population because it allows for the possibility that different participants use different models (Stephan et al. 2009). Given a candidate set of models $m = 1 \dots M$, we denoted r_m as the frequency with which a model *m* is employed in the population. The results can then be summarized in terms of the estimated frequencies of models within the group. For the analysis in this thesis, a random effects BMS was used.

A second approach in model selection is the family-level inference, which compares sets of models grouped by similar properties. Using this approach, we grouped our 8 models according to common features, namely local adaptation and synaptic plasticity, and used family-level inference to determine whether modulation of (1) post-synaptic gain in bilateral A1 or (2) inter-regional effective connectivity constituted important features of the model architecture.

4.10.6 Modeling adaptation under treatment with muscarinic agents

Adaptation can be modeled with DCM in two different ways: modulating the post-synaptic gain (changing the scaling of the excitatory postsynaptic potential (h_e)) or varying the slope of the sigmoid function (*cf.* 4.10.1) via the parameters p_1 and p_2 (Kiebel *et al.*, 2008). The free parameters p_1 and p_2 determine the slope of the function and its translation. Varying these parameters alters the transformation from average membrane potential to average firing rate. Increasing the parameter p_1 means that smaller changes in average membrane potential are needed to result in the same average firing rate. Increasing p_2, however, shifts the sigmoid to the right, meaning that a higher average membrane potential is needed for reaching an equivalent firing rate. In a biological sense, this also models adaptation.

In this thesis, the effect of the muscarinic agents was modeled by varying the scaling of the post-synaptic kernel (h_e) only.

5 Results preliminary studies

5.1 Brainstem audiometry

Pilot experiments with Lister hooded rats revealed difficulties regarding electrode implantation and detection of evoked potentials. In order to verify the hearing ability of the animals, an experimental setup for recording brainstem auditory evoked potentials (BAEPs) in anesthetized rats was developed.

For a gross estimation of hearing thresholds, BAEPs were elicited in six Lister hooded and six Black hooded rats. Even at first sight, considerable differences between the individual hearing thresholds in the two experimental groups became evident. Individual BAEP waveforms of two rats are shown in Figure 17 to exemplify these enormous strain differences. Lister hooded rats exhibited large amplitude BAEPs at 100 and 90 dB pSPL, but at 70 dB pSPL none of the recorded animals showed click-evoked potentials at all. On the contrary, in Black hooded rats, even with click sounds of 40 dB pSPL distinct potentials were visible in the recording tracks.

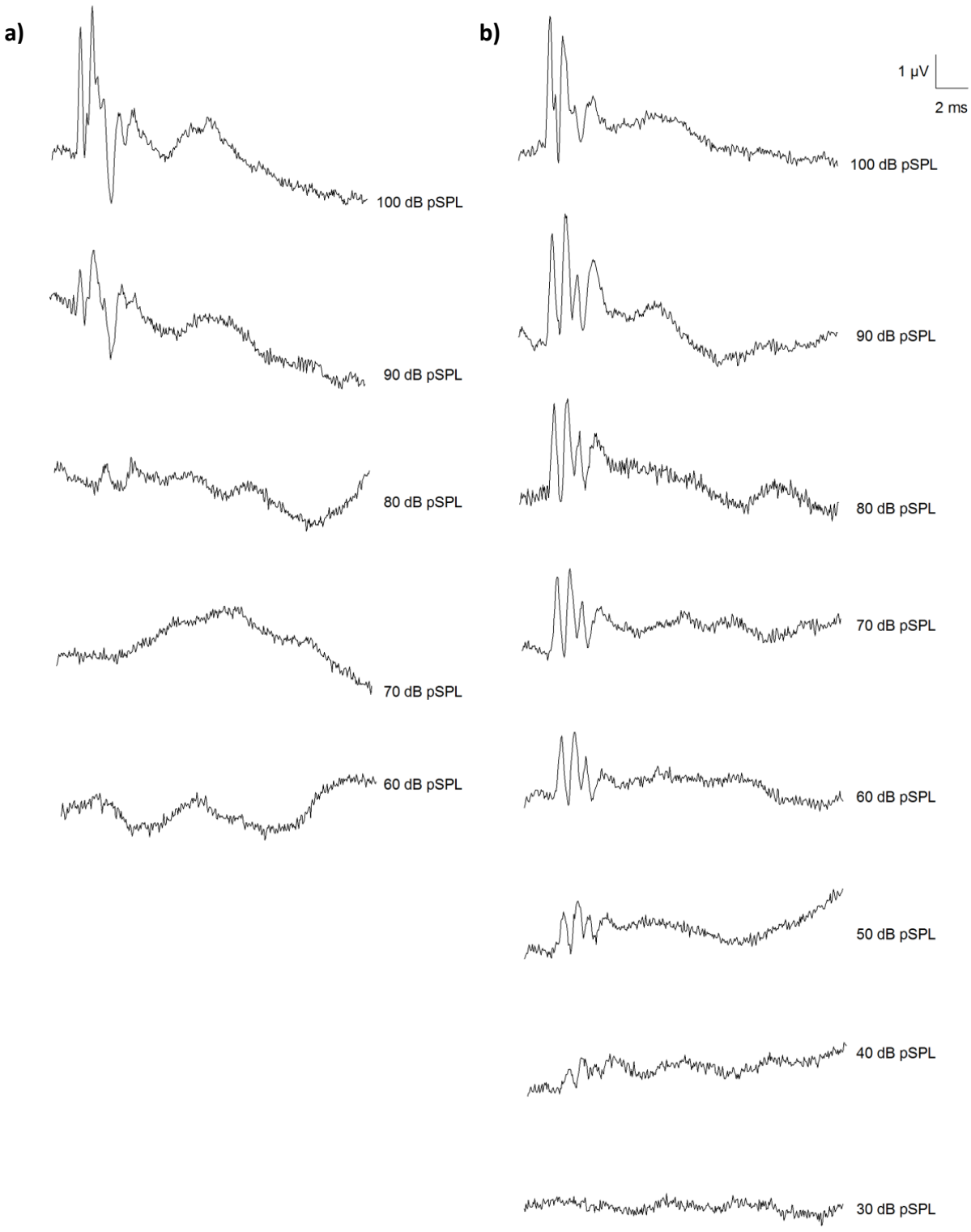

Figure 17: Brainstem potentials evoked with click stimuli recorded from two rats of different strains. a) BAEPs recorded in a Lister hooded rat. The individual hearing threshold of this animal was located at 75 dB pSPL. b) BAEPs recorded in a Black hooded rat with an individual hearing threshold of 35 dB pSPL.

The individual hearing thresholds of Black hooded rats are shown in Table 1. They exhibited a grand mean hearing threshold of 38 dB pSPL (SD = 3). Lister hooded rats, on the contrary, possessed a higher grand mean hearing threshold of 80 dB pSPL (SD = 4). The individual hearing thresholds are listed Table 2.

Table 1: Hearing thresholds of Black hooded rats. The individual hearing threshold of each ear is listed for the first and the second recording. Pooling of all values shows that Black hooded rats exhibited a grand mean hearing threshold of 38 dB pSPL (SD = 3).

Rat	Ear	1. Recording*	2. Recording*	Mean
R1J	left	35	35	35
	right	35	35	35
R2J	left	35	35	35
	right	45	35	40
R3J	left	45	35	40
	right	45	45	45
R4J	left	35	45	40
	right	35	35	35
R5J	left	45	35	40
	right	35	35	35
R6J	left	45	35	40
	right	35	35	35
* values are given in dB pSPL			**Grand mean**	38
			SD	3

Table 2: Hearing thresholds of Lister hooded rats. The individual hearing threshold of each ear is listed for two recordings. Lister hooded rats exhibited a grand mean hearing threshold of 80 dB pSPL (SD = 4).

Rat	Ear	1. Recording*	2. Recording*	Mean
R1H	left	85	75	80
	right	85	85	85
R2H	left	75	75	75
	right	75	75	75
R3H	left	85	85	85
	right	85	85	85
R4H	left	75	75	75
	right	85	85	85
R5H	left	75	85	80
	right	75	75	75
R6H	left	85	75	80
	right	85	75	80
* values are given in dB pSPL			**Grand mean**	80
			SD	4

Statistical comparison of the two rat strains with a two way mixed design ANOVA on ranks (factors: ear, strain) revealed a significant main effect of factor "strain" on the hearing threshold ($F(1,10) = 66.207$, $p < 0.001$, with significantly higher hearing thresholds in Lister hooded rats), but no main effect of factor "ear" ($F(1,10) = 0$, $p = 1$). The lack of a difference between left and right ears applies to both strains since there was no statistical interaction of the factors strain and ear ($F(1,10) = 1$, $p = 0.331$).

Due to the experimental results described above, Black hooded rats were selected to establish an audiogram. Therefore, brief tone-bursts of five different frequencies (4, 8, 16, 32 and 43 kHz) were presented. The grand mean audiogram of all animals is shown in Figure 18. The range of best hearing started at 8 kHz (37 ± 2 dB peSPL) and lasted until 32 kHz (38 ± 4 dB peSPL), whereas at 16 kHz the lowest sound pressure level (30 ± 3 dB peSPL) was needed to evoke brainstem activity.

For all further oddball experiments, bandpass-filtered stimuli of 7-9 kHz and 16-18 kHz were used.

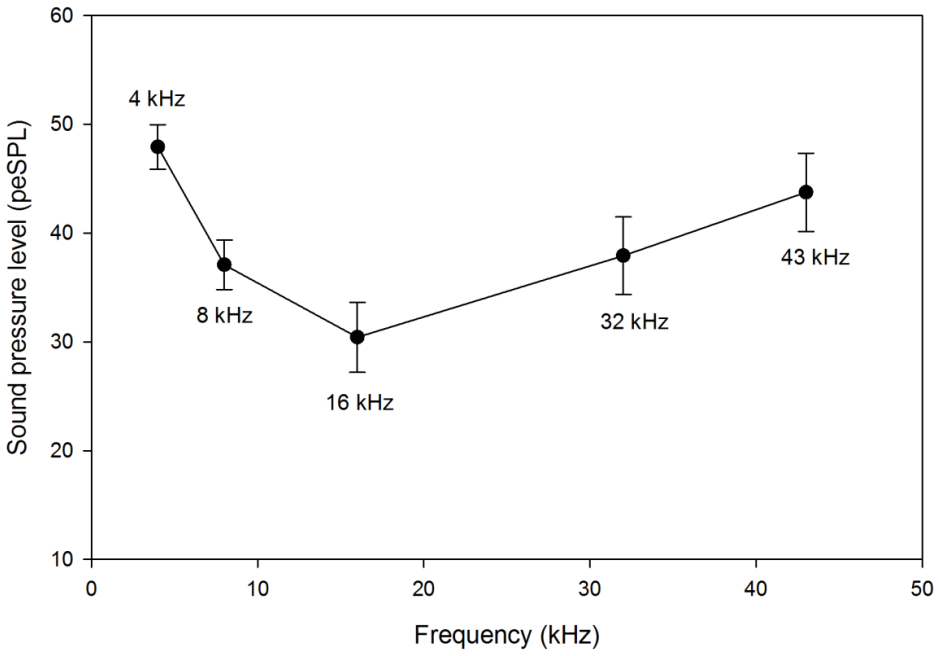

Figure 18: Audiogram of six Black Hooded rats established with tone-bursts of five different frequencies. Considering the five frequencies tested in this study, the range of best hearing starts at 8 kHz and ends at 32 kHz. Best hearing was determined for the stimulus of 16 kHz that evoked BAEPs at the lowest sound pressure level. The error bars display the standard error of the mean.

5.2 Offset responses

In an initial series of oddball experiments with four rats, stimuli of different duration were applied. The shortest stimulus was of 40 ms duration with an additional rise- and fall time of 5 ms. Afterwards, the duration of the stimuli was further increased in 10 ms steps with a rise- and fall time of 10 ms. Resulting average deviant and standard potentials are displayed in Figure 19.

Independent from stimulus duration, deviant- and standard-AEP[2] always differed. Besides stimulus-evoked activity at the beginning of the stimulus (onset-response) an offset-response was elicited. The first obvious difference between standard- and deviant-AEP affected the latency range of the first negative peak (N1) of the onset response. A second difference component in the latency range of 60 to 130 ms was observed after offset-response for short stimuli (up to 80 ms stimulus duration). The latter difference component increased in amplitude whenever longer stimuli were presented (starting at a stimulus duration of around 100 ms).

These pilot experiments lead us to choose stimuli of 120 ms duration (including 10 ms ramp) for all further experiments to induce a maximum difference between standard and deviant response, which emerges in the gap between on- and offset response.

[2] Deviant- and standard-AEP were calculated as the averaged potentials evoked by the high (16-18 kHz) and low (7-9 kHz) stimulus used once as standard and once as deviant in two consecutive blocks ("flip-flop" oddball paradigm)

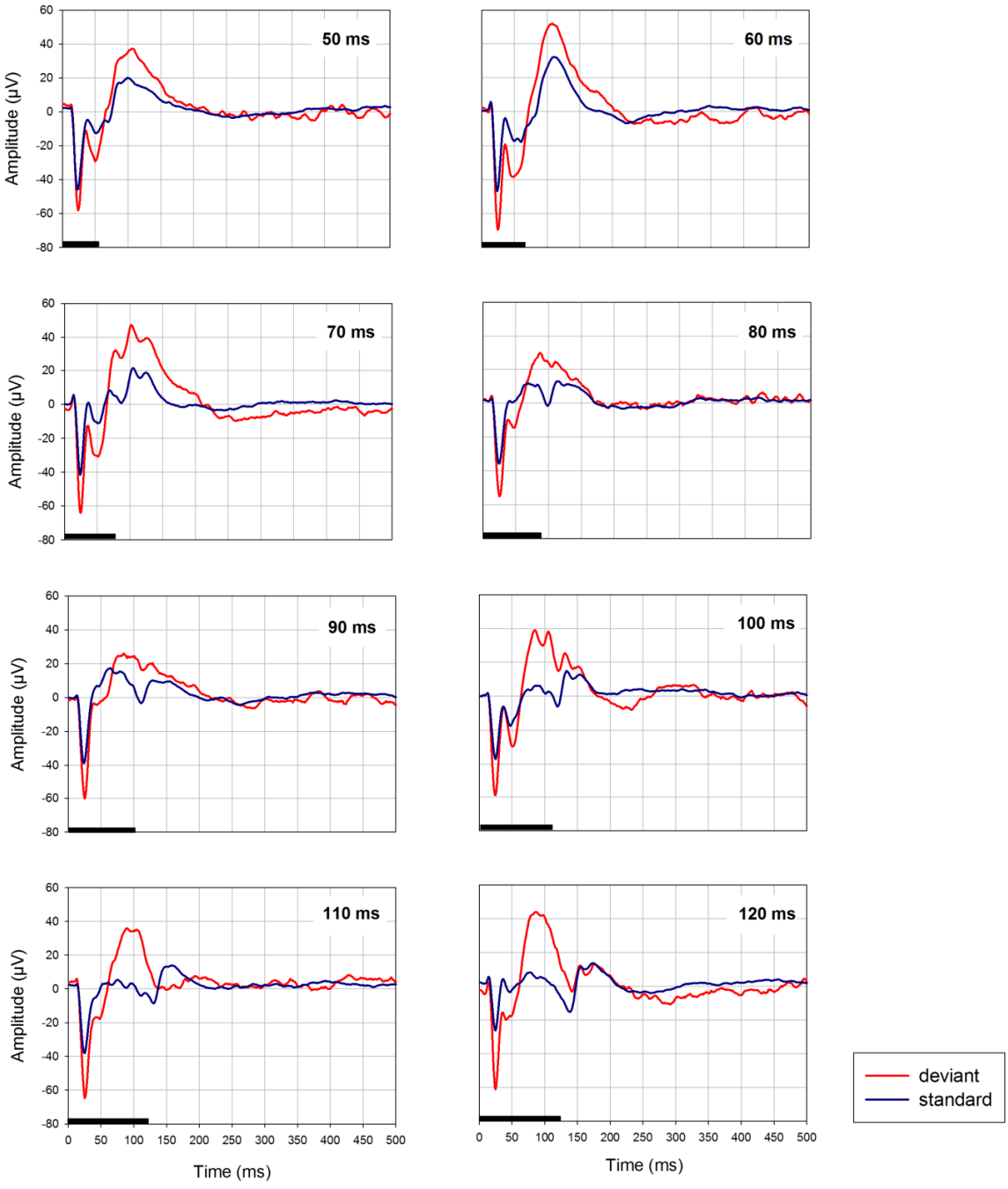

Figure 19: Oddball paradigm with stimuli of eight different durations (electrode PAF right only). Deviant potentials are depicted in red, standard potentials in blue. The upper left graph shows potentials elicited with stimuli of 50 ms length (including 5 ms rise- and fall time). Subsequently, the stimulus duration was increased in 10 ms steps (including 10 ms rise- and fall time). The difference between standard and deviant potentials increased with increasing stimulus duration. The black bar on the x-axis represents the stimulus, whereas the stimulus duration is depicted in the upper right corner of each graph.

5.3 Auditory evoked responses

Subsequent to the choice of the rat strain most suitable for the acoustic experiments and the decision for the best frequency and duration of the stimuli, animals were stimulated with a homogenous sequence of stimuli using the high (16-18 kHz) and the low (7-9 kHz) frequency stimulus in two consecutive trials.

Comparison of the elicited potentials across five different recording sessions revealed a change in potential waveforms from the first to the second recording. In subsequent sessions, however, the shape of the waveforms remained stable. This applied for the low (Figure 20) as well as the high (Figure 21) frequency stimulus.

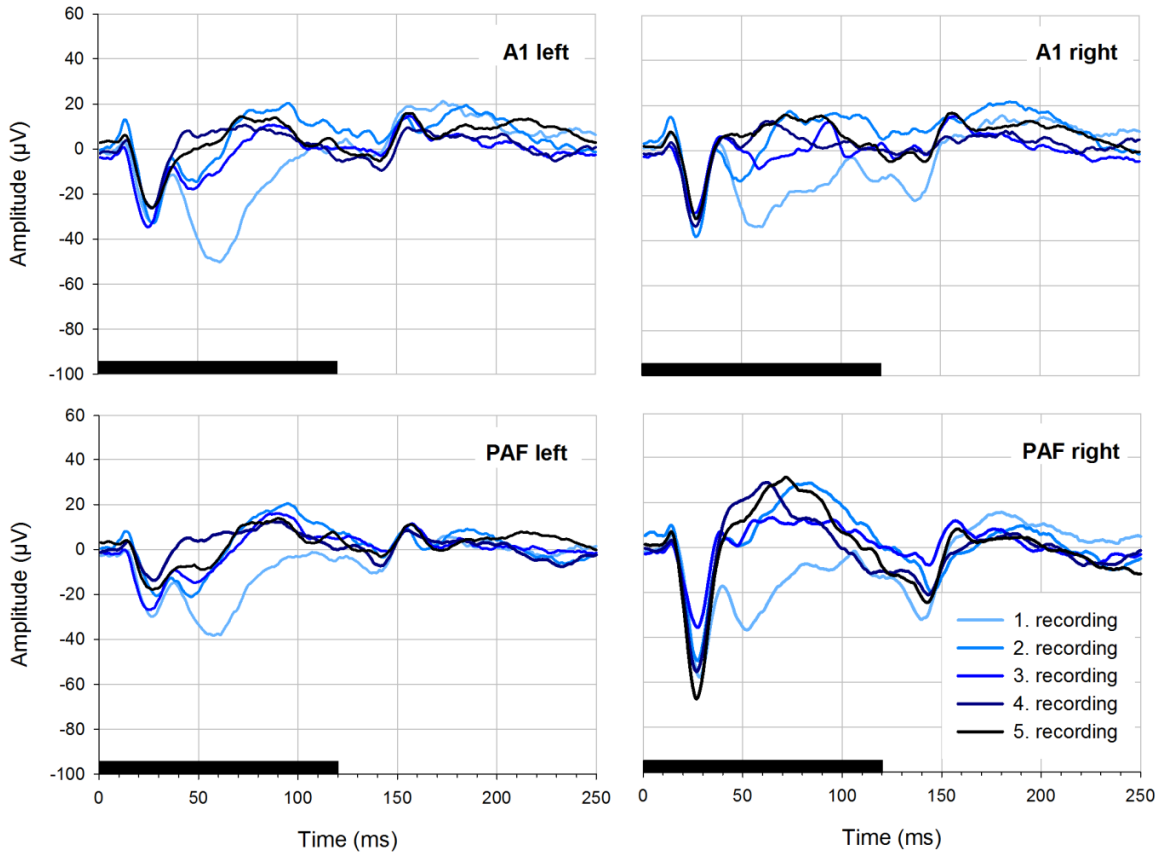

Figure 20: Grand averaged (n = 9) AEPs elicited with an acoustic stimulus of 7-9 kHz in five recording sessions. Changes in the waveforms from the first to the second recording session became apparent in AEPs. After the second recording, the waveform remained stable. The black bar on the x-axis represents the stimulus duration, and the position of the recording electrode is displayed in the upper right corner of each graph.

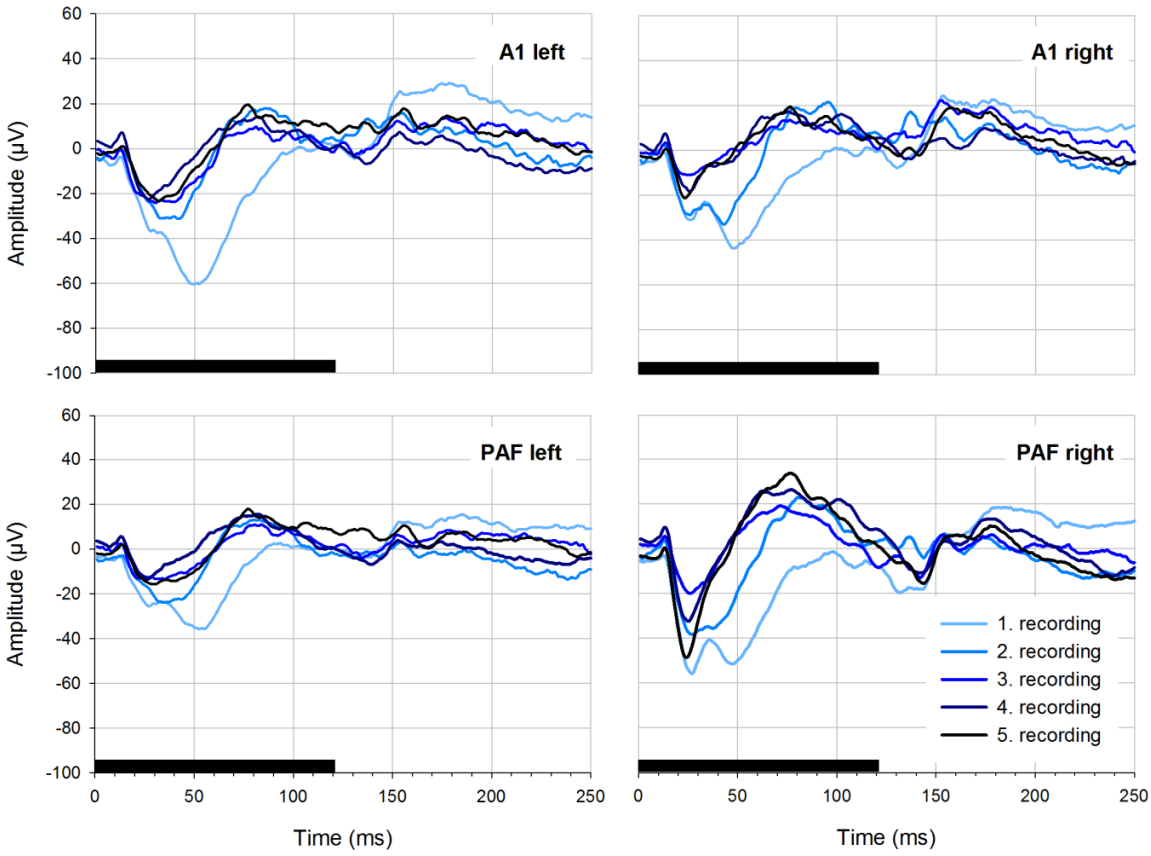

Figure 21: Grand averaged (n = 9) AEPs elicited with an acoustic stimulus of 16-18 kHz in five recording sessions. From the AEPs it became evident that there were changes in the waveforms from the first to the second recording session. After the second recording, the waveform remained stable. The black bar on the x-axis represents the stimulus duration, and the position of the recording electrode is displayed in the upper right corner of each graph.

Due to the remarkable waveform changes, data of the first recording session were discarded and not further analyzed in all subsequent experiments.

For a closer inspection of cortial AEPs elicited with the two different stimuli (7-9 kHz, 16-18 kHz) the potentials were averaged across the 2nd to 5th recording sessions. Potentials invariably consisted of an onset response comprising a fast, small positive peak around 13 ms and a fast large negative deflection around 26 ms (Figure 22). This was followed by a slow positive deflection that started around 50 ms and was finally terminated by the offset response around 140 ms. The offset response itself consisted of a fast negative deflection that continued with a slower positive deflection. In addition, small differences between the potentials evoked by the low and the high frequency stimulus became evident: potentials elicited with 7-9 kHz exihibted a larger amplitude N1-peak with a rapidly descending slope. The N1-peak in potentials evoked with 16-18 kHz, on the contrary, was smaller in amplitude and decayed more slowly. Amplitudes of the positive peaks P1 and P2 were nearly similar in both AEPs.

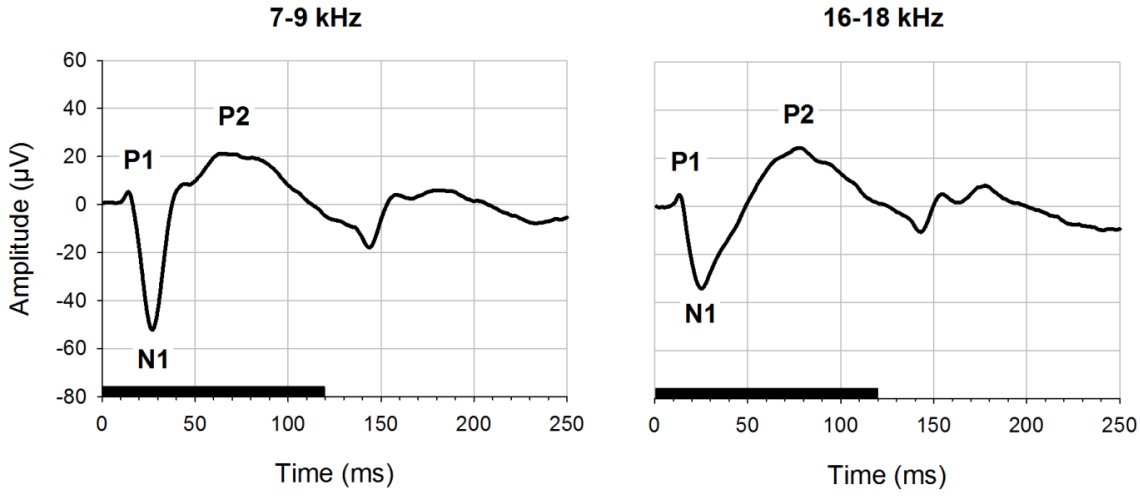

Figure 22: AEPs elicited with 7-9 kHz and 16-18 kHz. Potentials elicited with the low frequency stimulus are displayed on the left, potentials elicited with the high frequency stimulus on the right. The averages are derived from four recording sessions. The most prominent peaks are labeled according to their order of occurrence and polarity (P1, N1, P2). The black bar on the x-axis shows the stimulus duration.

6 Discussion preliminary studies

The preliminary studies were conducted in order to assess the optimal experimental conditions for evoking AEPs and mismatch responses in awake rats. In the following, the steps leading to the chosen rat strain and experimental procedure will be discussed.

6.1 Brainstem audiometry

6.1.1 Hearing thresholds

The experimental setup for recording BAEPs in rats was developed to counteract serious difficulties with recording of cortical auditory evoked activity in awake rats, which occurred at the beginning of the study.

One reason might have been the fact that implantation of silverball electrodes posed a challenge because most of the temporal muscle had to be preserved in order to maintain the rats' ability to chew their food. Managing the implantation under spatial constraints became easier with practice, so that finally in most animals all four electrodes were functional. However, the crucial step for successful recordings was the change of the rat strain after the severe hearing impairments of Lister hooded rats were discovered.

Black hooded rats exhibited a mean hearing threshold of 38 dB pSPL. This is well in the range of the values reported for other strains, e.g. Wistar, Fisher 344, Long Evans (Brandt-Lassen *et al.*, 2000; Popelar *et al.*, 2006). Lister hooded rats on the contrary exhibited mean hearing thresholds of 80 dB pSPL. Click stimuli for evoking brainstem activity had to be measured as dB pSPL (peak sound pressure level) due to their very brief duration. A direct conversion from dB pSPL to dB SPL (with short time weighting), however, is not possible. Furthermore, click stimuli comprised a broad range of frequencies while the frequencies applied in the oddball paradigms were filtered in a small frequency band. Although the acoustic stimuli used in the oddball paradigms cannot be directly compared to click stimuli due to the above mentioned reasons it is conceivable that Lister hooded rats did not perceive the stimuli (75 dB SPL) at all. However, using Black hooded rats assured that all acoustic stimuli applied throughout the experiments were well above the hearing thresholds of the subjects.

6.1.2 Audiogram of Black hooded rats

Six Black hooded rats were used to establish an audiogram for the specific strain. Hearing thresholds determined with tone burst stimuli comply well with other studies. Compared to Fisher 344 (Popelar *et al.*, 2003; Popelar *et al.*, 2006; Bielefeld *et al.*, 2008) and Long Evans (Popelar *et al.*, 2006) rats, the minimum of the u-shaped curve designating best hearing was shifted slightly to lower frequencies. For Black hooded rats, the range of best hearing was between 8 and 32 kHz, and exhibited its lowest threshold at 16 kHz, whereas best hearing of the strains mentioned above was reported to be located between 8 and 16 kHz (Popelar *et al.*, 2006). The inter-individual differences were found to be very small in the tested subjects.

According to the audiogram of Black hooded rats, 7-9 and 16-18 kHz stimuli were chosen for the oddball experiments. A further increase in stimulus frequency was avoided due to practical reasons: stimulus frequencies below 20 kHz can be perceived by the human ear, therefore the experimenter was always able to monitor the acoustic stimulus presentation. We chose bandpass-filtered noise stimuli over sine tones because the neurons in the auditory cortex adapt rapidly to pure tone stimulation and we wanted to ensure the largest possible response amplitude over time.

6.2 Offset responses

Oddball studies in rats are usually done with stimuli of 50 ms duration (Ruusuvirta *et al.*, 1998; Astikainen *et al.*, 2006; Tikhonravov *et al.*, 2008; Tikhonravov *et al.*, 2010; Astikainen *et al.*, 2011). However, in the preliminary experiments, the use of longer stimulus durations resulted in larger amplitude differences between deviant and standard-AEP. This was mainly due to the latency range of the offset response that was located after the late difference component when longer stimuli where used.

Auditory evoked offset responses have been previously detected throughout the auditory pathway, in the brainstem of mice (Henry, 1985), the inferior colliculus of bats (Casseday *et al.*, 1994) and the auditory cortex of rats (Takahashi *et al.*, 2004) and cats (He *et al.*, 1997). Single unit studies have shown that about 10-30 % of neurons in the auditory

pathway are responsive to the termination of an acoustic stimulus (as summarized by Takahashi *et al.* (2004)). Those neurons are named off-neurons and are important for perception of sound durations.

With respect to the present study, it is conceivable that the response of specific off-neurons in the latency range of mismatch components would superimpose or modify MMN-like potentials. After presenting longer stimuli in the oddball paradigm, the difference between standard and deviant potential was located between the on- and the offset response. For our main experiments we therefore chose stimulus durations of 120 ms stimuli (100 ms plus 10 ms ramp).

6.3 AEPs in five subsequent recordings

AEPs elicited with the chosen stimuli of 120 ms with carrier frequencies of 7-9 kHz and 16-18 kHz presented in a homogenous sequence of sounds, revealed differences with respect to the stimulus waveform between five subsequent recordings conducted on different days. The potentials recorded in the first session differed from all other measurements. In this first session, the rats were exposed to the acoustic stimulation for the first time or, in other words, the first session corresponds to the habituation phase of the animals to the experimental setup and the acoustic stimuli. Due to that reason, there may be several factors influencing the evoked responses on the first day of recording that cannot be controlled.

Learning induced neuronal plasticity in primary and secondary sensory cortices has been shown to be a common phenomenon. In primates (Recanzone *et al.*, 1993) and rats (Rutkowski & Weinberger, 2005; Polley *et al.*, 2006), for example, an expansion of frequency maps in the primary cortex develops in response to learned acoustic stimuli during operant training. Moreover, it was shown that the learning induced expansion of the sound representation was correlated with the behavioral importance of a stimulus (Rutkowski & Weinberger, 2005). In the present study, animals did not need to respond to the auditory stimulation but were listening passively. As a consequence, it can be hypothesized that a potential change in receptive field size corresponding to the employed frequencies that may have occurred would be rather small.

However, with regard to AEP waveforms recorded with epidural electrodes, a large negative deflection present in the first but not subsequent recording sessions was observed. This finding may be due to effects of attention and/ or arousal that may have been present in the first recording session and decreased with habituation to the stimulation. Visually evoked potentials in humans have been shown to exhibit larger amplitudes when the overall arousal level of the subjects was high (stimulus combined with the threat of a shock; Eason *et al.* (1969)). Furthermore, attending an auditory stimulation in order to detect an occasional softer stimulus was shown to enhance human auditory peaks (N1, P2, Picton & Hillyard (1974)).

Due to these findings, all data from the habituation phase were omitted and not further analyzed.

6.4 AEPs in awake rats

In awake rats, AEPs invariably consisted of an onset response comprising a fast, small positive peak (P1) around 13 ms and a fast large negative deflection (N1) around 26 ms. Cortical AEPs in ketamine-xylazine anesthetized rats consisted of a fast positive-negative deflection followed by a slower positive-negative wave (Barth & Di, 1990). In the latter study, P1 emerged with an approximate latency of 15-20 ms after stimulus onset. The slightly earlier occurrence of the P1-peak in our study can be explained with the effect of anesthesia in other studies or differences in the physical stimulus features. The P1-peak is likely to reflect the depolarization of supragranular pyramidal neurons in the auditory cortex following direct afferent input from the ventral division of the medial geniculate body (MGB). The subsequent N1-peak exhibits a latency of 25-30 ms (Barth & Di, 1990), which is well in line with the findings in the present thesis. The P1/N1-complex is presumably generated directly inside the auditory cortex because lesion studies of the auditory cortex conducted in cats affected both potential components (Kaga *et al.*, 1980). Moreover, electrical stimulation of the MGB evoked the potential complex within the auditory cortex, suggesting thalamo-cortical input to be responsible for its generation (Barth & Di, 1990; Di & Barth, 1992).

In the present study, the fast onset response was followed by a slow positive deflection, the P2-peak that started around 50 ms and was finally terminated by the offset response at 140 ms. Barth & Di (1990) reported a latency of 50-60 ms for the P2-peakBarth & Di (1990). It may emerge from two distinct processes: (1) repolarization of the neurons that were excited during P1 and N1 generation and (2) depolarization after thalamo-cortical input arising from the MGm, whereby activities from supra- and infragranular neurons overlap. It has been proposed that P1 and N1 are generated by stimulus-specific thalamo-cortical inputs while later components are generated by non-specific thalamo-cortical inputs and cortico-cortical connections (Hall & Borbely, 1970; Shaw, 1988).

The offset response also consisted of a fast negative deflection that continued with a slower positive deflection. Offset responses comparable to the ones detected in the present study have been previously described by Takahashi *et al.* (2004) (*cf.* 6.2). They have been shown to exhibit little tonotopy and the neuronal sources seem to differ slightly from the onset sources. This resembles also results of human studies (Hari *et al.*, 1987).

With respect to the AEPs elicited with the two different frequencies in the present study, small differences between the potentials were observable: potentials elicited with 7-9 kHz exihibt a larger amplitude N1-peak with a rapidly descending slope. The N1-peak in potentials evoked with 16-18 kHz, on the contrary, was smaller in amplitude but decayed more slowly. Amplitudes of the positive peaks P1 and P2 are nearly similar in both AEPs. Due to frequency specific differences in AEPs, a “flip-flop” oddball paradigm (*cf.* 4.7.1) was employed in order to control for frequency specific effects.

6.5 Conclusion

Black hooded rats were shown to be suitable for acoustic experiments due to their low hearing threshold as compared to Lister hooded rats. With the chosen strain it was possible to record AEPs in awake rats. Stimuli of 120 ms duration with the frequencies 7-9 kHz and 16-18 kHz fit the rats hearing range and evoke large amplitude, long lasting

differences between standard and deviant potentials in an oddball paradigm. In addition, it was demonstrated that it is crucial to habituate the animals to the experimental setup and acoustic stimulation in order to obtain stable AEP recordings.

After the preliminary studies were completed and the optimal rat strain and acoustic stimulation identified, the main oddball experiments were conducted.

7 Results mismatch responses

Human studies demonstrated that the amplitude of MMN potentials depends on the probability of the deviant stimulus: the MMN increases with decreasing deviant probability. Therefore, two different oddball paradigms were applied: a high (0.2) and a low (0.1) deviant probability condition. At first, the results of the high deviant probability condition (0.2) will be presented.

7.1 Deviant probability 0.2

Figure 23 shows the grand average results of the four recording electrodes. AEPs recorded in an oddball paradigm comprising deviant probability 0.2 again exhibited obligatory peaks P1, N1 and P2. Furthermore, a pronounced offset response was observed. After the N1 peak, there was a small deflection towards positive voltage values around 40 ms observable that was terminated by a negative deflection (N2) around 50 ms.

The waveforms of standard and deviant potentials were compared with a point-by-point analysis using Wilcoxon Signed Rank Tests for every data point from 0 to 250 ms after stimulus presentation. The resulting p-values were corrected for multiple comparisons using the false discovery rate (FDR) and are displayed below each graph. Significant differences between standard and deviant potentials were found in all four electrodes. Notably, the difference components invariably split into an early and a late significant distinction. The corresponding latency values of significantly different time periods are summarized in Table 3.

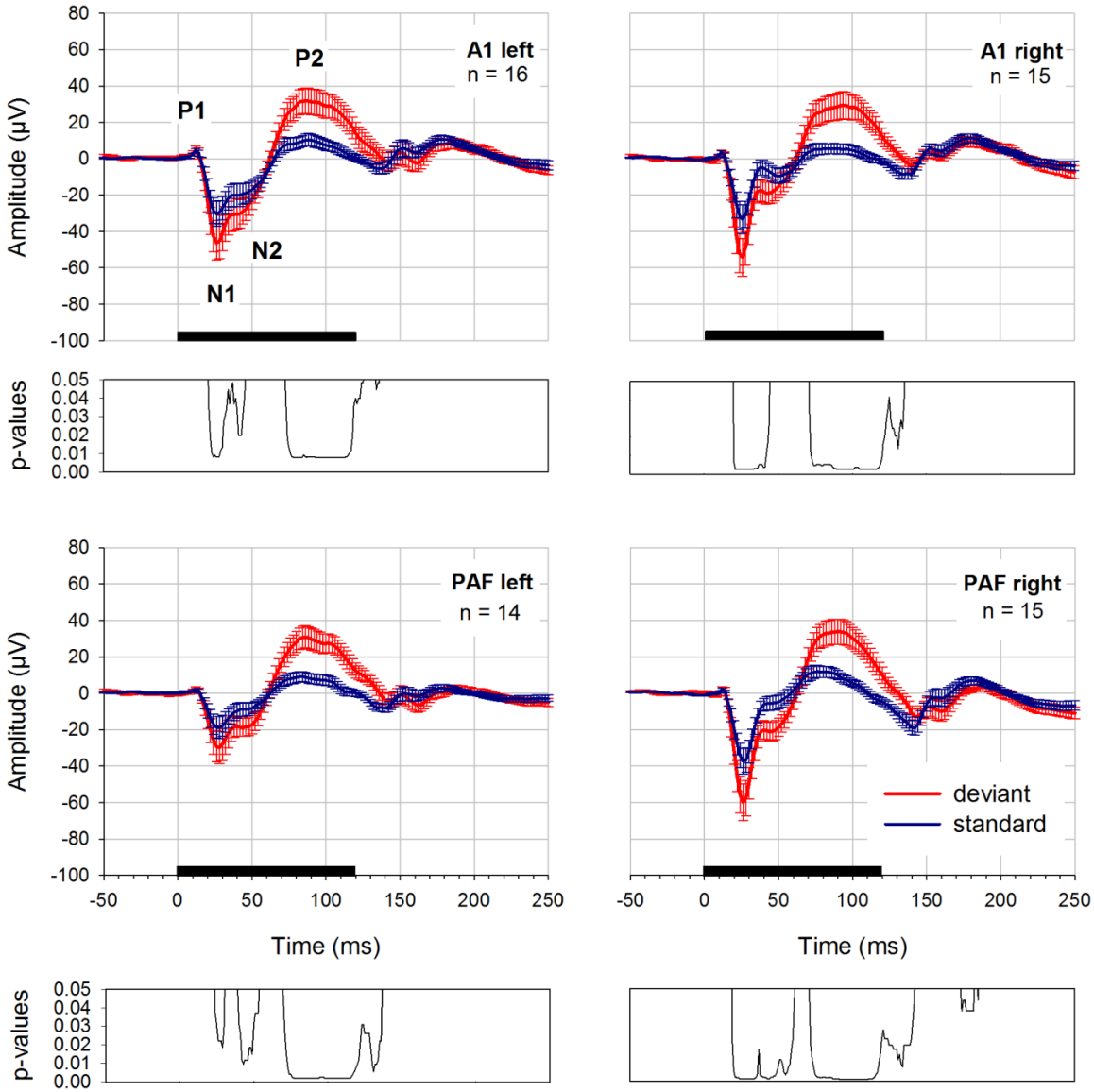

Figure 23: Potentials evoked with an oddball paradigm of deviant probability 0.2. Significant differences between standard (blue curve) and deviant potentials (red curve) were found in all four electrodes. FDR-corrected p-values that indicate significant differences between both potentials are displayed below each graph. The black bar on the x-axis represents the stimulus, whereas the error bars designate the standard error of the mean. The position of the recording electrode and the number of electrodes that was averaged for displaying AEPs are depicted in the upper right corner of each graph.

Table 3: Significant differences between standard and deviant deflections for deviant probability 0.2. The respective latency values and corresponding largest and smallest W-and p-values (FDR-corrected) as well as degrees of freedom are given for each time interval separately for the four recording electrodes.

Electrode	Latency range (in ms)	W-values	df	p-values
A1 left	21-46	4 < W < 21	15	0.04 < p < 0.044
	71-128	0 < W < 22	15	0.007 < p <0.049
	133-136	19 < W < 22	15	0.007 < p < 0.049
A1 right	20-44	0 < W < 15	14	0.002 < p < 0.024
	71-135	1 < W < 19	14	0.002 < p < 0.018
PAF left	24-30	9 < W < 13	13	0.016 < p < 0.031
	38-54	6 < W < 15	13	0.008 < p < 0.045
	69-136	0 < W < 15	13	0.002 < p < 0.045
PAF right	19-62	1 < W < 21	14	0.001 < p < 0.049
	71-142	0 < W < 20	14	0.001 < p < 0.043
	172-185	18 < W < 21	14	0.032 < p < 0.049

In addition to differences between standard and deviant potentials with respect to their potential amplitude, latencies of the most prominent peaks were analyzed. The latencies of the first negative peak (N1) are displayed in Figure 24. Standard potentials exhibited latencies of 29 ms (SD = 8, A1 left), 25 ms (SD = 5, A1 right), 28 ms (SD = 7, PAF left) and 27 ms (SD = 5, PAF right). Deviant potentials exhibited the following N1-latencies: 28 ms (SD = 7, A1 left), 26 ms (SD = 4, A1 right), 26 ms (SD = 7, PAF left) and 26 ms (SD = 6, PAF right).

A two-way repeated measures ANOVA on ranks (factors: stimulus type, electrode) showed that the latency of the N1-peak was independent of stimulus type ($F(1,33) = 1.8$, $p = 0.208$) and electrode ($F(3,33) = 0.1$, $p = 0.96$) and there was no interaction between the factors ($F(3,33) = 0.4$, $p = 0.775$).

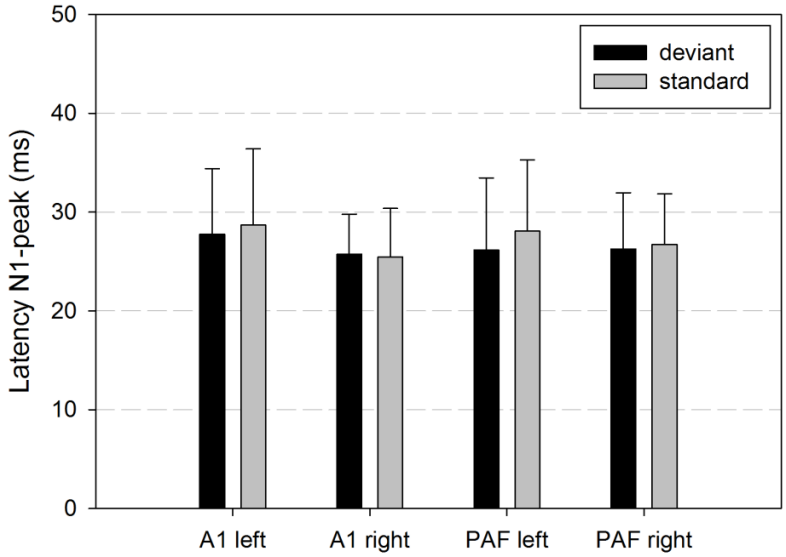

Figure 24: Latency values of the first negative peak (N1) of deviant and standard potentials in the 0.2 deviant probability condition. There were no significant differences between the latency values. The position of the recording electrode was not influencing the latency of the N1-peak. The displayed error bars designate the standard deviation.

For standard potentials, the latency values of the P2-peak were: 88 ms (SD = 22; A1 left), 80 ms (SD = 28; A1 right), 82 ms (SD = 15; PAF left) and 74 ms (SD = 20; PAF right), whereas for deviant potentials latencies of 91 ms (SD = 16 ms; A1 left), 93 ms (SD = 20; A1 right), 88 ms (SD = 19; PAF left) and 87 ms (SD = 17; PAF right) were measured. The respective results are displayed in Figure 25.

Statistical analysis (two-way repeated measures ANOVA on ranks (factors: stimulus type, electrode)) revealed a significant main effect of stimulus type ($F(1,33) = 6.7$, $p = 0.025$) and electrodes ($F(3,33) = 3.9$, $p = 0.018$). Post hoc test Holm-Sidak illustrates that standard potentials had significantly shorter P2-latencies compared to deviant potentials ($p = 0.025$). In addition, potentials recorded above A1 on the left hemisphere exhibited significantly longer latencies compared to electrodes above PAF in the right ($p = 0.002$) hemisphere.

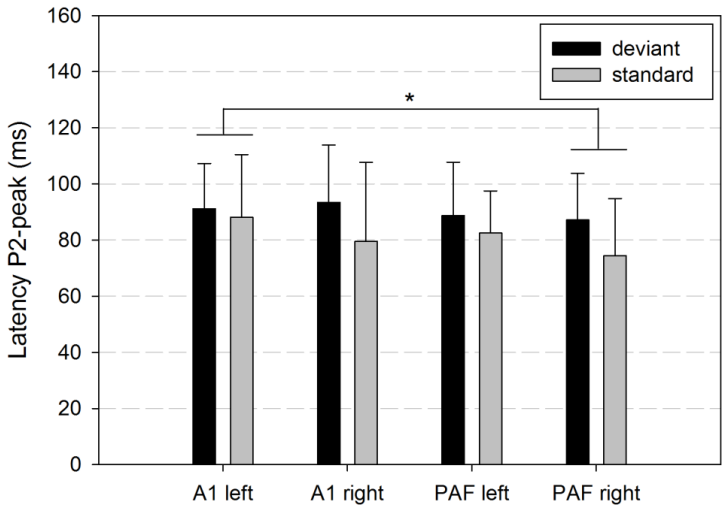

Figure 25: Latency values of the second positive peak (P2) of deviant and standard potentials in the 0.2 deviant probability condition. The position of the recording electrode and the stimulus type significantly influenced the latency of the P2-peak. Latencies of the potentials recorded from A1 left were significantly longer compared to PAF right. Furthermore, standard potentials exhibited shorter latencies than deviants with respect to the P2-peak.

7.2 Deviant probability 0.1

In Figure 26 the results of the oddball experiment with 0.1 deviant probability are displayed. Significant differences between standard and deviant potentials were again found in all four electrodes. Once more, the difference components were split up into an early difference and a late difference, which is explicitly visualized in the graph showing the FDR-corrected p-values. The corresponding latencies, W- and p-values are listed in Table 4.

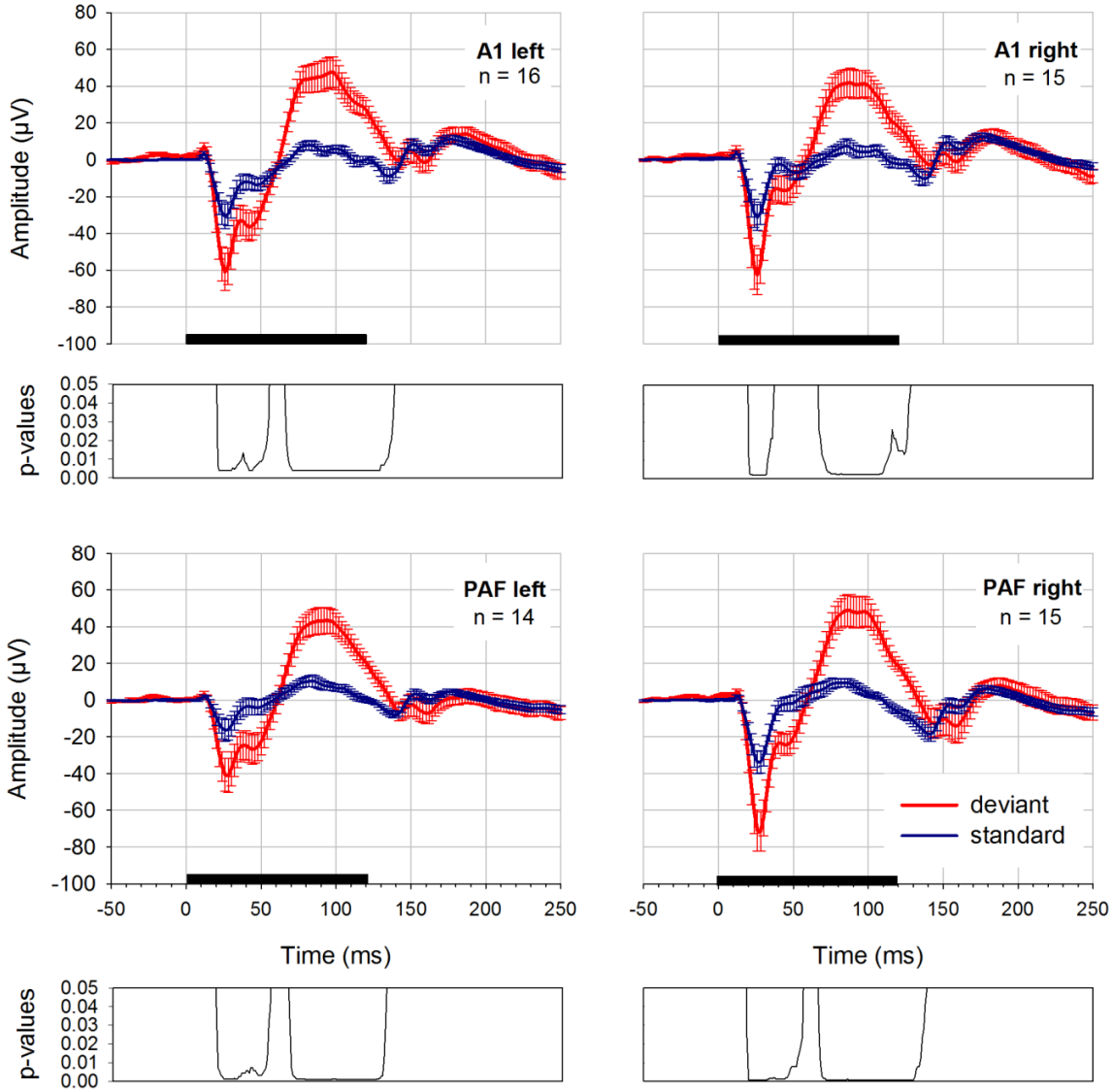

Figure 26: Potentials evoked with an oddball paradigm of deviant probability 0.1. Significant differences between standard (blue curve) and deviant potentials (red curve) were found in all four electrodes. FDR-corrected p-values that indicate significant differences between both potentials are displayed below each graph. The black bar on the x-axis represents the stimulus, whereas the error bars designate the standard error of the mean. The position of the recording electrode and the number of electrodes that was averaged for displaying AEPs is depicted in the upper right corner of each graph.

Table 4: Significant differences between standard and deviant deflections for deviant probability 0.1. The respective latency values and corresponding largest and smallest W-and p-values as well as degrees of freedom are given for each time interval separately for the four recording electrodes.

Electrode	Latency range (in ms)	W-values	df	p-values
A1 left	20-54	1 < W < 19	15	0.003 < p < 0.026
	65-138	1 < W < 22	15	0.003 < p < 0.04
A1 right	20-38	0 < W < 18	14	0.002 < p < 0.046
	67-129	3 < W < 18	14	0.002 < p < 0.046
PAF left	19-55	1 < W < 14	13	0.001 < p < 0.049
	67-133	0 < W < 16	13	0.001 < p < 0.049
PAF right	19-56	1 < W < 15	14	0.001 < p < 0.02
	67-140	0 < W < 20	14	0.001 < p < 0.048

In standard potentials, latencies for the N1-peak were 26 ms (SD = 7, A1 left), 27 ms (SD = 5, A1 right), 26 ms (SD = 8, PAF left) and 28 ms (SD = 5, PAF right). Deviant potentials exhibited the following N1-latencies: 27 ms (SD = 6, A1 left), 27 ms (SD = 3, A1 right), 26 ms (SD = 7, PAF left) and 28 ms (SD = 2, PAF right). The results are summarized in Figure 27.

For comparison of the N1-peak latency of deviant and standard potentials in the lower deviant probability condition, a two-way repeated measures ANOVA on ranks (factors: stimulus type, electrode) was performed. Neither the stimulus type ($F(1,33)$ 0.6, $p = 0.447$) nor the recording electrode ($F(3,33) = 2.7$, $p = 0.063$) had an influence on the latency of the N1-peak. Furthermore, there was no interaction between both factors ($F(3,33) = 0.4$, $p = 0.753$).

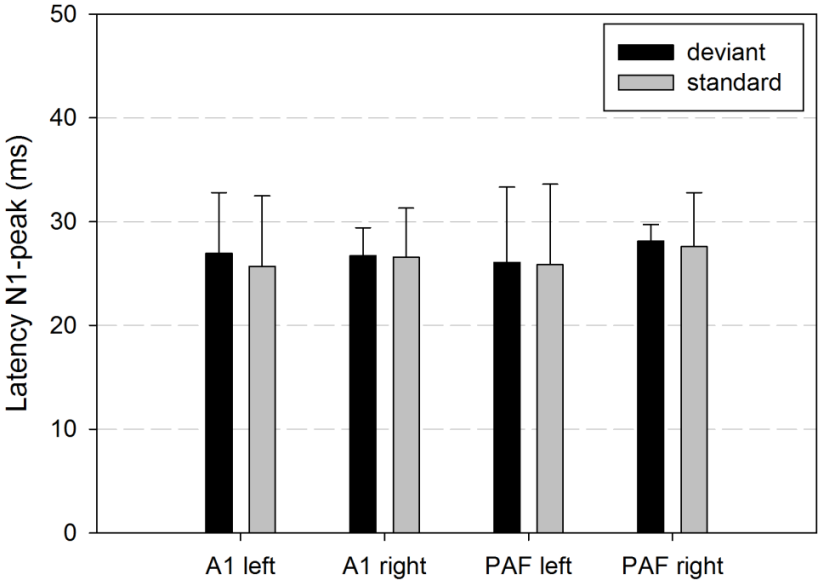

Figure 27: Latency of the first negative peak (N1) in the 0.1 probability condition. There were no significant differences between the latency values of the four electrodes and the different stimulus types (standard, deviant). The displayed error bars designate the standard deviation.

For standard potentials, the latency values of the P2-peak were detected as 84 ms (SD = 20; A1 left), 78 ms (SD = 30; A1 right), 83 ms (SD = 21; PAF left) and 74 ms (SD = 23; PAF right). Latencies of deviant potentials were 89 ms (SD = 18 ms; A1 left), 89 ms (SD = 21; A1 right), 89 ms (SD = 18; PAF left) and 87 ms (SD = 11; PAF right).

The latency of the P2-peak was again compared using a two-way repeated measures ANOVA on ranks (factors: stimulus type, electrode). There was no effect of stimulus type ($F(1,33) = 4$, $p = 0.072$) or recording electrode ($F(3,33) = 0.7$, $p = 0.552$). Furthermore, there was no interaction between the factors ($F(3,33) = 0.1$, $p = 0.968$). The latency of the P2-peak is depicted in Figure 28.

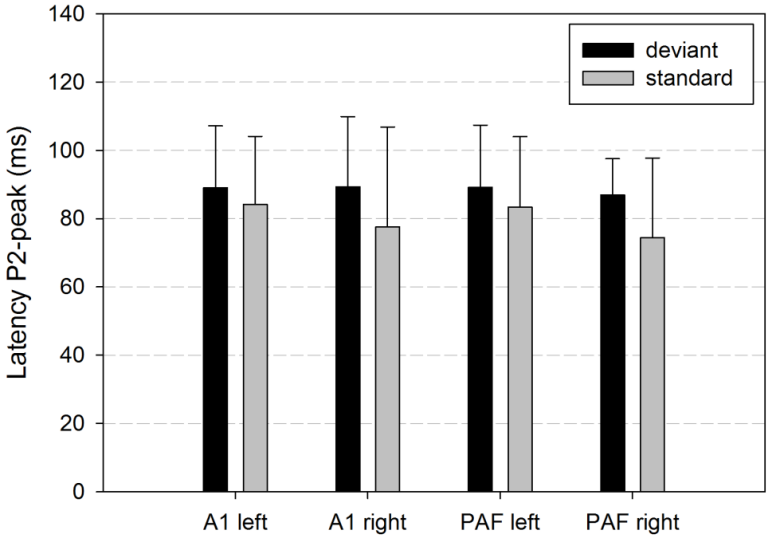

Figure 28: Latency of the second positive peak (P2) in the 0.1 probability condition. There were no significant differences between the latencies of deviant and standard potentials. The position of the recording electrode did not influence the latency of the P2-peak. The displayed error bars designate the standard deviation.

7.3 Comparison of the two deviant probabilities

The mismatch negativity, however, is procedurally defined as the difference between standard and deviant potentials. Subtracting standard from deviant potential led to difference waveforms consisting of an early negative and a later positive component (Figure 29). The resulting difference waves for 0.1 and 0.2 deviant probability were compared with Wilcoxon Signed Rank Tests for corresponding sample points. Significant differences occurred in three of four recording electrodes (A1 left, A1 right and PAF left). In the lower deviant probability condition mismatch negativity-like responses invariably exhibited larger amplitudes than in the higher probability condition.

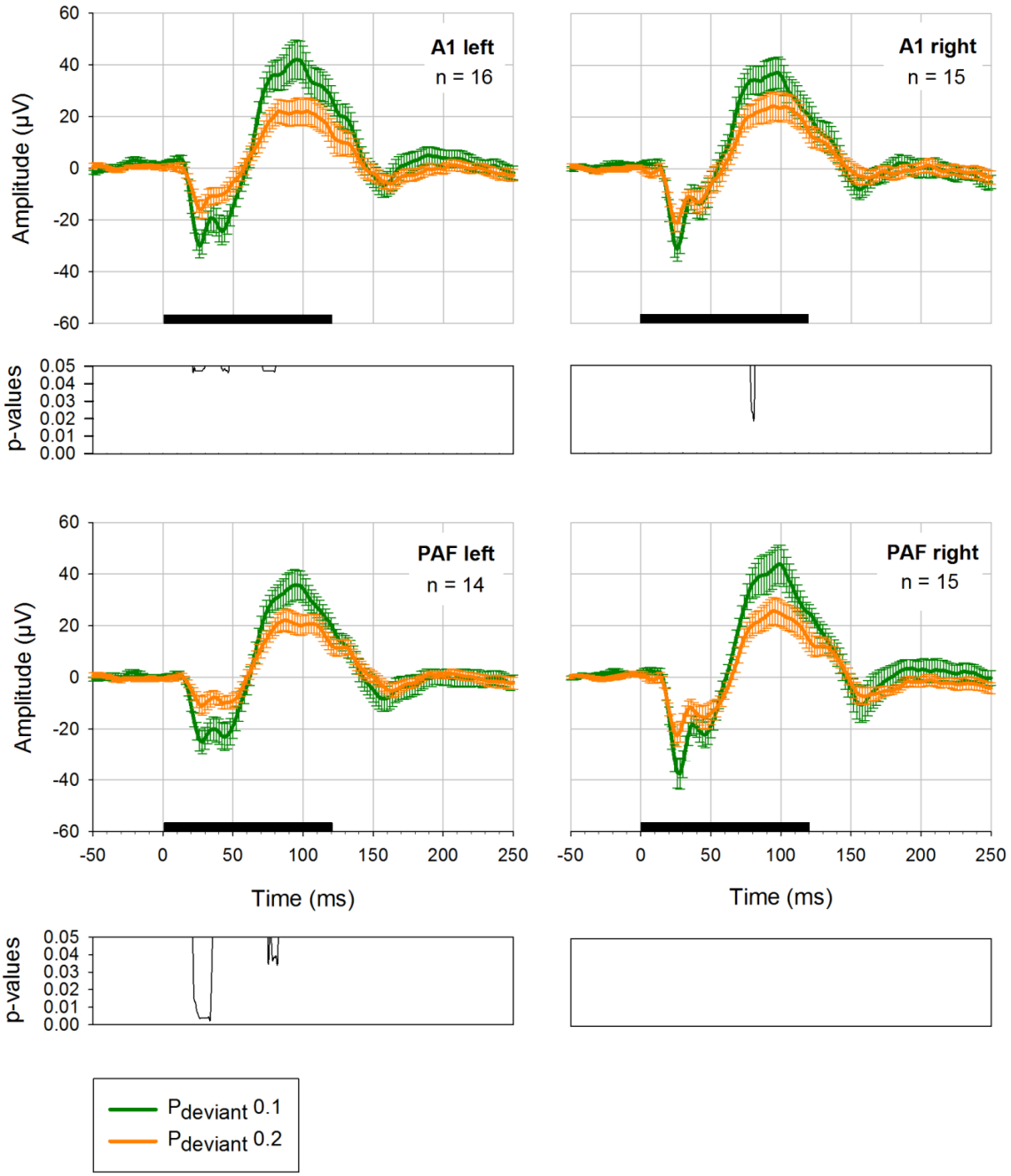

Figure 29: Mismatch responses displayed as difference waveforms for the two probability conditions. Difference waveforms, calculated as "deviant minus standard" potential, are displayed for all electrodes. In three electrodes (A1 left, A1 right and PAF left), waveforms elicited in the lower probability condition (green curve) were significantly larger than those obtained from the deviant 0.2 condition (orange curve). The black bar on the x-axis shows the stimulus duration whereas the position of the recording electrode and the number of electrodes that was averaged for displaying AEPs is depicted in the upper right corner of each graph. Below each graph FDR-corrected p-values are shown.

As displayed in Figure 30 there was no difference between the standard AEPs evoked in the two distinct probability conditions.

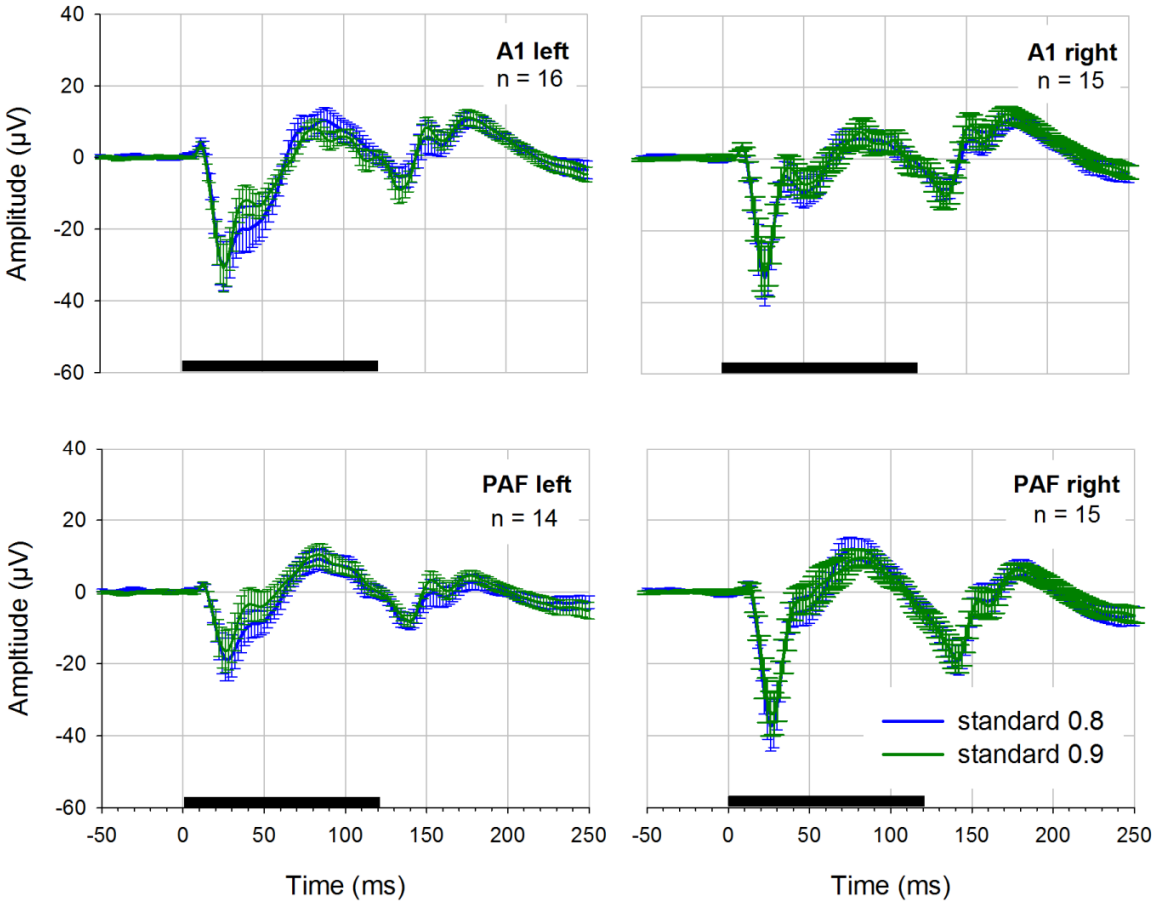

Figure 30: Standard potentials in the two probability conditions. Standards elicited in the high deviant probability (0.2) oddball paradigm are displayed in blue, standards in the low deviant probability (0.1) condition in green. The black bar on the x-axis shows the stimulus duration whereas the position of the recording electrode and the number of electrodes that was averaged for displaying AEPs is depicted in the upper right corner of each graph.

8 Discussion mismatch responses

The mismatch negativity (MMN) in humans is a special component of AEPs that reflects the violation of predictable stimulus regularities, established by the previous auditory sequence (for review see Näätänen *et al.*, 2005). MMN studies in rats were so far almost exclusively conducted under anesthesia and the previous results have not provided explicit evidence whether an MMN analogue exists in rats. The present results from awake rats clearly demonstrate an MMN-like difference between the amplitudes of standard- and deviant-evoked AEPs. The following parts of this study are dedicated to discover possible underlying physiological mechanisms in order to assess whether rat MMN-like potentials can be considered as analogues of their human counterparts.

When comparing the presented results to previous rodent studies, it is important to take into account differences in the physical attributes of the acoustic stimuli, like for example carrier frequency and duration. The most important difference, however, is the effect of anesthesia. Therefore, in the present study, epidural recordings in awake rats from two auditory cortical areas in both hemispheres were conducted to avoid confounding effects of anesthetics. At first, the impact of anesthesia on MMN-like potentials in rats will be discussed by summarizing results of previous studies.

8.1 Effect of anesthesia

Fentanyl-medetomidine anesthesia was shown to change the shape of AEPs in rats and reverse the polarity of MMN-like potentials that were detected under anesthesia with an approximate latency of 67 to 120 ms after stimulus onset (Nakamura *et al.*, 2011). Under urethane anesthesia, Ruusuvirta *et al.* (1998) detected mismatch responses from 63 to 253 ms from stimulus onset. The AEP waveforms recorded under fentanyl-medetomidine (Nakamura *et al.*, 2011) and under urethane anesthesia (Ruusuvirta *et al.*, 1998) are not comparable, as the typical fast onset responses are completely absent under urethane anesthesia but preserved under fentanyl-medetomidine. Potentials evoked under urethane anesthesia exhibit a slow positive followed by a smaller slow negative component (Ruusuvirta *et al.*, 1998; Astikainen *et al.*, 2011). In contrast to the study

presented by Ruusuvirta *et al.* (1998), Lazar and Metherate (2003) did not find mismatch-negativity like potentials under similar conditions. However, this may be due to the use of a stricter control condition (*cf.* 9.3.1). Pentobarbital-sodium anesthesia seems to preserve also fast onset responses (Tikhonravov *et al.*, 2008; Tikhonravov *et al.*, 2010). In the two MMN studies using this anesthetic, mismatch responses have also been reported within 31 to 90 ms, 151 to 210 ms, 270 to 300 ms (Tikhonravov *et al.*, 2008) and 91 to 180 ms (Tikhonravov *et al.*, 2010).

In addition, there is one rat study not using the classical "flip-flop" design but separating melodically ascending and descending deviants within their analysis (Astikainen *et al.*, 2011). The authors reported mismatch responses of positive polarity from 60 to 100 ms after stimulus onset only for melodically ascending deviants under urethane anesthesia. However, those results are difficult to compare to other MMN rat studies since there was no control for frequency specific effects of the stimuli employed.

Although the synaptic effects of anesthetic agents are not fully understood they significantly affect mismatch responses. Even in human studies, it is not clear whether an MMN can be recorded in the anesthetized state. Propofol anesthesia for example was shown to block the MMN even before patients lost consciousness (Simpson *et al.*, 2002). However, Heinke *et al.* (2004) observed MMN under propofol in deeply sedated subjects.

The use of various anesthetics in MMN studies leads to unequivocal results that are difficult to compare and to interpret. Even if mismatch responses occur under anesthesia, verifying the presence of a deviance detection mechanism comparable to the human counterpart can be done only in awake animals.

8.2 Comparison of oddball elicited potentials to previous studies

In the main experiments two different oddball conditions were employed: a high (0.2) and a low (0.1) deviant probability. In both conditions, significant differences between standard and deviant potentials were found that were present in all four electrodes. These differences were divided into an early difference with the deviant being more

negative than the standard, and a late difference with the deviant reaching more positive amplitude values. This was observed again in both probability conditions.

Today, there is only one other study recording AEPs to oddball stimulation with frequency mismatch epidurally in awake rats (Nakamura *et al.*, 2011). The potentials presented in this study are similar to the present results regarding the first two peaks. AEPs exhibited an initial small positive response followed by a negative peak (named "N29" by the authors to indicate its latency). This peak corresponds to the N1-peak in the present study that was detected with a similar latency. Furthermore, the positive peak P38 reported by Nakamura et al. appears to correspond to the small positive deflection around 40 ms observed in AEPs reported in this thesis. However, a more prominent finding in the present study was the large amplitude positive peak (P2) that commenced around 55 ms, reached its maximum amplitude around 100 ms and lasted until the end of the stimulus, which was not reported by Nakamura et al. This difference might be explained by the frequencies of the acoustic stimuli used in the study of Nakamura *et al.* (2011) that were located at the lower end of the rats' hearing range (2500 and 3600 Hz). The stimuli applied in the present study fit the rats' hearing ability much better and consequently evoked higher amplitude AEPs with more pronounced peaks and overall longer lasting sustained activity. In addition, one paper reported mismatch responses to duration deviants in awake rats (Roger *et al.*, 2009). However, these data cannot be directly compared to the data of the present thesis. The first reason is the different type of mismatch that is employed. As described by Nelken & Ulanovsky (2007), mismatch responses to duration deviants are difficult to interpret in general because off-responses may mimic MMN-like activity. Furthermore, the rats were implanted with electrodes above two primary motor cortices, two parietal cortices and the anterior cingulate cortex, thus a direct comparison to the present data is not possible.

8.3 Latencies

With respect to peak latencies there was no difference between the latencies found for the N1-peak of deviant and standard potentials in both probability conditions. As described in the discussion of the preliminary experiments (*cf.* 6.4), the N1-peak is likely

generated by stimulus-specific thalamo-cortical inputs (Hall & Borbely, 1970; Shaw, 1988) and its latency is found to be independent on whether the stimulus is a repeatedly presented standard or a rarely occurring deviant. In a single neuron study, recording from the MGB of anesthetized rats revealed that neurons responded with a much shorter latency to deviant as to standard potentials (Antunes *et al.*, 2010). This latency difference seems not to persist up to the auditory cortex as it was not detected with single neuron recordings from the auditory cortex of rats (von der Behrens *et al.*, 2009) and at least is not reflected in the summed up and averaged activity represented by the AEPs in this thesis.

For the second positive peak P2 is has to be mentioned that it exhibited rather a plateau than a sharp peak, especially in standard potentials, so it was difficult to determine a common maximum. This is reflected by large standard deviation values. However, there was a significant effect of latency found in probability condition 0.2. Latencies detected with the posterior electrodes (recording from PAF) on the left and right hemisphere were significantly shorter than latencies detected with the electrode positioned above A1 left. This is surprising, because PAF is supposed to be located downstream of A1 (Simpson & Knight, 1993b) and has been shown to exhibit longer latencies compared to A1 as determined by single neuron recordings (Doron *et al.*, 2002). The inverted latency difference found in the present study might be explained by the fact that with the use of epidural recordings the recorded signal is not that spatially confined. In other words, the recorded signal results from the summed activity of many underlying neurons. In addition, processes like volume conduction act on primary signals during transmission of the initial electric fields from the primary current source through biological tissue like the dura towards the sensor (electrode). Therefore, it is conceivable that the signals from A1 and PAF partially overlapped, as reflected by the highly similar potential shapes detected with the anterior and posterior electrodes, and maybe even activity from neighboring auditory areas was captured. In addition, the processing in the auditory system is conducted not only hierarchical but also in parallel what may result in simultaneous input to primary and secondary auditory areas.

Besides this P2-peak latency difference with regard to electrode position in the 0.2 probability condition, a significantly shorter P2-peak latency in standards compared to deviant potentials was found. This finding might be also based on the above-mentioned difficulty to detect a local maximum for the P2-peak.

Overall, the latencies of the N1-peak detected in this study conform with previous data (Barth & Di, 1990; Tikhonravov *et al.*, 2008; Nakamura *et al.*, 2011). The P2-peak seems to be more variable and may, as discussed previously (*cf.* 8.3 and Nakamura *et al.* (2011)) depend more strongly on the physical attributes of the acoustic stimuli employed.

8.4 Mismatch responses (difference waveforms)

The mismatch negativity (MMN) in humans is calculated as the difference between the averaged evoked deviant potential minus the averaged evoked standard potential. In awake rats, those difference waveforms consisted of a large amplitude biphasic wave. The early negative as well as the late positive potential component increased with decreasing deviant probability. Notably, this result mirrors the findings from the human MMN literature (Näätänen, 1992 ; Imada *et al.*, 1993; Javitt *et al.*, 1998; Shelley *et al.*, 1999; Sabri & Campbell, 2001; Sonnadara *et al.*, 2006).

With respect to the difference waveforms, there were no striking latency or shape differences, *i.e.*, additional potential components, between the four electrodes.

In guinea pigs (Kraus *et al.*, 1994b), cats (Pincze *et al.*, 2001) and humans (Sams *et al.*, 1985b) additional potential components in response to oddball deviants have been found in secondary cortical areas and interpreted as MMN-like. In the present study, there were no differences between mismatch responses recorded from primary and secondary auditory fields.

Nevertheless, mismatch responses detected in the present study are comparable to difference waves elicited with higher frequency deviants and standards (3600 Hz) by Nakamura *et al.* (2011) in awake rats. Both start with a double negative peak followed by a waveform of positive polarity.

8.5 Standard potentials

Although the MMN is calculated as “deviant minus standard”-potential, standards had no effect on the overall difference waveform when comparing oddball paradigms comprising deviant probability 0.1 and 0.2. This is due to the fact that after repeated presentation of standard stimuli, the overall potential waveform decreased in the same manner in the two conditions.

At the single neuron level, this effect is known as stimulus-specific adaptation (SSA) (Movshon & Lennie, 1979). The frequent presentation of the same acoustic stimulus leads to an overall reduced response. As discussed by Nelken & Ulanovsky (2007), the term “adaptation” is not appropriate because the key properties of this mechanism argue for “habituation” rather than “adaptation”. Habituation is characterized by a reduction in response amplitude to repeated stimulation with the same stimulus but the initial response can be restored by a different stimulus (dishabituation). This has to be differentiated from neuronal adaptation that is specified by the use-dependent fatigue of the neurons, *i.e.* changes in ion concentrations inside the neuron that leads to a reduced response to the presentation of a different stimulus compared to the initial response amplitude. Because the term SSA has been used so often in the literature, however, it seems not reasonable to change it (Nelken & Ulanovsky, 2007). Therefore, in this thesis, the term SSA will be used to designate the described mechanism.

SSA is a ubiquitous mechanism in the whole brain and has already been detected in the visual (Woods & Frost, 1977; Sobotka & Ringo, 1994; Muller *et al.*, 1999), somatosensory (Katz *et al.*, 2006) and auditory (Ulanovsky *et al.*, 2003; Reches & Gutfreund, 2008; Malmierca *et al.*, 2009; Anderson *et al.*, 2009; Antunes *et al.*, 2010) system. With respect to the auditory system, a reduced response to standard stimuli but restoring of the initial response amplitude by the deviant stimulus, has been detected in various structures of the auditory pathway. Those are the IC (Perez-Gonzalez *et al.*, 2005; Reches & Gutfreund, 2008; Malmierca *et al.*, 2009; Lumani & Zhang, 2010; Netser *et al.*, 2011; Zhao *et al.*, 2011), MGB (Anderson *et al.*, 2009; Antunes *et al.*, 2010; Bäuerle *et al.*, 2011), and A1 (Ulanovsky *et al.*, 2003; von der Behrens *et al.*, 2009; Taaseh *et al.*, 2011). In the brainstem, however, SSA has not been found in the VCN and DCN (Ayala *et al.*, 2012). This

finding may suggest that the IC is the first station of the auditory pathway that exhibits SSA (Malmierca *et al.*, 2009), but there are several brainstem nuclei between the cochlear nucleus and the IC that have not been investigated so far.

The idea that adaptation alone might be responsible for the reduced response to the standard stimulus compared to the deviant has been put forward previously (May *et al.*, 1999). However, SSA was the first single-neuron correlate that has been suggested to account for all properties shown by surface recorded MMN (Ulanovsky *et al.*, 2003; Ulanovsky *et al.*, 2004). As an underlying cellular mechanism, Ulanovsky *et al.* (2003) proposed synaptic depression and facilitation or inhibition because those processes may affect distinct portions of the dendritic tree of neurons and therefore can be stimulus-specific. Mechanisms operating at the output of neurons, on the contrary, like activation of voltage-dependent conductances or tonic hyperpolarization are not able to exhibit stimulus-specificity.

8.6 The relationship of MMN and stimulus specific adaptation

Differentiating between SSA and other possible mechanisms generating MMN-like phenomena like “model adjustment”, “prediction error signaling” or the detection of deviances in general only experimentally is difficult. First, it is important to bore in mind, as explicitly stated by Nelken & Ulanovsky (2007), that the MMN in humans is a cortical phenomenon that is recorded with scalp electrodes and therefore catches the activity of several cortical areas that superimpose at a given sensor. Therefore, single or multi-unit recordings in animals that have been previously described when discussing SSA are not capable of detecting MMM-like phenomena. It is conceivable, however, that epidural recordings comprising a spatial scale of about 3 mm (Freeman *et al.*, 2003) can be used to detect genuine mismatch responses (Nelken & Ulanovsky, 2007).

SSA and MMN share many features: the amplitude of both is enhanced with increasing physical differences between standard and deviant stimuli, moreover, both phenomena increase with decreasing deviant probability (Ulanovsky *et al.*, 2003; Ulanovsky *et al.*, 2004). However, the overall temporal dynamics of SSA are too fast to account for the surface recorded MMN. A possible explanation for this can be found in the paper of

Nelken & Ulanovsky (2007). The authors state that SSA may be located in A1 and therefore upstream of MMN generation so that the deviance is detected in A1 but the MMN itself is generated in higher auditory areas. This would be in line with studies reviewed above that demonstrate MMN in secondary cortical areas (guinea pigs (Kraus *et al.*, 1994b), cats (Pincze *et al.*, 2001) and humans (Sams *et al.*, 1985b)). In the present study, however, there were no differences with respect to mismatch responses between the primary auditory cortex and the posterior auditory field. Furthermore, there are several points as summarized by Näätänen *et al.* (2005) that argue against adaptation as the only mechanism leading to a surface recorded MMN. Amongst others, the presence of MMN to omitted stimuli and MMN to abstract changes occurring in an auditory sequence.

8.7 Conclusion

It has been shown that mismatch responses, *i.e.* large amplitude differences between standard and deviant potential, can be recorded in awake Black hooded rats from A1 and PAF. Those responses share properties with the human MMN, since MMN-like potentials increase with decreasing deviant probability. Some of the amplitude reduction of standard compared to deviant potentials is most likely due to SSA, a mechanism that is present in the whole brain and also in various stations throughout the auditory pathway. As a consequence, the operational definition of the MMN that is used mainly in MMN research ("deviant minus standard potential") identifies only habituation and cannot be sufficient to demonstrate other possible mechanisms like the detection of deviances in the environment.

It has to be concluded, that with the oddball paradigms conducted so far, it is not possible to distinguish between opposing mechanisms explaining the MMN. Subsequently, several other experimental conditions were conducted in order to differentiate between the above described mechanisms.

9 Results control experiments

In a smaller subsample of rats (n = 6) four additional paradigms were tested. Among these were two classical control conditions that have been already applied in earlier studies (deviant alone control condition, equiprobable control condition) and two additional paradigms (deviant probability 0.4, deviant omission) to further evaluate the effect of deviant probability or deviant presentation in general.

In the first section, the results of the oddball paradigm using deviant probability 0.4 will be summarized, whereas the other control conditions will be outlined one by one.

9.1 Deviant probability 0.4

AEPs evoked with an oddball paradigm in which deviant and standard probability converged compared to earlier experiments are shown in Figure 31. After the probability of the deviant was increased to 0.4, there was no difference between deviant and standard potentials present.

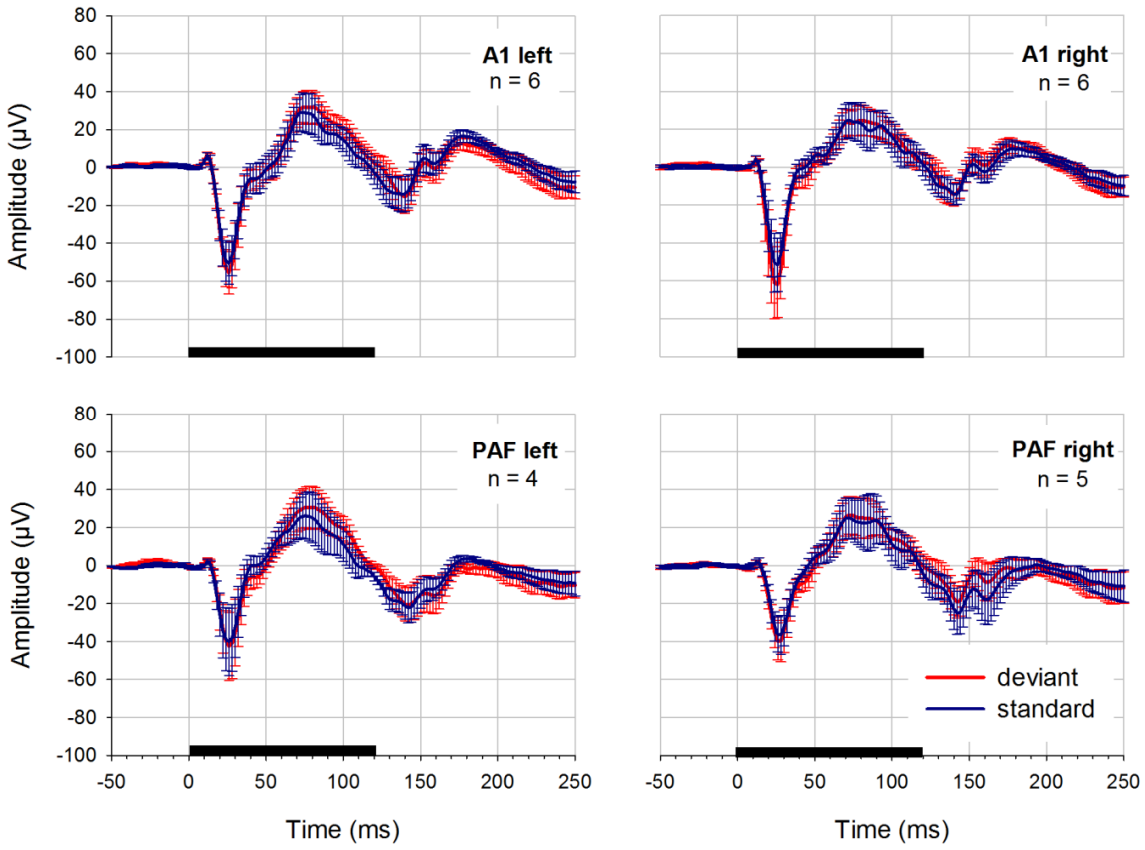

Figure 31: Potentials evoked with an oddball paradigm of deviant probability (0.4). There were no significant differences between standard (blue curve) and deviant potentials (red curve). The black bar on the x-axis represents the stimulus, whereas the error bars designate the standard error of mean. The position of the recording electrode and the number of electrodes that were averaged for displaying AEPs is depicted in the upper right corner of each graph.

9.2 Deviant omission experiment

The results of the deviant omission paradigm in which gaps were interspersed into a sequence of regularly delivered standards (probability of 0.1) are displayed in Figure 32. There was no evoked activity as response to the omission of an acoustic stimulus in an otherwise homogenous sequence detectable.

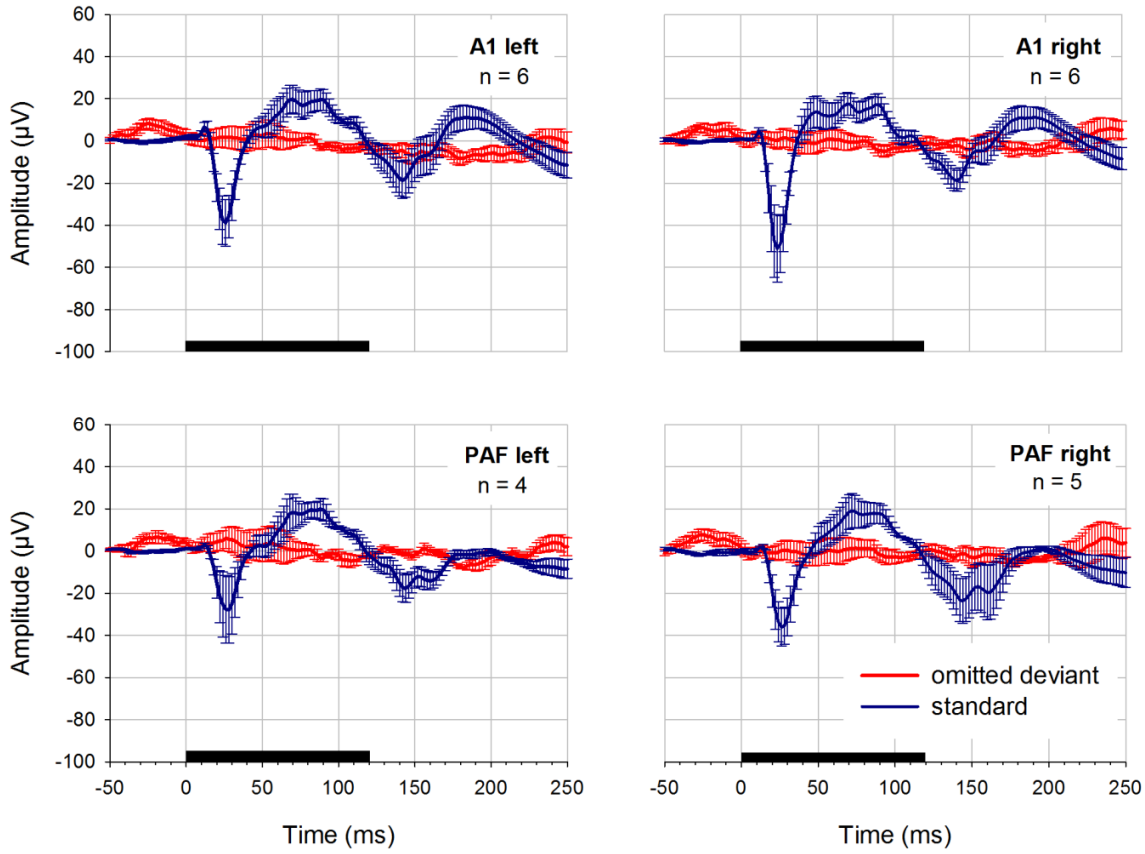

Figure 32: Responses to the omitted deviants and regularly presented standards (deviant probability 0.1). There was no activity evoked by the omitted deviants (red line).The black bar on the x-axis represents the stimulus, whereas the error bars designate the standard error of the mean. The position of the recording electrode and the number of electrodes that were averaged for displaying AEPs is depicted in the upper right corner of each graph.

9.3 Control conditions

9.3.1 Deviant alone control condition

The second classical control condition that was employed in this study was the "deviant alone" condition in which deviants were presented with the same probability as in the oddball paradigms (0.1 and 0.2) but without preceding standards. The results of this experiment are displayed in Figure 33 in which deviant alone potentials are compared to standard and deviant potentials elicited in an oddball paradigm. The results of the statistical comparison are listed in Table 5.

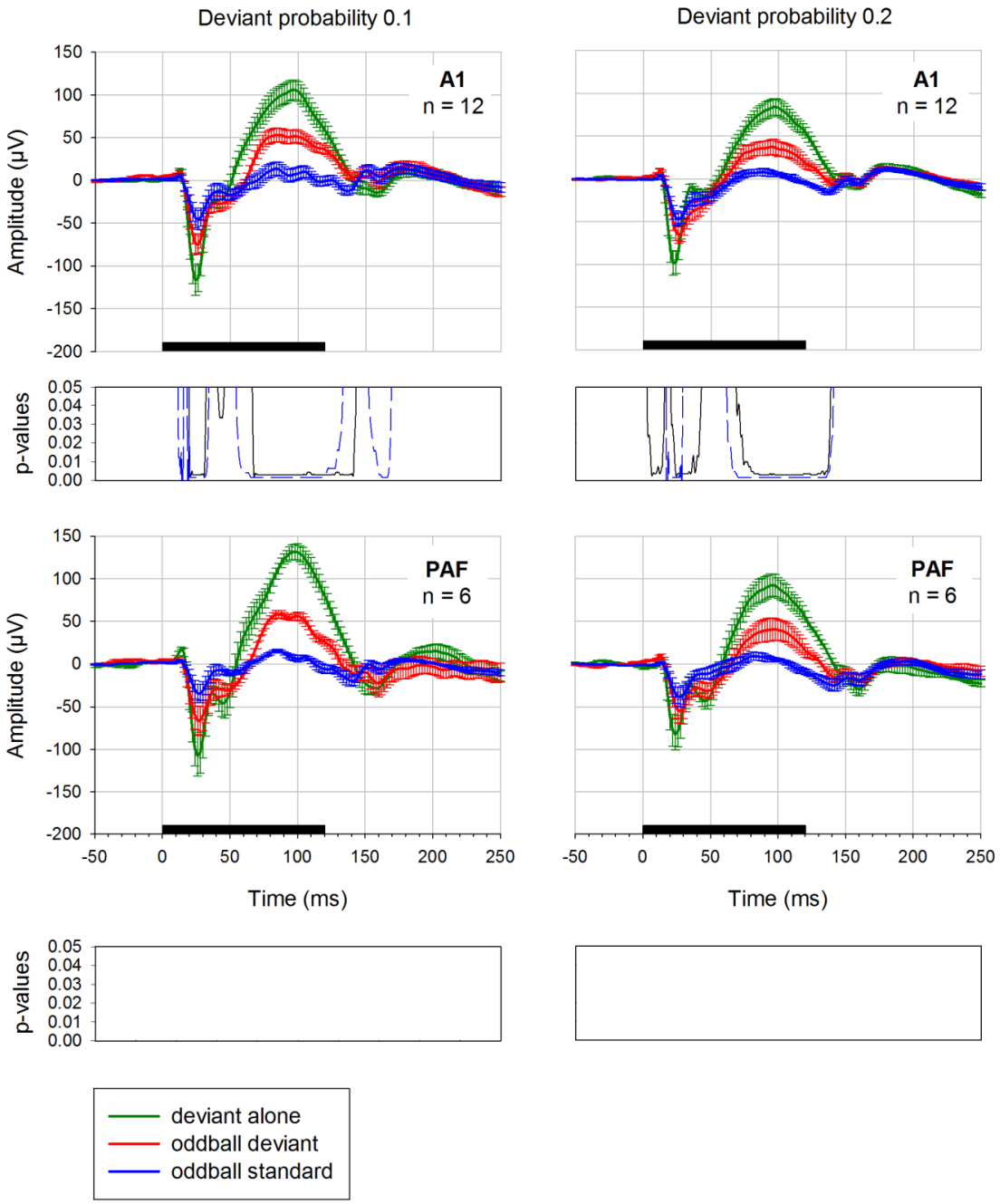

Figure 33: Oddball deviant compared to the deviant alone control condition. Oddball deviant (red curve), deviant alone (green curve) and oddball standard (blue curve) potentials were elicited with either 0.1 deviant probability (diagrams on the left side) or 0.2 deviant probability (diagrams on the right side). Data is derived from 6 rats. The posterior electrodes on the left and right hemisphere as well as anterior electrodes on the left and right hemisphere were pooled for displaying the results and statistical calculation. Black bar on the x-axis shows stimulus duration. Below each graph FDR-corrected p-values are shown. The black curve displays the differences between oddball deviants and the deviant-alone whereas the blue dashed curve displays significant differences between oddball standard and control deviant.

Table 5: Results of the statistical comparison between deviant alone control and oddball paradigm. The significant differences that were found between the deviant presented alone and the oddball deviant as well as differences between deviant alone and standards in the oddball condition are listed in the table.

Deviant probability		Electrode	Latency range (in ms)	w-values	df	p-values
0.1	Oddball deviant vs. Oddball standard	A1	20-31	0 < W < 4	11	0.003 < p < 0.01
			41-45	8 < W < 9	11	0.034 < p < 0.043
			67-142	0 < W < 7	11	0.003 < p < 0.026
		PAF				
	Deviant alone vs. Oddball standard	A1	12-15	1 < W < 6	11	0.003 < p < 0.016
			18-33	0 < W < 8	11	0.002 < p < 0.237
			153-168	0 < W < 9	11	0.002 < p < 0.035
		PAF				
0.2	Oddball deviant vs. Oddball standard	A1	3-15	1 < W < 8	11	0.004 < p < 0.03
			21-43	0 < W < 10	11	0.003 < p < 0.05
			69-138	0 < W < 9	11	0.003 < p < 0.038
		PAF				
	Deviant alone vs. Oddball standard	A1	17-28	0 < W < 6	11	0.002 < p < 0.019
			62-140	0 < W < 8	11	0.002 < p < 0.033
		PAF				

9.3.2 Equiprobable control condition

Potentials elicited in the equiprobable control condition were compared to potentials elicited in two classical oddball paradigms comprising deviant probability 0.1 and 0.2. In the equiprobable control condition again both probabilities were employed leading to the design of a control condition in which either ten or five stimuli were randomly presented. The results of these measurements are displayed in Figure 34. The data was pooled for the anterior electrodes (left and right hemisphere) and for the posterior electrodes (left and right hemisphere). Deviant potentials in the oddball condition comprising deviant probability 0.1 had higher amplitudes compared to equiprobable “deviants” in the control condition in the anterior electrodes. For posterior electrodes, p-values did not reach significance after FDR-correction. In addition, there were significant differences between oddball standard and control "deviant" potentials. These differences were also limited to the anterior electrodes. For probability 0.2, again, oddball deviant and standard were significantly different from control "deviant" in the anterior electrodes. There were no significant differences after correction of the p-values for multiple comparisons in the posterior electrodes.

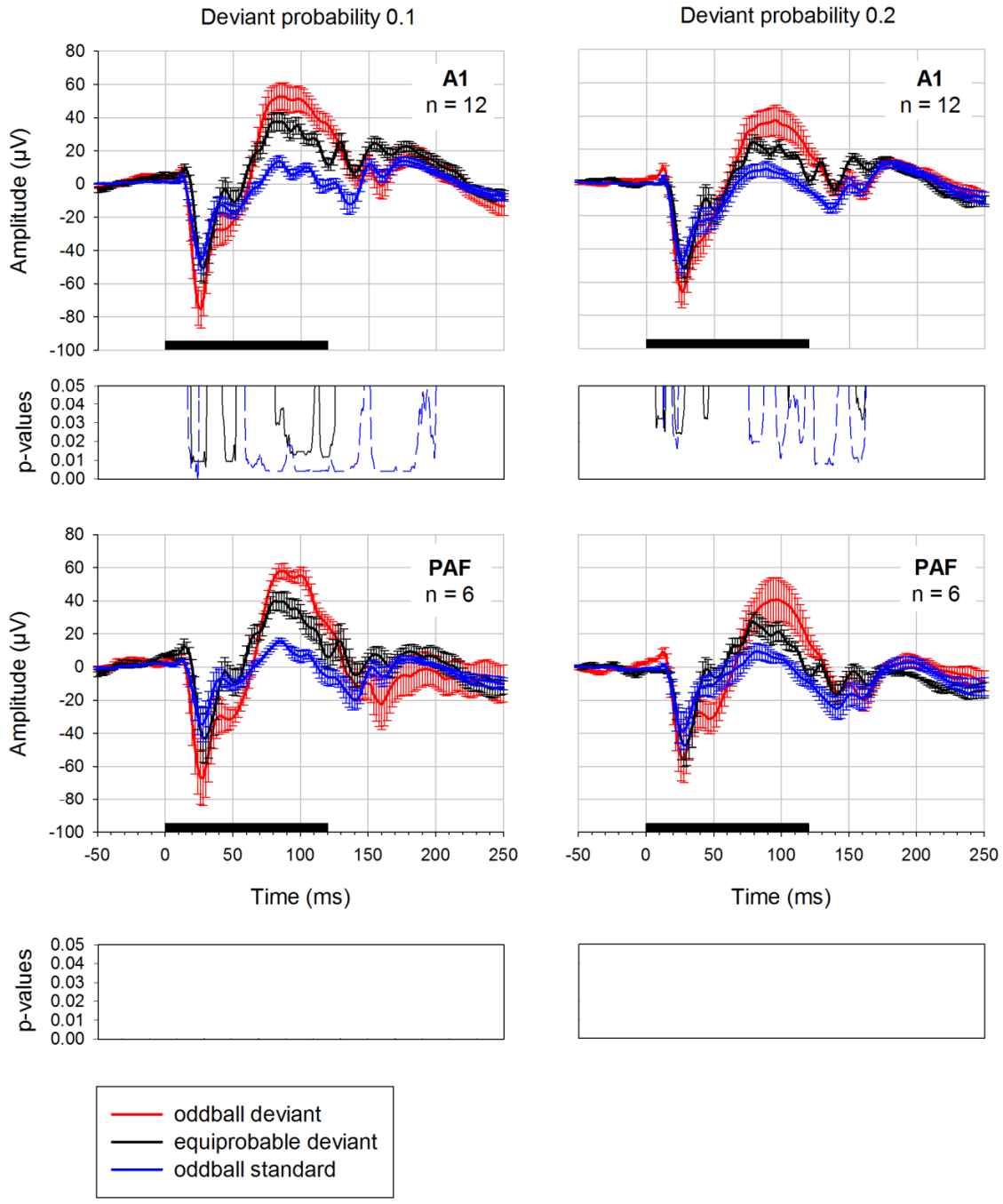

Figure 34: Oddball deviant compared to the equiprobable control condition. Oddball deviant (red curve), control "deviant" (black curve) and oddball standard (blue curve) potentials were elicited with either 0.1 deviant probability (diagrams on the left side) or 0.2 deviant probability (diagrams on the right side). Data is derived from 6 rats. The posterior electrodes on the left and right hemisphere as well as anterior electrodes on the left and right hemisphere were pooled for displaying the results and statistical calculation. Black bar on the x-axis shows stimulus duration. Below each graph FDR-corrected p-values are shown. The black curve displays the differences between oddball deviants and control deviants whereas the blue dashed curve displays significant differences between oddball standard and control deviant.

Table 6: Results of the statistical comparison between equiprobable control and oddball paradigm. The significant differences that were found between the equiprobable control deviant and the oddball deviant as well as differences between equiprobable deviant and standards in the oddball condition are listed in the table.

Deviant probability		Electrode	Latency range (in ms)	w-values	df	p-values
0.1	Equiprobable deviant vs. Oddball deviant	A1	19-33	0 < W < 4	11	0.009 < p < 0.018
			42-51	0 < W < 7	11	0.009 < p < 0.037
			81-110	2 < W < 8	11	0.013 < p < 0.048
			114-125	1 < W < 6	11	0.012 < p < 0.03
		PAF				
	Equiprobable deviant vs. Oddball standard	A1	17-24	0 < W < 7	11	0.004 < p < 0.018
			59-146	0 < W < 10	11	0.004 < p < 0.037
			152-199	0 < W < 11	11	0.004 < p < 0.047
		PAF				
0.2	Equiprobable deviant vs. Oddball deviant	A1	7-14	2 < W < 5	11	0.032 < p < 0.044
			21-27	0 < W < 3	11	0.024 < p < 0.032
			42-45	3 < W < 5	11	0.032 < p < 0.044
			105	W = 4	11	p = 0.037
			155-161	3 < W < 5	11	0.032 < p < 0.044
		PAF				
	Equiprobable deviant vs. Oddball standard	A1	19-23	3 < W < 8	11	0.019 < p < 0.044
			76-86	3 < W < 6	11	0.019 < p < 0.031
			96-117	1 < W < 8	11	0.011 < p < 0.044
			124-141	0 < W < 8	11	0.008 < p < 0.044
			150-162	0 < W < 8	11	0.008 < p < 0.044
		PAF				

9.3.3 Comparison of the control conditions

In order to compare the whole potential waveforms in the two control conditions to the potentials elicited in the oddball paradigms, integrals of the absolute values where calculated for the three conditions separately for deviant and standard potentials. The results of the comparison for deviant probability 0.1 are presented in Figure 35. To summarize the relationship between integral values belonging to the three experimental conditions, a regression line was drawn for the three data points.

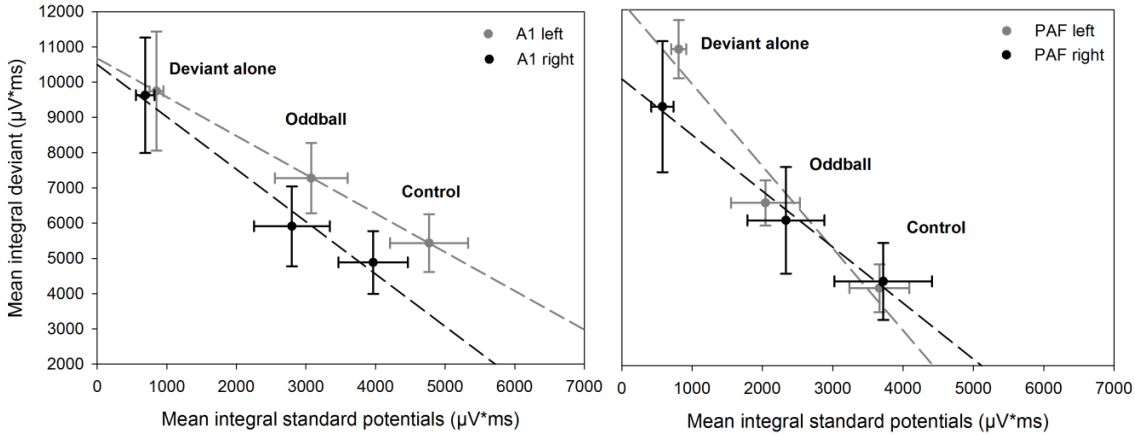

Figure 35: Mean integral of the absolute value of standard and deviant potentials. The data shown here, results from the oddball paradigm and the two control conditions (equiprobable control and deviant alone) with a probability of 0.1. The error bars display the standard error of the mean. Data derived from 6 rats (A1 left = 6, A1 right = 6, PAF left = 4, PAF right = 5).

The results of the calculation of integral values for deviant probability 0.2 derived from three experimental conditions are displayed in Figure 36. Overall, the relationship of the data points resembled the results from deviant probability 0.1 but integral values were smaller.

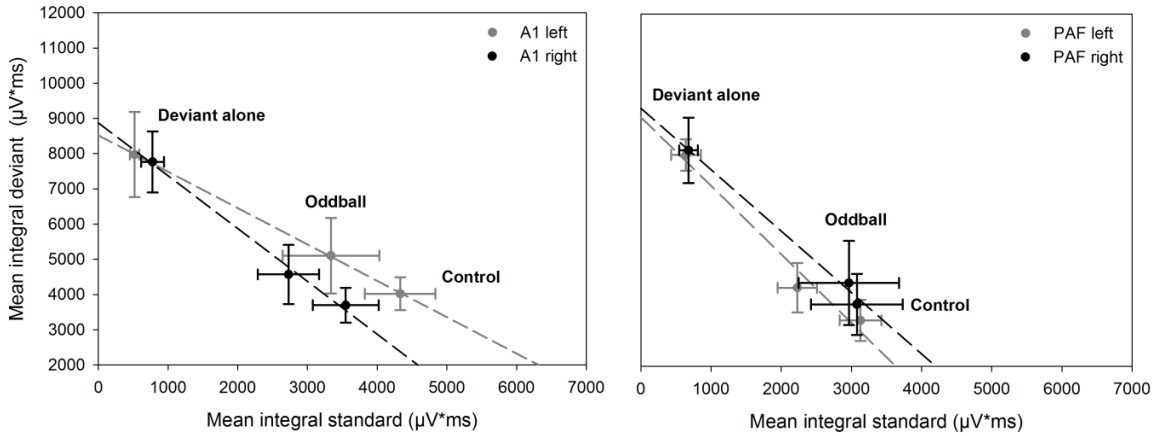

Figure 36: Mean integral of the absolute value of standard and deviant potentials. The data shown here, results from the oddball paradigm and the two control conditions (equiprobable control and deviant alone) with a probability of 0.2. The error bars display the standard error of the mean. Data derived from 6 rats (A1 left = 6, A1 right = 6, PAF left = 4, PAF right = 5).

Our results show that there is a linear inverse relationship between the strength of standard and deviant responses: the higher the integral of the standard potential the lower the integral of the deviant potential (and vice versa).

10 Discussion control experiments

As discussed in the previous section (*cf.* 8.7), the operational definition of the MMN ("deviant minus standard potential") is not sufficient to demonstrate mechanisms distinct from SSA. This is mostly due to the fact that deviant and standard stimuli differ enormously with respect to their overall presentation rate and this effect cannot be controlled for in a classical "flip-flop" oddball paradigm. Therefore, several control conditions have been previously suggested to distinguish between potential components derived by mechanisms of deviance detection *e.g.* prediction error generation and those that can be addressed to adaptation. In this study, two classical control conditions were presented to the rats. Furthermore, two additional paradigms where employed in order to investigate the effect of deviant probability and deviant omission.

10.1 Deviant probability 0.4

Further increasing the deviant probability to 0.4 showed that there was essentially no difference between the potentials. The employed paradigm was related to the 50 %-50 % control condition that has been used in other studies (von der Behrens *et al.*, 2009; Taaseh *et al.*, 2011) showing equal amplitudes and waveforms for "deviants" and "standards". With respect to deviant potentials, the large number of deviant presentations within the sequence of standards may have led to stimulus-specific adaptation (SSA) (*cf.* 8.6) occurring over the course of deviant presentations. However, arguing with the theory of prediction error signaling, the large number of deviants may have not allowed for generating a prediction about an upcoming sequence thus leading to the generation of prediction errors for both stimuli.

10.2 Deviant omission experiment

In human MMN-experiments it has been shown that MMN potentials can be also elicited by omission of sounds (Joutsiniemi & Hari, 1989; Nordby *et al.*, 1994; Yabe *et al.*, 1997; Hughes *et al.*, 2001; Wacongne *et al.*, 2011). To this end, evoked potentials to an oddball paradigm comprising deviant probability 0.1 were recorded, but deviant sounds were

replaced by silence. In this study, there was no evoked activity to the omission of sounds detectable. However, comparing the present results with previous human findings has to be done cautiously. The interstimulus interval of 380 ms that was used in the present study was longer than in human studies (*e.g.* Yabe *et al.* (1997): interstimulus interval 40 and 65 ms, Wacongne *et al.* (2011): 86 ms). However, Yabe *et al.* (1997) showed that there was a strong dependency of omission evoked activity on the interstimulus interval, with longer intervals being unable to evoke omission related potentials. The use of long interstimulus intervals may have led to the finding in the present study.

10.3 Control conditions

10.3.1 Deviant alone control condition

The deviant alone control condition was designed by Sams *et al.* (1985a). In this condition, deviants are presented within silent intervals of randomly changing lengths. The rationale for designing this control condition was that there was no regularity to break by the deviant while the presentation rate of deviants from the oddball paradigm was preserved.

In the present study, deviants presented alone evoked larger amplitudes compared to oddball deviants or oddball standards. However, there were no additional potential components arising in oddball deviants compared to control deviants. The shape of the waveform remained the same but obligatory potential components were enhanced for the deviant presented alone. Furthermore, the time interval in which oddball standard and oddball deviant differed overlapped with the time interval in which oddball deviant and deviant alone differed. Tikhonravov *et al.*, (2008, 2010) for example operationalized the MMN-like activity detected in their study with this concept. MMN-like responses were defined as “Deviant minus standard_before_deviant”-difference wave that significantly differed from the 0-level but that did not overlap in time with the “deviant-alone minus standard_before_deviant”-difference wave that significantly differed from the 0-level. This analysis was performed in order to detect activity that was only present when comparing oddball standards to oddball deviants but not oddball standards to deviants presented alone.

Although this control condition has been employed in several studies (Lazar & Metherate, 2003; Umbricht *et al.*, 2005; Tikhonravov *et al.*, 2008; Tikhonravov *et al.*, 2010), it neglects the fact that neuronal responses are strongly dependent on the overall presentation rate of stimuli, meaning that the "deviant alone" condition mixes the effect of stimulation duty cycle with the effect of the rarity of the deviant. This may account for the fact that MMN-like responses have not been detected reliably in rodents (Nelken & Ulanovsky, 2007). Mismatch responses were reported in awake mice by Umbricht *et al.* (2005) and in urethane-anesthetized rats Lazar & Metherate (2003) for the comparison of oddball deviants and oddball standards. When comparing oddball deviants to deviants alone, however, the differences disappeared and the authors consequently concluded that there was no true deviance detection present. In cats, MMN-like activity was reported when comparing 4 kHz standards to 3 kHz deviants (Csépe *et al.*, 1987; Csépe, 1995). In the latter study, however, there was no control condition employed and even no “flip-flop” design balancing frequency specific effects. Nevertheless, in primates, MMN was reported to frequency and loudness deviants, where deviants were softer compared to standards (Javitt *et al.*, 1994). Although there was no control condition employed, the presence of additional activity to the presentation of a softer deviant sound is a very strong result arguing for deviance detection rather than adaptation.

The above mentioned studies are examples for how the choice of the control condition can bias the interpretation of MMN. Today, there is consensus that the most reliable control condition is the “deviant within many standards” control (Jacobsen & Schröger, 2001) that has been employed in the present thesis but is termed the equiprobable control condition here (*cf.* 4.7.2).

10.3.2 Equiprobable control condition

In the equiprobable control condition the overall presentation rate of deviants is the same as in the oddball condition but standards are replaced by a number of acoustic stimuli with different frequencies. Each stimulus is presented with the same probability and in random manner so that no regularity is formed and consequently with respect to the

theory of prediction error generation, no prediction about an upcoming stimulus can be established.

In the present study, “deviants” presented in the equiprobable control condition had significantly smaller amplitudes than deviants in the oddball condition. Furthermore, there was a significant difference between standard stimuli and control “deviants”.

The amplitude differences between the standard response in the oddball condition and "deviant" response in the equiprobable control condition are most likely caused by SSA, reducing the amplitude of the standard potential over repeated stimulations. On the other hand, amplitude differences which occurred between the deviant in the oddball condition and the "deviant" in the equiprobable condition could be interpreted as resulting from deviance detection.

However, there is another possible explanation to this finding that can be addressed to the design of the control conditions: The frequencies of the stimuli in the equiprobable control were closely spaced (for deviant probability 0.2) or did even overlap at the boarders of the frequency bands (for deviant probability 0.1). Therefore, it is possible that cross-frequency adaptation due to the close spacing of the frequencies may have contributed to an overall amplitude reduction in the control condition (*cf.* Taaseh *et al.* (2011)). Cross-frequency adaptation is a special form of SSA, which has been reported to occur not only for the presented stimulus itself but also for the presentation of tones with adjacent frequencies (Taaseh *et al.*, 2011).

Under the experimental design chosen for this study, it cannot be determined how extensive the possible contribution of cross-frequency adaptation was altogether. This is clearly a limitation of this study. However, some information on this constraint can be gained from previous studies. In a recent study using LFP and multiunit recordings (Farley et al., 2010), stimulus frequencies in the equiprobable control were equally and sufficiently broadly spaced so that cross-frequency adaptation did not occur. For fast responses (latency 20 ms) SSA was the only detectable mechanism, whereas for late responses, in the same latency range as in the present study (around 110 ms), there was no evidence for either SSA or other mechanisms because of high response variability.

Another study (von der Behrens et al., 2009) showed that adaptation indeed plays a role for the late positive wave, but in a less pronounced fashion as for the first negative peak. Furthermore, using this control condition Astikainen et al. (2011) confirmed the existence of MMN-like potentials as significant differences between control and oddball deviants, recorded epidurally in urethane anaesthetized rats for melodically ascending deviants. Similarly, mismatch responses were reported by Nakamura et al. (2011) with epidurally recorded potentials in awake and anesthetized rats. However, both studies exhibit methodological limitation: In the first study (Astikainen et al., 2011), frequency specific effects were not controlled. In the latter study (Nakamura et al., 2011), rather low frequency stimuli were employed that did not fit the rats hearing ability very well (*cf.* 8.4).

A recent study recording MMN-like activity in awake macaque monkeys, on the contrary, demonstrated that deviants in the equiprobable control condition and deviants presented in an oddball paradigm were comparable (Fishman & Steinschneider, 2012). However, in the latter study, there were also methodological limitations with respect to the control condition present: the probability of each tone in the control experiment was less than the probability of the tones in the oddball condition (about 5 % versus 10 %). This may have led to less adaptation in the control compared to the oddball paradigm with respect to deviant potentials. However, the authors interpret their findings as derived from SSA rather than deviance detection.

Taken together, these studies show that contribution of SSA to MMN seems reliable, while not providing a stringent demonstration for the existence of deviance detection or prediction error generation in animals. In humans, on the contrary, the evidence for involvement of other mechanisms besides adaptation to MMN generation is much stronger. As summarized by Näätänen et al. (2005) and Garrido et al. (2009b), some properties of the human MMN cannot be explained by adaptation.

10.3.3 Comparison of the control conditions

The comparison of the two control conditions (equiprobable control, deviant alone) to the employed oddball paradigms showed that there was no additional activity present for oddball deviants. Active deviance detection mechanisms should lead to an increase in

amplitude of deviant compared to standard potentials or even to additional potential components. In the figure this would shift the data point for oddball deviants to larger integral values and consequently would not allow a linear regression fit of these data. However, this result has to be interpreted cautiously due to the low number of data points for fitting the linear regression. Hence, this analysis gives an idea on how the processing energy was subdivided on all stimuli presented in a paradigm.

10.4 Statistical analysis

Due to the relatively small sample used in this study, especially in the control experiments (n = 6), the data frequently differs significantly from normal distribution. Due to the lack of normality, non-parametric tests had to be used. Waveforms were for example compared with a number of Wilcoxon Sign Rank tests for corresponding data points. When samples are large, the statistical power of non-parametric tests is almost comparable to the power of their parametric counterparts (Altman & Bland, 2009). In small samples, however, non-parametric methods are less powerful (Bland & Altman, 2009). Therefore it is possible that an actual difference in the data was not detected.

Since comparison of waveforms requires multiple comparisons, a correction of p-values had to be employed. The false discovery rate (Benjamini & Hochberg, 1995) was chosen over the Bonferroni-correction since the latter is a way too conservative method that leads to an increased type II error rate and consequently a loss of power (Shi *et al.*, 2012). However, even the FDR was very strict applied to the present data, because it assumes data points to be independent. In the present thesis, neighboring data points, however, exhibit a certain dependency since the voltage can change only in a certain range from one millisecond to another.

The combination of both procedures led to very strict statistics that resulted in non-significant results for small samples (n = 6), for example in electrodes covering PAF in the control conditions, even if two waveforms and the respective error bars indicate differences between two distinct potentials.

10.5 Conclusion

With the classical “flip-flop” oddball paradigm, mismatch responses were demonstrated in awake rats. In order to differentiate between two opposing theories explaining the MMN, several control experiments were conducted. These paradigms led to the following results: 1) Increasing deviant probability to 0.4 and consequent converging of probabilities of deviant and standard stimulus resulted in an extinction of differences between the potentials. 2) The omission of deviant stimuli from the sequence did not lead to evoked activity in the present study. 3) The deviant-alone condition resulted in enlarged obligatory peaks compared to oddball deviants but not to additional potential components that may indicate active deviance detection. However, this control condition seems not appropriate to demonstrate the involvement of deviance detection mechanisms. 4) Mismatch responses significantly diminished in the equiprobable control condition that removed the predictive context while controlling for presentation rate of deviants. However, the present study does not allow for disambiguating the relative contribution of cross-frequency adaptation and deviance detection mechanisms like for example prediction error signaling to the observed mismatch responses.

Contemporary MMN theories have already begun to integrate adaptation and prediction error signaling within a unified explanation of MMN. In this framework (Garrido et al., 2009), prediction error dependent synaptic plasticity of inter-regional connections implements the online adjustment of a predictive model, while, at faster timescales, adaptation regulates the relative postsynaptic sensitivity to top-down predictions and bottom-up stimulus information. Modeling attempts have been undertaken to investigate predictive coding theories in order to uncover mechanisms contributing to the human surface recorded MMN. Therefore, dynamic causal models (DCMs) have already been applied successfully to human MMN data (Garrido *et al.*, 2008; Schmidt *et al.*, 2012) whilst arguing for a combination of adaptation and prediction error signaling.

Since it turned out very difficult to infer mechanisms of mismatch response generation in awake rats only from distinct experimental paradigms, subsequently DCM was applied to the recorded data.

11 Results dynamic causal modeling

Dynamic causal modeling (DCM) was used in order to infer on individual models and model architecture that can explain the effect of the deviant stimulus on the coupling between primary (A1) and secondary auditory regions (PAF). In practice, this was modeled by defining a space of 8 models in which mechanisms of adaptation in A1 were systematically combined with synaptic plasticity expressed by different extrinsic connections between primary and secondary areas in the left and right hemisphere. Within the predictive coding framework explaining the MMN (Garrido *et al.*, 2008; Schmidt *et al.*, 2012) synaptic plasticity of glutamatergic connections was supposed as a mechanism establishing predictions and transmitting those and the corresponding errors across hierarchical levels within the brain.

DCM was performed on the evoked potential data for deviant probability 0.1 and 0.2 (n = 12). First, the modeling results of the low probability condition (0.1) will be summarized below.

11.1 Deviant probability 0.1

Random effects Bayesian model selection indicates that model 6, which explains the effect of the deviant by changes in local adaptation in A1 and synaptic plasticity in forward connections from A1 to PAF exhibited higher log model evidence compared to all other models with exceedance probability > 80 % (Figure 37).

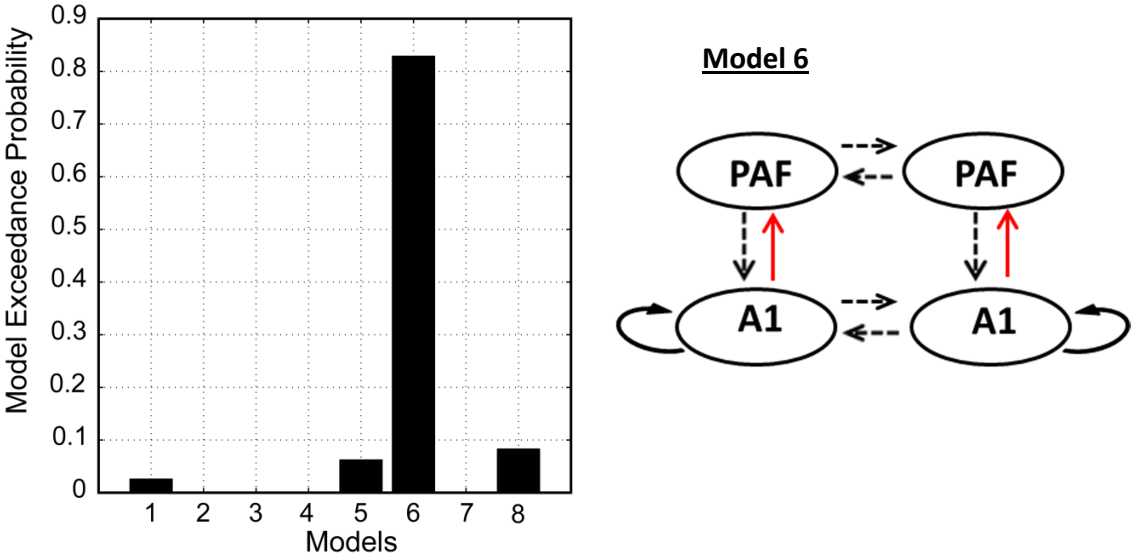

Figure 37: Results of the random effects BMS for eight models describing the effect of the deviant on the investigated network. Model 6 exhibited higher log model evidence compared to the other models included in the BMS analysis (exceedance probability > 80 %). This model explained the effect of the deviant with adaptation in A1 and plasticity in forward connections from A1 to PAF.

Furthermore, the importance of each model feature (adaptation and synaptic plasticity) was examined on its own by using random effects family-level BMS. The results of the family-level comparison are depicted in Figure 38. Models allowing for adaptation in A1 (models 5 to 8) were superior to models that did not allow for adaptation in A1 (models 1 to 4) (exceedance probability > 95 %). In addition, models that included synaptic plasticity in form of changes in forward and backward connectivity induced by the deviant stimulus (models 2 to 4 and 6 to 8) were superior to models that did not include plasticity (model 1 and 5) (exceedance probability > 90 %).

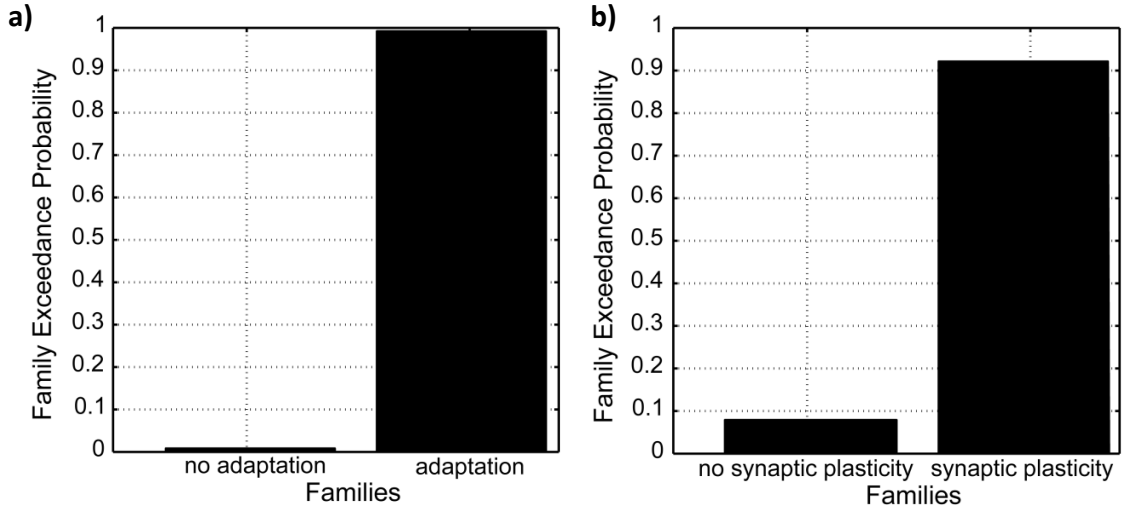

Figure 38: Family-level BMS comparing families with adaptation to families without adaptation and families with synaptic plasticity to families without synaptic plasticity. a) Family-level BMS showed that models allowing for adaptation (models 5-8) exhibited larger log model evidence than models without adaption in A1 (models 1-4) with an exceedance probability of > 95 %. b) Family-level BMS revealed models with synaptic plasticity (model 2-4 and 6-8, which included the modulation of forward and backward connections between A1 and PAF) were superior to models without synaptic plasticity (models 1 and 5) with an exceedance probability of > 90 %.

11.2 Deviant probability 0.2

For deviant probability 0.2 the same analysis was performed. Random effects BMS did not reveal one of the eight models being superior to the others (Figure 39).

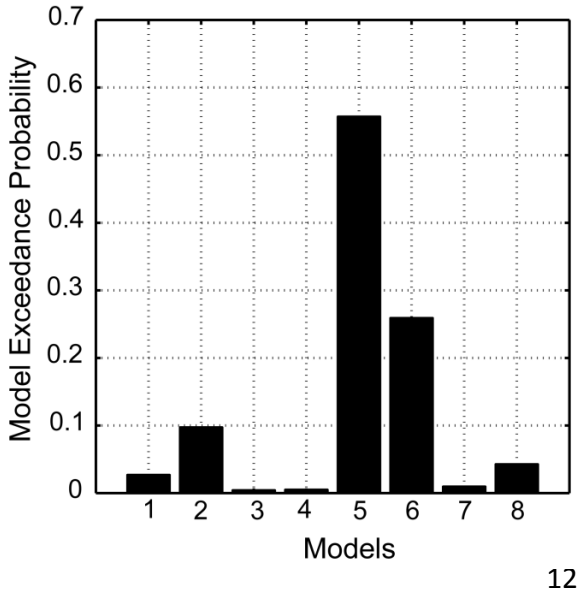

Figure 39: Results of the random effects BMS for eight models describing the effect of the deviant on the investigated network. There was no model superior.

Family-level comparison for deviant probability 0.2 demonstrated that the implementation of adaptation was an important mechanistic factor (exceedance probability > 85 %). With respect to the synaptic plasticity factor, the families could not be distinguished with respect to their model evidences.

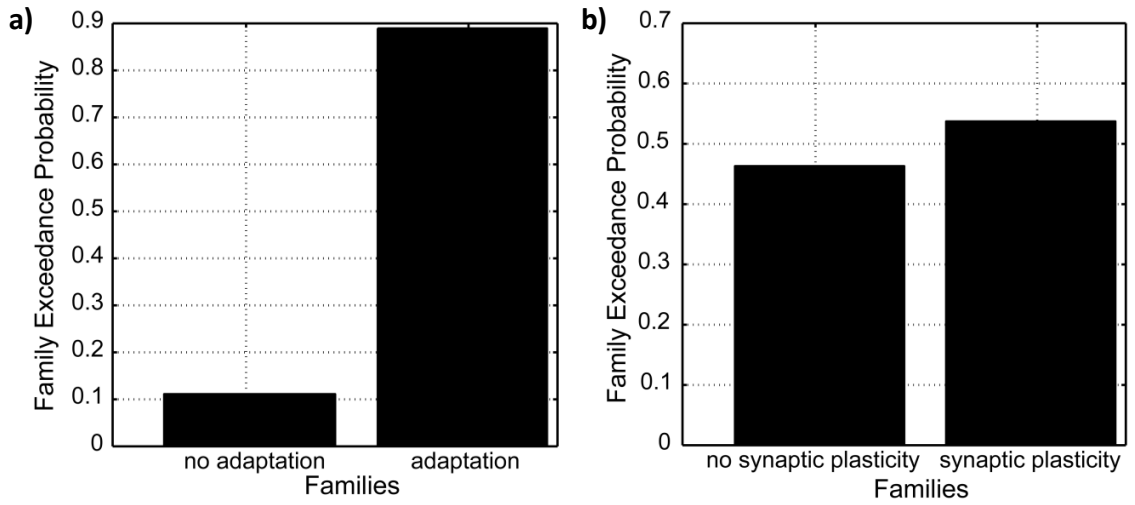

Figure 40: Family-level BMS comparing families with adaptation to families without adaptation and families with synaptic plasticity to families without synaptic plasticity. a) Family-level BMS showed that models allowing for adaptation (models 5-8) exhibited greater log model evidence than models without adaption in A1 (models 1-4, exceedance probability > 85 %) b) Family-level BMS revealed that synaptic plasticity seems not to be an important mechanistic factor to explain the effect of the deviant in the higher probability condition.

12 Discussion dynamic causal modeling

DCM was performed in order to investigate the predictive coding hypothesis (for a review see Garrido *et al.*, 2009b) a contemporary theory of MMN generation that combines adaptation and prediction error signaling. In this theory, prediction error-dependent synaptic plasticity of inter-regional connections generates the online adjustment of a predictive model, while adaptation changes the relative post-synaptic sensitivity to top-down predictions and bottom-up stimulus information. The modeling of human MMN data strongly argues for a combination of both mechanisms to the generation of the surface recorded MMN (Garrido *et al.*, 2008; Schmidt *et al.*, 2012).

For investigating how the presentation of a deviant stimulus changed synaptic plasticity and adaptation in the primary and secondary auditory cortex network, a model-based approach was used, in which eight different models were specified. With respect to the first mechanistic factor, namely synaptic plasticity, four models were designed to explain the effect of the deviant stimulus: no modulation of extrinsic connectivity (model 1), modulation of either forward or backward connectivity between A1 and PAF (models 2 and 3), and modulation of both forward and backward connectivity between the two regions (model 4). The second mechanistic factor concerned neuronal adaptation. In models 5 to 8, the variations in synaptic plasticity were repeated as above, but crossed with the presence versus the absence of neuronal adaptation (expressed via post-synaptic gain modulation in A1).

12.1 Selection of a winning model

Random effects BMS indicated that model 6, which included adaptation in A1 and modulation of synaptic plasticity in the forward connections from A1 to PAF was superior to the other models. This is, however, weak evidence that model 6 is much superior to the rest of the models (for 8 models about 6.5 times higher than equality (indistinguishability) of the models).

As stated by Raftery (1995), “positive” evidence corresponds to a posterior model probability of 75-95 %, “strong” evidence to 95-99 % whereas “very strong” evidence is expressed by a posterior probability of > 99 %.

There are several caveats that should be considered when interpreting the model selection results. First of all, DCM was originally designed to model human ERP data (Jansen & Rit, 1995) and contains priors and time constants chosen to capture the temporal dynamics of human evoked potentials. With respect to the present data, this may result in a rather poor model fit compared to studies modeling human AEPs. As illustrated in the introduction (*cf.* 0), central auditory conduction time, i.e. the time for an afferent volley to travel through the auditory pathway, is much shorter in rats (6.6 ms) compared to humans (12 ms) (Shaw, 1990; 1995), due to the shorter fiber lengths in rats. The difference with respect to time constants may have resulted in a poorer fit of rat AEP data in the present study.

In addition, DCM for human MMN data was performed for the bilateral primary auditory cortex, the bilateral superior temporal gyrus and the right inferior frontal gyrus (Garrido *et al.*, 2008; Schmidt *et al.*, 2012). Between the human AEP sources that were modeled, there was a pronounced hierarchy, especially between temporal and frontal areas. However, there is no strict hierarchy between A1 and PAF from which AEPs were recorded in the present study. Even in the present thesis, it was demonstrated (*cf.* 8.3) that some peak components arose earlier in PAF compared to A1. Throughout the auditory system, signal processing is performed in both a serial and a parallel manner. In other words, an afferent volley might reach both areas simultaneously. Furthermore, there may be volume conduction through biological tissue like the dura leading to a partial overlap of primary currents generated by neurons located in A1 and those located in PAF at the recording sites due to the relatively close spacing of electrodes.

Taken together, the above mentioned reasons may have led to the fact that there was not strong evidence that Model 6, which included adaptation and modulation of forward connectivity, could explain the underlying effect of the deviant best.

12.2 Family-level BMS

The family-level BMS, however, was conclusively suggesting that both adaptation and synaptic plasticity were important factors, contributing to the model evidence. The introduction of adaptation as a mechanistic factor improved the model evidence substantially with very strong evidence for models including adaptation in both the 0.1 and 0.2 deviant probability conditions. Further support that adaptation is an important mechanism involved in MMN generation was found in a recent study of human MMN data in the auditory modality (Schmidt *et al.*, 2012).

In addition, the implementation of synaptic plasticity improved the model fit to the data for the 0.1 probability condition. This did not apply to the 0.2 deviant probability condition, in which no family was superior to the other with respect to synaptic plasticity. With respect to the above mentioned DCM study using human MMN data (Schmidt *et al.*, 2012), the evidence for synaptic plasticity found in the rat study was not as strong and was also not consistent across the two experimental conditions.

12.3 Conclusion

The family-level inference strongly favored the involvement of adaptation in the generation of mismatch responses in awake rats. This finding is also supported by the experimental results that were presented in the two previous sections. From the overall modeling and experimental results, it can therefore be concluded that neuronal adaptation is a key mechanism underlying the generation of mismatch responses in rats. With respect to the second mechanism that was investigated, namely synaptic plasticity, we found evidence for the models including plasticity compared to the models without. Yet, the overall confidence was weaker compared to the family inference results for adaptation.

13 Pharmacological treatment

In order to investigate cellular mechanisms underlying MMN generation, two different substances (scopolamine: muscarinic receptor antagonist, pilocarpine: muscarinic receptor agonist) in two concentrations were applied to evaluate the effects of muscarinic receptor modulation on mismatch responses in awake rats.

13.1 Statistical annotation

In the present study, pharmacological treatment was compared across the two different stimulus types (deviant, standard) with the calculation of two-way repeated measures ANOVA separately for each of the four electrodes. The reason why this has been done is that the effect of treatment was of primary interest. In order to correct for multiple testing, however, the resulting p-values were multiplied by the number of tests conducted (Bonferroni procedure).

13.2 AEPs after drug treatment

AEPs evoked in an oddball paradigm (deviant probability 0.1) after injection of muscarinic drugs and vehicle are shown in Figure 41.

Drug treatment induced obvious waveform differences compared to vehicle injection. The injection of 1 mg/kg scopolamine seems to reduce the amplitude of the P2-peak in deviant potentials whereas this component in standard potentials is sustained. Interestingly, 2 mg/kg scopolamine seems to shift the P2-peak to earlier latencies. In addition, after scopolamine treatment, an increase of the slow positive waveform arising subsequently to the fast negative offset response with an approximate latency of 150 ms can be observed. On the other hand, treatment with 3 mg/kg pilocarpine reduced the amplitude of deviant potentials and led to a pronounced negative peak (N2) arising at about 50 ms latency from stimulus onset directly after the N1-peak. Deviant potentials were also modified by treatment with 6 mg/kg pilocarpine. The P2-component seems to exhibit a sharper peak with slightly earlier latency compared to vehicle treatment. Furthermore, again the

negative peak component around 50 ms arose. Waveforms of standard potentials appear to be reduced during treatment with pilocarpine compared to vehicle and scopolamine.

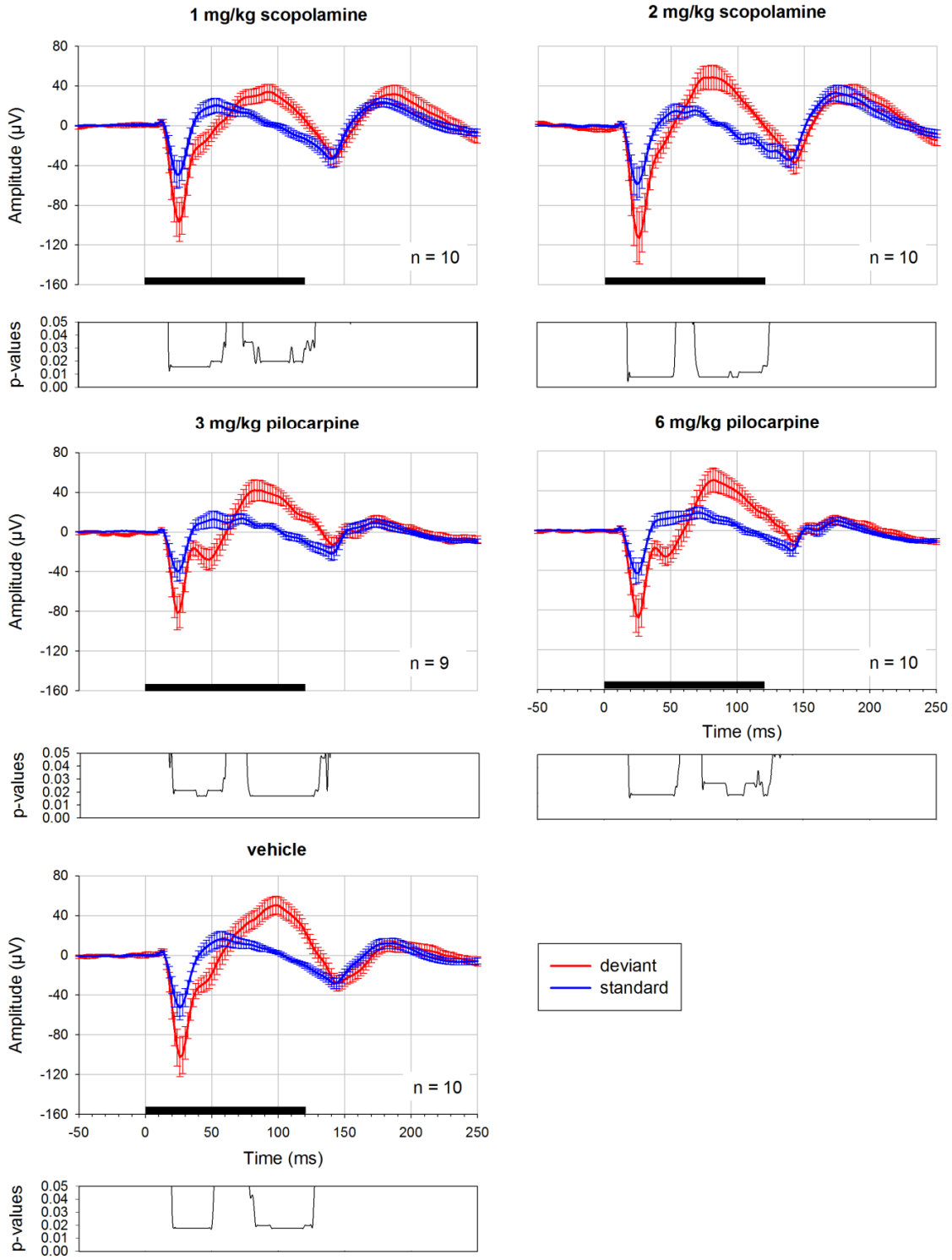

Figure 41: AEPs evoked in an oddball paradigm comprising deviant probability 0.1 under different treatments. AEPs are displayed for PAF right only. The significant differences between deviant (red curve) and standard (blue curve) are displayed as the FDR-corrected p-values below each graph.

13.3 Latencies of the N1- and P2-peak

The latency of the N1-peak was compared across the different treatment conditions and the respective results are displayed in Figure 42. Statistical comparison was performed using a two-way repeated measures ANOVA on ranks (factors: treatment, stimulus type) for each recording electrode. Potentials recorded with electrode A1 right showed a tendency to differ with regard to treatment ($F(4, 32) = 3.095$, $p = 0.029$, $p_{corrected} = 0.116$) and stimulus type ($F(1, 32) = 5.532$, $p = 0.047$, $p_{corrected} = 0.188$). In addition, an interaction between both factors ($F(4, 32) = 4.456$, $p = 0.006$, $p_{corrected} = 0.024$) was detected. Post hoc test Holm-Sidak revealed that treatment with 2 mg/kg scopolamine resulted in significantly shorter overall latencies compared to vehicle ($p = 0.005$, $p_{corrected} = 0.02$). On the other hand, standard latency was significantly shorter compared to deviant latency after treatment with 2 mg/kg scopolamine ($p = 0.006$, $p_{corrected} = 0.024$) and vehicle ($p = 0.012$, $p_{corrected} = 0.048$). Furthermore, the N1-peak in deviant potentials occurred earlier after treatment with 3 mg/kg pilocarpine compared to vehicle ($p < 0.001$, $p_{corrected} < 0.004$).

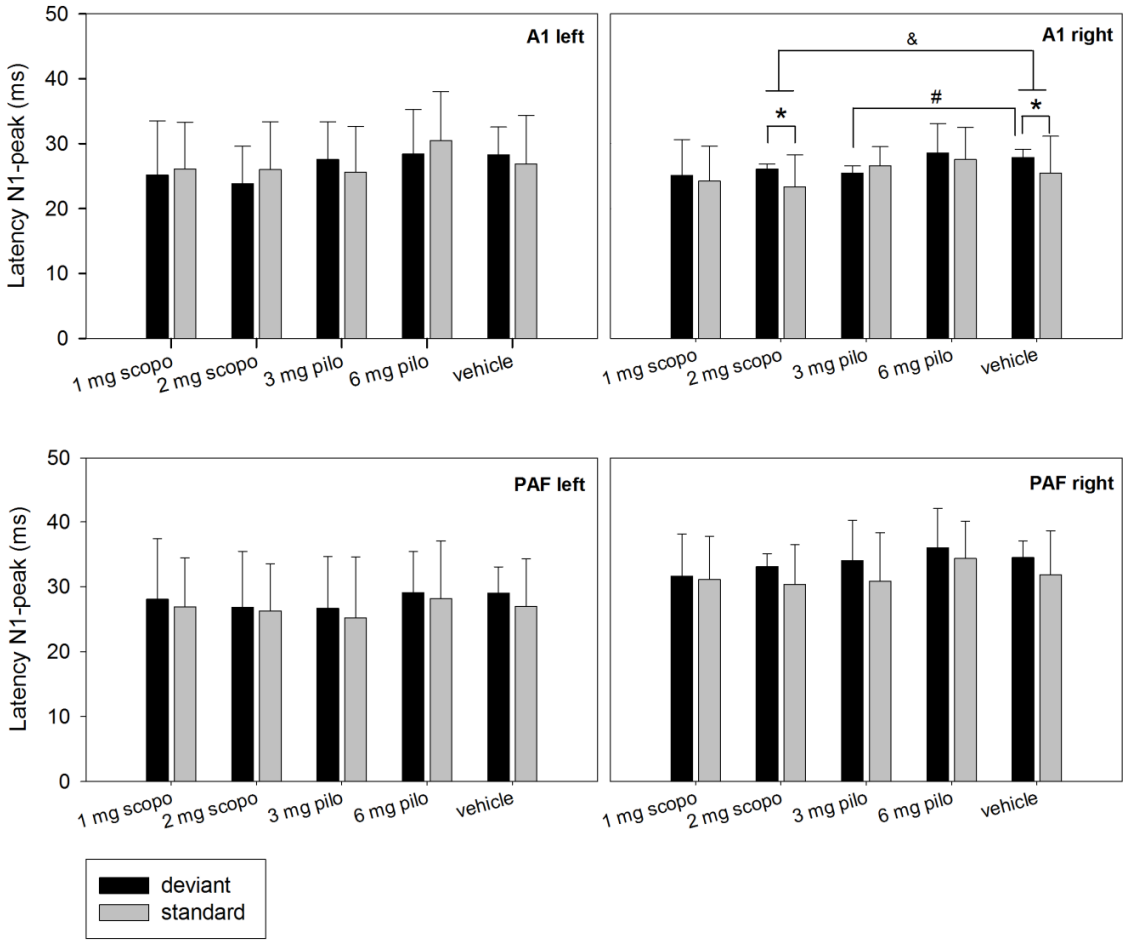

Figure 42: Latency of the N1-peak in five treatment conditions. Significant differences with respect to the latency values were only found for potentials recorded with electrode A1 right. Standard potentials had significantly shorter latencies than deviant potentials after treatment with 2mg/kg scopolamine and vehicle injection (designated by an asterisk), whereas latencies of deviant potentials were found to be significantly shorter after treatment with 3 mg/kg pilocarpine compared to vehicle treatment (designated by a hash). Overall, latencies of the N1-peak were significantly longer after vehicle compared to 2 mg/ kg scopolamine (designated by an ampersand).

Results of the latency measures for the P2-peak are displayed in Figure 43. Again, a two-way repeated measures ANOVA on ranks with the factors “treatment” and “stimulus type” was calculated for each electrode. There was a significant interaction of both factors for electrode A1 left ($F(4, 36) = 3.8$, $p = 0.011$, $p_{corrected} = 0.044$). Post hoc test Holm-Sidak revealed that latencies detected for standard potentials showed shorter latencies than deviant potentials after treatment with 6 mg/kg pilocarpine by trend ($p = 0.02$, $p_{corrected} = 0.08$).

With respect to electrode A1 right, a significant main effect of stimulus type was observed ($F(1, 32) = 76$, $p < 0.001$, $p_{corrected} < 0.004$). The same was found for the electrode PAF right ($F(1, 36) = 38.4$, $p < 0.001$, $p_{corrected} < 0.004$) and by trend also for electrode PAF left ($F(1, 36) = 7.2$; $p = 0.025$, $p_{corrected} = 0.1$). For PAF right, however, the equal variance test failed.

There was no main effect of treatment in all electrodes tested.

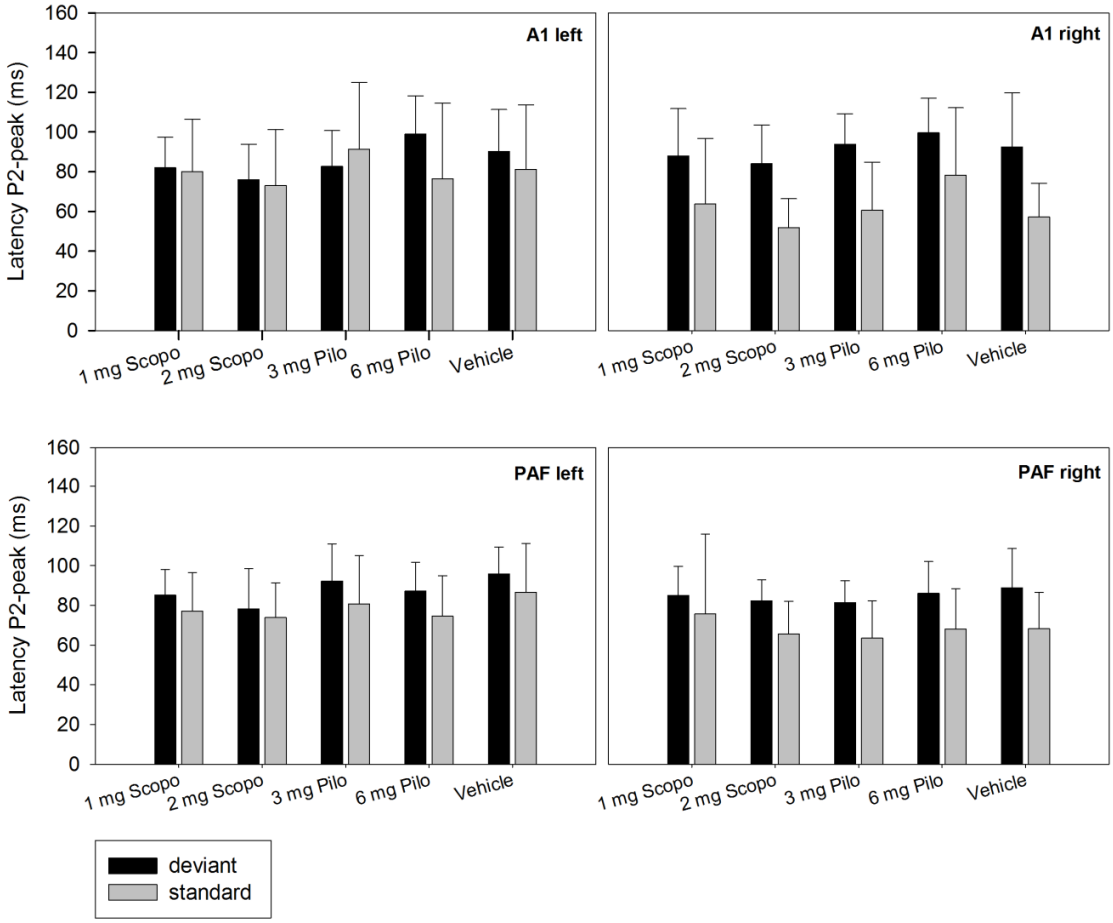

Figure 43: Latency of the P2-peak in five treatment conditions. For electrode A1 right and PAF right there was a significant main effect of stimulus type detected. Due to clarity of the figure this effect is not depicted.

13.4 Difference waveforms

Difference waveforms calculated as “deviant minus standard” potential for all four electrodes are displayed in Figure 44. There were no significant waveform differences after treatment with 1 or 2 mg/kg scopolamine as well as 3 or 6 mg/kg pilocarpine or vehicle.

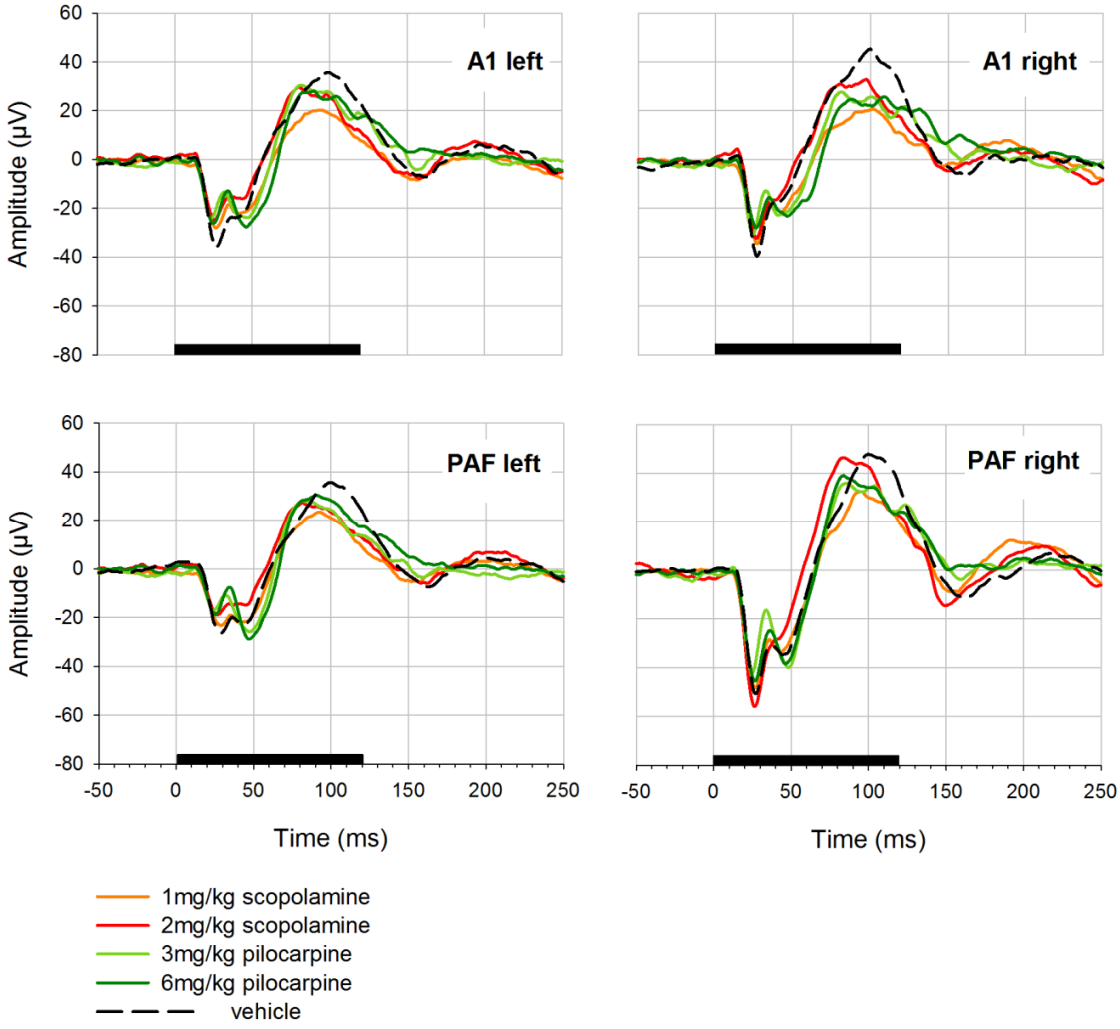

Figure 44: Difference waveforms after pharmacological treatment. The difference waveforms calculated as “deviant minus standard” potential were found to be similar over the different treatments. Potentials recorded with the electrode covering PAF right seemed to exhibit overall higher amplitudes compared to potentials recorded with the other three electrodes.

13.5 Integrals of standard and deviant potentials in five treament conditions

In order to compare the whole waveforms of deviant and standard potentials across the five different treatments, integrals of the potentials were calculated. The respective data is displayed in Figure 45. Integrals of standard potentials are shifted to larger values after scopolamine treatment whereas pilocarpine reduces standard integrals. The data points for vehicle treatment seem to be located in between the values for the two treatments.

A two-way repeated measures ANOVA on ranks (factors: treatment, stimulus type) was calculated separately for each electrode. Within A1 left, a significant effect of treatment ($F(4, 36) = 5.3$, $p = 0.002$, $p_{corrected} = 0.008$), stimulus type ($F(1, 36) = 83.4$, $p < 0.001$, $p_{corrected} < 0.004$) as well as a significant interaction between both factors ($F(4, 36) = 6.3$, $p < 0.001$, $p_{corrected} < 0.004$) was determined. Post hoc test Holm-Sidak revealed that in general, integrals recorded after treatment with 1 mg/kg ($p < 0.001$, $p_{corrected} < 0.004$) and 2 mg/kg scopolamine ($p < 0.001$, $p_{corrected} < 0.004$) were larger compared to integrals after treatment with 3 mg/kg pilocarpine. Moreover, integral values calculated for standard potentials were significantly smaller as integrals calculated for deviants across all treatments ($0.001 < p < 0.003$, $0.004 < p_{corrected} < 0.012$). Furthermore, integrals of deviant potentials were significantly attenuated after treatment with 3 mg/kg pilocarpine as compared to vehicle ($p = 0.002$, $p_{corrected} = 0.008$). Within standard potentials, integrals significantly increased after treatment with 2 mg/kg scopolamine compared to 3 mg/kg pilocarpine ($p < 0.001$, $p_{corrected} < 0.004$), 6 mg/kg pilocarpine ($p = 0.001$, $p_{corrected} = 0.004$) and vehicle treatment ($p < 0.001$, $p_{corrected} < 0.004$). After 1 mg/kg scopolamine administration, standards exhibited significantly larger integral values than after treatment with 3 mg/kg pilocarpine ($p < 0.001$, $p_{corrected} < 0.004$).

For electrode A1 right there was again a significant main effect of treatment ($F(4, 32) = 5.6$, $p = 0.002$, $p_{corrected} = 0.008$), stimulus type ($F(1, 32) = 70.2$, $p < 0.001$, $p_{corrected} < 0.004$) as well as a tendency for an interaction of both factors ($F(4, 32) = 3.5$, $p = 0.018$, $p_{corrected} = 0.072$). As revealed by the post hoc test Holm-Sidak,

integrals recorded after treatment with 1 mg/kg ($p = 0.001$, $p_{corrected} = 0.004$) and 2 mg/kg scopolamine ($p = 0.005$, $p_{corrected} = 0.02$) were in general significantly larger compared to integrals after treatment with 3 mg/kg pilocarpine. The same was found for treatment with 6 mg/kg pilocarpine compared to 1 mg/kg ($p = 0.005$, $p_{corrected} = 0.02$) and 2 mg/kg scopolamine ($p = 0.005$, $p_{corrected} = 0.02$). In addition, deviant integrals were larger than standard integrals for all treatments ($0.001 < p < 0.003$, $0.004 < p_{corrected} < 0.012$). There was no effect of treatment present for deviant potentials only. However, administration of 1 mg/kg scopolamine resulted in significantly enhanced standard potential integrals compared to 3 mg/kg ($p < 0.001$, $p_{corrected} < 0.004$) and 6 mg/kg pilocarpine ($p < 0.001$, $p_{corrected} < 0.004$), as well as vehicle ($p = 0.006$, $p_{corrected} = 0.024$) treatment. In addition, standard integrals were significantly larger after treatment with 2 mg/kg scopolamine when compared to 3 mg/kg ($p = 0.001$, $p_{corrected} = 0.004$) and 6 mg/kg pilocarpine ($p < 0.001$, $p_{corrected} < 0.004$) administration.

The statistical analysis of integral values of the potentials recorded above PAF left revealed a significant main effect of treatment ($F(4,36) = 13$, $p < 0.001$, $p_{corrected} < 0.004$) and stimulus type ($F(1, 36) = 96.4$, $p < 0.001$, $p_{corrected} < 0.004$). In general, integral values were larger after treatment with 1 mg/kg scopolamine compared to integrals after treatment with 3 mg/kg ($p < 0.001$, $p_{corrected} < 0.004$) and 6 mg/kg pilocarpine ($p < 0.001$, $p_{corrected} < 0.004$). Furthermore, integrals were larger after treatment with 2 mg/kg scopolamine compared to 3 mg/kg ($p < 0.001$, $p_{corrected} < 0.004$) and 6 mg/kg pilocarpine ($p = 0.003$, $p_{corrected} = 0.012$). In addition, integral values after vehicle injection were significantly larger compared to integrals after treatment with 3 mg/kg pilocarpine ($p < 0.001$, $p_{corrected} < 0.004$).

For PAF right a main effect of treatment ($F(4,32) = 3.1$, $p = 0.031$, $p_{corrected} = 0.124$) and stimulus type ($F(1, 32) = 51.9$, $p < 0.001$, $p_{corrected} < 0.004$) was observed as well as an interaction of both factors ($F(4, 32) = 3.9$, $p = 0.012$, $p_{corrected} = 0.048$). Post hoc test Holm-Sidak showed that standard integrals were significantly smaller than deviant integrals for all treatments ($0.001 < p > 0.002$, $0.004 < p_{corrected} < 0.008$). For standard potentials, integrals after treatment with 2 mg/kg scopolamine were significantly

enhanced compared to 3 mg/kg ($p = 0.003$, $p_{corrected} = 0.012$) and 6 mg/kg pilocarpine ($p = 0.004$, $p_{corrected} = 0.016$).

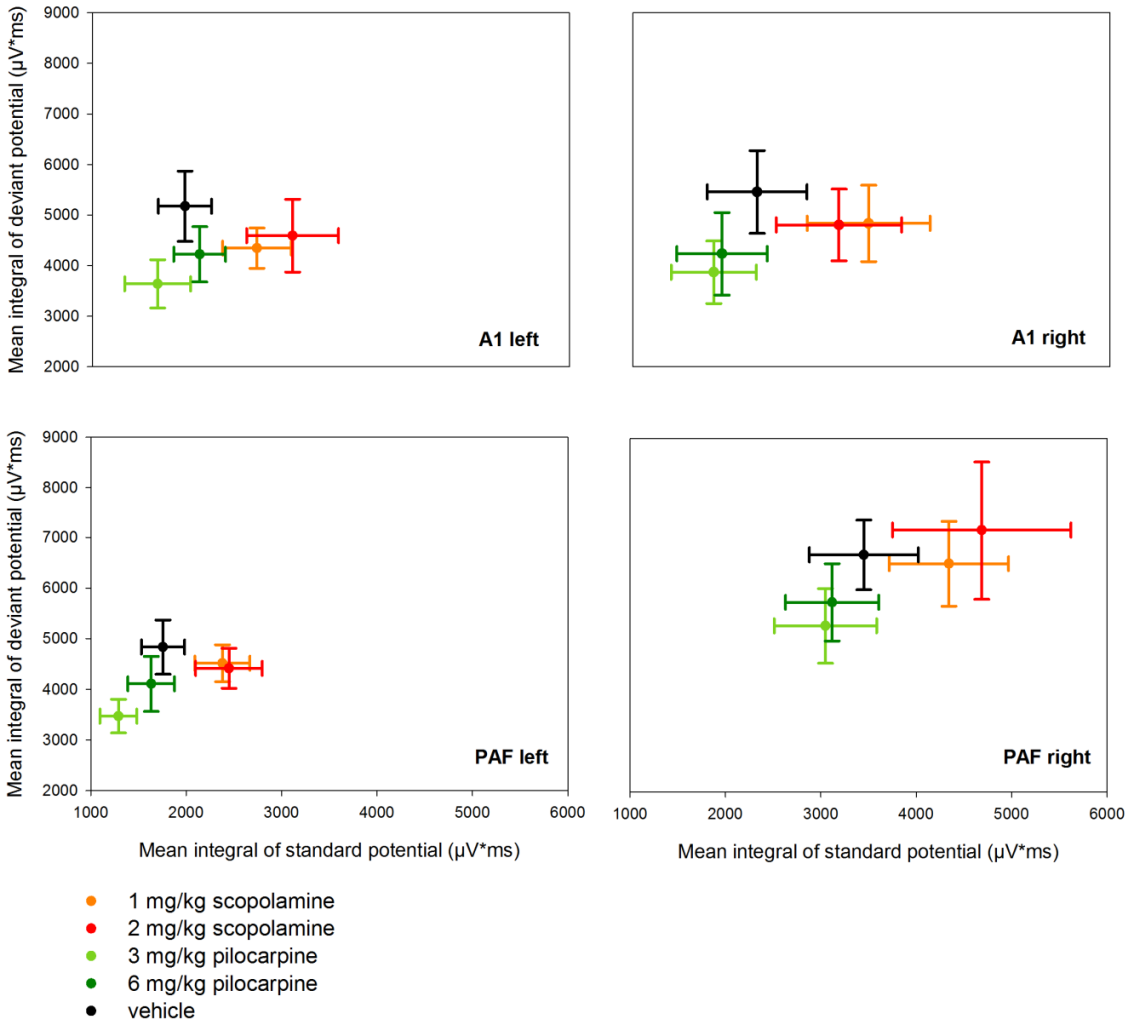

Figure 45: Integrals for deviant and standard potentials in five different treatment conditions. Integral values of standard potentials are shifted to larger integral values after scopolamine treatment (1 mg/kg depicted in orange, 2 mg/kg depicted in red). After treatment with pilocarpine (3 mg/kg displayed in light green, 6 mg/kg depicted in dark green) standard integral values seem to be reduced whereas after vehicle treatment (displayed in black) integrals are located in between the data points of the four different drugs. The details of the statistical comparison of integral values are given in the main text. Electrodes are designated in the lower right corner of each graph.

14 Discussion pharmacology

In this thesis, a pharmacological manipulation of the muscarinic acetylcholine receptor state was attempted. The motivation for this intervention was to explore one theory of MMN generation assuming that the difference wave, obtained by subtracting standard from deviant potentials, can be explained solely by adaptation of neurons in A1. A special type of adaptation, namely spike frequency adaptation, *i.e.* the decrease in response rate after repeated firing, is regulated particularly through muscarinic acetylcholine receptors. The activation of muscarinic receptors (pilocarpine) reduces slow calcium-activated potassium currents (Krause & Pedarzani, 2000) that hyperpolarize neurons after action potentials were generated thus enhancing the overall firing rate (Faber & Sah, 2003). Hence, blocking the muscarinic receptors with one of its antagonists (scopolamine) has opposite effects resulting in a reduction of the firing rate. As a consequence, after pharmacological treatment, attenuation of AEPs by scopolamine was expected because adaptation was thought to be enhanced. Pilocarpine on the contrary, was supposed to enhance AEPs due to an overall reduction of adaptation. Because standard potentials are most affected by adaptation due to the overall higher number of stimuli presented, those potentials were believed to show the highest drug effects. In order to interpret the present results, the function and distribution of muscarinic receptors has to be examined first.

14.1 Muscarinic receptors

14.1.1 Subtypes: transduction and distribution

Human muscarinic receptors are expressed at various sites throughout the CNS. Overall, five receptor subtypes have been cloned (m1, m2, m3, m4, m5) which are divided into two distinct classes based upon their properties of signal transduction (for review see Wess *et al.*, 2007). In rats, the existence of the same five receptor subtypes was demonstrated (Tice *et al.*, 1996).

The subtypes m1, m3 and m5 are coupled to the G-protein Gq/11 and thereby activate the phospholipase C that causes a release of calcium from intracellular stores. The stimulation of m2 and m4 receptors, however, leads to the inhibition of adenylate cyclase and reduces intracellular concentrations of cAMP (cyclic adenosine monophosphate). Subtypes m2 and m4 are supposed to act as cholinergic autoreceptors and inhibit ACh release in peripheral and central neurons (Starke *et al.*, 1989; Yan & Surmeier, 1996).

The most abundant human subtype in the CNS is the m1 receptor that can be found on postsynaptic neurons in the cortex, hippocampus, striatum and thalamus. The m2-receptors reside at cholinergic synaptic terminals in the brainstem, thalamus, cortex, hippocampus and striatum. The overall CNS levels of m3 and m5 are much lower compared to m1 and m2. The receptor subtype m3 is located in the cortex and hippocampus. Although m4 can be found in these areas too, it is particularly numerous in the striatum and appears to play a crucial role in controlling dopamine release and locomotor activity. The human m5 receptor seems to be restricted to the substantia nigra only (for review see Langmead *et al.*, 2008). In rats, the existence of the same five receptor subtypes was demonstrated (Tice *et al.*, 1996).

14.1.2 Cellular processes

The activation/ blocking of slow calcium activated potassium currents, i.e. the specific process that ought to be targeted in the present study, is supposed to be G-protein-mediated but phospholipase C-independent (Krause & Pedarzani, 2000). However, due to a lack of knowledge about the specific muscarinic subtype that is engaged in spike frequency adaptation, pilocarpine and scopolamine were employed in this thesis. Both substances bind non-specifically to all muscarinic receptor subtypes, whereas pilocarpine exhibits agonistic and scopolamine antagonistic properties.

The present study did not show the expected results (*cf.* 14). On the contrary, activating muscarinic receptors by the application of pilocarpine reduced AEP amplitudes in contrast to the blocking of the respective receptors by scopolamine that increased amplitudes. At the receptor level, inhibitory effects by the activation of muscarinic receptors were described for the subtypes m2 and m4 (Brown *et al.*, 1997; Bosch & Schmid, 2006). The

reduction of activity has been proposed (among other mechanisms) to be caused by the increase of potassium conductance (Brown *et al.*, 1997) or down-regulation of presynaptic Ca^{2+} influx (Yan & Surmeier, 1996). Carbachol, an agonist of muscarinic receptors, for example was shown to reduce excitatory postsynaptic potentials in recordings from pyramidal neurons in hippocampal slice preparations (Seeger & Alzheimer, 2001).

Cellular processes regulated by muscarinic receptors become even more complex taking into account that ACh modulates also non-cholinergic neurotransmission via the same receptors (Aigner, 1995). The application of oxotremorine (agonist) depressed AMPA (α-amino-3-hydroxy-5-methyl-4-isoxazolepropionic acid) receptor-mediated currents in rat auditory cortex slices presumably due to a presynaptic effect (Atzori *et al.*, 2005). However, there are also studies reporting opposing effects of muscarinic agonists on slice preparations of the rat auditory cortex. Activation of muscarinic receptors (by acetyl-β-methylcholine) was shown to result in a long-lasting enhancement of NMDA (N-Methyl-D-aspartate)-mediated neurotransmission (Aramakis *et al.*, 1997).

The studies described above illustrate only a small proportion of the various cellular actions throughout the CNS that are mediated or modulated via muscarinic receptor subtypes. It can be concluded that the particular response that is provoked by activation or inhibition of muscarinic receptors depends primarily on the location of the respective receptor subtype (Wess *et al.*, 2007). Due to the various actions and pathways that can be altered by these receptors, the specific muscarinic effect found in the present study cannot be attributed to a single receptor subtype or pathway.

In the following, the effects of the two substances will be interpreted at the level of evoked potentials.

14.2 Drug effects on evoked responses

14.2.1 Mismatch responses

The present literature reporting muscarinic effects on the MMN is not yet conclusive. In one study (Pekkonen, 2001), the amplitude of the magnetic MMN to frequency changes was attenuated by the application of the muscarinic antagonist scopolamine whereas the

MMN to duration mismatch was not affected. In a later study, presented by the same group, however, no effect of scopolamine on the electric and magnetic MMN could be demonstrated (Pekkonen *et al.*, 2005). In the present study, mismatch responses calculated as the difference between deviant and standard potential were preserved across treatments. The effect of scopolamine and pilocarpine treatment on deviant and standard AEPs is discussed below.

14.2.2 Effect of scopolamine

In the present study, the administration of 2 mg/kg scopolamine provoked an earlier occurrence of the N1-peak compared to vehicle treatment in electrode A1 right. No significant effect of treatment was observable with respect to the later P2-peak. In general, scopolamine was shown to enhance potential amplitude as explicitly demonstrated by comparison of integrals. In the present literature describing the effect of scopolamine on AEPs, however, opposite effects were reported.

Obligatory AEP components (P18, N40) recorded epidurally from the vertex of awake rats were shown to decrease after treatment with 0.1-1.0 mg/kg scopolamine (Campbell *et al.*, 1995). Miyazato *et al.* (1995) reported similarly that intravenous injections of scopolamine dose-dependently blocked specific vertex recorded AEP components of awake rats with a final disappearance. This effect was reversed by subsequent injections of physostigmine, a substance that inhibits the acetylcholinesterase and thereby stimulates indirectly muscarinic receptors.

However, vertex responses have to be distinguished from cortical AEPs since both potential classes mainly derive from two functionally distinct pathways. Vertex AEPs are generated by the extralemniscal pathway that is non-tonotopically organized, excited by multimodal stimuli and broadly tuned (Lennartz & Weinberger, 1992). Cortical AEPs, however, derive from projections of the lemniscal pathway, ascending from the core region of the inferior colliculus, crossing the ventral nucleus of the MGB and finally targeting the core region of the primary auditory cortex. The latter fiber tract is known to exhibit precise frequency tuning and tonotopic arrangement.

In rats, activity of the primary auditory cortex does not contribute to the responses recordable at the vertex (Knight *et al.*, 1985). Peaks generated inside the primary auditory cortex can be detected only at a very small area on the lateral surface of the brain (Barth & Di, 1990; Simpson & Knight, 1993a). In humans, on the contrary, vertex waves 1-7 reflect activation of generators inside the auditory cortex (Buchwald *et al.*, 1981) whereas later potential components originate from lemniscal generators.

The two potential classes were also shown to possess different properties: Cortical AEPs recorded directly above the temporal lobe of cats are unaffected by sleep (Chen & Buchwald, 1986), barbiturate anesthesia (Galambos *et al.*, 1961) and high stimulus repetition rates (Knight *et al.*, 1985). On the contrary, vertex recorded potential components which are independent of generators in the auditory cortex, are attenuated by slow wave sleep (Chen & Buchwald, 1986; Buchwald *et al.*, 1991) as well as barbiturate anesthesia (Galambos *et al.*, 1961; Buchwald *et al.*, 1991; Simpson & Knight, 1993b) and stimulation rates higher than 1 Hz (Buchwald *et al.*, 1981). The latter potential class has been proposed to derive from ascending cholinergic fibers from the reticular activating system which is a major source of cholinergic projections to the cortex. This is especially in line with the sleep-wake dependence of the AEP components.

The overall distinction of the two pathways generating the described potential classes may explain the effect of scopolamine observed in the present study. In contrast to decreased AEP components of the vertex potential class described in literature, this thesis determined significantly enhanced integrals especially of standard potentials after injection of scopolamine. This effect was mainly observed for late potential components arising after the offset response. However, AEP components recorded from the auditory cortex of rats were shown to remain stable after treatment with 0.2, 1.0, or 5.0 mg/kg scopolamine (Miyazato *et al.*, 1995), although the late potential components were not investigated. The importance of the separate analysis of distinct potential components was additionally demonstrated in a study recording from the auditory cortex of awake cats. It was shown that cholinergic agonists provoked heterogeneous, selective effects on different components of the responses (“on” response versus “off” response) rather than simply increasing or decreasing overall discharge levels (McKenna *et al.*, 1988). In human

subjects middle latency AEP components which are known to be generated inside the auditory cortex seem to be enhanced by scopolamine (Jääskelainen et al., 1999). An increase for a potential component after scopolamine treatment was also found for the human Pa peak that can be detected at the vertex but is most likely generated by the auditory cortex (Buchwald *et al.*, 1991).

With respect to EEG frequency, scopolamine was shown to decrease low voltage fast activity and leads to a shift towards high voltage low activity patterns after i. p. injection of 5 mg/kg recorded from the sensory-motor cortex in anesthetized rats (Dringenberg & Vanderwolf, 1997) or 0.8 mg/kg scopolamine in awake rats recorded from frontal and occipital areas (Riekkinen *et al.*, 1990). As already mentioned in the introduction (*cf.* 3.2.2), there is a close relationship between the cholinergic transmission to the cortex and the occurrence of rhythmic EEG activity. During periods of low voltage and fast activity, the cortical release of ACh from cat neocortex was observed to be higher than during periods of large amplitude irregular slow activity (Celesia & Jasper, 1966). Although the EEG frequency was not investigated in the present study the finding of enhanced voltage values represented in enlarged amplitudes that was present in the averaged potentials after treatment with scopolamine may not be explained by the irregularly occurring low frequency, high voltage activity present in the EEG that has been reported to be induced by low cortical ACh levels in general. This EEG activity would be temporally independent of the acoustic stimulation and thereby averaged out by calculating evoked potentials. Enhancement of components in cortical AEPs after scopolamine treatment can be most likely explained by specific properties of the lemniscal pathway transmitting auditory information to the core of the auditory cortex.

14.2.3 Effect of pilocarpine

In this study, pilocarpine was shown to decrease the overall potential waveforms as demonstrated by the comparison of integral values across five treatments. Pharmacologically, pilocarpine has opposite effects as scopolamine by activating the muscarinic acetylcholine receptor and consequently enhancing cholinergic signaling. This treatment did indeed result in opposite effects as those observed for scopolamine.

However, pilocarpine was thought to reduce spike frequency adaptation and thereby supposed to enhance potential amplitudes especially of standard potentials.

Until today, pilocarpine is used to induce chronic epilepsy in rats to study this disease and possibilities of its treatment. Therefore, pilocarpine is injected in very high doses from 80 mg/kg up to 400 mg/kg. Sub-convulsive doses and their effect on EEG or evoked potentials are rarely investigated.

Some studies were focused on the effects of cholinergic system modulation on visually evoked potentials. These results resemble those of the present study, although the underlying pathway is different. For example, treatment with pilocarpine resulted in attenuated amplitudes of late potential components of visually evoked potentials recorded in awake rats. Nevertheless, early components remained unchanged (Fleming *et al.*, 1974). Furthermore, the effect of a cholinergic agonist (AF102B) on the auditory P3 component in the macaque was studied (O'Neill *et al.*, 2000). The P3 is a special peak component which is only evoked in oddball paradigms were the deviant stimulus is attended. P3 amplitude was significantly enhanced following systemic administration at "cognition-enhancing" doses as a response to rare tones associated with fruit-juice reinforcement. However, the present study and the results presented by Fleming *et al.* (1974) indicate that pilocarpine also attenuates evoked potentials. This finding, as discussed in the previous section (*cf.* 14.2.2), may be dependent on the functional pathway that is engaged in the generation of a specific peak. The P3 peak that was investigated in the above mentioned study (O'Neill *et al.*, 2000), for example, is no obligatory component of auditory evoked potentials but can be generated in specific tasks and with a subject focusing its attention on the acoustic stimulus. Therefore, cognitive processes seem to be also involved in P3 generation, which suggests that this peak is at least partially generated by a pathway different from the core auditory projection. Due to the lack of studies using experimental designs comparable to our study, it is difficult to interpret the demonstrated effects of pilocarpine on AEPs in awake rats.

Nevertheless, scopolamine and pilocarpine were shown to exhibit opposite effects on AEP in the present study. This suggests that the same pathway was modulated by the two

substances. However, the detected effect seems to be independent of spike frequency adaptation.

14.3 Peripheral side effects

A possible limitation of the chosen experimental design is that no control for peripheral side effects of the muscarinic drugs was implemented. Both substances were injected i. p. and consequently also affect muscarinic receptors located on peripheral organs and smooth muscles, causing contraction or dilatation in the respiratory, vascular and gastrointestinal system (Eglen *et al.*, 1996). Scopolamine for example is known to dilate the pupil and impair lens accommodation (Leopold & Comroe, 1948). It also reduces salivation and, in addition, might induce gastrointestinal distress (*e.g.* constipation) or cause changes in cerebral blood flow and glucose consumption due to vasodilation/ vasoconstriction (for review see Klinkenberg & Blokland, 2010). The injection of pilocarpine was shown to induce salivation and thirst in rats (Sato *et al.*, 2006) and it can also provoke cardiovascular responses (Takakura *et al.*, 2005).

A possible way to deal with the problem of peripheral side effects with respect to scopolamine is the application of methyl-scopolamine, a quaternary form of scopolamine. It is known to bind to the muscarinic receptor with the same properties as scopolamine but cannot cross the blood-brain barrier (Pradhan & Roth, 1968) since it is highly polarized. Introducing a control group receiving only methyl-scopolamine, facilitates the control for possible peripheral effects: if an effect is seen in the scopolamine-treated subjects only, but not in those who received methyl-scopolamine, it can be concluded that the observed effect is due to the central action of scopolamine (Evans, 1975). However, in the last decades the solely peripheral action of methyl-scopolamine has been doubted because the substance seems to have effects on cognition in animals (van Haaren & van Hest, 1989; Pakarinen & Moerschbaecher, 1993; Andrews *et al.*, 1994). This finding indeed strongly suggests central effects of methyl-scopolamine while it has also been shown by a microdialysis study that methyl-scopolamine increases cortical acetylcholine release and may even reach the central nervous system itself (Moore *et al.*, 1992). From the above

mentioned results it can be concluded that the control for peripheral effects employed so far may be unsufficient to distinguish peripheral from central muscarinic effects.

A substance that was used in epilepsy studies in order to block peripheral effects of pilocarpine is atropine methylbromide which is known not to interact with status epilepticus (for review see Curia *et al.*, 2008) but binds to peripheral muscarinic receptors and inhibits cholinergic transmission.

However, due to the various interactions and the possibility that even quaternary, polarized substances interact with the cholinergic metabolism in the CNS, the additional application of drugs was avoided in the present study.

14.4 Relationship of spike frequency adaptation and stimulus specific adaptation

The rationale for employing muscarinic drugs in the present study was to investigate whether adaptation alone can account for the overall difference between standard and deviant potential. Therefore, a manipulation of spike frequency adaptation was attempted.

The theory of adaptation as a mechanism for explaining MMN has been put forward several years ago (May *et al.*, 1999) and in addition, a single-neuron correlate, namely stimulus specific adaptation (SSA) was suggested that may account for all properties of the surface recorded MMN (Ulanovsky *et al.*, 2003; Ulanovsky *et al.*, 2004). This correlate, however, may be a mechanism independent of spike frequency adaptation, and it is questionable whether muscarinergic drugs do affect SSA.

SSA was shown to exhibit stimulus-specificity even at the neuron level (Ulanovsky *et al.*, 2003), whereas spike frequency adaptation that was targeted in the present study, is a process that reduces the overall excitability of a neuron after the generation of action potentials. As a consequence, spike frequency adaptation cannot tune the response of a single cell specifically for a particular auditory stimulus. In a review presented by Nelken & Ulanovsky (2007) the difference between adaptation and the suggested single neuron correlate, which the authors suggest to explain the MMN, namely SSA is described in

detail (*cf.* 8.6). SSA is defined as "single neuron habituation" as opposed to adaptation because the initial response amplitude can be restored by a different stimulus. According to the authors (Ulanovsky *et al.*, 2004), stimulus specificity can only be expressed by a mechanism that is able to affect distinct proportions of the dendritic tree namely the input to the neuron. Therefore, synaptic depression and facilitation (Abbott *et al.*, 1997; Tsodyks & Markram, 1997) or inhibition (Zhang *et al.*, 2003) have been proposed as cellular mechanisms. Spike frequency adaptation, however, changes the output of neurons and can therefore not account for properties of SSA that was demonstrated by Ulanovsky *et al.* (2003) in auditory neurons as a response to acoustic oddball stimulation.

Whether SSA alone can account for MMN and/ or MMN-like phenomena is still a subject of debate (Ulanovsky *et al.*, 2004). However, the pharmacological manipulation of SSA has to be attempted at the single neuron level first, if successful, should be employed at a higher recording level in order to investigate whether surface recordable difference waves can be changed in the same manner. Therefore, the involved receptors and neurotransmitter have to be uncovered first.

From the recorded potential waveforms evoked after treatment with pilocarpine or scopolamine no final conclusions can be drawn whether spike frequency adaptation is involved in the generation of MMM-like potentials or not. The chosen experimental design was unsuccessful to detect the manipulation of this very specific mechanism that has been demonstrated at the single cell level, due to the various muscarinic actions and pathways that are present in the CNS.

14.5 Conclusion

It has been shown in the present thesis that cholinergic signaling is involved in the generation of cortical AEPs that arise from generators in the lemniscal pathway. Scopolamine was demonstrated to enhance evoked potentials whereas pilocarpine had opposite effects. However, with the chosen experimental setup it was not possible to alter either spike frequency adaptation or detect these manipulations at the level of epidural AEP recordings from the auditory cortex.

The pharmacological study was initially conceived to validate dynamic causal models by attempting a detection of parametric receptor modulation with the mathematical model. Modeling results will be presented in the next section of this thesis.

15 Results dynamic causal modeling after pharmacological treatment

Dynamic causal modeling (DCM) was performed on the evoked potential data recorded after treatment with muscarinic drugs (agonist: pilocarpine, antagonist: scopolamine) and vehicle injection. For simplicity, the results of the single model selection are not displayed if the model exceedance probability was below 50 %. First, the DCM results after vehicle treatment will be presented.

The results of the family-level Bayesian model selection (BMS) are depicted in Figure 46. Models allowing for adaptation in A1 (models 5 to 8) were superior to models that did not allow for adaptation in A1 (models 1 to 4) (exceedance probability > 90 %). In addition, models that included synaptic plasticity modeled in form of deviant-induced changes in forward and backward connectivity (models 2 to 4 and 6 to 8) were superior to models that did not include plasticity (model 1 and 5) (exceedance probability > 85 %).

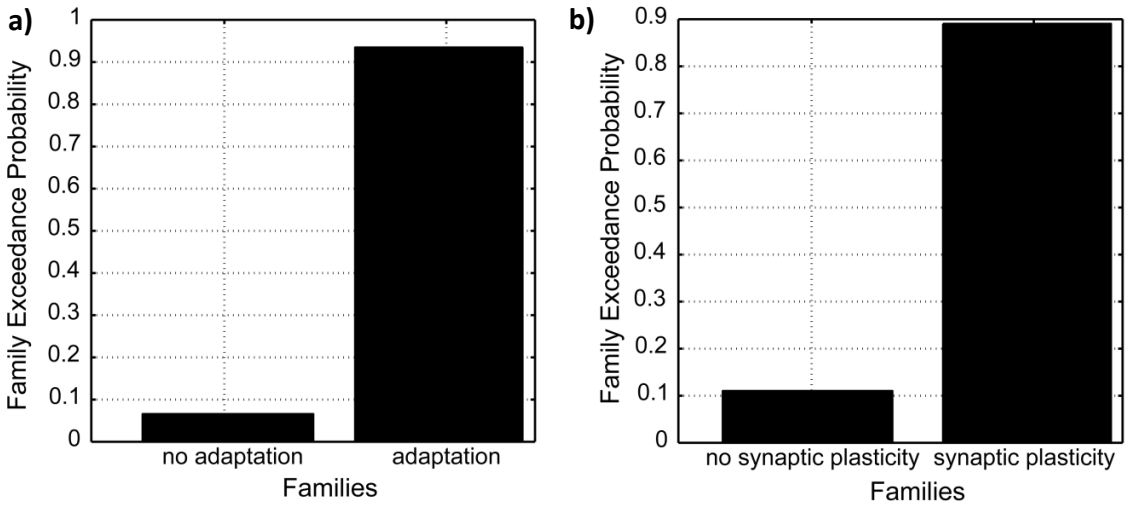

Figure 46: Family-level BMS comparing families with adaptation to families without adaptation and families with synaptic plasticity to families without synaptic plasticity after vehicle treatment. a) Family-level BMS showed that models allowing for adaptation (models 5-8) exhibited greater log model evidence than models without adaption in A1 (models 1-4, exceedance probability > 90 %). b) Family-level BMS revealed models with synaptic plasticity (model 2-4 and 6-8, which included the modulation of forward and backward connections between A1 and PAF) were superior to models without synaptic plasticity (models 1 and 5) with an exceedance probability > 85 %.

The BMS results for the comparison of model families after treatment with 1 mg/kg scopolamine are displayed in Figure 47. Models including adaptation exhibited a family exceedance probability > 60 %, whereas models including synaptic plasticity were superior to models without synaptic plasticity with a model exceedance probability > 75 %.

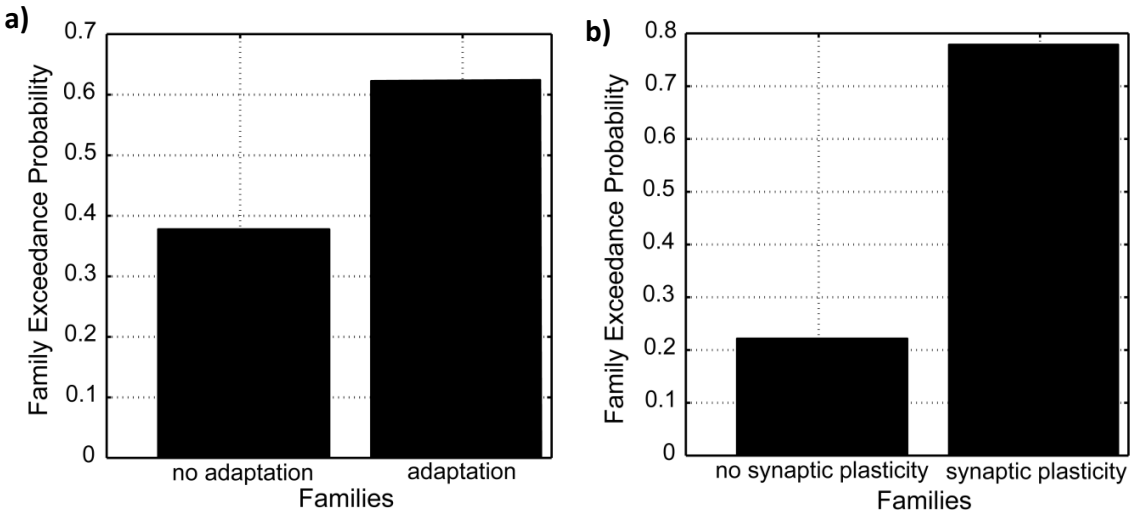

Figure 47: Family-level BMS comparing families with adaptation to families without adaptation and families with synaptic plasticity to families without synaptic plasticity after treatment with 1 mg/kg scopolamine. a) Family-level BMS showed that models allowing for adaptation (models 5-8) exhibited greater log model evidence than models without adaption in A1 (models 1-4, exceedance probability > 60 %). b) Family-level BMS revealed models with synaptic plasticity (model 2-4 and 6-8, which included the modulation of forward and backward connections between A1 and PAF) were superior to models without synaptic plasticity (models 1 and 5) with an exceedance probability > 75 %.

The results of the family-level comparison for the 2 mg/kg scopolamine condition are depicted in Figure 48. The implementation of adaptation led to a family exceedance probability > 70 %. With respect to the factor synaptic plasticity, the model families could not be differentiated, because they exhibited nearly equal model evidences.

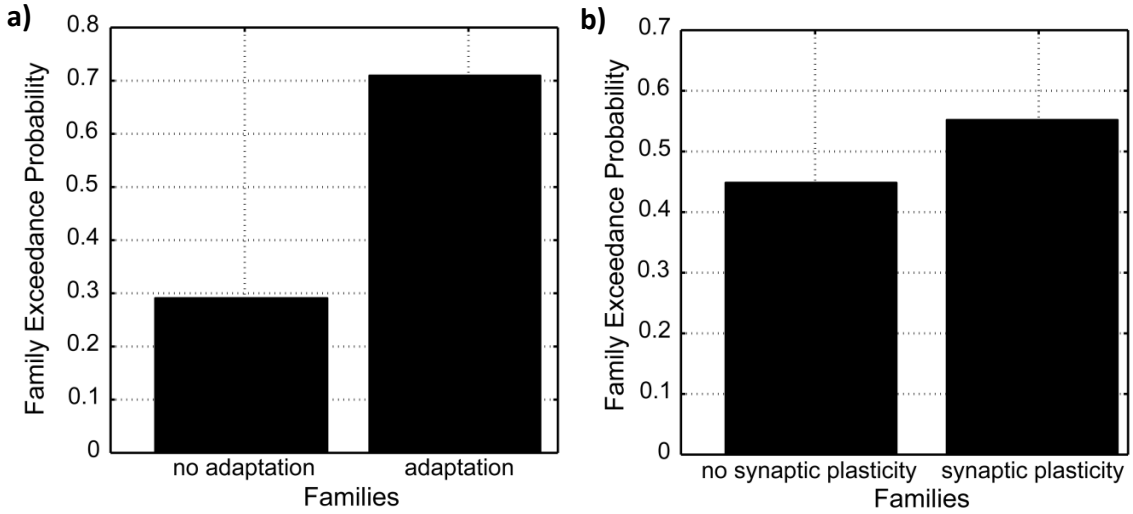

Figure 48: Family-level BMS comparing families with adaptation to families without adaptation and families with synaptic plasticity to families without synaptic plasticity after treatment with 2 mg/kg scopolamine. a) Family-level BMS showed that models allowing for adaptation (models 5-8) exhibited greater log model evidence than models without adaption in A1 (models 1-4, exceedance probability > 70 %). b) Family-level BMS revealed that synaptic plasticity seems not to be an important mechanistic factor to explain the effect of the deviant after treatment with 2 mg/kg scopolamine.

Random effects BMS indicates that after treatment with 3 mg/kg pilocarpine, model 8, which explains the effect of the deviant by changes in local adaptation in A1 and synaptic plasticity in forward connections from A1 to PAF as well as backward connections from PAF to A1, exhibited higher log model evidence compared to all other models with exceedance probability > 85 % (Figure 49).

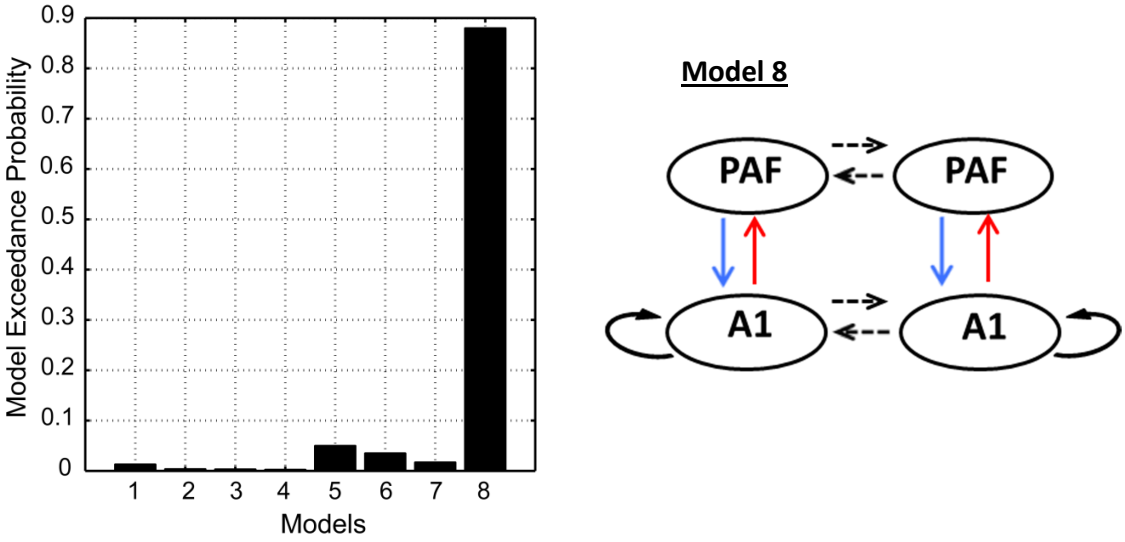

Figure 49: Results of the random effects BMS for eight models describing the effect of the deviant on the investigated network after treatment with 3 mg/kg pilocarpine. Model 8 exhibited higher log model evidence compared to the other models included in the BMS analysis (exceedance probability > 85 %). This model explained the effect of the deviant with adaptation in A1 and plasticity in forward connections from A1 to PAF as well as backward connections from PAF to A1.

Family-level BMS conducted for models after treatment with 3 mg/kg pilocarpine showed that models allowing for adaptation in A1 were superior to models that did not allow for adaptation in A1 (exceedance probability > 95 %, Figure 50). Furthermore, models that included synaptic plasticity in form of changes in forward and backward connectivity induced by the deviant stimulus were superior to models that did not include synaptic plasticity (exceedance probability > 90 %).

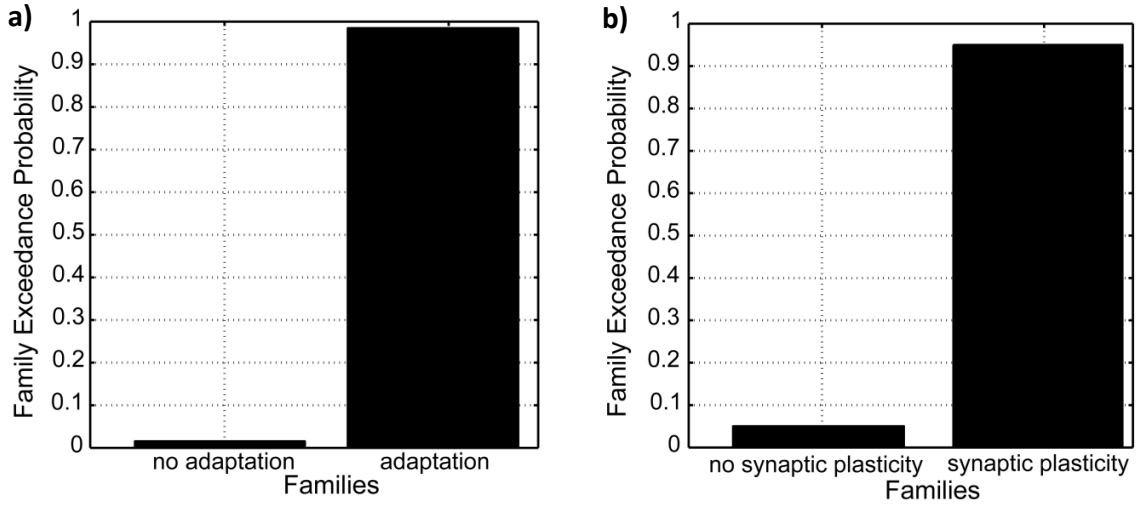

Figure 50: Family-level BMS comparing families with adaptation to families without adaptation and families with synaptic plasticity to families without synaptic plasticity after treatment with 3 mg/kg pilocarpine. a) Family-level BMS showed that models allowing for adaptation (models 5-8) exhibited greater log model evidence than models without adaption in A1 (models 1-4, exceedance probability > 95 %). b) Family-level BMS revealed models with synaptic plasticity (model 2-4 and 6-8, which included the modulation of forward and backward connections between A1 and PAF) were superior to models without synaptic plasticity (models 1 and 5) with an exceedance probability > 90 %.

Random effects BMS performed for models after treatment with 6 mg/kg pilocarpine revealed a single superior model (Figure 51). Model 6, which explains the effect of the deviant by changes in local adaptation in A1 and synaptic plasticity in forward connections from A1 to PAF, exhibited higher log model evidence with exceedance probability > 85 %.

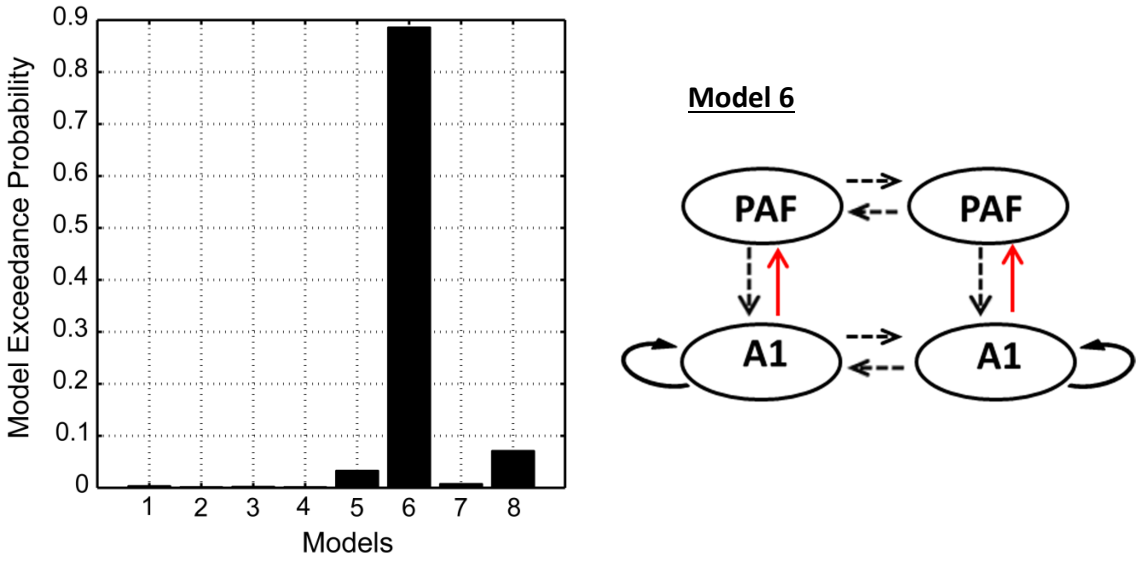

Figure 51: Results of the random effects BMS for eight models describing the effect of the deviant on the investigated network. Model 6 exhibited higher log model evidence compared to the other models included in the BMS analysis (exceedance probability > 85 %). This model explained the effect of the deviant with adaptation in A1 and plasticity in forward connections from A1 to PAF.

With respect to the family-level comparison that was performed for models after treatment with 6 mg/kg pilocarpine, adaptation and synaptic plasticity were both important mechanistic factors (Figure 52). The model family allowing for adaptation reached an exceedance probability > 95 %. In addition, the model family including synaptic plasticity exhibited an exceedance probability > 95 %.

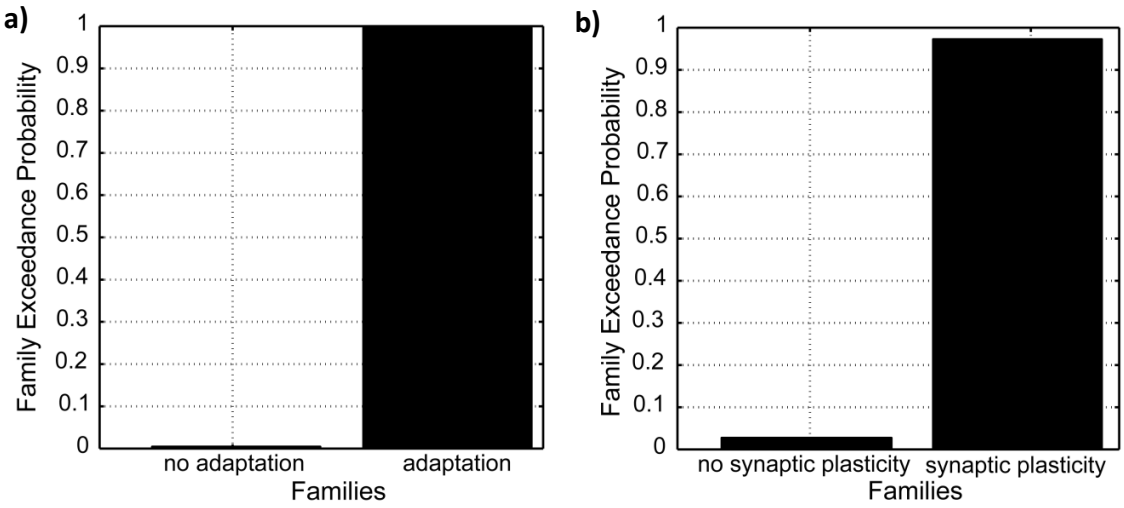

Figure 52: Family-level BMS comparing families with adaptation to families without adaptation and families with synaptic plasticity to families without synaptic plasticity after treatment with 6 mg/kg pilocarpine. a) Family-level BMS showed that models allowing for adaptation (models 5-8) exhibited greater log model evidence than models without adaption in A1 (models 1-4, exceedance probability > 95 %). b) Family-level BMS revealed models with synaptic plasticity (model 2-4 and 6-8, which included the modulation of forward and backward connections between A1 and PAF) were superior to models without synaptic plasticity (models 1 and 5) with an exceedance probability> 95 %.

16 Discussion dynamic causal modeling after treatment

With a parametric modulation of muscarinic acetylcholine receptors, we aimed to investigate the effect of changes in adaptation, namely spike frequency adaptation on mismatch responses and ask whether DCM for ERPs can successfully detect these manipulations.

In a previous study using the same experimental setup with epidural electrodes placed above A1 and PAF but in the isoflurane-anesthetized rat it has been shown that anesthesia induced effects can indeed be detected with DCM (Moran *et al.*, 2011). In this study, no oddball stimulation was employed but the continuous EEG to silence and acoustic white noise stimulation was recorded. The resulting parameter estimates indicated that the amplitude of fast glutamatergic EPSPs and IPSPs in addition changed as predicted by previous neurophysiological studies. Glutamatergic EPSPs were shown to decrease linearly with increasing levels of isoflurane whereas fast GABAergic IPSPs displayed a nonlinear (saturating) increase. This study argues for the vability of DCM to infer on specific synaptic processes from macroscopic electrophysiological data.

With respect to the pharmacological manipulation of muscarinic acetylcholine receptors in the awake animal that was intended in the present thesis, a specific manipulation of spike frequency adaptation was attempted. However, as discussed in the previous section (*cf.* 14), scopolamine was shown to enhance particularly late potential components whereas pilocarpine application led to opposite effects, *i.e.* decreasing AEPs in awake rats. It has to be concluded that a possible alteration of this particular adaptational mechanism could not be detected with the chosen experimental setup. As a consequence, our model was ill-defined and DCM could not reveal further details about an involvement of spike frequency adaptation in the generation of MMN-like phenomena. Due to completeness, however, the DCM results after muscarinic treatment were presented and will be discussed below.

16.1 Vehicle

BMS for models after vehicle treatment revealed no single superior model. However, family-level comparison showed that adaptation as well as synaptic plasticity was an important mechanistic factor explaining the effect of the deviant on the investigated network. This finding resembles the results of the family-level comparison conducted for models fit to AEP data from non-treated animals (*cf.* 12.2). The reproducibility of these results again supports our findings: adaptation seems to be a key mechanism underlying the generation of mismatch responses, while also evidence for an involvement of synaptic plasticity exists.

16.2 Scopolamine

The analysis performed for models after treatment with scopolamine demonstrated that no single model could explain the effect of the deviant after treatment with 1 or 2 mg/kg scopolamine. The lack of a single superior model explaining the underlying data in both the vehicle and scopolamine condition may be due to the caveats mentioned in the previous DCM section: DCM for ERPs is based on a neural mass model, originally designed to simulate the dynamics of human evoked potential data. In addition, the electrodes in the present study were closely spaced; therefore, there is no strict hierarchy between the primary and secondary auditory areas from which AEPs were recorded in the present study. This may have led to an indistinguishability of forward and backward connections between the areas.

In the low scopolamine condition, family-based inference for models allowing for adaptation and models without adaptation led to nearly equal exceedance probabilities suggesting that the two model families could not be distinguished. For the second mechanistic factor that was investigated, i.e. synaptic plasticity, there was not strong evidence that the presence of synaptic plasticity was an important factor that explained the effect of the deviant on the auditory network.

Family-level inference after treatment with 2 mg/kg scopolamine revealed weak evidence for the family, which included adaptation. With respect to the analysis comparing models

with synaptic plasticity to models without synaptic plasticity, families exhibited nearly equal probability; therefore, they could not be distinguished from each other.

Certainly, the application of scopolamine induced a change in the event-related potentials compared to the vehicle treatment, which that can also be observed in terms of differences in the family-level BMS results. In this drug condition, adaptation no longer seems to be an important mechanistic factor for explaining the effect of the deviant. This may be also reflected by enhancement of AEPs after scopolamine treatment.

16.3 Pilocarpine

Random-effects BMS after pilocarpine treatment, compared to the vehicle and scopolamine, revealed that model 8 was the winning model. This model explained the effect of the deviant as changes in forward and backward effective connectivity from A1 to PAF (and vice versa) and local adaptation in A1. Furthermore, family-level BMS demonstrated strong evidence for adaptation as an important mechanistic factor. In addition, synaptic plasticity was also important for explaining the effect of the deviant. The evidence for both mechanistic factors was also strong after treatment with 3 mg/kg pilocarpine.

After treatment with 6 mg/kg pilocarpine, model 6 that explained the effect of the deviant as changes in forward effective connectivity from A1 to PAF and adaptation in A1 was superior to all other models. This finding replicates BMS results in untreated animals (*cf.* 12.1). This suggests that the overall effect of the deviant was not altered by the application of 6 mg/kg pilocarpine. The family-level inference after treatment with 6 mg/kg pilocarpine demonstrates that there is strong evidence for adaptation and synaptic plasticity explaining the effect of the deviant.

16.4 Conclusion

The parametric modulation of spike frequency adaptation could not be detected by the recording of AEPs and as a consequence the modeling approach using DCM for

event-related potentials was ill-defined. However, the analysis of the spectral EEG components and modeling of adaptation with the second approach described previously (*cf.* 4.10.6) is outstanding. By varying the slope of the sigmoid function via an alteration of the parameters p_1 and p_2 the transformation from average membrane potential to average firing rate can be modulated (Kiebel et al., 2008). The analysis of spectral EEG components may shed light on alterations induced by the application of muscarinic drugs that were present in the background EEG but not time-locked to the acoustic stimulation and therefore averaged out by calculating AEPs. Nevertheless, general alterations of spike frequency adaptation may not be expected because the presence of this mechanism depends on the activation of neurons by the presentation of acoustic stimuli.

The present thesis shows, however, that results after vehicle injection replicate previous results with adaptation and synaptic plasticity being important for explaining the effect of the deviant. DCM results after pilocarpine treatment demonstrate that the substance did not alter the effect of the deviant on the investigated network compared to vehicle treatment. With respect to family-inference after scopolamine treatment, adaptation seems to be less important.

The modeling attempt using DCM for ERPs on rat data, which has been presented in this thesis, is only one step within this type of modeling studies. The present study shows that DCM can be successfully applied to AEPs recorded in awake rats, however it has to be mentioned that family-inference results were most conclusive. With respect to the single model selection, choosing one superior model was not successful several times suggesting that the model fit to the data has to be improved for further studies, maybe by the use of a set of priors accounting for faster time constants underlying rat AEPs.

17 General discussion

The present thesis demonstrates that robust MMN-like potentials can be recorded in awake and unrestrained Black hooded rats, if some basic methodological requirements are fulfilled: As preliminary studies revealed, acoustic experiments require a careful selection of the suitable rat strain in advance, because the hearing ability can differ enormously between strains. Therefore, the evaluation of hearing thresholds prior to acoustic experiments is indispensable.

Frequencies employed for acoustic stimulation were shown to fit well the rats hearing range and evoked large amplitude auditory evoked potentials (AEPs). In addition, the implementation of longer duration stimuli compared to other MMN studies in rats (Ruusuvirta *et al.*, 1998; Astikainen *et al.*, 2006; Tikhonravov *et al.*, 2008; Tikhonravov *et al.*, 2010; Astikainen *et al.*, 2011) is recommended because differences between both potentials increased with increasing stimulus duration. Furthermore, the present thesis demonstrated that habituating animals to the experimental setup and acoustic stimulation is important for obtaining stable electrophysiological recordings.

In the main oddball experiments, MMN-like potentials in terms of large amplitude differences between standard and deviant potential were observed in awake rats. Those were recorded from both the primary auditory cortex A1 and the posterior auditory field (PAF). The detected mismatch responses share key properties with human MMN (Näätänen, 1992 ; Imada *et al.*, 1993; Javitt *et al.*, 1998; Shelley *et al.*, 1999; Sato *et al.*, 2000; Sabri & Campbell, 2001; Sonnadara *et al.*, 2006): differences between standard and deviant potential were enhanced by the reduction of the overall probability of deviant occurrence. However, the operational definition of the MMN determined as “deviant minus standard potential” identifies only adaptation, *i.e.* a reduced response to the standard stimulus as a result of repeated stimulus presentation, and cannot be employed solely to reveal mechanisms like prediction error generation.

In order to differentiate between adaptation and other possible mechanisms explaining MMN-like phenomena like deviance detection or prediction error signaling, four control experiments were conducted.

(1) One paradigm showed that an increased deviant probability resulting in a nearly equal number of deviant and standard stimuli (0.4 versus 0.6 probability), led to an extinction of the differences between both potentials. This may indicate that due to the large number of deviants presented, adaptation occurred also for deviant sounds. On the other hand, arguing with prediction error signaling the large number of deviants may have not allowed for generating a prediction about an upcoming sequence and thereby a prediction error for both stimulus types may have been generated.

(2) Although in humans MMN is provoked by the complete omission of deviant stimuli from the sequence (Joutsiniemi & Hari, 1989; Nordby *et al.*, 1994; Yabe *et al.*, 1997; Hughes *et al.*, 2001; Wacongne *et al.*, 2011), omission-evoked activity was not observed in awake rats with the chosen experimental setup. However, the same experiment should be repeated with the use of shorter interstimulus intervals because in humans, the elicitation of omission-evoked activity has been shown to depend on the chosen interval between standard stimuli (*cf.* 10.2 and Yabe *et al.* (1997)).

(3) The deviant-alone control condition resulted in enlarged obligatory peaks compared to oddball deviants but no additional potential components that were present only in oddball-elicited deviant potentials. Those components may have indicated generation mechanisms distinct from adaptation. However, this control condition is probably not appropriate for uncovering such mechanisms because the effect of neuronal responses on the overall duty cycle of the stimulation is completely neglected (*cf.* 9.3.1).

(4) Nevertheless, mismatch responses significantly diminished in the equiprobable control condition that removed the predictive context but preserved the overall presentation rate of the deviants. A limitation of the chosen design, however, was the close spacing of the frequencies thus not allowing for disambiguating precisely between cross-frequency adaptation and deviance detection or prediction error signaling.

It has to be concluded from the implemented control conditions that MMN-like potentials can be recorded in awake rats but the underlying mechanism have to be further investigated.

One possible approach is the use of dynamic causal models (DCM). In the present thesis, DCM was employed on the basis of the predictive coding framework explaining the MMN by local adaptation of neurons in A1 and synaptic plasticity of glutamatergic long-range connections, the latter establishing the prediction about the upcoming auditory sequence and signaling predictions and corresponding prediction errors across the hierarchy of the auditory system (Garrido *et al.*, 2008; Garrido *et al.*, 2009b; Schmidt *et al.*, 2012). DCM analyses indicated that adaptation is a key factor for explaining the effects of the deviant on the investigated network. This was demonstrated for both experimental conditions employed, namely 0.1 and 0.2 deviant probability. Although DCM revealed also evidence for the involvement of synaptic plasticity, the overall confidence was weaker compared to the family inference results for adaptation because this result derived from one experimental condition (0.1 deviant probability) only.

While the theory of prediction error generation has gained a lot of support from modeling studies (Garrido *et al.*, 2008; Schmidt *et al.*, 2012), there are other possible mechanisms that may explain MMN generation which are distinct from simple adaptation. The active detection of novelty or deviances in the acoustic environment and gating only those to a subject's awareness may be even more efficient than establishing a prediction about upcoming sensory stimuli each time a stimulus is presented. The latter theory of prediction error signaling may apply for stimuli which are rewarded or important to a subject and therefore have to be learned rapidly. However, short-term synaptic plasticity leading to learning of a recurring stimulus without any behavioral significance, as it is the case in oddball paradigms, may be inefficient and too energy-consuming. Crucial for an adequate reaction to novel sensory stimuli is the fast detection of deviances and to channel this information to awareness. For this, only one sudden strong response is needed, that may be explained by dishabituation caused by a novel stimulus at the single neuron level (Nelken & Ulanovsky, 2007).

In the next part of this project, the dependence of MMN-like potentials on adaptation in general was investigated. Treatment with muscarinic drugs (pilocarpine, scopolamine) was intended to alter a particular form of adaptation, namely spike frequency adaptation in order to investigate whether the generation of mismatch responses in awake rats is

dependent on this mechanism. The systemic treatment, however, either did not manipulate spike frequency adaptation or, if this process was affected, the effect was not detected with epidurally recorded AEPs in awake rats. In addition, there is an ongoing discussion if actually spike frequency adaptation or another adaptation mechanism, namely stimulus specific adaptation (SSA) may underlie MMN generation (Ulanovsky *et al.*, 2004). Nevertheless, it has been shown in the present thesis that cholinergic signaling is involved in the generation of potentials recorded from the lemniscal pathway with electrodes placed at the core of the auditory cortex. AEPs were altered by the treatment with muscarinic drugs in opposing directions: scopolamine enhanced the potentials while they were reduced after treatment with pilocarpine suggesting that both substances manipulated the same pathway.

The detection of the pharmacological manipulation using DCM was ill-defined because the specific mechanism (spike frequency adaptation) was not altered or the alteration could not be detected in the first place. However, the observed changes in the potential waveforms after drug treatment may be reflected in the results of the family-level comparison. DCM results after vehicle treatment indeed support previous findings demonstrating that both adaptation and synaptic plasticity were important mechanistic factors explaining the effect of the deviant on the investigated network for the 0.1 deviant probability condition.

The presented study indicates that mismatch responses can be obtained in awake rats, providing a basis for experimental investigations of the mechanisms that underlie MMN generation. With the established experimental setup it is possible to record AEPs without worrying about possible confounds of anesthesia. Investigating rodent analogues of human MMN is important because many diseases have been shown to be accompanied by reduced MMN amplitudes (Pekkonen *et al.*, 1994; Pekkonen *et al.*, 1995b; Shelley *et al.*, 1999; Baldeweg *et al.*, 1999; Näätänen, 2003; Umbricht & Krljes, 2005). Uncovering mechanisms underlying MMN generation can facilitate the detection of therapeutic targets at the cellular level for treating or ameliorating these disorders.

18 References

Abbott LF, Varela JA, Sen K, Nelson SB (1997) Synaptic depression and cortical gain control. Science 275(5297):220-224

Adrian ED (1942) Olfactory reactions in the brain of the hedgehog. J Physiol 100(4):459-473

Ahmed M, Mallo T, Leppanen PH, Hamalainen J, Ayravainen L, Ruusuvirta T, Astikainen P (2011) Mismatch brain response to speech sound changes in rats. Front Psychol 2:283

Aigner TG (1995) Pharmacology of memory: cholinergic-glutamatergic interactions. Curr Opin Neurobiol 5(2):155-160

Alain C, Woods DL, Knight RT (1998) A distributed cortical network for auditory sensory memory in humans. Brain Res 812(1-2):23-37

Alcaini M, Giard MH, Thevenet M, Pernier J (1994) Two separate frontal components in the N1 wave of the human auditory evoked response. Psychophysiology 31(6):611-615

Alho K, Sams M, Paavilainen P, Näätänen R (1986) Small pitch separation and the selective-attention effect on the ERP. Psychophysiology 23(2):189-197

Alho K, Woods DL, Algazi A, Knight RT, Näätänen R (1994) Lesions of frontal cortex diminish the auditory mismatch negativity. Electroencephalogr Clin Neurophysiol 91(5):353-362

Altman DG, Bland JM (2009) Parametric v non-parametric methods for data analysis. BMJ 338:a3167

Anderson LA, Christianson GB, Linden JF (2009) Stimulus-specific adaptation occurs in the auditory thalamus. J Neurosci 29(22):7359-7363

Andrews JS, Jansen JH, Linders S, Princen A (1994) Effects of disrupting the cholinergic system on short-term spatial memory in rats. Psychopharmacology (Berl) 115(4):485-494

Antle MC, Mistlberger RE (2005) Circadian Rhythms. . In: Whishaw IQ (ed) The Behavior of the Laboratory Rat. A Handbook with Tests. Oxford University Press, pp 183-194

Antunes FM, Nelken I, Covey E, Malmierca MS (2010) Stimulus-Specific Adaptation in the Auditory Thalamus of the Anesthetized Rat. PLoS ONE 5(11):e14071

Aramakis VB, Bandrowski AE, Ashe JH (1997) Activation of muscarinic receptors modulates NMDA receptor-mediated responses in auditory cortex. Experimental brain research. Experimentelle Hirnforschung. Experimentation cerebrale 113(3):484-496

Ashmore J (2008) Cochlear outer hair cell motility. Physiological reviews 88(1):173-210

Astikainen P, Ruusuvirta T, Wikgren J, Penttonen M (2006) Memory-based detection of rare sound feature combinations in anesthetized rats. Neuroreport 17(14):1561-1564

Astikainen P, Stefanics G, Nokia M, Lipponen A, Cong F, Penttonen M, Ruusuvirta T (2011) Memory-based mismatch response to frequency changes in rats. PLoS ONE 6(9):e24208

Atzori M, Kanold PO, Pineda JC, Flores-Hernandez J, Paz RD (2005) Dopamine prevents muscarinic-induced decrease of glutamate release in the auditory cortex. Neuroscience 134(4):1153-1165

Ayala YA, Perez-Gonzalez D, Duque D, Nelken I, Malmierca MS (2012) Frequency discrimination and stimulus deviance in the inferior colliculus and cochlear nucleus. Frontiers in neural circuits 6:119

Baldeweg T, Richardson A, Watkins S, Foale C, Gruzelier J (1999) Impaired auditory frequency discrimination in dyslexia detected with mismatch evoked potentials. Ann Neurol 45(4):495-503

Baldeweg T, Wong D, Stephan KE (2006) Nicotinic modulation of human auditory sensory memory: Evidence from mismatch negativity potentials. International journal of psychophysiology : official journal of the International Organization of Psychophysiology 59(1):49-58

Barth DS, Di S (1990) Three-dimensional analysis of auditory-evoked potentials in rat neocortex. Journal of Neurophysiology 64(5):1527-1536

Bäuerle P, von der Behrens W, Kossl M, Gäese BH (2011) Stimulus-specific adaptation in the gerbil primary auditory thalamus is the result of a fast frequency-specific habituation and is regulated by the corticofugal system. J Neurosci 31(26):9708-9722

Benda J, Herz AV (2003) A universal model for spike-frequency adaptation. Neural computation 15(11):2523-2564

Benjamini Y, Hochberg D (1995) The control of the false discovery rate in multiple testing under dependency. Journal of the Royal Statistical Society 57(1):289–300

Berger H (1929) Über das Elektroenkephalogramm des Menschen. pp 527-570

Bielefeld EC, Coling D, Chen GD, Li M, Tanaka C, Hu BH, Henderson D (2008) Age-related hearing loss in the Fischer 344/NHsd rat substrain. Hear Res 241(1-2):26-33

Bland JM, Altman DG (2009) Analysis of continuous data from small samples. BMJ 338:a3166

Bordi F, LeDoux JE (1994) Response properties of single units in areas of rat auditory thalamus that project to the amygdala. II. Cells receiving convergent auditory and somatosensory inputs and cells antidromically activated by amygdala stimulation. Experimental brain research. Experimentelle Hirnforschung. Experimentation cerebrale 98(2):275-286

Bosch D, Schmid S (2006) Activation of muscarinic cholinergic receptors inhibits giant neurones in the caudal pontine reticular nucleus. Eur J Neurosci 24(7):1967-1975

Böttcher-Gandor C, Ullsperger P (1992) Mismatch negativity in event-related potentials to auditory stimuli as a function of varying interstimulus interval. Psychophysiology 29(5):546-550

Brandt-Lassen R, Lund SP, Jepsen GB (2000) Rats exposed to Toluene and Noise may develop Loss of Auditory Sensitivity due to Synergistic Interaction. Noise Health 3(9):33-44

Brodmann K (1909) Vergleichende Lokalisationslehre der Grosshirnrinde. Barth, Leipzig

Brown DA, Abogadie FC, Allen TG, Buckley NJ, Caulfield MP, Delmas P, Haley JE, Lamas JA, Selyanko AA (1997) Muscarinic mechanisms in nerve cells. Life sciences 60(13-14):1137-1144

Brown JH (1992) Atropine, scopolamine, and related antimuscarinic drugs. In: The Pharmacological Basis of Therapeutics. Gilman, A.G., Rall, T.W., Nies, A.S., Taylor, P., Singapore, pp 150-165

Brown JH, Taylor B (2005) Muscarinic Receptor Agonists and Antagonists. In: Goodmann & Gilman's The pharmalogical basis of therepeutics. pp 183-200

Brown WS, Marsh JT, LaRue A (1982) Event-related potentials in psychiatry: differentiating depression and dementia in the elderly. Bulletin of the Los Angeles neurological societies 47:91-107

Buchwald JS, Hinman C, Norman RJ, Huang CM, Brown KA (1981) Middle- and long-latency auditory evoked responses recorded from the vertex of normal and chronically lesioned cats. Brain Res 205(1):91-109

Buchwald JS, Rubinstein EH, Schwafel J, Strandburg RJ (1991) Midlatency auditory evoked responses: differential effects of a cholinergic agonist and antagonist. Electroencephalogr Clin Neurophysiol 80(4):303-309

Burkard R (2006) Calibration of acoustic transients. Brain Research 1091(1):27-31

Buzsaki G, Anastassiou CA, Koch C (2012) The origin of extracellular fields and currents--EEG, ECoG, LFP and spikes. Nat Rev Neurosci 13(6):407-420

Buzsaki G, Draguhn A (2004) Neuronal oscillations in cortical networks. Science 304(5679):1926-1929

Campbell KA, Kalmbacher CE, Specht CD, Gregg TR (1995) Dependence of rat vertex auditory evoked potentials on central muscarinic receptor activation. Brain Res 702(1-2):110-116

Campbell KB, Bartoli EA (1986) Human auditory evoked potentials during natural sleep: the early components. Electroencephalogr Clin Neurophysiol 65(2):142-149

Carral V, Corral MJ, Escera C (2005) Auditory event-related potentials as a function of abstract change magnitude. Neuroreport 16(3):301-305

Casseday JH, Ehrlich D, Covey E (1994) Neural tuning for sound duration: role of inhibitory mechanisms in the inferior colliculus. Science 264(5160):847-850

Celesia GG, Jasper HH (1966) Acetylcholine released from cerebral cortex in relation to state of activation. Neurology 16(11):1053-1063

Chapman RM, Nowlis GH, McCrary JW, Chapman JA, Sandoval TC, Guillily MD, Gardner MN, Reilly LA (2007) Brain event-related potentials: diagnosing early-stage Alzheimer's disease. Neurobiol Aging 28(2):194-201

Chen BM, Buchwald JS (1986) Midlatency auditory evoked responses: differential effects of sleep in the cat. Electroencephalogr Clin Neurophysiol 65(5):373-382

Cheung SW, Nagarajan SS, Bedenbaugh PH, Schreiner CE, Wang X, Wong A (2001) Auditory cortical neuron response differences under isoflurane versus pentobarbital anesthesia. Hearing Research 156(1-2):115-127

Colburn HS, Han YA, Culotta CP (1990) Coincidence model of MSO responses. Hear Res 49(1-3):335-346

Covey E, Casseday JH (1991) The monaural nuclei of the lateral lemniscus in an echolocating bat: parallel pathways for analyzing temporal features of sound. J Neurosci 11(11):3456-3470

Creutzfeldt O, Struck G (1962) Neurophysiologie und Morphologie der chronisch isolierten Cortexinsel der Katze: Hirnpotentiale und Neuronentätigkeit einer isolierten Nervenzellpopulation ohne afferente Fasern. European Archives of Psychiatry and Clinical Neuroscience 203(6):708-731

Csépe V (1995) On the origin and development of the mismatch negativity. Ear and hearing 16(1):91-104

Csépe V, Karmos G, Molnar M (1987) Evoked potential correlates of stimulus deviance during wakefulness and sleep in cat--animal model of mismatch negativity. Electroencephalogr Clin Neurophysiol 66(6):571-578

Curia G, Longo D, Biagini G, Jones RS, Avoli M (2008) The pilocarpine model of temporal lobe epilepsy. J Neurosci Methods 172(2):143-157

Curro Dossi R, Pare D, Steriade M (1991) Short-lasting nicotinic and long-lasting muscarinic depolarizing responses of thalamocortical neurons to stimulation of mesopontine cholinergic nuclei. J Neurophysiol 65(3):393-406

Dallos P, Corey ME (1991) The role of outer hair cell motility in cochlear tuning. Curr Opin Neurobiol 1(2):215-220

David O, Harrison L, Friston KJ (2005) Modelling event-related responses in the brain. NeuroImage 25(3):756-770

David O, Kiebel SJ, Harrison LM, Mattout J, Kilner JM, Friston KJ (2006) Dynamic causal modeling of evoked responses in EEG and MEG. NeuroImage 30(4):1255-1272

Davis H, Mast T, Yoshie N, Zerlin S (1966) The slow response of the human cortex to auditory stimuli: recovery process. Electroencephalogr Clin Neurophysiol 21(2):105-113

Deschenes M, Veinante P, Zhang ZW (1998) The organization of corticothalamic projections: reciprocity versus parity. Brain Res Brain Res Rev 28(3):286-308

Destexhe A, Contreras D, Steriade M (1999) Spatiotemporal analysis of local field potentials and unit discharges in cat cerebral cortex during natural wake and sleep states. J Neurosci 19(11):4595-4608

Di S, Barth DS (1992) The functional anatomy of middle-latency auditory evoked potentials: thalamocortical connections. J Neurophysiol 68(2):425-431

Doron NN, Ledoux JE, Semple MN (2002) Redefining the tonotopic core of rat auditory cortex: physiological evidence for a posterior field. J. Comp. Neurol. 453(4):345-360

Dringenberg HC, Vanderwolf CH (1997) Neocortical activation: modulation by multiple pathways acting on central cholinergic and serotonergic systems. Experimental brain research. Experimentelle Hirnforschung. Experimentation cerebrale 116(1):160-174

Dunbar G, Boeijinga PH, Demazieres A, Cisterni C, Kuchibhatla R, Wesnes K, Luthringer R (2007) Effects of TC-1734 (AZD3480), a selective neuronal nicotinic receptor agonist, on cognitive performance and the EEG of young healthy male volunteers. Psychopharmacology (Berl) 191(4):919-929

Eason RG, Harter R, White CT (1969) Effects of attention and arousal on visually evoked cortical potentials and reaction time in man. Physiology and Behavior 4:283-289

Eccles JC (1951) Interpretation of action potentials evoked in the cerebral cortex. Electroencephalogr Clin Neurophysiol 3(4):449-464

Edwards MS, Powers SK, Baringer RA, Jewett DL, Bolger C, Phillips TL (1983) Evoked potentials in rats with misonidazole neurotoxicity. I. Brain stem auditory evoked potentials. Journal of neuro-oncology 1(2):115-123

Eglen RM, Hegde SS, Watson N (1996) Muscarinic receptor subtypes and smooth muscle function. Pharmacological reviews 48(4):531-565

Engeland C, Mahoney C, Mohr E, Ilivitsky V, Knott VJ (2002) Acute nicotine effects on auditory sensory memory in tacrine-treated and nontreated patients with Alzheimer's disease: an event-related potential study. Pharmacol Biochem Behav 72(1-2):457-464

Eriksson J, Villa A (2005) Event-related potentials in an auditory oddball situation in the rat. Biosystems 79(1-3):207-212

Escera C, Alho K, Winkler I, Näätänen R (1998) Neural mechanisms of involuntary attention to acoustic novelty and change. J Cogn Neurosci 10(5):590-604

Evans HL (1975) Scopolamine effects on visual discrimination: modifications related to stimulus control. The Journal of pharmacology and experimental therapeutics 195(1):105-113

Faber ES, Sah P (2003) Calcium-activated potassium channels: multiple contributions to neuronal function. The Neuroscientist : a review journal bringing neurobiology, neurology and psychiatry 9(3):181-194

Farley BJ, Quirk MC, Doherty JJ, Christian EP (2010) Stimulus-specific adaptation in auditory cortex is an NMDA-independent process distinct from the sensory novelty encoded by the mismatch negativity. J Neurosci 30(49):16475-16484

Felleman DJ, Van Essen DC (1991) Distributed hierarchical processing in the primate cerebral cortex. Cereb Cortex 1(1):1-47

Fishman YI, Steinschneider M (2012) Searching for the mismatch negativity in primary auditory cortex of the awake monkey: deviance detection or stimulus specific adaptation? J Neurosci 32(45):15747-15758

Fleming DE, Shearer DE, Creel DJ (1974) Effect of pharmacologically-induced arousal on the evoked potential in the unanesthetized rat. Pharmacol Biochem Behav 2(2):187-192

Freeman WJ, Holmes MD, Burke BC, Vanhatalo S (2003) Spatial spectra of scalp EEG and EMG from awake humans. Clin Neurophysiol 114(6):1053-1068

Friston K (2005) A theory of cortical responses. Philosophical Transactions of the Royal Society B: Biological Sciences 360(1456):815-836

Friston KJ, Harrison L, Penny W (2003) Dynamic causal modelling. NeuroImage 19(4):1273-1302

Gaese BH, Ostwald J (2001) Anesthesia changes frequency tuning of neurons in the rat primary auditory cortex. Journal of Neurophysiology 86(2):1062-1066

Galambos R, Myers RE, Sheatz GC (1961) Extralemniscal activation of auditory cortex in cats. The American journal of physiology 200:23-28

Garrido MI, Friston KJ, Kiebel SJ, Stephan KE, Baldeweg T, Kilner JM (2008) The functional anatomy of the MMN: a DCM study of the roving paradigm. NeuroImage 42(2):936-944

Garrido MI, Kilner JM, Kiebel SJ, Stephan KE, Baldeweg T, Friston KJ (2009a) Repetition suppression and plasticity in the human brain. NeuroImage 48(1):269-279

Garrido MI, Kilner JM, Stephan KE, Friston KJ (2009b) The mismatch negativity: a review of underlying mechanisms. Clin Neurophysiol 120(3):453-463

Giard MH, Perrin F, Echallier JF, Thevenet M, Froment JC, Pernier J (1994) Dissociation of temporal and frontal components in the human auditory N1 wave: a scalp current density and dipole model analysis. Electroencephalogr Clin Neurophysiol 92(3):238-252

Giard MH, Perrin F, Pernier J, Bouchet P (1990) Brain generators implicated in the processing of auditory stimulus deviance: a topographic event-related potential study. Psychophysiology 27(6):627-640

Glowatzki E, Fuchs PA (2002) Transmitter release at the hair cell ribbon synapse. Nat Neurosci 5(2):147-154

Golebiewski H, Eckersdorf B, Konopacki J (2002) Septal cholinergic mediation of hippocampal theta in the cat. Brain Res Bull 58(3):323-335

Groppe DM, Urbach TP, Kutas M (2011) Mass univariate analysis of event-related brain potentials/fields I: a critical tutorial review. Psychophysiology 48(12):1711-1725

Grundy BL, Jannetta PJ, Procopio PT, Lina A, Boston JR, Doyle E (1982) Intraoperative monitoring of brain-stem auditory evoked potentials. J Neurosurg 57(5):674-681

Halgren E, Baudena P, Clarke JM, Heit G, Liegeois C, Chauvel P, Musolino A (1995) Intracerebral potentials to rare target and distractor auditory and visual stimuli. I. Superior temporal plane and parietal lobe. Electroencephalogr Clin Neurophysiol 94(3):191-220

Hall RD, Borbely AA (1970) Acoustically evoked potentials in the rat during sleep and waking. Experimental brain research Experimentelle Hirnforschung Expérimentation cérébrale 11(1):93-110

Hari R, Aittoniemi K, Jarvinen ML, Katila T, Varpula T (1980) Auditory evoked transient and sustained magnetic fields of the human brain. Localization of neural generators. Experimental brain research. Experimentelle Hirnforschung. Experimentation cerebrale 40(2):237-240

Hari R, Pelizzone M, Makela JP, Hallstrom J, Leinonen L, Lounasmaa OV (1987) Neuromagnetic responses of the human auditory cortex to on- and offsets of noise bursts. Audiology : official organ of the International Society of Audiology 26(1):31-43

Hari R, Rif J, Tiihonen J, Sams M (1992) Neuromagnetic mismatch fields to single and paired tones. Electroencephalogr Clin Neurophysiol 82(2):152-154

Hasselmo ME (1995) Neuromodulation and cortical function: modeling the physiological basis of behavior. Behav Brain Res 67(1):1-27

He J, Hashikawa T, Ojima H, Kinouchi Y (1997) Temporal integration and duration tuning in the dorsal zone of cat auditory cortex. J Neurosci 17(7):2615-2625

Heinke W, Kenntner R, Gunter TC, Sammler D, Olthoff D, Koelsch S (2004) Sequential effects of increasing propofol sedation on frontal and temporal cortices as indexed by auditory event-related potentials. Anesthesiology 100(3):617-625

Henry KR (1985) Tuning of the auditory brainstem OFF responses is complementary to tuning of the auditory brainstem ON response. Hear Res 19(2):115-125

Howard MA, Volkov IO, Mirsky R, Garell PC, Noh MD, Granner M, Damasio H, Steinschneider M, Reale RA, Hind JE, Brugge JF (2000) Auditory cortex on the human posterior superior temporal gyrus. The Journal of comparative neurology 416(1):79-92

Hu B (2003) Functional organization of lemniscal and nonlemniscal auditory thalamus. Experimental brain research. Experimentelle Hirnforschung. Experimentation cerebrale 153(4):543-549

Hudspeth AJ (2000) Hearing. In: Kandel ER, Schwartz JH, Jessell TM (eds) Principles of neural science. The McGraw-Hill Companies, pp 590-613

Hughes HC, Darcey TM, Barkan HI, Williamson PD, Roberts DW, Aslin CH (2001) Responses of human auditory association cortex to the omission of an expected acoustic event. Neuroimage 13(6 Pt 1):1073-1089

Hyde M (1997) The N1 response and its applications. Audiol Neurootol 2(5):281-307

Imada T, Hari R, Loveless N, McEvoy L, Sams M (1993) Determinants of the auditory mismatch response. Electroencephalogr Clin Neurophysiol 87(3):144-153

Inami R, Kirino E, Inoue R, Arai H (2005) Transdermal nicotine administration enhances automatic auditory processing reflected by mismatch negativity. Pharmacol Biochem Behav 80(3):453-461

Jääskelainen IP, Ahveninen J, Bonmassar G, Dale AM, Ilmoniemi RJ, Levanen S, Lin FH, May P, Melcher J, Stufflebeam S, Tiitinen H, Belliveau JW (2004) Human posterior auditory cortex gates novel sounds to consciousness. Proc Natl Acad Sci U S A 101(17):6809-6814

Jacobsen T, Schröger E (2001) Is there pre-attentive memory-based comparison of pitch? Psychophysiology 38(4):723-727

Jansen BH, Rit VG (1995) Electroencephalogram and visual evoked potential generation in a mathematical model of coupled cortical columns. Biological cybernetics 73(4):357-366

Javitt DC, Grochowski S, Shelley AM, Ritter W (1998) Impaired mismatch negativity (MMN) generation in schizophrenia as a function of stimulus deviance, probability, and interstimulus/interdeviant interval. Electroencephalogr Clin Neurophysiol 108(2):143-153

Javitt DC, Schroeder CE, Steinschneider M, Arezzo JC, Vaughan HG, Jr. (1992) Demonstration of mismatch negativity in the monkey. Electroencephalogr Clin Neurophysiol 83(1):87-90

Javitt DC, Steinschneider M, Schroeder CE, Arezzo JC (1996) Role of cortical N-methyl-D-aspartate receptors in auditory sensory memory and mismatch negativity generation: implications for schizophrenia. Proc Natl Acad Sci U S A 93(21):11962-11967

Javitt DC, Steinschneider M, Schroeder CE, Vaughan HG, Arezzo JC (1994) Detection of stimulus deviance within primate primary auditory cortex: intracortical mechanisms of mismatch negativity (MMN) generation. Brain Research 667(2):192-200

Joutsiniemi SL, Hari R (1989) Omissions of Auditory Stimuli May Activate Frontal Cortex. Eur J Neurosci 1(5):524-528

Kaga K, Hink RF, Shinoda Y, Suzuki J (1980) Evidence for a primary cortical origin of a middle latency auditory evoked potential in cats. Electroencephalogr Clin Neurophysiol 50(3-4):254-266

Kähkönen S, Ahveninen J, Jääskeläinen IP, Kaakkola S, Näätänen R, Huttunen J, Pekkonen E (2001) Effects of haloperidol on selective attention: a combined whole-head MEG and high-resolution EEG study. Neuropsychopharmacology : official publication of the American College of Neuropsychopharmacology 25(4):498-504

Kähkönen S, Mäkinen V, Jääskeläinen IP, Pennanen S, Liesivuori J, Ahveninen J (2005) Serotonergic modulation of mismatch negativity. Psychiatry research 138(1):61-74

Katz Y, Heiss JE, Lampl I (2006) Cross-whisker adaptation of neurons in the rat barrel cortex. J Neurosci 26(51):13363-13372

Kiebel SJ, David O, Friston KJ (2006) Dynamic causal modelling of evoked responses in EEG/MEG with lead field parameterization. Neuroimage 30(4):1273-1284

Kiebel SJ, Garrido MI, Friston KJ (2007) Dynamic causal modelling of evoked responses: the role of intrinsic connections. Neuroimage 36(2):332-345

Kiebel SJ, Garrido MI, Moran RJ, Friston KJ (2008) Dynamic causal modelling for EEG and MEG. Cognitive neurodynamics 2(2):121-136

Klinkenberg I, Blokland A (2010) The validity of scopolamine as a pharmacological model for cognitive impairment: A review of animal behavioral studies. Neuroscience & Biobehavioral Reviews 34(8):1307-1350

Knight RT, Brailowsky S, Scabini D, Simpson GV (1985) Surface auditory evoked potentials in the unrestrained rat: component definition. Electroencephalogr Clin Neurophysiol 61(5):430-439

Knight RT, Scabini D, Woods DL, Clayworth C (1988) The effects of lesions of superior temporal gyrus and inferior parietal lobe on temporal and vertex components of the human AEP. Electroencephalogr Clin Neurophysiol 70(6):499-509

Korzyukov O, Alho K, Kujala A, Gumenyuk V, Ilmoniemi RJ, Virtanen J, Kropotov J, Näätänen R (1999) Electromagnetic responses of the human auditory cortex generated by sensory-memory based processing of tone-frequency changes. Neurosci Lett 276(3):169-172

Kramer K, Kinter L, Brockway BP, Voss HP, Remie R, Van Zutphen BL (2001) The use of radiotelemetry in small laboratory animals: recent advances. Contemporary topics in laboratory animal science / American Association for Laboratory Animal Science 40(1):8-16

Kraus N, McGee T, Carrell T, King C, Littman T, Nicol T (1994a) Discrimination of speech-like contrasts in the auditory thalamus and cortex. J Acoust Soc Am 96(5 Pt 1):2758-2768

Kraus N, McGee T, Littman T, Nicol T, King C (1994b) Nonprimary auditory thalamic representation of acoustic change. Journal of Neurophysiology 72(3):1270-1277

Krause M, Pedarzani P (2000) A protein phosphatase is involved in the cholinergic suppression of the Ca(2+)-activated K(+) current sI(AHP) in hippocampal pyramidal neurons. Neuropharmacology 39(7):1274-1283

Kreitschmann-Andermahr I, Rosburg T, Demme U, Gaser E, Nowak H, Sauer H (2001) Effect of ketamine on the neuromagnetic mismatch field in healthy humans. Brain Res Cogn Brain Res 12(1):109-116

Kropotov JD, Näätänen R, Sevostianov AV, Alho K, Reinikainen K, Kropotova OV (1995) Mismatch negativity to auditory stimulus change recorded directly from the human temporal cortex. Psychophysiology 32(4):418-422

Langmead CJ, Watson J, Reavill C (2008) Muscarinic acetylcholine receptors as CNS drug targets. Pharmacology & Therapeutics 117(2):232-243

Lazar R, Metherate R (2003) Spectral interactions, but no mismatch negativity, in auditory cortex of anesthetized rat. Hearing Research 181(1-2):51-56

Lennartz RC, Weinberger NM (1992) Frequency selectivity is related to temporal processing in parallel thalamocortical auditory pathways. Brain Res 583(1-2):81-92

Leopold IH, Comroe JH, Jr. (1948) Effect of intramuscular administration of morphine, atrophine, scopolamine and neostigmine on the human eye. Archives of ophthalmology 40(3):285-290

Leung S, Croft RJ, Baldeweg T, Nathan PJ (2007) Acute dopamine D(1) and D(2) receptor stimulation does not modulate mismatch negativity (MMN) in healthy human subjects. Psychopharmacology (Berl) 194(4):443-451

Leung S, Croft RJ, Guille V, Scholes K, O'Neill BV, Phan KL, Nathan PJ (2010) Acute dopamine and/or serotonin depletion does not modulate mismatch negativity (MMN) in healthy human participants. Psychopharmacology (Berl) 208(2):233-244

Liegeois-Chauvel C, Musolino A, Badier JM, Marquis P, Chauvel P (1994) Evoked potentials recorded from the auditory cortex in man: evaluation and topography of the middle latency components. Electroencephalogr Clin Neurophysiol 92(3):204-214

Liljenstrom H, Hasselmo ME (1995) Cholinergic modulation of cortical oscillatory dynamics. J Neurophysiol 74(1):288-297

Litvak V, Jha A, Flandin G, Friston K (2013) Convolution models for induced electromagnetic responses. Neuroimage 64:388-398

Loftus WC, Malmierca MS, Bishop DC, Oliver DL (2008) The cytoarchitecture of the inferior colliculus revisited: a common organization of the lateral cortex in rat and cat. Neuroscience 154(1):196-205

Lumani A, Zhang H (2010) Responses of neurons in the rat's dorsal cortex of the inferior colliculus to monaural tone bursts. Brain Res 1351:115-129

Lütkenhoner B, Steinsträter O (1998) High-precision neuromagnetic study of the functional organization of the human auditory cortex. Audiol Neurootol 3(2-3):191-213

Malmierca MS (2003) The structure and physiology of the rat auditory system: an overview. Int Rev Neurobiol 56:147-211

Malmierca MS, Cristaudo S, Perez-Gonzalez D, Covey E (2009) Stimulus-specific adaptation in the inferior colliculus of the anesthetized rat. J Neurosci 29(17):5483-5493

Malmierca MS, Hackett TA (2010) Structural organization of the ascending auditory pathway. In: The Oxford Handbook of Auditory Science. Oxford University Press, pp 9-41

Malmierca MS, Leergaard TB, Bajo VM, Bjaalie JG, Merchan MA (1998) Anatomic evidence of a three-dimensional mosaic pattern of tonotopic organization in the ventral complex of the lateral lemniscus in cat. J Neurosci 18(24):10603-10618

May P, Tiitinen H, Ilmoniemi RJ, Nyman G, Taylor JG, Näätänen R (1999) Frequency change detection in human auditory cortex. J Comput Neurosci 6(2):99-120

McCallum WC, Curry SH (1980) The form and distribution of auditory evoked potentials and CNVs when stimuli and responses are lateralized. Prog Brain Res 54:767-775

McCarley RW, Faux SF, Shenton ME, Nestor PG, Adams J (1991) Event-related potentials in schizophrenia: their biological and clinical correlates and a new model of schizophrenic pathophysiology. Schizophr Res 4(2):209-231

McEvoy L, Makela JP, Hamalainen M, Hari R (1994) Effect of interaural time differences on middle-latency and late auditory evoked magnetic fields. Hear Res 78(2):249-257

McKenna TM, Ashe JH, Hui GK, Weinberger NM (1988) Muscarinic agonists modulate spontaneous and evoked unit discharge in auditory cortex of cat. Synapse 2(1):54-68

Metherate R, Cox CL, Ashe JH (1992) Cellular bases of neocortical activation: modulation of neural oscillations by the nucleus basalis and endogenous acetylcholine. J Neurosci 12(12):4701-4711

MGIPharma (2001) Salagen (pilocarpine).55343 [monograph]. Minneapolis (MN).

Miyazato H, Skinner RD, Reese NB, Boop FA, Garcia-Rill E (1995) A middle-latency auditory-evoked potential in the rat. Brain Res Bull 37(3):247-255

Molholm S, Martinez A, Ritter W, Javitt DC, Foxe JJ (2005) The neural circuitry of pre-attentive auditory change-detection: an fMRI study of pitch and duration mismatch negativity generators. Cereb Cortex 15(5):545-551

Moller AR, Jannetta P, Bennett M, Moller MB (1981) Intracranially recorded responses from the human auditory nerve: new insights into the origin of brain stem evoked potentials (BSEPs). Electroencephalogr Clin Neurophysiol 52(1):18-27

Moore DR (1991) Anatomy and physiology of binaural hearing. Audiology : official organ of the International Society of Audiology 30(3):125-134

Moore DR (2003) Cortical neurons signal sound novelty. Nat Neurosci 6(4):330-332

Moore H, Dudchenko P, Comer KS, Bruno JP, Sarter M (1992) Central versus peripheral effects of muscarinic antagonists: the limitations of quaternary ammonium derivatives. Psychopharmacology (Berl) 108(1-2):241-243

Moran RJ, Jung F, Kumagai T, Endepols H, Graf R, Dolan RJ, Friston KJ, Stephan KE, Tittgemeyer M (2011) Dynamic causal models and physiological inference: a validation study using isoflurane anaesthesia in rodents. PLoS ONE 6(8):e22790

Moran RJ, Stephan KE, Seidenbecher T, Pape HC, Dolan RJ, Friston KJ (2009) Dynamic causal models of steady-state responses. Neuroimage 44(3):796-811

Morest DK (1964) THE NEURONAL ARCHITECTURE OF THE MEDIAL GENICULATE BODY OF THE CAT. Journal of anatomy 98:611-630

Moruzzi G, Magoun HW (1949) Brain stem reticular formation and activation of the EEG. Electroencephalogr Clin Neurophysiol 1(4):455-473

Movshon JA, Lennie P (1979) Pattern-selective adaptation in visual cortical neurones. Nature 278(5707):850-852

Muller JR, Metha AB, Krauskopf J, Lennie P (1999) Rapid adaptation in visual cortex to the structure of images. Science 285(5432):1405-1408

Mulroney SE, Myers AK (2009) Sensory Physiology. In: Netter's essential physiology. Saunders/ Elsevier,

Näätänen R (1990) The role of attention in auditory information processing as revealed by event-related potentials and other brain measures of cognitive function. Behav Brain Res (13):201-288

Näätänen R (1992) Attention and brain function. Lawrence Erlbaum Associates, Hillsdale, NJ:193

Näätänen R (2003) Mismatch negativity: clinical research and possible applications. International journal of psychophysiology : official journal of the International Organization of Psychophysiology 48(2):179-188

Näätänen R, Gaillard AW, Mäntysalo S (1978) Early selective-attention effect on evoked potential reinterpreted. Acta psychologica 42(4):313-329

Näätänen R, Jacobsen T, Winkler I (2005) Memory-based or afferent processes in mismatch negativity (MMN): a review of the evidence. Psychophysiology 42(1):25-32

Näätänen R, Michie PT (1979) Early selective-attention effects on the evoked potential: a critical review and reinterpretation. Biol Psychol 8(2):81-136

Näätänen R, Paavilainen P, Alho K, Reinikainen K, Sams M (1989a) Do event-related potentials reveal the mechanism of the auditory sensory memory in the human brain? Neurosci Lett 98(2):217-221

Näätänen R, Paavilainen P, Reinikainen K (1989b) Do event-related potentials to infrequent decrements in duration of auditory stimuli demonstrate a memory trace in man? Neurosci Lett 107(1-3):347-352

Näätänen R, Picton T (1987) The N1 wave of the human electric and magnetic response to sound: a review and an analysis of the component structure. Psychophysiology 24(4):375-425

Näätänen R, Winkler I (1999) The concept of auditory stimulus representation in cognitive neuroscience. Psychol Bull 125(6):826-859

Nakagome K, Ichikawa I, Kanno O, Akaho R, Suzuki M, Takazawa S, Watanabe H, Kazamatsuri H (1998) Overnight effects of triazolam on cognitive function: an event-related potentials study. Neuropsychobiology 38(4):232-240

Nakamura T, Michie PT, Fulham WR, Todd J, Budd TW, Schall U, Hunter M, Hodgson DM (2011) Epidural Auditory Event-Related Potentials in the Rat to Frequency and duration Deviants: Evidence of Mismatch Negativity? Front Psychol 2:367

Nelken I, Ulanovsky N (2007) Mismatch negativity and stimulus-specific adaptation in animal models. Journal of Psychophysiology 21(3-4):214-223

Netser S, Zahar Y, Gutfreund Y (2011) Stimulus-specific adaptation: can it be a neural correlate of behavioral habituation? J Neurosci 31(49):17811-17820

Nordby H, Hammerborg D, Roth WT, Hugdahl K (1994) ERPs for infrequent omissions and inclusions of stimulus elements. Psychophysiology 31(6):544-552

O'Neill J, Halgren E, Marinkovic K, Siembieda D, Refai D, Fitten LJ, Perryman K, Fisher A (2000) Effects of muscarinic and adrenergic agonism on auditory P300 in the macaque. Physiol Behav 70(1-2):163-170

Obleser J, Boecker H, Drzezga A, Haslinger B, Hennenlotter A, Roettinger M, Eulitz C, Rauschecker JP (2006) Vowel sound extraction in anterior superior temporal cortex. Hum Brain Mapp 27(7):562-571

Osen KK, Mugnaini E, Dahl AL, Christiansen AH (1984) Histochemical localization of acetylcholinesterase in the cochlear and superior olivary nuclei. A reappraisal with emphasis on the cochlear granule cell system. Archives italiennes de biologie 122(3):169-212

Paavilainen P, Alho K, Reinikainen K, Sams M, Näätänen R (1991) Right hemisphere dominance of different mismatch negativities. Electroencephalogr Clin Neurophysiol 78(6):466-479

Paavilainen P, Simola J, Jaramillo M, Näätänen R, Winkler I (2001) Preattentive extraction of abstract feature conjunctions from auditory stimulation as reflected by the mismatch negativity (MMN). Psychophysiology 38(2):359-365

Pakarinen ED, Moerschbaecher JM (1993) Comparison of the effects of scopolamine and methylscopolamine on the performance of a fixed-ratio discrimination in squirrel monkeys. Pharmacol Biochem Behav 44(4):815-819

Pandya PK, Rathbun DL, Moucha R, Engineer ND, Kilgard MP (2008) Spectral and temporal processing in rat posterior auditory cortex. Cereb Cortex 18(2):301-314

Pekkonen E (2001) Auditory Sensory Memory and the Cholinergic System: Implications for Alzheimer's Disease. NeuroImage 14(2):376-382

Pekkonen E, Hirvonen J, Ahveninen J, Kahkonen S, Kaakkola S, Huttunen J, Jääskeläinen IP (2002) Memory-based comparison process not attenuated by haloperidol: a combined MEG and EEG study. Neuroreport 13(1):177-181

Pekkonen E, Huotilainen M, Virtanen J, Sinkkonen J, Rinne T, Ilmoniemi RJ, Naatanen R (1995a) Age-related functional differences between auditory cortices: a whole-head MEG study. Neuroreport 6(13):1803-1806

Pekkonen E, Jääskeläinen IP, Kaakkola S, Ahveninen J (2005) Cholinergic modulation of preattentive auditory processing in aging. NeuroImage 27(2):387-392

Pekkonen E, Jousmaki V, Kononen M, Reinikainen K, Partanen J (1994) Auditory sensory memory impairment in Alzheimer's disease: an event-related potential study. Neuroreport 5(18):2537-2540

Pekkonen E, Jousmaki V, Reinikainen K, Partanen J (1995b) Automatic auditory discrimination is impaired in Parkinson's disease. Electroencephalogr Clin Neurophysiol 95(1):47-52

Penny WD, Stephan KE, Mechelli A, Friston KJ (2004) Comparing dynamic causal models. NeuroImage 22(3):1157-1172

Perez-Gonzalez D, Malmierca MS, Covey E (2005) Novelty detector neurons in the mammalian auditory midbrain. Eur J Neurosci 22(11):2879-2885

Picton TW, Alain C, Woods DL, John MS, Scherg M, Valdes-Sosa P, Bosch-Bayard J, Trujillo NJ (1999) Intracerebral sources of human auditory-evoked potentials. Audiol Neurootol 4(2):64-79

Picton TW, Hillyard SA (1974) Human auditory evoked potentials. II. Effects of attention. Electroencephalogr Clin Neurophysiol 36(2):191-199

Picton TW, Hillyard SA, Krausz HI, Galambos R (1974) Human auditory evoked potentials. I. Evaluation of components. Electroencephalogr Clin Neurophysiol 36(2):179-190

Pincze Z, Lakatos P, Rajkai C, Ulbert I, Karmos G (2001) Separation of mismatch negativity and the N1 wave in the auditory cortex of the cat: a topographic study. Clin Neurophysiol 112(5):778-784

Pincze Z, Lakatos P, Rajkai C, Ulbert I, Karmos G (2002) Effect of deviant probability and interstimulus/interdeviant interval on the auditory N1 and mismatch negativity in the cat auditory cortex. Brain Res Cogn Brain Res 13(2):249-253

Polley DB, Read HL, Storace DA, Merzenich MM (2007) Multiparametric auditory receptive field organization across five cortical fields in the albino rat. Journal of Neurophysiology 97(5):3621-3638

Polley DB, Steinberg EE, Merzenich MM (2006) Perceptual learning directs auditory cortical map reorganization through top-down influences. J Neurosci 26(18):4970-4982

Ponton CW, Eggermont JJ, Kwong B, Don M (2000) Maturation of human central auditory system activity: evidence from multi-channel evoked potentials. Clin Neurophysiol 111(2):220-236

Popelar J, Groh D, Mazelova J, Syka J (2003) Cochlear function in young and adult Fischer 344 rats. Hear Res 186(1-2):75-84

Popelar J, Groh D, Pelanova J, Canlon B, Syka J (2006) Age-related changes in cochlear and brainstem auditory functions in Fischer 344 rats. Neurobiol Aging 27(3):490-500

Pradhan SN, Roth T (1968) Comparative behavioral effects of several anticholinergic agents in rats. Psychopharmacologia 12(4):358-366

Raftery AE (1995) Bayesian Model Selection in Social Research. Sociological Methodology 25:111-163

Recanzone GH, Schreiner CE, Merzenich MM (1993) Plasticity in the frequency representation of primary auditory cortex following discrimination training in adult owl monkeys. J Neurosci 13(1):87-103

Reches A, Gutfreund Y (2008) Stimulus-specific adaptations in the gaze control system of the barn owl. J Neurosci 28(6):1523-1533

Riekkinen P, Sirviö J, Valjakka A, Pitkänen A, Partanen J, Riekkinen P (1990) The effects of concurrent manipulations of cholinergic and noradrenergic systems on neocortical EEG and spatial learning. Behav Neural Biol 54(2):204-210

Rodriguez R, Kallenbach U, Singer W, Munk MH (2004) Short- and long-term effects of cholinergic modulation on gamma oscillations and response synchronization in the visual cortex. J Neurosci 24(46):10369-10378

Roger C, Hasbroucq T, Rabat A, Vidal F, Burle B (2009) Neurophysics of temporal discrimination in the rat: a mismatch negativity study. Psychophysiology 46(5):1028-1032

Romanski LM, Bates JF, Goldman-Rakic PS (1999) Auditory belt and parabelt projections to the prefrontal cortex in the rhesus monkey. The Journal of comparative neurology 403(2):141-157

Romanski LM, LeDoux JE (1993) Organization of rodent auditory cortex: anterograde transport of PHA-L from MGv to temporal neocortex. Cereb Cortex 3(6):499-514

Rosburg T, Marinou V, Haueisen J, Smesny S, Sauer H (2004) Effects of lorazepam on the neuromagnetic mismatch negativity (MMNm) and auditory evoked field component N100m. Neuropsychopharmacology : official publication of the American College of Neuropsychopharmacology 29(9):1723-1733

Rose JE, Galambos R, Hughes JR (1959) Microelectrode studies of the cochlear nuclei of the cat. Bulletin of the Johns Hopkins Hospital 104(5):211-251

Rowntree CI, Bland BH (1986) An analysis of cholinoceptive neurons in the hippocampal formation by direct microinfusion. Brain Res 362(1):98-113

Rutkowski RG, Weinberger NM (2005) Encoding of learned importance of sound by magnitude of representational area in primary auditory cortex. Proc Natl Acad Sci U S A 102(38):13664-13669

Ruusuvirta T, Astikainen P, Wikgren J, Nokia M (2010) Hippocampus responds to auditory change in rabbits. Neuroscience 170(1):232-237

Ruusuvirta T, Koivisto K, Wikgren J, Astikainen P (2007) Processing of melodic contours in urethane-anaesthetized rats. Eur J Neurosci 26(3):701-703

Ruusuvirta T, Penttonen M, Korhonen T (1998) Auditory cortical event-related potentials to pitch deviances in rats. Neurosci Lett 248(1):45-48

Saarinen J, Paavilainen P, Schoger E, Tervaniemi M, Näätänen R (1992) Representation of abstract attributes of auditory stimuli in the human brain. Neuroreport 3(12):1149-1151

Sabri M, Campbell KB (2001) Effects of sequential and temporal probability of deviant occurrence on mismatch negativity. Brain Res Cogn Brain Res 12(1):171-180

Sams M, Hamalainen M, Antervo A, Kaukoranta E, Reinikainen K, Hari R (1985a) Cerebral neuromagnetic responses evoked by short auditory stimuli. Electroencephalogr Clin Neurophysiol 61(4):254-266

Sams M, Hamalainen M, Hari R, McEvoy L (1993a) Human auditory cortical mechanisms of sound lateralization: I. Interaural time differences within sound. Hear Res 67(1-2):89-97

Sams M, Hari R (1991) Magnetoencephalography in the study of human auditory information processing. Ann N Y Acad Sci 620:102-117

Sams M, Hari R, Rif J, Knuutila J (1993b) The Human Auditory Sensory Memory Trace Persists about 10 sec: Neuromagnetic Evidence. Journal of Cognitive Neuroscience 5(3):363-370

Sams M, Paavilainen P, Alho K, Näätänen R (1985b) Auditory frequency discrimination and event-related potentials. Electroencephalogr Clin Neurophysiol 62(6):437-448

Sato N, Ono K, Honda E, Haga K, Yokota M, Inenaga K (2006) Pilocarpine-induced Salivation and Thirst in Conscious Rats. Journal of Dental Research 85(1):64-68

Sato Y, Yabe H, Hiruma T, Sutoh T, Shinozaki N, Nashida T, Kaneko S (2000) The effect of deviant stimulus probability on the human mismatch process. Neuroreport 11(17):3703-3708

Scheel M (1988) Topographic organization of the auditory thalamocortical system in the albino rat. Anatomy and embryology 179(2):181-190

Scherg M, Berg P (1991) Use of prior knowledge in brain electromagnetic source analysis. Brain topography 4(2):143-150

Schmidt A, Diaconescu AO, Kometer M, Friston KJ, Stephan KE, Vollenweider FX (2012) Modeling Ketamine Effects on Synaptic Plasticity During the Mismatch Negativity. Cereb Cortex

Schröger E, Wolff C (1998) Attentional orienting and reorienting is indicated by human event-related brain potentials. Neuroreport 9(15):3355-3358

Schwender D, Klasing S, Conzen P, Finsterer U, Poppel E, Peter K (1996) Midlatency auditory evoked potentials during anaesthesia with increasing endexpiratory concentrations of desflurane. Acta anaesthesiologica Scandinavica 40(2):171-176

Seeger T, Alzheimer C (2001) Muscarinic activation of inwardly rectifying K(+) conductance reduces EPSPs in rat hippocampal CA1 pyramidal cells. J Physiol 535(Pt 2):383-396

Shaw NA (1988) The auditory evoked potential in the rat--a review. Prog Neurobiol 31(1):19-45

Shelley AM, Silipo G, Javitt DC (1999) Diminished responsiveness of ERPs in schizophrenic subjects to changes in auditory stimulation parameters: implications for theories of cortical dysfunction. Schizophrenia Research 37(1):65-79

Shi CJ, Cassell MD (1997) Cortical, thalamic, and amygdaloid projections of rat temporal cortex. The Journal of comparative neurology 382(2):153-175

Shi Q, Pavey ES, Carter RE (2012) Bonferroni-based correction factor for multiple, correlated endpoints. Pharmaceutical statistics 11(4):300-309

Simpson GV, Knight RT (1993a) Multiple brain systems generating the rat auditory evoked potential. I. Characterization of the auditory cortex response. Brain Res 602(2):240-250

Simpson GV, Knight RT (1993b) Multiple brain systems generating the rat auditory evoked potential. II. Dissociation of auditory cortex and non-lemniscal generator systems. Brain Res 602(2):251-263

Simpson TP, Manara AR, Kane NM, Barton RL, Rowlands CA, Butler SR (2002) Effect of propofol anaesthesia on the event-related potential mismatch negativity and the auditory-evoked potential N1. Br J Anaesth 89(3):382-388

Singer W, Gray CM (1995) Visual feature integration and the temporal correlation hypothesis. Annual review of neuroscience 18:555-586

Smith PH, Populin LC (2001) Fundamental differences between the thalamocortical recipient layers of the cat auditory and visual cortices. The Journal of comparative neurology 436(4):508-519

Sobotka S, Ringo JL (1994) Stimulus specific adaptation in excited but not in inhibited cells in inferotemporal cortex of macaque. Brain Res 646(1):95-99

Sonnadara R, Alain C, Trainor L (2006) Effects of spatial separation and stimulus probability on the event-related potentials elicited by occasional changes in sound location. Brain Research 1071(1):175-185

Starke K, Gothert M, Kilbinger H (1989) Modulation of neurotransmitter release by presynaptic autoreceptors. Physiological reviews 69(3):864-989

Stephan KE, Penny WD, Moran RJ, den Ouden HE, Daunizeau J, Friston KJ (2010) Ten simple rules for dynamic causal modeling. NeuroImage 49(4):3099-3109

Stone JL, Calderon-Arnulphi M, Watson KS, Patel K, Mander NS, Suss N, Fino J, Hughes JR (2009) Brainstem auditory evoked potentials--a review and modified studies in healthy subjects. J Clin Neurophysiol 26(3):167-175

Strominger NL (1973) The origins, course and distribution of the dorsal and intermediate acoustic striae in the rhesus monkey. The Journal of comparative neurology 147(2):209-233

Sumich A, Harris A, Flynn G, Whitford T, Tunstall N, Kumari V, Brammer M, Gordon E, Williams LM (2006) Event-related potential correlates of depression, insight and

negative symptoms in males with recent-onset psychosis. Clin Neurophysiol 117(8):1715-1727

Sussman E, Winkler I (2001) Dynamic sensory updating in the auditory system. Brain Res Cogn Brain Res 12(3):431-439

Taaseh N, Yaron A, Nelken I (2011) Stimulus-specific adaptation and deviance detection in the rat auditory cortex. PLoS ONE 6(8):e23369

Takahashi H, Nakao M, Kaga K (2004) Cortical mapping of auditory-evoked offset responses in rats. Neuroreport 15(10):1565-1569

Takakura AC, Moreira TS, De Luca LA, Jr., Renzi A, Menani JV, Colombari E (2005) Effects of AV3V lesion on pilocarpine-induced pressor response and salivary gland vasodilation. Brain Res 1055(1-2):111-121

Tervaniemi M, Maury S, Näätänen R (1994) Neural representations of abstract stimulus features in the human brain as reflected by the mismatch negativity. Neuroreport 5(7):844-846

Tice MA, Hashemi T, Taylor LA, McQuade RD (1996) Distribution of muscarinic receptor subtypes in rat brain from postnatal to old age. Brain research. Developmental brain research 92(1):70-76

Tiitinen H, Alho K, Huotilainen M, Ilmoniemi RJ, Simola J, Näätänen R (1993) Tonotopic auditory cortex and the magnetoencephalographic (MEG) equivalent of the mismatch negativity. Psychophysiology 30(5):537-540

Tiitinen H, May P, Reinikainen K, Näätänen R (1994) Attentive novelty detection in humans is governed by pre-attentive sensory memory. Nature 372(6501):90-92

Tikhonravov D, Neuvonen T, Pertovaara A, Savioja K, Ruusuvirta T, Näätänen R, Carlson S (2008) Effects of an NMDA-receptor antagonist MK-801 on an MMN-like response recorded in anesthetized rats. Brain Research 1203:97-102

Tikhonravov D, Neuvonen T, Pertovaara A, Savioja K, Ruusuvirta T, Näätänen R, Carlson S (2010) Dose-related effects of memantine on a mismatch negativity-like response in anesthetized rats. NSC 167(4):1175-1182

Tollin DJ (2003) The lateral superior olive: a functional role in sound source localization. The Neuroscientist : a review journal bringing neurobiology, neurology and psychiatry 9(2):127-143

Tsodyks MV, Markram H (1997) The neural code between neocortical pyramidal neurons depends on neurotransmitter release probability. Proc Natl Acad Sci U S A 94(2):719-723

Ulanovsky N, Las L, Farkas D, Nelken I (2004) Multiple time scales of adaptation in auditory cortex neurons. Journal of Neuroscience 24(46):10440-10453

Ulanovsky N, Las L, Nelken I (2003) Processing of low-probability sounds by cortical neurons. Nat Neurosci 6(4):391-398

Umbricht D, Krljes S (2005) Mismatch negativity in schizophrenia: a meta-analysis. Schizophr Res 76(1):1-23

Umbricht D, Schmid L, Koller R, Vollenweider FX, Hell D, Javitt DC (2000) Ketamine-induced deficits in auditory and visual context-dependent processing in healthy volunteers: implications for models of cognitive deficits in schizophrenia. Archives of general psychiatry 57(12):1139-1147

Umbricht D, Vollenweider FX, Schmid L, Grubel C, Skrabo A, Huber T, Koller R (2003) Effects of the 5-HT2A agonist psilocybin on mismatch negativity generation and AX-continuous performance task: implications for the neuropharmacology of cognitive deficits in schizophrenia. Neuropsychopharmacology : official publication of the American College of Neuropsychopharmacology 28(1):170-181

Umbricht D, Vyssotki D, Latanov A, Nitsch R, Lipp H (2005) Deviance-related electrophysiological activity in mice: is there mismatch negativity in mice? Clinical Neurophysiology 116(2):353-363

van Haaren F, van Hest A (1989) The effects of scopolamine and methylscopolamine on visual and auditory discriminations in male and female Wistar rats. Pharmacol Biochem Behav 32(3):707-710

Vaughan HG, Jr., Ritter W (1970) The sources of auditory evoked responses recorded from the human scalp. Electroencephalogr Clin Neurophysiol 28(4):360-367

Vaughan HG, Jr., Ritter W, Simson R (1980) Topographic analysis of auditory event-related potentials. Prog Brain Res 54:279-285

Verkindt C, Bertrand O, Perrin F, Echallier JF, Pernier J (1995) Tonotopic organization of the human auditory cortex: N100 topography and multiple dipole model analysis. Electroencephalogr Clin Neurophysiol 96(2):143-156

von der Behrens W, Bäuerle P, Kössl M, Gaese BH (2009) Correlating stimulus-specific adaptation of cortical neurons and local field potentials in the awake rat. J Neurosci 29(44):13837-13849

Wacongne C, Labyt E, van Wassenhove V, Bekinschtein T, Naccache L, Dehaene S (2011) Evidence for a hierarchy of predictions and prediction errors in human cortex. Proc Natl Acad Sci U S A 108(51):20754-20759

Wallace MN, Harper MS (1997) Callosal connections of the ferret primary auditory cortex. Experimental brain research. Experimentelle Hirnforschung. Experimentation cerebrale 116(2):367-374

Warr WB, Guinan JJ, Jr. (1979) Efferent innervation of the organ of corti: two separate systems. Brain Res 173(1):152-155

Weaver ML, Tanzer JM, Kramer PA (1992) Pilocarpine disposition and salivary flow responses following intravenous administration to dogs. Pharmaceutical research 9(8):1064-1069

Wess J, Eglen RM, Gautam D (2007) Muscarinic acetylcholine receptors: mutant mice provide new insights for drug development. Nature reviews. Drug discovery 6(9):721-733

West CD (1985) The relationship of the spiral turns of the cochlea and the length of the basilar membrane to the range of audible frequencies in ground dwelling mammals. J Acoust Soc Am 77(3):1091-1101

Winer JA (1985) Structure of layer II in cat primary auditory cortex (AI). The Journal of comparative neurology 238(1):10-37

Winer JA, Larue DT (1996) Evolution of GABAergic circuitry in the mammalian medial geniculate body. Proc Natl Acad Sci U S A 93(7):3083-3087

Winer JA, Morest DK (1983) The medial division of the medial geniculate body of the cat: implications for thalamic organization. J Neurosci 3(12):2629-2651

Winkler I, Karmos G, Näätänen R (1996) Adaptive modeling of the unattended acoustic environment reflected in the mismatch negativity event-related potential. Brain Research 742(1-2):239-252

Woods EJ, Frost BJ (1977) Adaptation and habituation characteristics of tectal neurons in the pigeon. Experimental brain research. Experimentelle Hirnforschung. Experimentation cerebrale 27(3-4):347-354

Yabe H, Tervaniemi M, Reinikainen K, Näätänen R (1997) Temporal window of integration revealed by MMN to sound omission. Neuroreport 8(8):1971-1974

Yan Z, Surmeier DJ (1996) Muscarinic (m2/m4) receptors reduce N- and P-type Ca2+ currents in rat neostriatal cholinergic interneurons through a fast, membrane-delimited, G-protein pathway. J Neurosci 16(8):2592-2604

Yokoyama S (2000) Molecular evolution of vertebrate visual pigments. Progress in retinal and eye research 19(4):385-419

Zhang LI, Tan AY, Schreiner CE, Merzenich MM (2003) Topography and synaptic shaping of direction selectivity in primary auditory cortex. Nature 424(6945):201-205

Zhao L, Liu Y, Shen L, Feng L, Hong B (2011) Stimulus-specific adaptation and its dynamics in the inferior colliculus of rat. Neuroscience 181:163-174

Zschocke S (2012) Klinische Elektroenzephalographie. Springer-Verlag Berlin Heidelberg,

Zurita P, Villa AE, de Ribaupierre Y, de Ribaupierre F, Rouiller EM (1994) Changes of single unit activity in the cat's auditory thalamus and cortex associated to different anesthetic conditions. Neurosci Res 19(3):303-316

19 Acknowledgments

This dissertation would not have been possible without the help of the following persons who contributed in various ways to its preparation and completion.

First of all I would like to thank PD Dr. Heike Endepols for the excellent supervision of my thesis, for scientific discussions and patiently answering all my questions. This thesis would not have been possible without her guidance and encouragement. Dr. Marc Tittgemeyer I would like to thank for contributing to the development of the study, for giving me the opportunity to work on this project and helpful comments during the preparation of this thesis. Furthermore, I would like to express my gratitude to Prof. Dr. Graf for scientific discussions and numerous advices. Prof. Dr. Dr. med Klaas Enno Stefan I would like to thank for contributing to the development of the study, for his help with writing the paper and giving me the opportunity to learn how to employ “dynamic causal models” in his group.

Special thanks are due to M.Sc. Elena Höfener, Dipl. Biol. Hanna Mertgens and Dr. Cathrin Rohleder who never got tired of giving me professional advice and emotional support in every circumstance. M.Sc. Markus Gramer I would like to thank for the patient help with the use of Matlab and programming as well as Dr. Heiko Backes for scientific discussions and interpretation of the data. Furthermore, I want to express my gratitude to Dr. med Tetsuya Kumagai who initially developed the method of electrodes implantation and instructed me in this technique. B.Sc. Felix Neumaier I would like to thank for the conduction of the brainstem audiometry.

In addition, I would like to thank PhD Andreea Oliviana Diaconescu for teaching me how to use „dynamic causal models“ and for taking the time to answer many questions. Thanks are also due to PhD Kay Henning Brodersen for providing me with the Matlab scripts for the model inversion.

Moreover, I am grateful to the IT-group of the MPI, especially Ingo Alt, Dr. Stefan Vollmar and Dipl. Inf. Andreas Hüsgen for support and help at any time and for providing me with the “jobrunner” script.

In particular I would like to express my gratitude to my parents Maria and Hans Jürgen Jung who always supported and encouraged me and without whom none of this would have been possible. Thanks are also due to my brother Christoph Jung, especially for cheering me up during the last weeks, and my grandparents Renate and Heinz Jung.

Furthermore, I would like to thank all my friends for nice hours far from work.

20 Erklärung

"Ich versichere, dass ich die von mir vorgelegte Dissertation selbständig angefertigt, die benutzten Quellen und Hilfsmittel vollständig angegeben und die Stellen der Arbeit − einschließlich Tabellen, Karten und Abbildungen −, die anderen Werken im Wortlaut oder dem Sinn nach entnommen sind, in jedem Einzelfall als Entlehnung kenntlich gemacht habe; dass diese Dissertation noch keiner anderen Fakultät oder Universität zur Prüfung vorgelegen hat; dass sie − abgesehen von unten angegebenen Teilpublikationen − noch nicht veröffentlicht worden ist sowie, dass ich eine solche Veröffentlichung vor Abschluss des Promotionsverfahrens nicht vornehmen werde. Die Bestimmungen der Promotionsordnung sind mir bekannt. Die von mir vorgelegte Dissertation ist von PD Dr. Heike Endepols betreut worden."

Köln, den 06.05.2013 _____

Fabienne Jung